

The Preparation and  
Characterisation Of Some Novel  
Transition Metal Pentafluoride  
Adducts And The  
Reduction Of Some Transition  
Metal Fluorides

A thesis presented for the degree of  
Doctor of Philosophy  
in the  
Department of Chemistry  
of the  
Faculty of Science  
at the University of Leicester  
by  
Peter James Holliman.  
1992.

UMI Number: U050654

All rights reserved

INFORMATION TO ALL USERS

The quality of this reproduction is dependent upon the quality of the copy submitted.

In the unlikely event that the author did not send a complete manuscript and there are missing pages, these will be noted. Also, if material had to be removed, a note will indicate the deletion.



UMI U050654

Published by ProQuest LLC 2015. Copyright in the Dissertation held by the Author.  
Microform Edition © ProQuest LLC.

All rights reserved. This work is protected against  
unauthorized copying under Title 17, United States Code.



ProQuest LLC  
789 East Eisenhower Parkway  
P.O. Box 1346  
Ann Arbor, MI 48106-1346



7501439523

X752271732

For Judith and for Richard.

## Abstract

A review of the transition-metal pentafluoride structures and the theories put forward to explain them is held in Chapter 1, along with a brief discussion of the transition-metal oxide fluorides which have structures related to them.

Chapters 2–5 detail the preparation and characterisation of  $\text{NbF}_5:\text{TaF}_5$  [x:y] (Chapter 2),  $\text{RuF}_5:\text{TaF}_5$  [x:y] (Chapter 3),  $\text{VF}_5:\text{TaF}_5$  [x:y] (Chapter 4) and  $\text{RuF}_5:\text{VF}_5$  [x:y] and  $\text{RuF}_5:\text{NbF}_5$  [x:y] are grouped together in Chapter 5. Characterisation of these compounds has involved XRF analysis, infrared and Raman spectroscopy, mass spectrometry and X-ray diffraction techniques.

In order to investigate the metal site occupancy of some of the mixed-metal pentafluorides the EXAFS spectra of suitable metal edges have been recorded and analysed. The results are reported in Chapter 6 along with a brief theoretical description of the technique and the method of data analysis used.

The possibility of using MICVD (Metal Inorganic Chemical Vapour Deposition) as a method of forming thin layers of pure metals or alloys by the reduction of metal fluorides or mixed-metal pentafluorides respectively has been investigated both theoretically and experimentally. This is discussed in Chapter 8.

Chapter 9 reports details of the experimental techniques used in the work in this thesis.

## Acknowledgements

The part that my wife Judith has played during and in the completion of my PhD studies cannot be overestimated, as I doubt it would have been finished without her support. She is my happiness that we all look for and some are not fortunate enough to find. I was also lucky enough to have Richard as my twin brother, which made growing up great fun, still does and will do, I have no doubt.

I would like to thank my family for their support throughout my life as a student. My parents, grandparents and my parents-in-law have done all that they could to help me and I am extremely grateful.

I would like to acknowledge the help of my supervisor John Holloway in the completion of this thesis and a number of people who have also helped, not least of which is Dr Alan Brisdon who unglued computers after I had superglued them up, gave advice and generally drove women to distraction.

Most of the single crystal structure data sets in this thesis were collected and solved at Leicester University by Dr John Fawcett, with the aid of Dr D. R. Russell and Mr Stuart Brewer. Many thanks to all, but especially to John as well as for some good gossips and fireworks. I would also like to thank Dr S. Blake at Edinburgh University who collected the data sets For  $\text{NbF}_5:\text{TaF}_5$  [1:3],  $\text{RuF}_5:\text{TaF}_5$  [1:1] and  $\text{TaF}_5:\text{VF}_5$  [1:1].

Many thanks to Dr Alan Brisdon, Dr Eric Hope and Mr Stuart Brewer for their help in collecting EXAFS data and to Dr Malcolm Atherton and the staff at BNFL Ltd for their help in the interpretation of the nature of the U deposits in Chapter 8. The group at Leicester was ever-changing, but ever cheerful and so I say thankyou to Matthias, Preston Paul, Mohammed, Saad, Scottish Paul and Leslie and Stu (my contemporaries), Chris, Ady, Graham and Martin.

Finally, a big thankyou goes to Mr George McCulloch who ran the SEM and

XRF analysis, Mrs Gill Lonaghan who ran the mass spectra, the workshop, my mate Roy the glass-blower, John Graham at Southampton University for running some FT-Raman spectra and letting me sleep on his floor and the Computer Centre at Leicester who provided the facilities to run Latex, which is the word processor used in this thesis. Also thankyou to the SERC who funded this work.

# Contents

<b>1</b>	<b>Introduction.</b>	<b>2</b>
1.1	Area of Study . . . . .	2
1.2	Review of Transition-Metal Fluoride and Related Oxide Fluoride Structures . . . . .	5
1.2.1	The Transition-Metal Pentafluorides . . . . .	6
1.2.2	Review of the Explanations for the Different Pentafluoride Structures . . . . .	19
1.2.3	Related Oxide Fluoride Structures . . . . .	27
1.2.4	Transition Metal Oxide Fluoride Structure Generalisations . . . . .	33
<b>2</b>	<b>The Preparation and Characterisation of NbF<sub>5</sub>:TaF<sub>5</sub> [3:1], [1:1] and [1:3].</b>	<b>35</b>
2.1	Introduction . . . . .	35
2.2	Preparation . . . . .	37
2.3	X-ray Fluorescence . . . . .	37
2.4	Mass Spectrometry . . . . .	39
2.4.1	NbF <sub>5</sub> :TaF <sub>5</sub> [1:3] . . . . .	40
2.4.2	NbF <sub>5</sub> :TaF <sub>5</sub> [3:1] . . . . .	43
2.4.3	NbF <sub>5</sub> :TaF <sub>5</sub> [1:1] . . . . .	43
2.5	Infrared Spectroscopy of Solid Samples . . . . .	44
2.6	Raman Spectroscopy . . . . .	45
2.6.1	The NbF <sub>5</sub> and TaF <sub>5</sub> Spectra . . . . .	47
2.6.2	The NbF <sub>5</sub> :TaF <sub>5</sub> [3:1], [1:1] and [1:3] Spectra . . . . .	47

2.7	Gas-Phase Infrared Spectroscopy . . . . .	48
2.7.1	NbF <sub>5</sub> . . . . .	48
2.7.2	TaF <sub>5</sub> . . . . .	50
2.7.3	NbF <sub>5</sub> :TaF <sub>5</sub> [x:y] . . . . .	51
2.8	X-ray Diffraction . . . . .	57
2.8.1	X-ray Powder Diffraction Studies . . . . .	57
2.8.2	X-ray Single Crystal Studies . . . . .	57
2.9	Conclusions . . . . .	59

**3 The Preparation and Characterisation of RuF<sub>5</sub>:TaF<sub>5</sub> [3:1], [1:1] and [1:3].** **65**

3.1	Introduction . . . . .	65
3.2	Preparation . . . . .	66
3.3	X-ray Fluorescence Analysis . . . . .	66
3.4	Infrared Spectroscopy of the Solids . . . . .	67
3.5	Raman Spectroscopy . . . . .	68
3.5.1	The Raman Spectra of (RuF <sub>5</sub> ) <sub>4</sub> and (TaF <sub>5</sub> ) <sub>4</sub> . . . . .	69
3.5.2	The Raman Spectrum of RuF <sub>5</sub> :TaF <sub>5</sub> [3:1] . . . . .	70
3.5.3	The Raman Spectrum of RuF <sub>5</sub> :TaF <sub>5</sub> [1:1] . . . . .	71
3.5.4	The Raman Spectrum of RuF <sub>5</sub> :TaF <sub>5</sub> [1:3] . . . . .	71
3.6	Gas-Phase Infrared Spectroscopy . . . . .	71
3.6.1	The Spectra of RuF <sub>5</sub> and TaF <sub>5</sub> . . . . .	72
3.6.2	RuF <sub>5</sub> :TaF <sub>5</sub> [3:1] . . . . .	74
3.6.3	RuF <sub>5</sub> :TaF <sub>5</sub> [1:1] . . . . .	76
3.6.4	RuF <sub>5</sub> :TaF <sub>5</sub> [1:3] . . . . .	76
3.7	X-ray Powder Diffraction . . . . .	76
3.8	X-ray Single Crystal Diffraction Studies . . . . .	78
3.8.1	The RuF <sub>5</sub> :TaF <sub>5</sub> [1:3] Structure . . . . .	78
3.8.2	The RuF <sub>5</sub> :TaF <sub>5</sub> [1:1] Structure . . . . .	82
3.9	Conclusions . . . . .	83

<b>4</b>	<b>The Preparation and Characterisation of <math>\text{VF}_5:\text{TaF}_5</math> [3:1], [1:1] and [1:3].</b>	<b>86</b>
4.1	Introduction . . . . .	86
4.2	Preparation . . . . .	87
4.3	X-ray Fluorescence Analysis . . . . .	87
4.4	Solid-Phase Infrared Spectroscopy . . . . .	88
4.4.1	$\text{VF}_5:\text{TaF}_5$ [1:1] . . . . .	88
4.4.2	$\text{VF}_5:\text{TaF}_5$ [3:1] . . . . .	89
4.5	Raman Spectroscopy . . . . .	90
4.6	Gas-Phase Infrared Spectroscopy . . . . .	92
4.7	X-ray Powder Diffraction . . . . .	93
4.8	X-ray Single Crystal Diffraction . . . . .	93
4.9	Conclusions . . . . .	97
<b>5</b>	<b>The Preparation and Characterisation of <math>\text{RuF}_5:\text{VF}_5</math> [1:1], <math>\text{RuF}_5:\text{NbF}_5</math> [3:1], [1:1] and [1:3].</b>	<b>100</b>
5.1	Introduction . . . . .	100
5.1.1	$\text{RuF}_5:\text{VF}_5$ . . . . .	100
5.1.2	$\text{RuF}_5:\text{NbF}_5$ . . . . .	101
5.2	The Preparation and Characterisation of $\text{RuF}_5:\text{VF}_5$ [1:1] . . . . .	102
5.2.1	Preparation . . . . .	102
5.2.2	X-ray Fluorescence Analysis . . . . .	102
5.3	Solid-Phase Infrared Spectroscopy . . . . .	102
5.4	Gas-Phase Infrared Spectroscopy . . . . .	103
5.5	X-ray Powder Diffraction . . . . .	104
5.6	X-ray Single Crystal Studies . . . . .	106
5.7	The Characterisation Of $\text{RuF}_5:\text{NbF}_5$ [3:1], [1:1] and [1:3] . . . . .	106
5.7.1	Preparation . . . . .	106
5.7.2	The Solid-Phase Infrared Spectroscopy . . . . .	106
5.7.3	Gas-Phase Infrared Spectroscopy . . . . .	107
5.7.4	X-ray Powder Diffraction . . . . .	108
5.7.5	X-ray Single Crystal Diffraction Work . . . . .	110

5.8	Conclusions . . . . .	112
5.8.1	$\text{RuF}_5:\text{VF}_5$ . . . . .	112
5.8.2	$\text{RuF}_5:\text{NbF}_5$ . . . . .	113
<b>6</b>	<b>Structural Studies Using EXAFS.</b>	<b>115</b>
6.1	Introduction . . . . .	115
6.2	EXAFS Theory . . . . .	116
6.2.1	Short-Range Single-Electron Single-Scattering Theory. . . . .	117
6.2.2	Curved Wave Theory . . . . .	120
6.2.3	EXAFS Data Analysis . . . . .	121
6.2.4	Error Estimation . . . . .	125
6.3	The Hexafluorometallates . . . . .	125
6.4	The Metal Pentafluorides . . . . .	126
6.4.1	Niobium Pentafluoride . . . . .	126
6.4.2	Tantalum Pentafluoride . . . . .	129
6.4.3	Ruthenium Pentafluoride . . . . .	130
6.5	The Mixed-Metal Pentafluorides . . . . .	132
6.5.1	$\text{NbF}_5:\text{TaF}_5$ [1:3] . . . . .	132
6.5.2	$\text{RuF}_5:\text{NbF}_5$ [1:1] . . . . .	139
6.5.3	$\text{RuF}_5:\text{VF}_5$ [1:1] . . . . .	143
6.5.4	$\text{TaF}_5:\text{VF}_5$ [1:1] . . . . .	143
6.5.5	$\text{RuF}_5:\text{TaF}_5$ [3:1] . . . . .	148
6.5.6	$\text{TaF}_5:\text{VF}_5$ [1:3] . . . . .	151
6.6	Conclusions . . . . .	152
<b>7</b>	<b>Solid-State Structural Conclusions</b>	<b>156</b>
7.1	Introduction . . . . .	156
7.2	The $\text{TaF}_5$ Structure . . . . .	157
7.3	Packing in the Transition-Metal Pentafluorides . . . . .	158
7.4	Comparison Of H.C.P. and C.C.P. Fluorine Lattices . . . . .	160
7.5	Future Work . . . . .	163

<b>8</b>	<b>Metal Inorganic Chemical Vapour Deposition Studies on Selected Metal Fluorides</b>	<b>165</b>
8.1	Introduction . . . . .	165
8.1.1	Area of Study . . . . .	165
8.1.2	Review of Previous Work . . . . .	166
8.1.3	The CVD Technique . . . . .	169
8.2	Theoretical Thermodynamic Investigation of MICVD . . . . .	169
8.2.1	The Transition-Metal Pentafluorides and Hexafluorides . . . . .	169
8.2.2	The Mixed-metal Pentafluorides . . . . .	173
8.3	The Reduction Apparatus . . . . .	176
8.4	Experimental Results . . . . .	180
8.5	Conclusions . . . . .	189
8.6	Future Work . . . . .	189
<b>9</b>	<b>Experimental</b>	<b>193</b>
9.1	Handling of Materials . . . . .	193
9.1.1	Metal Vacuum Lines . . . . .	193
9.1.2	Dry Box . . . . .	194
9.1.3	Reaction Vessels . . . . .	197
9.2	Analytical Techniques . . . . .	200
9.2.1	Infrared Spectroscopy . . . . .	200
9.3	The Preparation of the Transition Metal Pentafluorides and Mixed- Metal Pentafluorides . . . . .	204
9.3.1	NbF <sub>5</sub> , TaF <sub>5</sub> and RuF <sub>5</sub> . . . . .	204
9.3.2	The VF <sub>5</sub> Preparation . . . . .	206
9.3.3	The Mixed-Metal Pentafluoride Preparation . . . . .	206
9.4	The Reduction of the Metal Fluorides . . . . .	206
9.4.1	The First and Second Types of Reduction Apparatus (Marks 1 and 2). . . . .	206
9.4.2	The Third Type of Reduction Apparatus (Mark 3). . . . .	207
9.5	Sources of Chemicals and Methods of Purification . . . . .	208

# Chapter 1

## Introduction.

### 1.1 Area of Study

This thesis can be divided into four parts, the first of which is a review of the transition-metal pentafluoride and related oxide fluoride structures, along with the theories suggested to explain the differences between the atomic arrangements. These theories are no longer believed to adequately describe the solid states of the materials on the basis of new information from more recent structure determinations of NbF<sub>5</sub> [4], RuF<sub>5</sub>, TaF<sub>5</sub> (Chapter 2) and from novel mixed-metal pentafluorides (Chapters 2–6). Chapter 7 details conclusions based on this new information, which seem to offer more reasonable explanations for the structures. Finally, the area of metal inorganic chemical vapour deposition (MICVD) of the transition-metal and mixed-metal pentafluorides has not previously been studied and it is thought that work described in this thesis may yield a route to thin films and alloys difficult to obtain by other means. A theoretical investigation of this chemistry, combined with experimental work, is reported in Chapter 8.

Prior to the work in this thesis, the transition-metal pentafluorides had been reported to occur as three structural types; the TaF<sub>5</sub> type of structure [1] which was thought to be a straight *cis*-fluorine bridged tetramer, the RuF<sub>5</sub> type [2], which was described as a bent *cis*-fluorine bridged tetramer, and the VF<sub>5</sub> type [3] which was described as a bent *cis*-fluorine bridged endless chain.

$\text{TaF}_5$  was thought to be based on a cubic close-packed lattice of fluorine atoms with metal atoms in one fifth of the octahedral holes [1]. The  $\text{RuF}_5$  structure, on the other hand, was thought to be based on a hexagonal close-packed lattice of fluorine atoms with metal atoms in one fifth of the octahedral holes [2], whilst the atoms in  $\text{VF}_5$  were not thought to be close-packed but to have a structure based more closely on a hexagonal lattice of fluorine atoms than a cubic lattice [3].

Various theories have been put forward to explain the reasons why transition-metal pentafluorides adopt these different structures (see review section). However, these explanations have been based on single-crystal structure determinations carried out twenty years ago and some of the data is not as accurate as that obtained from crystal structure analyses carried out nowadays.

As part of the present study the structure of  $\text{TaF}_5$  has been redetermined and this has confirmed the overall, original tetrameric arrangement [1]. However, there are differences between this new structure and that of the original which must be assumed also to be the case for other materials isostructural with  $\text{TaF}_5$ . For  $\text{NbF}_5$ ,  $\text{TaF}_5$  and  $\text{RuF}_5$  the original structure determinations were two-dimensional and solved by visual estimation of photographic data rather than with the aid of modern computing methods.  $\text{NbF}_5$  [4] and  $\text{RuF}_5$  [5] have been redetermined recently three-dimensionally, using modern data collection and computer programmes. The three-dimensional structure determination carried out in 1969 on a single crystal of  $\text{VF}_5$  [3] was also done without the aid of modern computer programmes. There may also be errors associated with this structure due to the fact that the crystal was changing shape during the collection of the data because of its small residual vapour pressure at 8–10° C, the temperature at which the experiment was carried out [6].

In order to investigate further the factors which influence the types of solid-state structure the transition-metal pentafluorides adopt, novel compounds con-

taining two different transition-metal pentafluorides have been prepared as part of the present work. It was thought that the solid-state structures adopted by these mixed-metal pentafluorides might yield further information, not only about the parent transition-metal pentafluoride structures themselves, but also about the way in which the metal atoms interact within these solids. It was anticipated that this new investigation would also yield information about the relative Lewis acidities of the metal pentafluorides.

The characterisation of the metal pentafluorides in the gas phase has also led to some conflicting reports in the literature (see Chapter 2). The main area of uncertainty being the exact nature of the species dominant in the gas phase at different temperatures. The main techniques of investigation used so far have been gas-phase infrared spectroscopy [7–10], gas-phase Raman spectroscopy [11–13], mass spectroscopy [14–16] and electron diffraction [17–22]. It has been reported that of the transition metal pentafluorides only  $(\text{NbF}_5)_4$  and  $(\text{TaF}_5)_4$  do not decompose at temperatures less than  $100^\circ\text{C}$  [23]. However this may be because of the extreme reactivity of many of the metal pentafluorides and resultant attack on the container rather than their thermal instability and so can be discounted. The deduction made from the mass spectroscopy, electron diffraction and the more recent gas-phase vibrational spectroscopy is that the dominant species at  $\approx 90^\circ\text{C}$  is trimeric. However, vapour density measurements [24] imply that the chain-length of gas-phase species of  $\text{NbF}_5$  and  $\text{TaF}_5$  close to their boiling points (ie. above  $200^\circ$ ) is greater than expected for chains containing three  $\text{MF}_5$  units. This implies that, although the dominant species may be trimeric, there are also tetramers present. On the whole however, it can be seen that, with increasing temperature, the metal pentafluorides dissociate from tetramers to form trimers, dimers and monomers [14–16, 24].

By comparing the metal pentafluoride gas-phase infrared data with that from the mixed-metal pentafluorides prepared as part of the present work, it was thought likely that new insights into the dominant gas-phase species at less than  $100^\circ$  might become apparent. The nature of such gas-phase species is important in terms of

the factors affecting the bonding in the  $\text{MF}_5$  units, when they are not held in a crystalline lattice.

The dominant gas-phase species at a given temperature is important for a second reason. The metal pentafluorides and mixed-metal pentafluorides have been investigated as possible precursors in the chemical vapour deposition of pure metals and alloys (see Chapter 7). Because the precursor must be in the gas phase before reaching the substrate and reacting, the nature of the deposit will be affected by the nature of the gas phase species, as well as by the thermodynamics of the process.

Chemical vapour deposition using metal pentafluorides as precursors is a novel area of research and has implications for (a) the electronics industry [eg. 25–27], (b) for the preparation of thin metal or alloy films for heterogenous catalysis etc. [eg. 28, 29] and (c) for the metallurgical industry [eg. 30].

## 1.2 Review of Transition-Metal Fluoride and Related Oxide Fluoride Structures

There are a large number of transition-metal fluoride and oxide fluoride structures known but, for the purposes of this review, only the transition-metal pentafluorides or oxide fluorides where  $\text{M}:(\text{O} + \text{F})$  is 1:5 will be considered. The main purpose of the review is to consider compounds with similar structures to those of the transition-metal pentafluorides and explanations as to why they adopt the structures they do.

All of the  $\text{MF}_5$  and  $\text{MO}_a\text{F}_b$  species mentioned in the review have structures involving fluorine bridging; whether that be *cis*- or *trans*-fluorine bridging, whether the material is trimeric or tetrameric and regardless of the oxidation state of the metal. It should be noted that many metal fluorides in oxidation states other than five or six have structures which are also heavily dependent on fluorine bridging between metal centres, for instance, the transition-metal tetrafluorides [31–35] and

the transition-metal trifluorides [36–38, 73]. Many of the structures are also believed to be based on close-packed lattices of fluorine atoms, or a mixture of fluorine and oxide atoms, with metal atoms filling an appropriate proportion of octahedral holes.

### 1.2.1 The Transition-Metal Pentafluorides

The literature concerning the structures of the transition-metal pentafluorides is fairly extensive and, in the present section, the structures themselves will first be summarized and then the various theories which have been used to explain the differences between them will be outlined.

All of the transition-metal pentafluorides are polymeric in the solid state. Most are also polymeric at temperatures below  $\approx 200^\circ\text{C}$ , which is reflected in their very large liquid range (see Table 1.1). This implies a degree of association even at elevated temperatures.

Three structural types of the transition-metal pentafluorides are described in the literature. These are the  $\text{NbF}_5$  type structure [1], the  $\text{RuF}_5$  type structure [2] and the  $\text{VF}_5$  type structure [3]. All of the transition-metal pentafluorides characterised so far possess one of these structures. There is, however, a report in the literature of X-ray powder diffraction data for  $\text{AuF}_5$  [48], which suggests a new type of chain structure for this material, although Holloway and co-workers had previously reported that  $\text{AuF}_5$  possesses a structure similar to that of  $\text{RuF}_5$  [49]. This is discussed further later in the review (see section on the  $\text{RuF}_5$ -Type Structure). The unit cell dimensions and other crystallographic data for all the known transition-metal pentafluorides are shown in Table 1.2. The main-group and actinide-pentafluoride structures (eg.  $\text{SbF}_5$  [50],  $\text{UF}_5$  [51–53] and  $\text{BiF}_5$  [54]) are reported merely for comparison.

Table 1.1: Melting Points and Boiling Points of the Transition Metal Pentafluorides

Compound	Melting Point (°C)	Boiling Point (°C)	Reference
$\text{VF}_5$	19.5(5)	48.1(2)	6
$\text{CrF}_5$	50	-	47
$\text{TcF}_5$	50	-	39
$\text{ReF}_5$	48	221.3 <sup>*</sup>	41
$\text{NbF}_5$	80	234.9	40
$\text{TaF}_5$	95.1	229	40
$\text{MoF}_5$	67	214 <sup>*</sup>	41
$\text{WF}_5$	dec above 30	dec	44, 45
$\text{RuF}_5$	86.5	227	42
$\text{OsF}_5$	70	226	41
$\text{RhF}_5$	95.5	-	43
$\text{IrF}_5$	104	-	68
$\text{PtF}_5$	80	-	46

\* By extrapolation.

Table 1.2: Crystallographic Data For the Transition Metal Pentafluorides

MF <sub>5</sub>	Space Group	Symmetry	a (Å)	b (Å)	c (Å)	$\beta$ (°)	Ref.
VF <sub>5</sub>	Pmcn	Orth	5.40(1)	16.72(2)	7.53(1)	-	3
CrF <sub>5</sub>	Pmcn	Orth	5.5	16.3	7.4	-	47
TcF <sub>5</sub>	Pmcn	Orth	5.76(1)	17.01(2)	7.75(1)	-	55
ReF <sub>5</sub>	Pmcn	Orth	5.70(1)	17.23	7.67(1)	-	3
NbF <sub>5</sub>	C2/m	Mono	9.62(1)	14.43(2)	5.12(1)	96.1(3)	1
TaF <sub>5</sub>	C2/m	Mono	9.631(27)	14.466(41)	5.102(2)	96.34(2)	*
MoF <sub>5</sub>	C2/m	Mono	9.61(1)	14.22(2)	5.16(1)	94.3(3)	56
WF <sub>5</sub>	C2/m	Mono	9.61(2)	14.26(3)	5.23(2)	94.6(6)	57
RuF <sub>5</sub>	P2 <sub>1</sub> /c	Mono	5.4969(6)	9.946(1)	12.531(2)		5
OsF <sub>5</sub>	P2 <sub>1</sub> /a	Mono	12.59(15)	9.91(10)	5.53(3)	99.53(3)	58
RhF <sub>5</sub>	P2 <sub>1</sub> /a	Mono	12.3376(13)	9.9173(8)	5.5173(6)	100.42(2)	59
IrF <sub>5</sub>	P2 <sub>1</sub> /a	Mono	12.267(3)	9.982(4)	5.413(2)	99.9(2)	60,61
PtF <sub>5</sub>	P2 <sub>1</sub> /c	Mono	5.523(3)	9.942(6)	12.430(6)	99.98(4)	62
AuF <sub>5</sub>	C6 <sub>1</sub> 2 or C6 <sub>1</sub> <sup>†</sup>	Hex	5.664(2)	-	19.221(9)	-	48

Orth = Orthorhombic.

Mono = Monoclinic.

Hex = Hexagonal.

\* See Chapter 2.

<sup>†</sup> Most probable space groups.

## The NbF<sub>5</sub>-Type Structure

Edwards first examined the structures of NbF<sub>5</sub> and TaF<sub>5</sub> [1] by X-ray single crystal work and found them to be isostructural and made up of linear *cis*-fluorine bridged tetramers. The metal atoms are approximately at the four corners of a square with fluorine bridging atoms between the metal centres. The four metal atoms and four fluorine-bridging atoms are in a planar arrangement with each metal atom approximately octahedrally coordinated (see Figure 1.1).

The NbF<sub>5</sub> structure has been redetermined three-dimensionally recently [4] by the original author using modern computer programmes in order to gain more accurate atomic positions. This was necessary because the original structure was only a two-dimensional determination solved using photographic data. The redetermined structure has shown that the gross tetrameric structure is correct. However, the M-F<sub>b</sub>-M bond angle is changed from the original near-linear arrangement to 173.0(1)°. A second difference is that the average M-F<sub>t</sub> bond distance is 1.827(4) Å as compared with 1.77 Å in the original work.

The TaF<sub>5</sub> structure has now also been redetermined, as part of the work described in this thesis (see Chapter 2). This has allowed closer comparison of the structure with those of the mixed-metal pentafluorides. Here again the determination has confirmed the original tetrameric arrangement, but has again shown a departure from linearity of the M-F<sub>b</sub>-M bridge.

In the 1960's, Edwards also examined the structure of MoF<sub>5</sub> [56] but this, the first of the pentafluoride structure determinations, was not as accurate as those for NbF<sub>5</sub> and TaF<sub>5</sub>. MoF<sub>5</sub> was known, at this time, to be isostructural with NbF<sub>5</sub> and TaF<sub>5</sub> and yet it was suggested that there were two sites within the tetramer, at opposite corners. This suggestion was based on two sets of slightly different M-F distances, one set for each site. Bearing in mind the redetermination of the NbF<sub>5</sub> and TaF<sub>5</sub> structures this is clearly not the case.

Evidence for a second, trimeric phase for MoF<sub>5</sub>, based on magnetic susceptibility studies on crystalline, liquid and glassy MoF<sub>5</sub> in the temperature range 4.2–320K has also been published [63]. These measurements have been interpreted to suggest that only a percentage of trimer molecules occur in the glassy state and no other information has been reported to support this.

### The RuF<sub>5</sub>-Type Structure

The RuF<sub>5</sub> structure was first reported by Holloway et al [2] and was found to be a different structural form to that of NbF<sub>5</sub> and its structural relatives. Although tetrameric with four Ru atoms in a plane, these were at the four corners of a rhombus with bent *cis*-fluorine bridges between each metal atom. The four bridging fluorine atoms were also found not to be in the plane of the four metal atoms, but with two above the plane and two below (see Figure 1.2). Another difference between the RuF<sub>5</sub> and NbF<sub>5</sub> structures was that the Ru-F<sub>b</sub>-Ru bond angle was 138° as compared with 182.5° in NbF<sub>5</sub> [1]. This Ru-F<sub>b</sub>-Ru bond angle corresponded to a Ru-Ru° distance (Table 6.4) along one side of the tetramer of ≈ 3.7 Å which compared with ≈ 4.13 Å for the analogous distance in NbF<sub>5</sub> [1].

The RuF<sub>5</sub> structure was later redetermined by the same author [58] and more accurate data reported. However, both this new structure and the original were solved using data collected photographically as two-dimensional structures, without the use of modern computing methods.

More recently two new redeterminations of the RuF<sub>5</sub> structure [5, 64] have been carried out. Both are three-dimensional and have been solved using modern computer programmes. The redetermination by Bartlett and co-workers can be considered to be the more accurate in terms of a lower R-factor of 3 % as compared with 7% for the other work and because lower thermal parameters are obtained. This redetermination [5] shows that there are two slightly different M-F<sub>b</sub>-M bond angles of 136 and 140°. The overall structure, however, is the same as that in the original

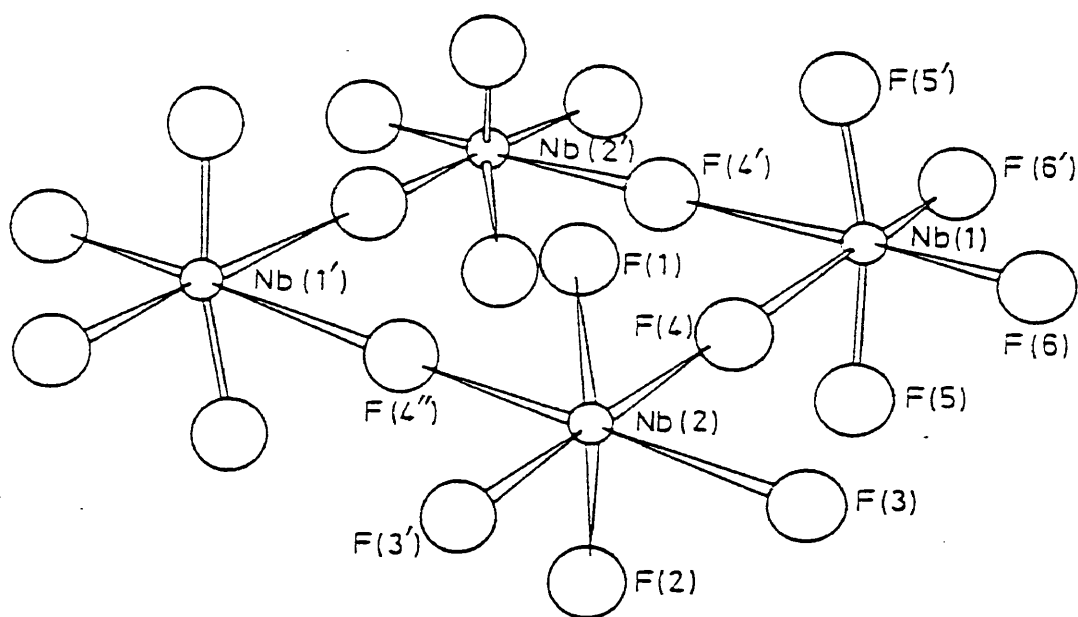


Figure 1.1: The  $\text{NbF}_5$  Tetramer

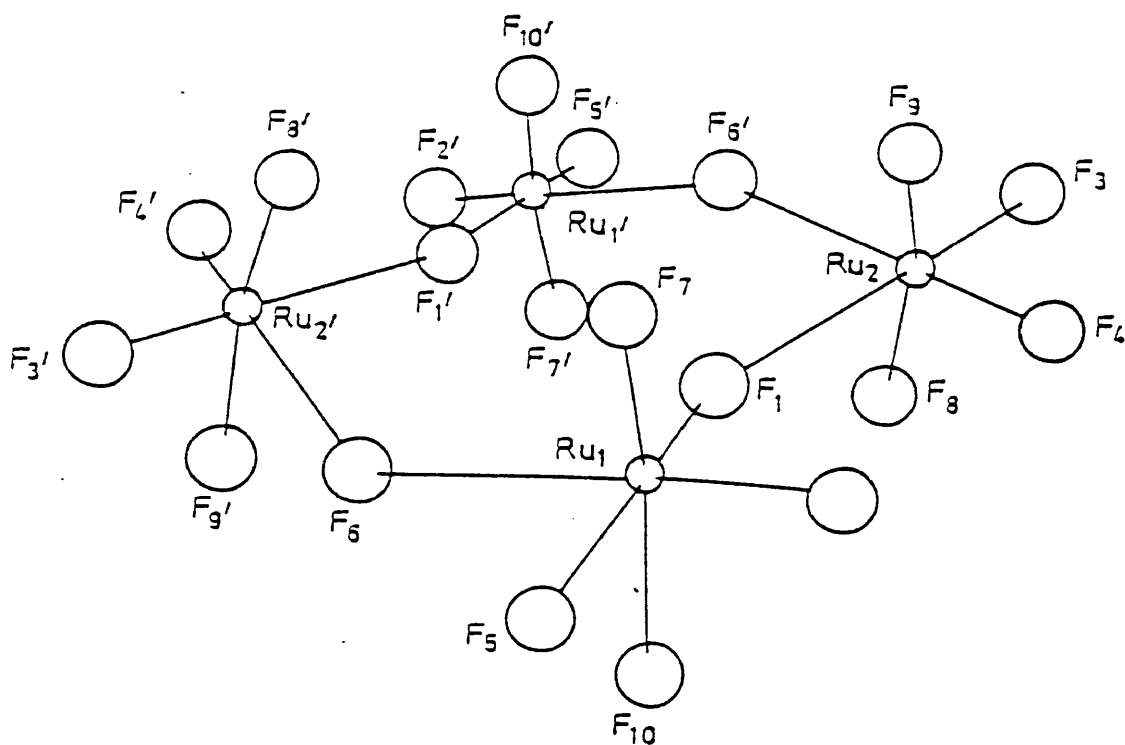


Figure 1.2: The  $\text{RuF}_5$  Tetramer

study [2].

Recently, there have been reports of a red form of  $\text{RuF}_5$  [65] produced, along with  $\text{RuF}_5$  and  $\text{RuF}_6$ , during the flow fluorination of Ru metal. This red material has only been characterised by mass spectroscopy so far but this suggests that it is a trimeric form of  $\text{RuF}_5$ . Attempts to collect X-ray diffraction data on the material were not successful as the compound appeared to decompose in the X-ray beam at room temperature [66].

After the first  $\text{RuF}_5$  structure determination was first published [58] the structure of  $\text{OsF}_5$  was also determined, and found, not surprisingly, to be essentially isomorphous with that of  $\text{RuF}_5$  [2]. It was also shown that the structure is based on a hexagonal close-packed lattice of fluorine atoms with the osmium atoms occupying one fifth of the octahedral holes.

$\text{RhF}_5$  [59] is also isostructural with  $\text{RuF}_5$  and, until the recent  $\text{RuF}_5$  structure redetermination was published, this was considered the most accurately determined structure of this type. The structure was solved from three-dimensional data, using modern computing methods, and yielded a final R-factor of 0.029. This work highlighted the more accurate fluorine atomic positions, and showed that there are two groups of  $\text{M-F}_t$  bond lengths; (a) those *trans* to a  $\text{M-F}_b$ , which are labelled  $\text{M-F}_{eq}$  here, and (b) those *trans* to a terminal fluorine atom, which are denoted  $\text{M-F}_{ax}$ . The  $\text{M-F}_{eq}$  distances range from 1.810–1.820 Å and the  $\text{M-F}_{ax}$  distances ranged from 1.796–1.803 Å. The average  $\text{M-F}_b$  bond length is 1.999 Å and there are two slightly different  $\text{Rh-F}_b\text{-Rh}$  bond angles of  $134.35(10)^\circ$  and  $135.71(11)^\circ$ .

$\text{IrF}_5$  [60, 61, 68],  $\text{AuF}_5$  [49] and  $\text{PtF}_5$  [62] are all known to exhibit the  $\text{RuF}_5$  type of structure. This has been ascertained both from X-ray powder diffraction and single-crystal work. Cell dimensions and other crystallographic parameters for these compounds are shown in Table 1.3 along with those for the other transition-metal pentafluorides for comparison. A full X-ray study of the structures of  $\text{IrF}_5$

and AuF<sub>5</sub> has not yet been carried out.

When AuF<sub>5</sub> was first prepared [49] it was suggested on the basis of X-ray powder diffraction data that it has a structure similar to that of RuF<sub>5</sub>. Recently a further X-ray powder diffraction study [48] on hexagonal crystals from an AuF<sub>5</sub> preparation has yielded different cell dimensions to those of the other transition-metal pentafluorides (see Table 1.2). The molar volume of AuF<sub>5</sub> corresponding to the formula unit (89 Å<sup>3</sup>), however is found to be consistent with that of the other MF<sub>5</sub> species. The suggestion here is that AuF<sub>5</sub> is a polymeric chain with a spiral arrangement in space. Mössbauer spectroscopy [72] has shown that, whichever is correct, the coordination about the gold atoms is in the form of a distorted octahedron. This new work suggests that the Au-F<sub>b</sub> bond lengths are identical and that the data can only be solved to reasonable R-factors when a six-fold axis is present. This data has been interpreted to give an Au-Au distance of 4.24 Å, which means that the Au-F<sub>b</sub> bonds would not be less than 2.12 Å. This is a much longer bridge bond than the analogous bonds in AuF<sub>3</sub> (2.03 Å) [73] or NbF<sub>5</sub> (2.06 Å) [1,4]. However, when it is considered with other M-F<sub>b</sub> bond lengths this does not seem unreasonable. For instance, in MOF<sub>4</sub> (where M = Re, Mo or Tc) the longer M-F<sub>b</sub> length is ≈ 2.3 Å [74] and the average W-F<sub>b</sub> bond length in WOF<sub>4</sub> is 2.11 Å [75]. The data were insufficient to permit determination of the positions of the fluorine atoms. The unit cell and symmetry of crystalline AuF<sub>5</sub> may thus indicate a different structural type from those of the other transition-metal pentafluorides. Until single crystals of AuF<sub>5</sub> can be obtained, however, a reliable structure for AuF<sub>5</sub> cannot be determined, but it seems more likely that AuF<sub>5</sub> would adopt the RuF<sub>5</sub>-type structure as originally stated by Holloway [49] because Au<sup>5+</sup> 0.57Å [67] is similar in size to Ru<sup>5+</sup> 0.565Å and these structures are believed to be based on packing (see Chapter 7).

### The VF<sub>5</sub> Type of Structure

The third type of transition-metal pentafluoride structure is typified by VF<sub>5</sub> [3]. This consists of bent *cis*-fluorine bridging atoms linking vanadium atoms arranged

in an endless chain (see Figure 1.3). The X-ray single crystal data from this compound has been solved as a three-dimensional structure, but without using modern computer programmes, to a final R-factor of 0.096. The V-F<sub>b</sub>-V bond angle was estimated to be 149.7(1)°, with an average V-F<sub>t</sub> bond length of 1.69(1) Å and an average V-F<sub>b</sub> bond length of 1.965 Å. Both the V-F<sub>t</sub> and the V-F<sub>b</sub> bond lengths are shorter than their equivalents in either RuF<sub>5</sub> or NbF<sub>5</sub> (see Table 1.3). The volume of the VF<sub>5</sub> unit cell is 680 Å<sup>3</sup>, and it was suggested that this contained a close-packed lattice of fluorine atoms on the basis of the volume of one fluorine atom being 17 Å<sup>3</sup>. It was also suggested that with a M-F<sub>b</sub>-M of 149.7(1)° the close-packed lattice was closer to hexagonal than cubic-close packing. It should be noted, however, that the crystals used for this study are reported as being small (maximum dimensions were 0.05 mm) and no absorption correction was used because the crystals changed shape during data collection on account of the fact that, at the temperature at which the data was collected (8–10°C), VF<sub>5</sub> has a small, residual vapour pressure [6]. The changing crystal size hindered the calculation of structure factors and the plotting of electron density maps. Further errors may also have been introduced through the way in which the data was collected. For instance, because the VF<sub>5</sub> crystal was close to its melting point, the atoms would be vibrating more than if the crystal had been at a lower temperature. This would obviously increase the errors in the atomic positions. For this reason it is now fairly common to collect X-ray data at -78°C [69], and it would be worthwhile to redetermine the VF<sub>5</sub> structure at this temperature.

CrF<sub>5</sub> [47], TcF<sub>5</sub> [55] and ReF<sub>5</sub> [3] are known to be orthorhombic, *P<sub>m</sub>cn* and with similar unit cell dimensions to those of VF<sub>5</sub> (see Table 1.2), although the compounds have been investigated only by X-ray powder diffraction and preliminary X-ray single crystal work.

It should be noted that, although MnF<sub>5</sub> [70] and PdF<sub>5</sub> [71] may have been prepared, no structural data has been collected. It might be expected that, because both TcF<sub>5</sub> and ReF<sub>5</sub> are isostructural with VF<sub>5</sub>, MnF<sub>5</sub> will also possess the same

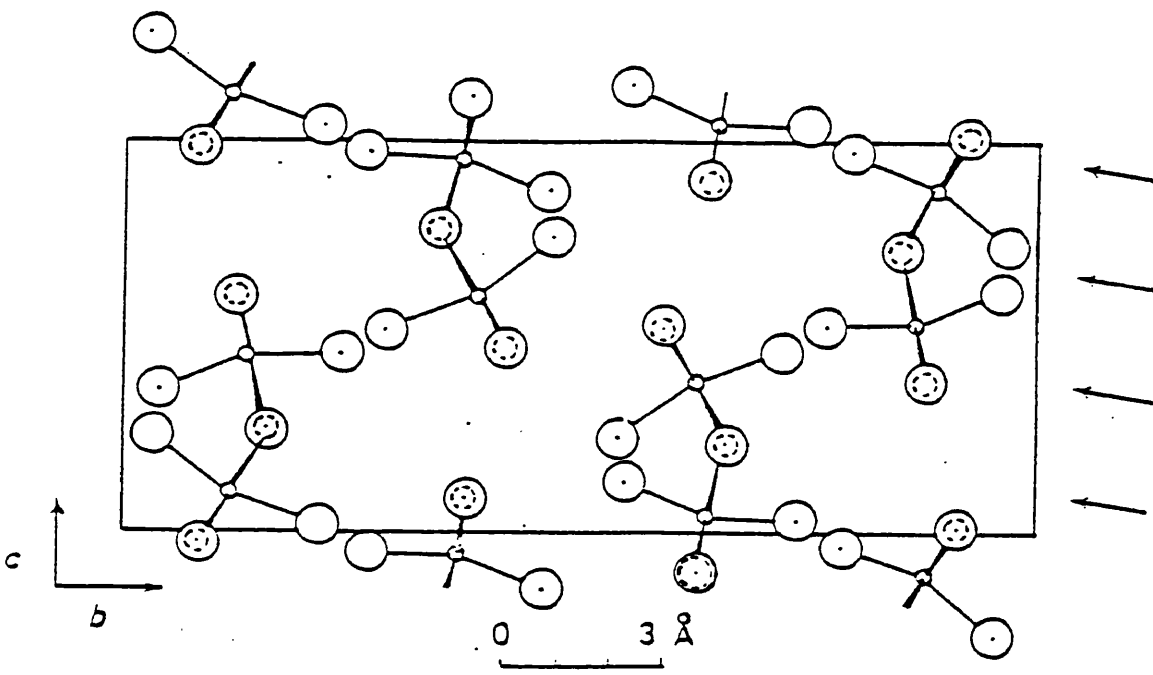


Figure 1.3: The  $\text{VF}_5$  Structure

structure since Mn is in the same group of the Periodic Table as Tc and Re. This is supported by the ionic radius of  $\text{Mn}^{5+}$  ( $0.33 \text{ \AA}$  [67]) which is smaller than the radius of an octahedral hole in a theoretical close-packed fluorine lattice ( $0.54 \text{ \AA}$ ) and so would not displace the fluorine atoms from their ideal positions. This eliminates the possibility of  $\text{MnF}_5$  adopting a close-packed structure and so the  $\text{VF}_5$  arrangement of atoms is then the most likely. The  $\text{VF}_5$  structure is discussed in more detail in Chapter 7. The  $\text{Pd}^{5+}$  ionic radius is not known, but it seems reasonable to expect  $\text{PdF}_5$ , if indeed it exists, to adopt the  $\text{RuF}_5$ -type structure.

### Other Metal Pentafluoride Structures

Other metal pentafluoride structures have been reported and are mentioned here for comparison. Perhaps the most interesting with respect to the  $\text{RuF}_5$ ,  $\text{NbF}_5$  and  $\text{VF}_5$  structures is that of frozen  $\text{SbF}_5$  [50]. This is reported as being tetrameric but with two bent *cis*-fluorine bridges and two near linear *cis*-fluorine bridges (see Figure 1.4). The structure is explained in terms of there being alternating layers of

Table 1.3: Selected Bond Lengths and Angles for the Transition Metal Pentafluorides

MF <sub>5</sub>	MF <sub>t</sub> (Å)	MF <sub>b</sub> (Å)	M-F <sub>b</sub> -M (°)	W (Å <sup>3</sup> ) <sup>†</sup>	Data	C	R	Ref.
VF <sub>5</sub>	1.69	1.97	149.71	84.9	3-D	no	0.096	3
CrF <sub>5</sub>	-	-	-	82.9	-	-	-	47
TcF <sub>5</sub>	-	-	-	94.9	-	-	-	55
ReF <sub>5</sub>	-	-	-	94.1	-	-	-	3
NbF <sub>5</sub>	1.827	2.066(2)	173.0(1)	88.3	3-D	yes		4
TaF <sub>5</sub>	1.853(20)	2.070(9)	171.9(6)	88.6	3-D	yes	0.070	*
MoF <sub>5</sub>	1.784(4)	2.063(2)	174.7(2)	87.8	3-D	yes		4
WF <sub>5</sub>	-	-	-	89.3	-	-	-	57
RuF <sub>5</sub>	1.808(1)	2.001(1)	138.8(6)	83.3	3-D	yes	0.024	5
OsF <sub>5</sub>	1.84	2.03	137.5(20)	85.0	2-D	no	0.106	58
RhF <sub>5</sub>	1.808	1.999	135(1)	84.4	3-D	yes	0.029	59
IrF <sub>5</sub>	-	-	-	81.9	-	-	-	60, 61
PtF <sub>5</sub>	1.818(17)	2.012(16)	132.9	82.4	3-D	yes	0.060	62
AuF <sub>5</sub>	-	-	-	89 <sup>48</sup>	-	-	-	-

All values for bond lengths and angles are the average values calculated from the crystal data.

\* See Chapter 2.

† These values are quoted from [60], unless otherwise stated.

W = Formula unit volume.

C = Use of computing in the data analysis.

R = Final error factor on crystal analysis.

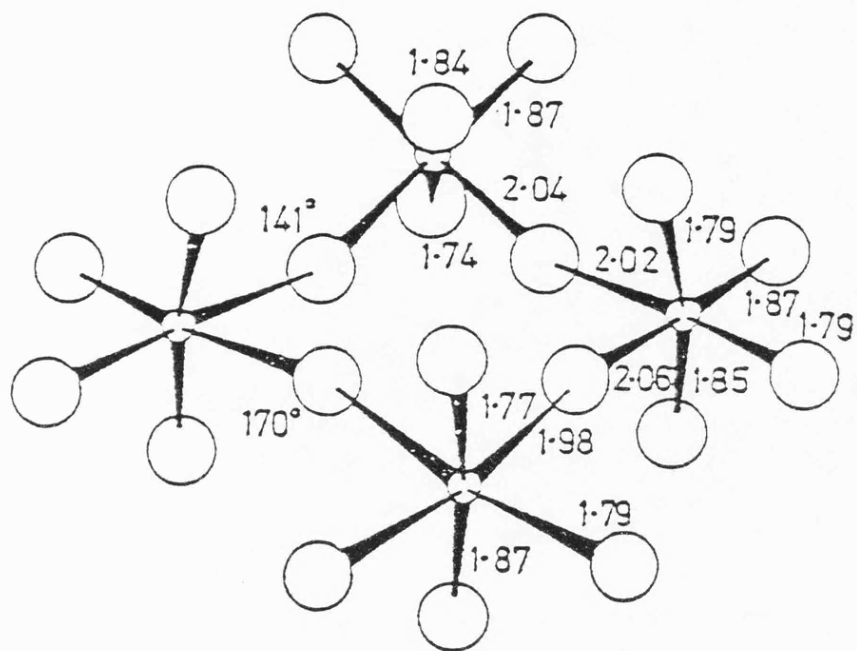


Figure 1.4: The  $\text{SbF}_5$  Tetramer

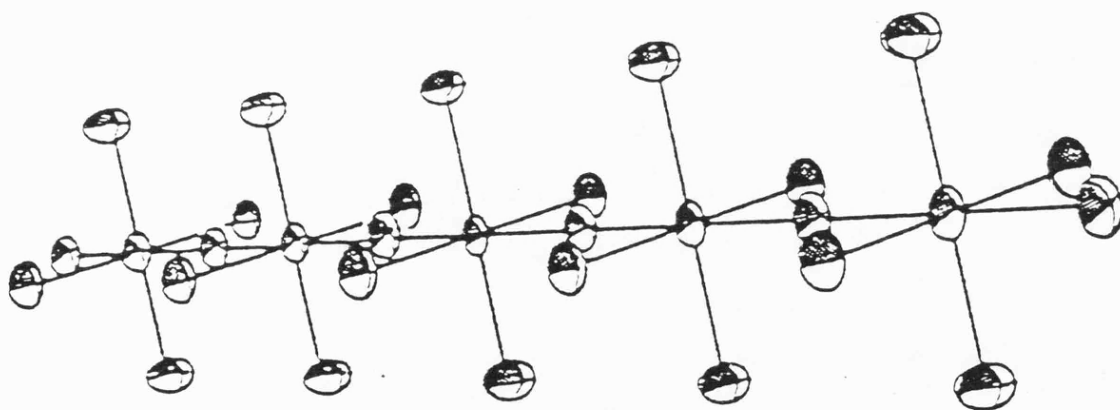


Figure 1.5: The  $\alpha\text{-UF}_5$  Structure

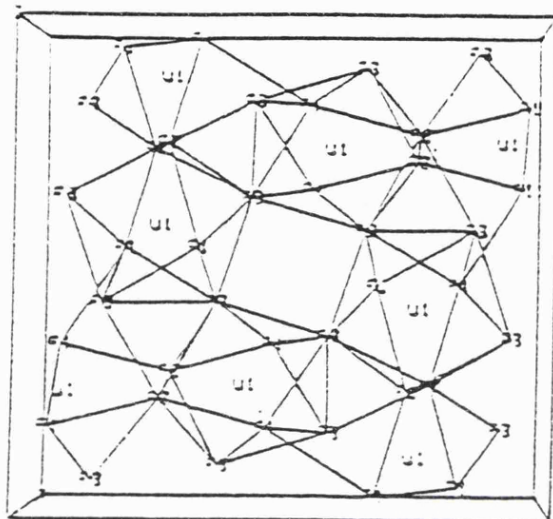


Figure 1.6: The  $\beta$ - $\text{UF}_5$  Structure

hexagonally and cubic-close packed fluorine atoms with metal atoms in one fifth of the octahedral holes. However, there is no attempt to explain why this occurs.

The other metal pentafluoride structures known are those of  $\text{UF}_5$  and  $\text{BiF}_5$ .  $\text{BiF}_5$  is a *trans*-fluorine bridged endless chain [54] (see Figure 1.5) and  $\text{UF}_5$  has been reported as having two structural forms,  $\alpha$ - $\text{UF}_5$  [51, 52] and  $\beta$ - $\text{UF}_5$  [51, 53], shown in Figures 1.5 and 1.6 respectively. In  $\alpha$ - $\text{UF}_5$  the U atoms are six-coordinate, linked in an endless chain arrangement by *trans*-fluorine bridges. The structure of  $\beta$ - $\text{UF}_5$  was originally believed to be based on seven-coordinate U atoms, but it has since been found that they are eight coordinate with a coordination geometry between that of a dodecahedron and a square antiprism [53].

## 1.2.2 Review of the Explanations for the Different Pentafluoride Structures

The solid-state structures of the transition-metal pentafluorides have been outlined above along with descriptions of the precise nature of their crystal lattices. From the review it can be said that the TaF<sub>5</sub> structure is based on cubic close-packed fluorine atoms [1], the RuF<sub>5</sub> structure on hexagonal close-packed fluorine atoms [2] with VF<sub>5</sub> somewhere in between these two [3].

The purpose of this section is to report explanations which have been postulated about why the different transition-metal pentafluorides adopt the structures they do. There are three explanations, the first of which is based on  $\pi$ -bonding, the second on ionicity and the third on packing. Each is reported separately along with the supporting evidence. However, some of the explanations are based on a combination of the three mentioned above and so are listed in the section considered to be most appropriate.

### $\pi$ -Bonding

The first attempt to rationalise the structures was by Canterford, Colton and O'Donnell [23], and their explanation was reported again without alteration in a later review [76]. The explanation was based on the assumption that the TaF<sub>5</sub> essentially linear M-F<sub>b</sub>-M bond angle reported by Edwards [1] implies  $\pi$ -bonding from the filled p-orbitals of the fluorine bridging atom into the vacant d-orbitals of the Ta atoms. The TaF<sub>5</sub> structure, at this time, was known to be adopted by NbF<sub>5</sub> (d<sup>0</sup>) [1] and MoF<sub>5</sub> (d<sup>1</sup>) [56] and has since been found to occur in WF<sub>5</sub> (d<sup>1</sup>) [57]. In each of these cases  $\pi$ -bonding from the fluorine atom on to the metal would be favourable. The M-F<sub>b</sub>-M bond angle of 138° in the RuF<sub>5</sub> type structure [2], it was argued, ruled out the possibility of  $\pi$ -bonding from the fluorine-bridging atom in this case because of the deviation from linearity. This was rationalised in terms of the fact that Ru<sup>5+</sup> (d<sup>3</sup>) has partially filled t<sub>2g</sub> orbitals which preclude weak p $\pi$  donation from fluorine.

When these papers were written the precise nature of the  $\text{VF}_5$  structure was not known. It was believed to be based on a slightly distorted form of the  $\text{MoOF}_4$  structure [74] incorporating bent *cis*-fluorine bridged endless chain of metal atoms in octahedral coordination. It was stated that the two compounds thought to adopt structure,  $\text{VF}_5$  and  $\text{CrF}_5$  [74, 47], were less amenable to  $\pi$ -bonding with fluorine and so did not adopt the  $\text{TaF}_5$  type structure despite having  $d^n$  configurations of  $d^0$  and  $d^1$  respectively. However, it has since been shown that  $\text{ReF}_5$  [3] and  $\text{TcF}_5$  [55] have the  $\text{VF}_5$  structure [3]. Tc and Re (second- and third-row transition metals respectively) should be no less amenable to  $\pi$ -bonding from fluorine than the elements on either side of them in the Periodic Table and their  $d^n$  configurations are both  $d^2$ . From this it can be seen that, although  $\pi$ -bonding offers some explanation of the influences on these structures, it does not provide a *complete* explanation.

Another approach by Glemser in 1984 [77] grouped the structures of the solid fluorides  $\text{MF}_2$ ,  $\text{MF}_3$ ,  $\text{MF}_4$  and  $\text{MF}_5$  into three types. These three types corresponded essentially to the three  $\text{MF}_5$  structural types (one based on c.c.p. fluorine atoms, one based on h.c.p. fluorine atoms and an intermediate structure). Glemser repeated the explanation for the occurrence of the three structural types given by Canterford, Colton and O'Donnell [23], but also quoted a review of the  $\text{MF}_3$  structures [78], which stated that the anion packing was of interest since it determined the  $\text{M-F}_b\text{-M}$  angle. Glemser, however, believed that it was the  $\text{M-F}_b\text{-M}$  angle which determined the anion packing. This point is crucial to a full explanation of these structures as it may explain why hexagonal- and cubic-close packed lattices occur for different pentafluorides.

### **Explanations Based on Ionicity.**

A more recent review of the transition-metal pentafluorides by Peacock [80] states that, although the fluorine-to-metal  $\pi$ -bonding is an attractive idea, the bond distances involved seemed rather long for  $\pi$ -bonding to be effective. Also the heats of polymerisation for  $\text{TaF}_5$ ,  $\text{NbF}_5$  and  $\text{MoF}_5$  would have been expected to have been

greater than those for  $\text{RuF}_5$  if  $\pi$ -bonding were present and there was no evidence to support this. Peacock suggested a polar model as more likely to account for the differences in the bond angles between the structures, assuming that the fluorine-bridging atom is a negatively charged entity between two positively charged metal atom centres. The increasing ionisation potentials of the metal atoms (for instance, across the series  $\text{Ta} \rightarrow \text{Au}$ ) increasingly polarise the bridging fluorine atom. In turn, the covalent directive forces at the fluorine bridging atom become more significant and the bond angle decreases. This explanation is supported by the fact that increasing ionisation potentials from left to right across the Periodic Table and the decreasing ionisation potentials down the Periodic Table result in  $\text{VF}_5$  [3] and  $\text{CrF}_5$  [47,74] having more bent bridging bond angles than  $\text{NbF}_5$  [1] and  $\text{MoF}_5$  [56] respectively. However, this hypothesis suggests a gradual decrease in the bridging bond angle in line with a gradual increase in the ionisation potential of the metal, while the X-ray structural data indicates three distinct structural types. This implies that the explanation is not entirely correct.

In an X-ray structure of  $\text{RhF}_5$  published in 1973 [59] the authors stressed the importance of fluorine-bridging and described the structure in terms similar to those of Peacock. Thus the changes in the  $\text{M-F}_\text{b}\text{-M}$  bond angles (decreasing from Nb to Rh and Ta to Pt) was suggested to be based on the increasing nuclear charge across these two series, which was not being screened by the formally non-bonding d-electrons occupying the  $\text{dt}_{2g}$  levels. This was believed to give rise to increased covalency across the range and therefore a more bent fluorine bridge angle. For  $\text{VF}_5$  and the related structures, it was suggested that the covalency restraint prevented adoption of the close-packed  $\text{NbF}_5$  type structure, but was not sufficient to make adoption of the  $\text{RuF}_5$  structure energetically feasible.

This rationalisation led to the suggestion that the fluorine-bridging in the  $\text{NbF}_5$  structure came closest to being ionic and so the  $\text{NbF}_5$  tetramer came closest to representing an ionic assembly  $(\text{NbF}_4^+\text{F}^-)_4$ . As such, it was believed that  $\text{NbF}_5$  would be most likely to form  $\text{MF}_4^+$  salts with strong Lewis acids. In support of

this the author quotes a paper where Edwards found evidence for  $\text{NbF}_4^+\text{SbF}_6^-$  [84].

There was also a discussion about the precise nature of the  $\text{M-F}_t$  and  $\text{M-F}_b$  bonds, which recalled the empirical relationship between bond length and order given by Pauling [81]. This predicted a bond order of unity to be  $0.18 \text{ \AA}$  shorter than one of order 0.5. If the shorter  $\text{M-F}_t$  bonds of  $\text{RhF}_5$  (average  $1.808 \text{ \AA}$ ) are represented as electron pair bonds, then the bridging  $\text{M-F}_b$  bonds (average  $1.999 \text{ \AA}$ ) would be single-electron bonds. This fluorine-bridging situation was compared to the bridging in  $\text{Al}_2\text{Cl}_6$  [82] and  $\text{Al}_2(\text{CH}_3)_6$  [83] where the geometries are similar. The bridging bonds in  $\text{Al}_2(\text{CH}_3)_6$  had been previously described in terms of two-electron three-centre bonds and it was suggested that this might be appropriate for  $\text{Al}_2\text{Cl}_6$  and  $\text{Rh-F}_b\text{-Rh}$  in  $\text{RhF}_5$ . However, not all of the transition-metal pentafluorides possess  $\text{M-F}_b\text{-M}$  bond angles similar to those in  $\text{RhF}_5$  and so the nature of the fluorine-bridge bonds was not thought to be the same for all the transition-metal pentafluorides.

The structural characteristics of the inorganic fluorides were reviewed by Klimov in 1990 [79], who also repeated the statement that it was a possibility that the different structural types are adopted on the basis of weak  $\pi$ -bonding. As to the nature of the fluorine-bridging bond, Klimov suggested that this might be ionic (where the bridging fluorine atoms carry a negative charge and react with the positively charged metal atoms) or covalent for elements having high ionisation potentials. This argument is based on those of Peacock [80] and Bartlett [59], detailed above.

The most recent discussion of the metal pentafluoride structures was by Bartlett and co-workers [5] and describes the differences between the  $\text{M-F}_{ax}$  and  $\text{M-F}_{eq}$  bond lengths in  $\text{RuF}_5$  and  $\text{RhF}_5$  in terms of  $\pi$ -bonding energy levels and ionicity arguments detailed above. In  $\text{RuF}_5$  the  $\text{M-F}_{ax}$  bond lengths are slightly shorter than the  $\text{M-F}_{eq}$  bond lengths and in  $\text{RhF}_5$  the opposite is the case. These are subtle differences ( $\approx 0.03 \text{ \AA}$ ) and are explained by the  $d^n$ -configurations of  $\text{RuF}_5$  and  $\text{RhF}_5$ . Thus, for these metal pentafluorides, the lowest lying orbital is of  $\pi^*$  character, de-

rived from the  $dt_{2g}$  and  $Fp\pi$  orbitals, and must be located in the plane of the M atom and its two fluorine bridging ligands. For  $Rh^{5+}$  this orbital is full and so the  $F_{eq}$  atoms experience more  $\pi^*$  character than those of the  $F_{ax}$ , where the appropriate  $\pi^*$  orbitals contain only one electron each. The situation in  $RuF_5$  is described differently. The  $t_{2g}$  levels are all singly occupied so that all of the terminal fluorine atoms experience the same  $\pi^*$  character. The fluorine-bridging atoms being considered to be more electron rich than the terminal fluorine atoms, could be viewed as being on the ionisation pathway to  $F^-$ . The  $F_{eq}$  electron clouds in the equatorial plane of the M and  $F_b$  atoms therefore contract towards the Ru atom making the  $Ru-F_{eq}$  shorter than for  $Ru-F_{ax}$ , a simple electrostatic effect.

This argument of d-orbital occupancy is extended for the other  $MF_5$  structures and used to explain the bonding in  $MoF_5$  and  $NbF_5$ . For  $MoF_5$  the one d electron is thought to be in the  $F_b-M-F_b$  plane and this is said to explain the slightly shorter  $Mo-F_{ax}$  distance compared with the  $Mo-F_{eq}$  distance. This is a similar situation to that in  $RhF_5$ .

For  $NbF_5$  on the other hand (with no d-electrons), the same *trans*-electrostatic effect as in  $RuF_5$  is believed to explain the slightly longer  $F_{ax}$  bonds compared with the  $M-F_{eq}$  bonds. This is supported by the recent structure analysis of  $NbF_5$  [4] where the  $M-F_{eq}$  bond distances are 1.807–1.812 Å and the  $M-F_{ax}$  bond distances are 1.839–1.846 Å.

In addition, a comparison of the  $M-F_b-M$  bond angle for  $RuF_5$  (136.8° and 140.8°) and  $RhF_5$  (134.3° and 135.71°) [59] and the bridging bond angle for perfect h.c.p. of 132° implies that the  $RhF_5$  structure is closer to ideal h.c.p. than  $RuF_5$ . This was explained by the fact that the Rh case is more covalent due to a lower nuclear charge for Ru. The paper also compares the  $RuF_5$  and  $RhF_5$  structures with those of their respective lower fluorides, which implies a packing argument and so this is dealt with in the next section.

## Packing

A review of the solid state structures of the binary fluorides by Edwards in 1983 [60] dealt mainly with the structures themselves and their descriptions in terms of the packing of the atoms. This approach seemed to offer a more comprehensive explanation for the structural types but the author stopped short of detailing a full hypothesis.

Taking the  $\text{TaF}_5$  structure to be based on cubic-close packed fluorine atoms with metal atoms in one fifth of the octahedral holes the expected  $\text{M-F}_b\text{-M}$  bond angle would be  $180^\circ$  for perfect packing. The corresponding value in the  $\text{RuF}_5$  structure based on hexagonal close-packed fluorine atoms with metal atoms in one fifth of the octahedral holes would be  $132^\circ$ . For  $\text{TaF}_5$  the value was thought to be  $182.5^\circ$  [1], while for  $\text{RuF}_5$  the average value was  $132^\circ$  [2]. The values from the more recent structure determinations are  $171.6^\circ$  (see Chapter 2) and  $\approx 138^\circ$  [5], respectively, which imply that there is not perfect packing in either of these materials.

Edwards suggested that the  $\text{VF}_5$  structure, with a  $\text{M-F}_b\text{-M}$  bond angle between that of  $\text{TaF}_5$  or  $\text{RuF}_5$ , could not be described either as cubic close-packed or hexagonal close-packed. Having calculated the structural unit volumes of all the pentafluorides (see Table 1.2), the values for  $\text{ReF}_5$  and  $\text{TcF}_5$  (which have similar structures to  $\text{VF}_5$ ) were seen to be anomalously high which suggested inefficient packing of the structural units. This supported the suggestion of inefficient packing in the  $\text{VF}_5$  structure.

Although this review gives no further information on why the three different structural types exist it does imply that a likely explanation for the structures is concerned with the packing of the atoms.

A report by Muller [85] described the transition-metal pentafluorides and related structures in terms of the arrangement of rings or chains of vertex sharing octahedra. The designation of the structures was based on the fact that a group of three con-

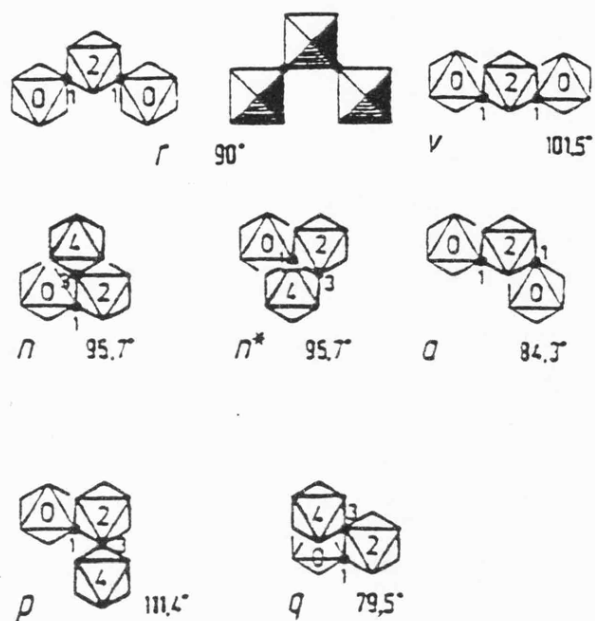
nected octahedra could adopt several structural types having characteristic M-M-M bond angles which were denoted by symbols (see Figure 1.7a). Thus for  $\text{RuF}_5$ , each metal site in the tetrameric ring could be described by a group of three connected octahedra,



The  $\text{anan}^*$  ring for  $\text{RuF}_5$  is shown in Figure 1.7c along with the  $\text{vqrq}^*$  ring for  $\text{SbF}_5$  (Figure 1.7b) and the  $z^4$  ring for  $\text{NbF}_5$  (Figure 1.7d). Close-packing was found to be possible for the rings  $\text{anan}^*$  and  $z_4$  (\* denotes enantiomeric). In addition to this,  $\text{SbF}_5$  was denoted as  $\text{vqrq}^*$  which allowed close-packing in two ways, and the  $\text{VF}_5$  structure was considered to have distorted  $v^2$  chains that did not allow close-packing. These observations are in line with the crystal structures of these compounds in that all four of the Nb atoms in  $\text{NbF}_5$  are equivalent [1,4] while the description of  $\text{RuF}_5$  as ring  $\text{anan}^*$  supports the presence of two metal sites at opposite corners of the tetramer. This corresponds to the two  $\text{M-F}_b\text{-M}$  bond angles in the recent  $\text{RuF}_5$  structure analysis of  $136^\circ$  and  $140^\circ$  [5]. Although his work does not attempt to explain why these structures are adopted, it does imply an explanation based on packing.

The paper by Bartlett and co-workers [5] is included in the previous section dealing with ionicity but is also discussed here because although it does not attempt to discuss why the different structures are adopted by the pentafluorides, it compares them to those of the lower fluorides which implies an explanation based on packing. For instance, the  $\text{M-F}_b$  bond distance in  $\text{RuF}_3$  and  $\text{RuF}_5$  (1.982 and 2.000 Å respectively) allowed that the  $\text{M-F}_b$  bond distances could be the same and independent of the oxidation state. The slight differences in the bond lengths were attributed to cis-fluorine repulsions which were thought to be greater than those in  $\text{RuF}_5$  because of the four non-bridging fluorine atoms at around 1.8 Å compared with the six bridging fluorine atoms in  $\text{RuF}_3$  [36].

This paper appears to suggest that although the oxidation state,  $d^n$  configuration and Lewis acidity do not appear to affect the overall structure of the metal

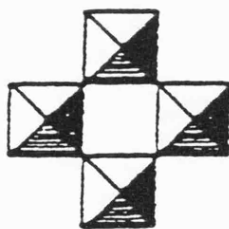


(a) Examples of Corner-Sharing Octahedra.



(b)  $SbF_5$ .

(c)  $RuF_5$ .



(d)  $NbF_5$ .

Figure 1.7: Theoretical Cis-octahedra and their Description of the Transition-Metal Pentafluoride Structures

pentafluoride (or lower fluoride), these factors *do* appear to influence the subtle differences between these structures.

### 1.2.3 Related Oxide Fluoride Structures

Some of the transition-metal oxide fluorides have similar structures to those of the transition-metal pentafluorides. For this reason, brief summaries of the relevant structures are included in this section. Only the transition metal fluorides with the overall stoichiometry of 1:5 (M:O+F) are included as these have obvious possible structural similarities to the pentafluorides. For more complete summaries of the transition-metal oxide fluorides, readers are referred to reviews by Laycock [86] and Townson [87].

The first report of a  $\text{MOF}_4$  crystal structure was that of  $\text{CrOF}_4$  [47]. Only the cell dimensions and space group were reported (see Table 1.4) and, although a full structure determination was said to be underway, it has been only briefly mentioned in the literature since [88]. In the meantime, crystal structure determinations of  $\text{WOF}_4$ ,  $\text{MoOF}_4$ ,  $\text{TcOF}_4$  and  $\text{ReOF}_4$  have been carried out [74], and their structural parameters are shown in Table 1.4.  $\text{WOF}_4$  is reported to have the tetrameric  $\text{NbF}_5$  type structure in the solid state.  $\text{MoOF}_4$ ,  $\text{ReOF}_4$  and  $\text{TcOF}_4$  have similar unit cells to those of  $\text{TcF}_5$ ,  $\text{CrF}_5$ ,  $\text{VF}_5$  and  $\text{ReF}_5$  (see Table 1.2). The  $\text{MoOF}_4$  and  $\text{ReOF}_4$  three-dimensional X-ray data, collected photographically, suggest that fluorine-bridging is involved between the metal centres, as opposed to oxygen-bridging which was initially suggested for  $\text{WOF}_4$  [75].  $\text{WOF}_4$  has now been shown to have fluorine-bridging also [80, 89–91].

The  $\text{ReOF}_4$  and  $\text{MoOF}_4$  structures are both *cis*-fluorine bridged endless chain structures with very similar bond lengths (Figure 1.8). The main difference between them is that the M-F<sub>b</sub>-M bond angle in  $\text{ReOF}_4$  is 139° and in  $\text{MoOF}_4$  it is 151°. There is also a difference in the way that the endless chains of atoms pack together in the two structures, leading to different crystal symmetries and unit cell dimen-

Table 1.4: Crystallographic Data for Selected Transition Metal Oxide Fluorides

Compound	Space Group	Symmetry	a (Å)	b (Å)	c (Å)	$\beta$ (°)	mp (°C)	bp (°C)	Ref.
CrOF <sub>4</sub>	-	Mono	12.3	5.4	7.3	104	55	95*	39
WOF <sub>4</sub>	C2/m	Mono	9.65	14.42	5.15	95.4	104	185	75,[90]
MoOF <sub>4</sub> <sup>†</sup>	P2 <sub>1</sub> /c	Mono	5.50	16.98	7.84	91.7	97	186	74,92,[90]
ReOF <sub>4</sub>	C2/c	Mono	19.01	5.57	14.72	114.0	108	172*	74,93,[90]
TcOF <sub>4</sub> <sup>†</sup>	-	Mono	18.83	5.49	14.43	114.0	134	-	74
TcOF <sub>4</sub> <sup>‡</sup>	P6 <sub>3</sub> /m	Hex	9.00	-	7.92	-	-	-	95,96
MoOF <sub>4</sub> <sup>‡</sup>	-	Hex	8.95	-	7.91	-	-	-	95,96
OsOF <sub>4</sub>	P2 <sub>1</sub> 22 <sub>1</sub>	Orth	5.56	9.56	12.83	-	-	-	97
OsO <sub>3</sub> F <sub>2</sub>							170–2	-	[100]
$\alpha$ -form	-	Mono	12.01	4.98	5.33	98.5	-	-	98
$\beta$ -form	-	Orth	11.63	10.37	5.51	-	-	-	98
$\gamma$ -form	-	Orth	5.55	16.29	7.60	-	-	-	98
RuOF <sub>4</sub>							115	184*	[42]
ReO <sub>2</sub> F <sub>3</sub>							90	185.4	[101]

References in square brackets are for melting points and boiling points.

\* By extrapolation.

<sup>†</sup> Endless chain form.

<sup>‡</sup> Trimeric form.

Mono = Monoclinic.

Orth = Orthorhombic.

Hex = Hexagonal.

sions (see Table 1.4). In both there is a very short terminal bond length *trans* to one of the fluorine bridging atoms (1.66 Å for ReOF<sub>4</sub> and 1.66 Å for MoOF<sub>4</sub>), which is attributed to a metal-oxygen bond with multiple-bond character.

## WOF<sub>4</sub>

The first detailed X-ray structure determination of WOF<sub>4</sub> was published in 1968 [75]. The three-dimensional data was solved photographically with a final R-factor of 0.128. The bridging atoms were thought to be oxygen atoms, but this is now known to be incorrect and the oxygen atoms are terminal, while the bridging atoms are fluorines [78, 89–91]. Bearing this in mind, there are similarities between the WOF<sub>4</sub> structure and those of MoOF<sub>4</sub>, ReOF<sub>4</sub> and TcOF<sub>4</sub> [74]. The light atoms in all cases make up slightly distorted octahedra around the metal atoms with the metal atoms displaced 0.3 Å from the centre of the octahedra towards the terminal oxygen atom. For WOF<sub>4</sub> this gives a W-O<sub>t</sub> bond distance of 1.64(4) Å (implying a tungsten-oxygen bond with multiple bond character) and an average W-F<sub>b</sub> distance of 2.11(4) Å. This displacement of the metal atom within the octahedron of light atoms is common to the WOF<sub>4</sub>, TcOF<sub>4</sub>, ReOF<sub>4</sub> and MoOF<sub>4</sub> structures.

One difference between WOF<sub>4</sub> and the others is that the WOF<sub>4</sub> fluorine bridges are all the same length within experimental error, whereas the other oxide fluorides mentioned here have asymmetric fluorine bridges. This bridging distance for WOF<sub>4</sub> is longer than the value of 2.06 Å for NbF<sub>5</sub> [1] and the W-F<sub>b</sub>-W bond angle is 173°. The positions of the light atoms in WOF<sub>4</sub> are believed to approximate to a cubic-close packed array with an average volume per light atom of 18 Å<sup>3</sup>. NbF<sub>5</sub> is also believed to be based on a cubic close-packed array of fluorine atoms, and the recent work on the redetermination of the NbF<sub>5</sub> structure reports an identical Nb-F<sub>b</sub>-Nb bond angle of 173° [4].

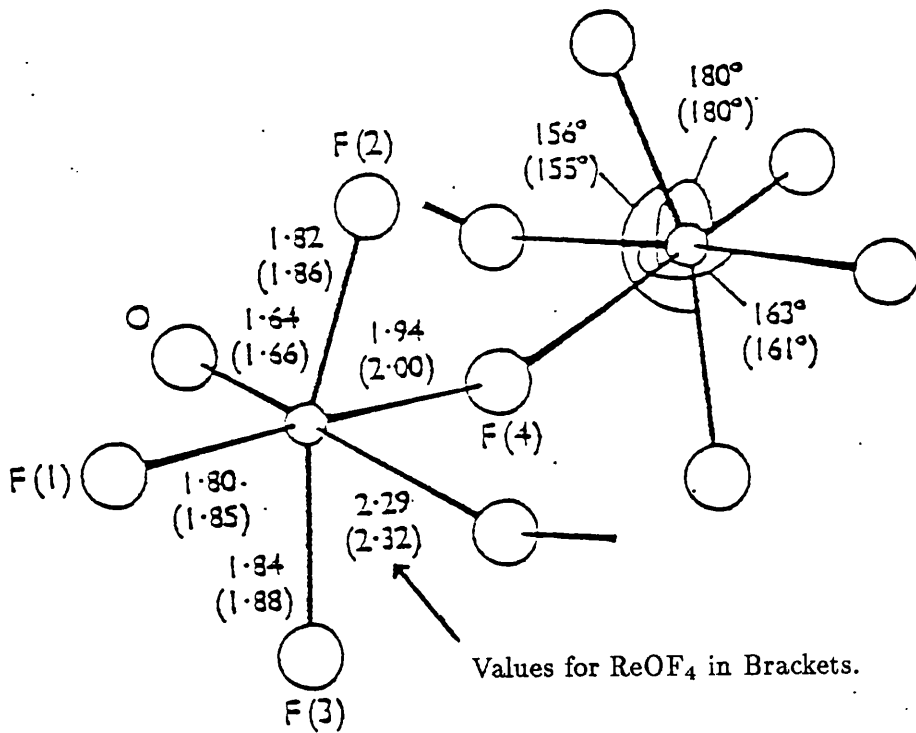


Figure 1.8: The  $\text{MoOF}_4$  and  $\text{ReOF}_4$  Structures

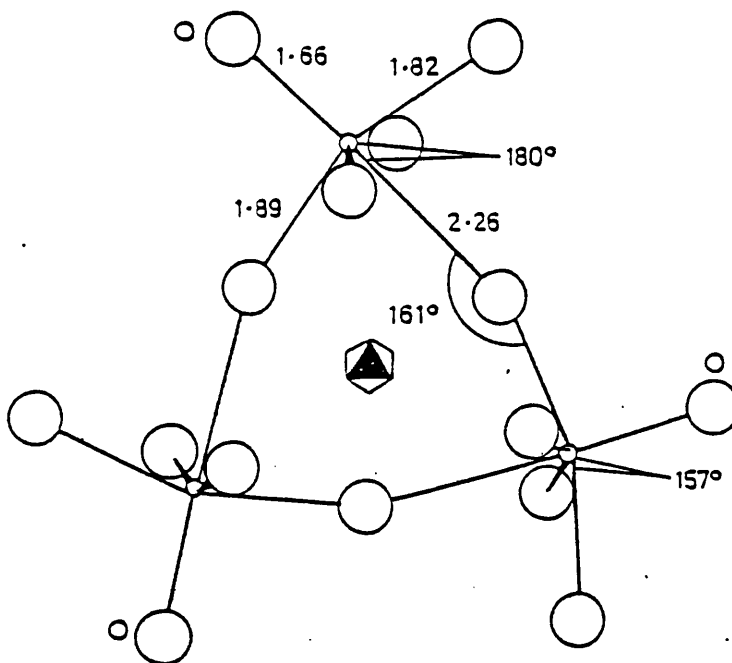


Figure 1.9: The Trimeric  $\text{TcOF}_4$  Structure

## MoOF<sub>4</sub>

A more detailed account of the MoOF<sub>4</sub> structure determination than the original report [74] was reported by Edwards [92]. The three-dimensional X-ray data was collected photographically, with a final R-factor of 0.102. The *cis*-fluorine bridged octahedra (Figure 1.8) are linked into endless chains parallel to the a-axis, similar to those in the VF<sub>5</sub>-type structure [3]. The fluorine bridge is asymmetric (in VF<sub>5</sub> it is symmetric) with Mo-F<sub>b</sub> bond lengths of 2.27(1) Å for the F-bridge bond *trans* to oxygen and 1.96(1) Å for the F-bridge bond *trans* to fluorine. As in WOF<sub>4</sub>, the light atoms make up an almost undistorted octahedron with the Mo atom displaced from the centre of the octahedron towards the terminal oxygen atom. The bond lengths within the octahedron fall into four groups: (a) 1.64 Å; the Mo-O<sub>t</sub> distance, (b) 1.82 Å the Mo-F<sub>t</sub> distance, (c) 1.94 Å; the shorter Mo-F<sub>b</sub> distance and (d) 2.27 Å the longer Mo-F<sub>b</sub> distance. The Mo-F<sub>b</sub>-Mo bond angle is 151° which is between the theoretical values of 132° and 180° for perfect h.c.p. and c.c.p. respectively. Thus this angle is not consistent with either close-packed system but is closer to the h.c.p. value.

## ReOF<sub>4</sub>

The ReOF<sub>4</sub> structure (Figure 1.8) is reported to be similar to that of MoOF<sub>4</sub> although with a different unit cell [93]. This structure is based on three-dimensional data, collected photographically, and the final R-factor is 0.112. One difference between the MoOF<sub>4</sub> and ReOF<sub>4</sub> structures is that there is an average lengthening of the rhenium-light atom distances of  $\approx 0.04$  Å over the corresponding Mo distances. The ReOF<sub>4</sub> and MoOF<sub>4</sub> structures also have different unit cells, which are believed to be due to the different packing of the endless chains. The other main discrepancy between these two structures is the M-F<sub>b</sub>-M bond angle which is 139° for ReOF<sub>4</sub> and 151° for MoOF<sub>4</sub>. This is again believed to be due to differences in packing as the value for ReOF<sub>4</sub> is close to the theoretical value of 132° for perfect h.c.p..

There is some indication in the literature that the transition-metal pentaflu-

oxides may crystallise to form more than one structure [63, 65, 94], though the structures reported in this review represent only the dominant structural types. Similar polymorphism is known also to occur in the transition-metal oxide fluorides. For instance,  $\text{TcOF}_4$  is normally blue but, during the fluorination of Tc metal, small amounts of a green volatile material are given off [95, 96]. Subsequent X-ray single crystal analysis has shown that this material is trimeric  $\text{TcOF}_4$  (see Figure 1.9). A brief report in 1968 [95], along with a more detailed one in 1970 [96], also mention a trimeric form of  $\text{MoOF}_4$ , but with no structural details. The structure shows similarities to those of the other oxide fluorides in that the trimer is made up of metal atoms joined by *cis*-fluorine bridges. The light atoms around the Tc atom make up a virtually undistorted octahedron with the Tc atom displaced 0.36 Å towards the oxygen atom. This, in turn, leads to asymmetric fluorine bridging with the  $\text{M-F}_b$  distance *trans* to the Tc-O distance of 2.26 Å, and the other  $\text{M-F}_b$  distance 1.89 Å. The Tc- $\text{F}_b$ -Tc bond angle of 161° in this structure precludes a close-packed arrangement of light atoms, and this is borne out further by the volume taken up by them which is 18.5 Å<sup>3</sup> as compared with 18.0 Å<sup>3</sup> for  $\text{WOF}_4$  and  $\text{ReOF}_4$ .

### The Osmium Oxide Fluorides

Preliminary X-ray single crystal work on  $\text{OsOF}_4$  has shown it to be orthorhombic with space group  $\text{P2}_122_1$  [97]. This space group, though unusual, was chosen to illustrate a relationship between the cell constants for  $\text{OsOF}_4$  and those of  $\text{OsF}_5$  [58]. The volume available for the light atoms is 17 Å<sup>3</sup> (the same as in  $\text{OsF}_5$ ). The assumption is that  $\text{OsOF}_4$  consists of tetramers, but with a structure and packing different to that of  $\text{OsF}_5$ .

$\text{OsO}_3\text{F}_2$  crystallises in three structural forms [98] which are shown in Table 1.4. Full single crystal structure determinations have not been carried out, but the unit cell dimensions and some limited X-ray diffraction work show that  $\beta$ - $\text{OsO}_3\text{F}_2$  is based on the  $\text{RuF}_5$  structure and that  $\gamma$ - $\text{OsO}_3\text{F}_2$  is based on the  $\text{MoOF}_4$  structure.

Crystals of  $\text{OsO}_2\text{F}_3$  [99] are believed to be isomorphous with the monoclinic  $\alpha$ -phase of  $\text{OsO}_3\text{F}_2$ , but no single crystal data has been recorded. Raman data supported the presence of a fluorine-bridged polymeric arrangement.

#### 1.2.4 Transition Metal Oxide Fluoride Structure Generalisations

It is evident that, in general, the transition-metal oxide fluoride structures are similar to those of the transition-metal pentafluorides. For example, like the pentafluorides all of the oxide fluoride structures mentioned are based on fluorine bridging between metal centres (not oxygen bridging), with an octahedral arrangement of light atoms around each metal atom. A second similarity lies in the fact that the  $\text{WOF}_4$  [75] structure is very like that of  $\text{NbF}_5$  [1] and, as such, is believed to be based on a cubic close-packed lattice of light atoms. Also, the  $\text{MoOF}_4$  structure is almost isomorphous with  $\text{VF}_5$ . It is interesting to note, however, that the  $\text{MoF}_5$  tetrameric structure [56] is based on close-packing and is isomorphous with  $\text{NbF}_5$  [1]. Effectively, the exchange of one oxygen atom for one fluorine atom ( $\text{MoF}_5$  to  $\text{MoOF}_4$ ) results in a complete change of structure.

The osmium oxide fluorides,  $\text{OsOF}_4$  [97] and  $\beta$ - $\text{OsO}_3\text{F}_2$  [98], appear to be based on the  $\text{OsF}_5$  structure so that all of the transition-metal pentafluoride structures are represented amongst the oxide fluorides.

The  $\text{ReOF}_4$  structure, although very similar to those of  $\text{MoOF}_4$  and  $\text{VF}_5$ , has a  $\text{Re-F}_b\text{-Re}$  bond angle of  $139^\circ$  and, as such, appears to be based on h.c.p. light atoms. The main difference between this and the  $\text{MoOF}_4$  structure seems to lie in the way the endless chains pack together. Why these chains pack differently is not yet known. However, some of the factors which influence this packing may be the different ionic sizes, ionisation potentials and the d-configuration of the metals. These are some of the factors which appear to effect the transition-metal pentafluoride structures either directly or indirectly.

A striking difference between the transition-metal oxide fluorides and transition-metal pentafluorides is that, apart from  $\text{WOF}_4$ , there are asymmetric fluorine bridges in the oxide fluorides. This appears to be a consequence of the very short metal-oxygen bond ( $\approx 1.66 \text{ \AA}$ ) which implies a multiple bond. The fluorine bridge *trans* to this terminal oxygen atom is then significantly longer ( $\approx 2.3 \text{ \AA}$ ) compared to the fluorine bridge *trans* to a terminal fluorine atom ( $\approx 1.92 \text{ \AA}$ ). Thus, as the electron density cloud of the oxygen atom is pulled closer to the metal atom, the  $\text{M-F}_b$  bridge becomes longer and the fluorine atom becomes closer to  $\text{F}^-$ . This is a simple electrostatic effect, similar to that used by Peacock [80] and Bartlett [59] to describe the bonding in the transition-metal pentafluorides. Asymmetry in the fluorine bridges has yet to be found in the transition-metal pentafluorides. However, some of the mixed-metal pentafluorides reported in this thesis appear to exhibit asymmetric-fluorine bridging (see Chapter 6). This is almost certainly due to differences in the Lewis acidity of the different metal atoms in the different metal sites.

## Chapter 2

# The Preparation and Characterisation of $\text{NbF}_5:\text{TaF}_5$ [3:1], [1:1] and [1:3].

### 2.1 Introduction

Niobium and tantalum pentafluorides were first synthesised in 1911 [102] and have been widely studied. The reader is referred to a review [80] which details much of this work. The first structural information on the compounds was based on X-ray single crystal structure determinations carried out by Edwards [1] who found that  $\text{NbF}_5$  and  $\text{TaF}_5$  were isostructural *cis*-fluorine bridged tetramers. This has been confirmed by recent three-dimensional X-ray work [4], and work described in this thesis. When the original  $\text{NbF}_5$  and  $\text{TaF}_5$  X-ray structure determinations were published [1], it was suggested that they were both based on a cubic close-packed lattice of fluorine atoms with metal atoms in one fifth of the octahedral holes.

$\text{NbF}_5$  and  $\text{TaF}_5$  are sufficiently similar that they form a solid solution on mixing with almost ideal behaviour [103]. In addition to this, they both form similar compounds with  $\text{SbF}_5$  [84]. The structure of  $\text{MF}_5.\text{SbF}_5$  [1:1] (where  $\text{M} = \text{Nb}$  or  $\text{Ta}$ ) consists of a *cis*-fluorine bridged endless chain similar to that of  $\text{VF}_5$  [3], with  $\text{M}$  and

Sb atoms alternating in the chain.  $\text{NbF}_5$  and  $\text{TaF}_5$  also form similar adducts with  $\text{UF}_5$  [104],  $\text{XeF}_2$  [105],  $\text{BrF}_3$  [105] and  $\text{ClF}_3$  [105]. The chemistry of  $\text{NbF}_5$  and  $\text{TaF}_5$  with organic molecules also shows similarities. Both form adducts with  $\text{Me}_2\text{O}$  [106],  $\text{Me}_2\text{S}$  [106], pyridine [107],  $\text{EtCN}$  [107] and  $\text{Me}_2\text{SO}$  [108]. Detailed structures of these adducts have not been determined but, from the spectroscopic data collected, there seems to be little difference between the  $\text{NbF}_5$ - and  $\text{TaF}_5$ -containing adducts.

$\text{TaF}_5$  is believed to be a stronger Lewis acid than  $\text{NbF}_5$  [109]. However, this has yet to be confirmed by X-ray single crystal data. This is partly due to the similarities in the chemical reactivities of the two pentafluorides, but also because of the difficulties in preparing suitable single crystals of their reaction products.

The similarities in the chemical reactivities are hardly surprising when it is considered that Nb and Ta are in the same group of the Periodic Table, that their outer electron configurations are the same and that  $\text{Nb}^{5+}$  and  $\text{Ta}^{5+}$  both have an ionic radius of  $0.64 \text{ \AA}$  [67]. The only difference between the two elements is that Ta has an extra shell of electrons than Nb. However, by investigating the compound formation between  $\text{NbF}_5$  and  $\text{TaF}_5$ , a direct comparison of their Lewis acidities may be possible. The combination of the two similarly-bridged tetrameric structures may also yield information about why these structures are formed, and why the  $\text{RuF}_5$ -type structure [2, 5] and the  $\text{VF}_5$  type structure [3] are present for other transition-metal pentafluorides. In addition to this,  $\text{NbF}_5:\text{TaF}_5$  [x:y] may be useful as precursors for CVD (see Chapter 8).

In order to compare the structures of  $\text{NbF}_5:\text{TaF}_5$  [x:y] compounds with those of  $\text{NbF}_5$  and  $\text{TaF}_5$ , the  $\text{TaF}_5$  structure has been redetermined. This new X-ray single crystal structure determination is three-dimensional, which gives significantly more accurate atomic positions when compared to the previously determined two-dimensional structure [1], which was carried out twenty five years ago. Edwards, who solved the original structure, has also redetermined  $\text{NbF}_5$  as a three-dimensional structure [4].

A preliminary theoretical investigation has also been carried out into the possibility of using the mixed-metal pentafluorides as precursors for the formation of alloys by chemical vapour deposition (see Chapter 8). A number of conflicting ideas are present in the literature as to exactly what species is dominant in the gas phase of the metal pentafluorides at  $\approx 90^\circ\text{C}$  [7–22]. The gas-phase variable temperature infrared spectra of the  $\text{NbF}_5\cdot\text{TaF}_5$  [x:y] series have therefore been recorded in order to try to establish the nature of the material in the gas phase. However, the mixed-metal pentafluoride spectra have been analysed more as a means of characterising these compounds rather than analysing the precise symmetry of the gas-phase molecules.

In order to achieve a complete characterisation of the  $\text{NbF}_5\cdot\text{TaF}_5$  [x:y] series of compounds mass spectral, XRF analysis, X-ray diffraction, Raman and infrared data have been recorded.

## 2.2 Preparation

$\text{NbF}_5\cdot\text{TaF}_5$  [3:1], [1:1] and [1:3] have been prepared as described in Chapter 9. The compounds have been stored in a dry box in stoppered, pre-seasoned 6mm FEP tubes and samples have been taken and analysed as required. The results of the analysis are reported below.

## 2.3 X-ray Fluorescence

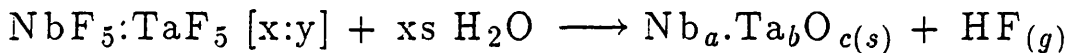
For each of the  $\text{NbF}_5\cdot\text{TaF}_5$  stoichiometries [3:1], [1:1] and [1:3], the X-ray fluorescence analysis of hydrolysed samples confirms the approximate overall metal ratio for the samples. The results are shown in Table 2.1, along with those from single crystals on which the X-ray diffraction data has been collected, where available. Hydrolysed samples have been used as there is no facility on the scanning electron microscope to handle air sensitive samples. It has been assumed that the hydrolysis

Table 2.1: X-ray Fluorescence Data for NbF<sub>5</sub>:TaF<sub>5</sub> [3:1], [1:1], [1:3] and Nb/Ta Metal Powder Samples.

Sample	Nb Expected (%)	Ta Expected (%)	Nb Found (%)	Ta Found (%)
NbF <sub>5</sub> :TaF <sub>5</sub> [3:1]	75	25	72.95	27.05
NbF <sub>5</sub> :TaF <sub>5</sub> [1:1]	50	50	52.92	47.08
NbF <sub>5</sub> :TaF <sub>5</sub> [1:1]*	50	50	58.24	41.76
NbF <sub>5</sub> :TaF <sub>5</sub> [1:3]	25	75	25.75	74.25
Nb-Ta Metal Powders				
Nb:Ta Ratio [3:1]	75	25	74.48	25.52
Nb:Ta Ratio [1:1]	50	50	51.28	48.72
Nb:Ta Ratio [1:3]	25	75	29.94	70.06

\* This was the single crystal on which the X-ray structure determination has been carried out. Unfortunately, there was some slight contamination of this sample with Fe from the SEM which may cause errors in this analysis not present the other data. Although the data are quoted to 2 decimal places, the values are  $\approx \pm 4\%$ .

occurs by the release of HF<sub>(g)</sub>, and that all the metal atoms remain in the sample. The samples are left for a period of hours before the analyses are recorded and so complete hydrolysis can be assumed to have occurred, as follows:



It should be noted that the X-ray fluorescence analysis technique analyses the surface of the material only and, consequently, errors may be caused by an uneven surface. All efforts to minimise errors have been made and, in particular, intimately mixed samples of Nb and Ta powders of known stoichiometry have also been analysed to verify the accuracy of the technique (see Table 2.1). However, the results using this technique do not distinguish whether the mixed niobium/tantalum pentafluorides are tetramers of single metal pentafluorides arranged at random throughout the crystal lattice, in approximately the correct stoichiometry, or whether there

Table 2.2: Relative Abundancies of the Dimeric Fragments Observed from the Mass Spectroscopy of NbF<sub>5</sub>:TaF<sub>5</sub> [3:1], [1:1] and [1:3].\*

Data	NbF <sub>5</sub> .TaF <sub>5</sub> [1:3]	NbF <sub>5</sub> .TaF <sub>5</sub> [1:1]	NbF <sub>5</sub> .TaF <sub>5</sub> [3:1]
Source temperature (°C)	140	100	130
(eV)	60	60	60
Nb <sub>2</sub> F <sub>9</sub> <sup>+</sup> (355 m.u.)	0	0.6	1.3
NbTaF <sub>9</sub> <sup>+</sup> (444 m.u.)	0.8	0.8	1.3
Ta <sub>2</sub> F <sub>9</sub> <sup>+</sup> (533 m.u.)	6.4	0.9	0.2

\* NbF<sub>4</sub><sup>+</sup>, TaF<sub>4</sub><sup>+</sup> and their fragmentation patterns are also present in each spectrum, which have only been recorded to 720 m.u. due to the limitations of the mass spectrometer.

are mixed-metal tetramers.

## 2.4 Mass Spectrometry

Mass spectrometry data for the NbF<sub>5</sub>:TaF<sub>5</sub> [3:1], [1:1] and [1:3] compounds are shown in Table 2.2. The results confirm the presence of mixed-metal fragments in all of the stoichiometries and rule out the possibility of single-metal tetramers randomly arranged through the lattice, assuming that no association of fragments has occurred in the mass spectrometer.

The fragments which would be expected from the mass spectrometry of the com-

pounds, and their approximate relative abundancies, are shown in Figure 2.1. The predominant species from which the fragmentation patterns should be derived is expected to be the trimeric, as the mass spectra have been recorded with a source temperature of between 100 and 140°C. This assumption is based on the fact that the dominant species in the gas phase of both NbF<sub>5</sub> and TaF<sub>5</sub> in this temperature range is believed to be the trimer (e.g. from the electron diffraction work [18, 19]). However, the species resulting from dimeric fragments or from tetramers are also shown in Figure 2.2 as, at a temperature of 140°C, there may be some dimer and tetramer present [24].

To briefly summarise the main findings of the predicted spectra, Figure 2.1 shows that for NbF<sub>5</sub>:TaF<sub>5</sub> [3:1] no Ta<sub>2</sub>F<sub>9</sub><sup>+</sup> fragment would be expected, while for NbF<sub>5</sub>:TaF<sub>5</sub> [1:3] no Nb<sub>2</sub>F<sub>9</sub><sup>+</sup> fragment would be expected. For NbF<sub>5</sub>:TaF<sub>5</sub> [1:1] all possible dimeric fragments would be expected regardless of how the two Ta atoms and the two Nb atoms are arranged in the tetramer.

#### 2.4.1 NbF<sub>5</sub>:TaF<sub>5</sub> [1:3]

For NbF<sub>5</sub>:TaF<sub>5</sub> [1:3], no Nb<sub>2</sub>F<sub>9</sub><sup>+</sup> (355 m.u.) fragment is present even though there is a NbTaF<sub>9</sub><sup>+</sup> peak at 444 m.u. (see Table 2.2). This would suggest the occurrence of only tetrameric rings containing three Ta atoms and one Nb atom. Had a random arrangement of metal atoms occurred, or if the material had consisted of a mixture of (NbF<sub>5</sub>)<sub>4</sub> and (TaF<sub>5</sub>)<sub>4</sub> rings Nb<sub>2</sub>F<sub>9</sub><sup>+</sup> peaks would have been observed.

The statistically expected ratio of NbTaF<sub>9</sub><sup>+</sup>:Ta<sub>2</sub>F<sub>9</sub><sup>+</sup> from Figure 2.1 is 1:2, whilst the actual value is approaching 1:8. This may be explained by the fact that at a source temperature of 140°C, at which this spectrum was recorded, there may be tetrameric and dimeric species as well as the trimer (see Figure 2.2). In addition, the ratio of ions in a mass spectrometer is a consequence of instrument geometry and so do not necessarily reflect the real ratio [110]. This may explain discrepancies between the expected and actual values. This applies to all the spectra reported

Figure 2.1: Expected Dimeric Fragments for the Mass Spectra of NbF<sub>5</sub>:TaF<sub>5</sub> [3:1], [1:1] and [1:3] with

Ordered Metal Sites (Based on Fragmentation from Trimeric Molecules).  = Ta

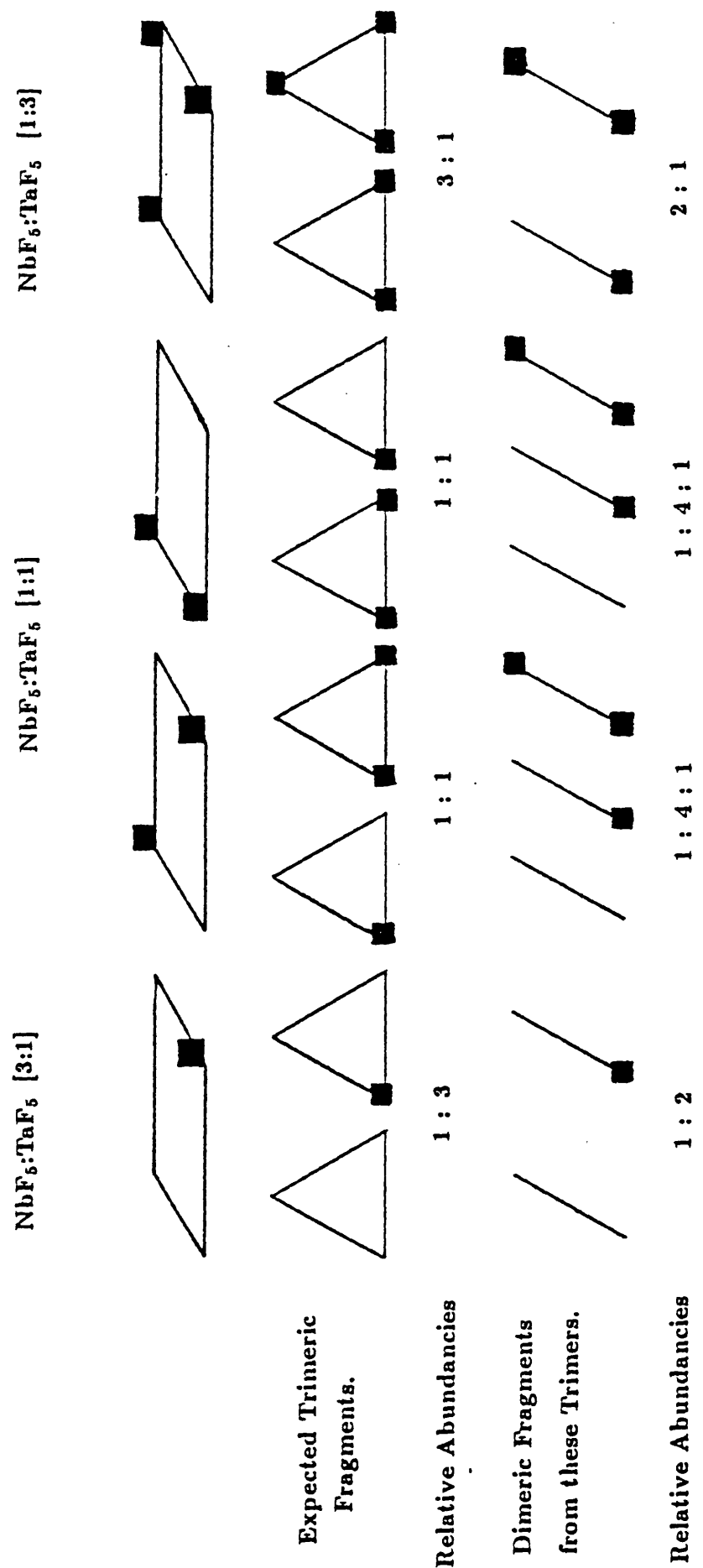
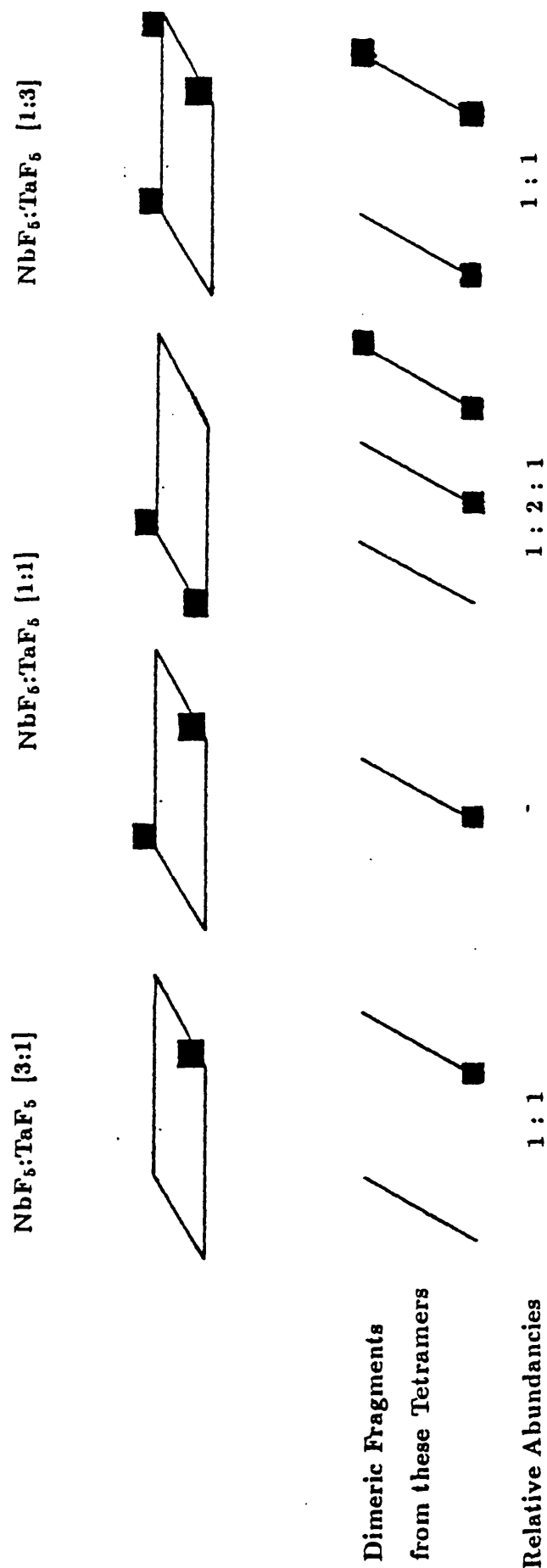


Figure 2.2: Expected Dimeric Fragments for the Mass Spectra of  $\text{NbF}_5$ : $\text{TaF}_5$  [3:1], [1:1] and [1:3] with

Ordered Metal Sites (Based on Fragmentation from Tetrameric Molecules).  $\blacksquare = \text{Ta}$



here.

#### 2.4.2 NbF<sub>5</sub>:TaF<sub>5</sub> [3:1]

In the NbF<sub>5</sub>:TaF<sub>5</sub> [3:1] mass spectrum, Nb<sub>2</sub>F<sub>9</sub><sup>+</sup> and NbTaF<sub>9</sub><sup>+</sup> fragments are both observed along with a trace peak at 533 m.u., which can be attributed to Ta<sub>2</sub>F<sub>9</sub><sup>+</sup> (Figure 2.2). This may be due to (a) a trace amount of (TaF<sub>5</sub>)<sub>4</sub> in the sample, (b) a small amount of disorder in the metal sites within the sample or (c) association of the fragments in the mass spectrometer.

For completely ordered metal sites in this compound the expected ratio of Nb<sub>2</sub>F<sub>9</sub><sup>+</sup>:NbTaF<sub>9</sub><sup>+</sup> would be 2:1. The actual value is closer to 1:1 but the expected value is based on the dominant species at the source temperature of 130°C being trimeric. If the dominant species was dimeric the expected ratio would be 1:1 and so it could be that there are fragments in this mass spectrum, derived from the dimer.

#### 2.4.3 NbF<sub>5</sub>:TaF<sub>5</sub> [1:1]

The mass spectrum of NbF<sub>5</sub>:TaF<sub>5</sub> [1:1] (see Table 2.2), shows the presence of Nb<sub>2</sub>F<sub>9</sub><sup>+</sup>, NbTaF<sub>9</sub><sup>+</sup> and Ta<sub>2</sub>F<sub>9</sub><sup>+</sup> fragments. This suggests the presence of both Nb and Ta in the same tetramer, but is not conclusive as to whether they occur in a 2:2 ratio or not. The reason for this is that the metal sites could be ordered in one of two ways (see Figure 2.3), although the arrangement of metal atoms shown in Figure 2.3a would appear to be more favourable because the tetramer has a higher degree of symmetry than that in Figure 2.3b. Both arrangements would give rise to Nb<sub>2</sub>F<sub>9</sub><sup>+</sup>, NbTaF<sub>9</sub><sup>+</sup> and Ta<sub>2</sub>F<sub>9</sub><sup>+</sup> fragments in a ratio of 1:4:1 (see Table 2.2). The actual ratio of the fragments is 1:1:1. The difference may be due to slight disorder in the crystal. The presence of a large proportion of the dimeric species in the gas phase can be ruled out as the spectrum was recorded at 100°C.

It should be remembered that the calculation of the exact ratios of the expected

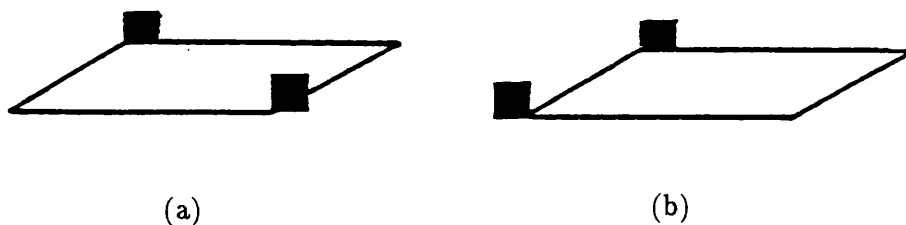


Figure 2.3: Possible Ordered Metal Sites for  $\text{MF}_5:\text{M}'\text{F}_5$  [1:1].

fragments is based on an assumption that all fragments have an equal probability of being formed. This may not be the case because of energetic considerations, in which case the  $\text{M}_2\text{F}_9^+$  fragment (where  $\text{M} = \text{Nb}$  or  $\text{Ta}$ ) might be expected to be favoured over the  $\text{NbTaF}_9^+$  fragment.

## 2.5 Infrared Spectroscopy of Solid Samples

The infrared spectra of  $(\text{NbF}_5)_4$ ,  $(\text{TaF}_5)_4$  and  $\text{NbF}_5:\text{TaF}_5$  [3:1], [1:1] and [1:3] are reported in Table 2.3. The spectra are from solid, powdered samples held between KBr discs, as the compounds react with nujol. Attempts to dilute the metal and mixed-metal pentafluorides with dry LiF, NaF or KF proved unsuccessful, because of reaction between these materials and the pentafluorides, even in the solid state. The spectra, therefore, are not well resolved and so peak assignments are difficult, especially for weakly absorbing bands. The spectra are all of similar shape and consist of a series of strongly absorbing, but poorly resolved peaks from  $\approx 750$ – $650$   $\text{cm}^{-1}$ , and a weak fluorine-bridging mode at  $\approx 510$   $\text{cm}^{-1}$ .

No attempt has been made to analyse the spectra in terms of the symmetries of the molecules involved because of the poor resolution of the bands. They are, therefore, reported purely for characterisation purposes. However, it is evident from the presence of a fluorine-bridging mode ( $\approx 500$   $\text{cm}^{-1}$ ) in each of the spectra that

Table 2.3: Infrared Frequencies of Solid, Powdered Samples of  $\text{NbF}_5$ ,  $\text{TaF}_5$ ,  $\text{NbF}_5:\text{TaF}_5$  [3:1], [1:1] and [1:3].

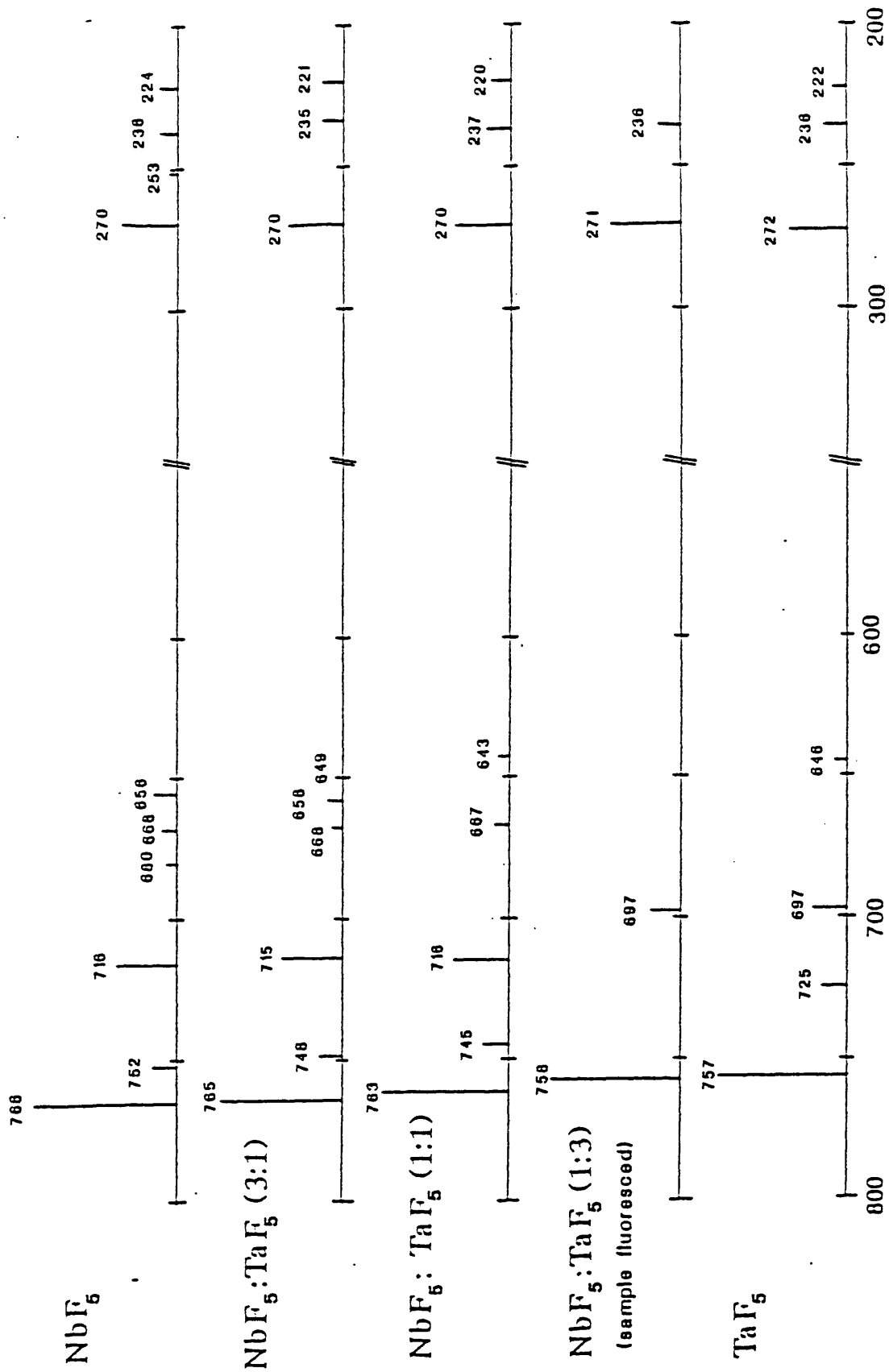
$\text{NbF}_5$	$\text{NbF}_5:\text{TaF}_5$ [3:1]	$\text{NbF}_5:\text{TaF}_5$ [1:1]	$\text{NbF}_5:\text{TaF}_5$ [1:3]	$\text{TaF}_5$
748 m	750 m	749 m	752 m	753 m
723 w	714 w	724 w	723 w	723 w
708 m		707 w		
693 vw			692 vw	
677 s	680 s	676 s	672 s	667 vw,br
661 s	664 m	655 vw		
	645 w	642 m	643 m	
				601 vw
				579 s
498 s	505 s	503 s	508 s	512 m,br

the materials are polymeric. Also, because the spectra do not appear to be made up of superimposed  $\text{NbF}_5$  and  $\text{TaF}_5$  spectra, it seems likely that the  $\text{NbF}_5:\text{TaF}_5$  [x:y] compounds are not made up of discrete single metal tetramers. This supports evidence from the mass spectra.

## 2.6 Raman Spectroscopy

The Raman spectra of  $\text{NbF}_5:\text{TaF}_5$  [3:1], [1:1] and [1:3] have been recorded and are reported in Figure 2.4, along with those of  $\text{NbF}_5$  and  $\text{TaF}_5$  for comparison. The spectra are shown between  $1200\text{ cm}^{-1}$  and  $200\text{ cm}^{-1}$  and no peaks were found outside of this region, in the range  $200\text{--}4000\text{ cm}^{-1}$ . Calibration of the spectrometer has been achieved using the well-documented, strong peak at  $766\text{ cm}^{-1}$  in  $(\text{NbF}_5)_4$  [111].

Figure 2.4: Raman Spectra of  $\text{NbF}_5$ ,  $\text{TaF}_5$ ,  $\text{NbF}_5:\text{TaF}_5$  [3:1], [1:1] and [1:3].



### 2.6.1 The NbF<sub>5</sub> and TaF<sub>5</sub> Spectra

The Raman spectra of NbF<sub>5</sub> and TaF<sub>5</sub> have been studied previously by Beattie and coworkers and a full interpretation of the NbF<sub>5</sub> spectrum has been reported [111]. The analysis is on the basis of vibration of the whole tetrameric molecule rather than that of the individual MF<sub>5</sub> units within each tetramer (ie. on the basis of the symmetry of the crystal structure [1, 4]). The analysis is also assumed to be correct for the TaF<sub>5</sub> Raman spectrum because of the similarity between the NbF<sub>5</sub> and TaF<sub>5</sub> structures [1] and the shapes of the two Raman spectra. However, differences in the intensities between calculated and experimental spectra are explained by the fact that the theoretical spectra have been calculated qualitatively assuming that (a) the polarisability change is mainly along the bond and (b) the coupling between the four corners of the tetramer across the fluorine bridge bonds is small. Some errors may have been incurred by these assumptions. It is worth noting that this analysis of the NbF<sub>5</sub> Raman spectrum was based on the original structure determination [1]. This has since been repeated [4]. This structure determination may increase the accuracy of the calculated Raman spectra, as the calculation of the spectrum is particularly sensitive to the bond angles of the molecule and the bridging bond angle is now known not to be linear.

### 2.6.2 The NbF<sub>5</sub>:TaF<sub>5</sub> [3:1], [1:1] and [1:3] Spectra

As a result of similarities of these Raman spectra and those of (NbF<sub>5</sub>)<sub>4</sub> and (TaF<sub>5</sub>)<sub>4</sub>, and their structures, it has been assumed that the analysis of the NbF<sub>5</sub> Raman spectrum [111] will also hold for the NbF<sub>5</sub>:TaF<sub>5</sub> [x:y] spectra.

The analysis of (NbF<sub>5</sub>)<sub>4</sub> by Beattie et al is supported by the Raman spectra of the NbF<sub>5</sub>.TaF<sub>5</sub> [x:y] compounds. Indeed, since the spectra consist of peaks at intermediate values between those of the (NbF<sub>5</sub>)<sub>4</sub> and (TaF<sub>5</sub>)<sub>4</sub> spectra, this suggests the presence of both metals within each tetramer.

The fact that the spectra of these mixed-metal pentafluorides are so closely re-

lated to  $(\text{TaF}_5)_4$  and  $(\text{NbF}_5)_4$  implies that a similar bonding situation occurs in all of the structures. This is perhaps not surprising bearing in mind that  $\text{Nb}^{5+}$  and  $\text{Ta}^{5+}$  are both  $d^0$  and have the same ionic radius ( $0.64 \text{ \AA}$  [67]).

## 2.7 Gas-Phase Infrared Spectroscopy

For analytical purposes the variable-temperature, gas-phase infrared spectra of the metal and mixed-metal pentafluorides have been investigated. It was hoped that this work would lead to the possibility of identifying gas-phase species, which may be important when considering these compounds as precursors for CVD of the metals (see Chapter 8). The spectra have been recorded at approximately  $15^\circ\text{C}$  intervals, between room temperature and  $\approx 90^\circ\text{C}$ . At  $\approx 50^\circ\text{C}$ , peaks are observed, the intensities of which increase with temperature. Between  $50$  and  $90^\circ\text{C}$  there are no changes in the relative intensities or any new peaks observed and so it seems that the spectra are associated with a single, or a single group of, species.

The spectra have been recorded between  $4000$  and  $400 \text{ cm}^{-1}$  but are only shown between  $1100$  and  $400 \text{ cm}^{-1}$ . Only bands associated with water and carbon dioxide are seen outside this region.

### 2.7.1 $\text{NbF}_5$

The gas-phase infrared spectrum of  $\text{NbF}_5$  obtained in the present study is shown in Table 2.4 and Figure 2.5. There are already reports in the literature of the gas-phase infrared spectrum of  $\text{NbF}_5$  and also interpretations of the spectrum [7, 10, 12]. The literature spectra are identical within experimental error with that shown in Figure 2.5.

The earliest analysis of the  $\text{NbF}_5$  spectrum was by Blanchard [7]. This assignment was made on the basis of a  $D_{3h}$ , trigonal bi-pyramidal monomer. More recent

Table 2.4: Gas-Phase Infrared Frequencies ( $\text{cm}^{-1}$ ) for  $\text{NbF}_5$ ,  $\text{TaF}_5$  and  $\text{NbF}_5:\text{TaF}_5$  [3:1], [1:1] and [1:3] at  $\approx 90^\circ\text{C}$

$\text{NbF}_5$	$\text{NbF}_5:\text{TaF}_5$ [3:1]	$\text{NbF}_5:\text{TaF}_5$ [1:1]	$\text{NbF}_5:\text{TaF}_5$ [1:3]	$\text{TaF}_5$
747.5 vs	747.3 s	747.2 vw	741.3 vw,sh	750.6 w*
732.4 vs	742.5 w	741.9 w	733.5 s	738.8 w*
687.9 m	732.7 s	733.9 s	713.8 m	714.2 m
	705.2 vw	711.5 vw	705.0 vw,sh	702.7 ms
	691.1 vw	704.5 vw	702.3 m	686.7 m
	686.8 m	691.4 vw	691.2 vw,sh	
		685.2 s	685.5 ms	
516.7 w	517.6 w	517.5	517.6	519.9 w

\* Assigned to non-gas phase species.

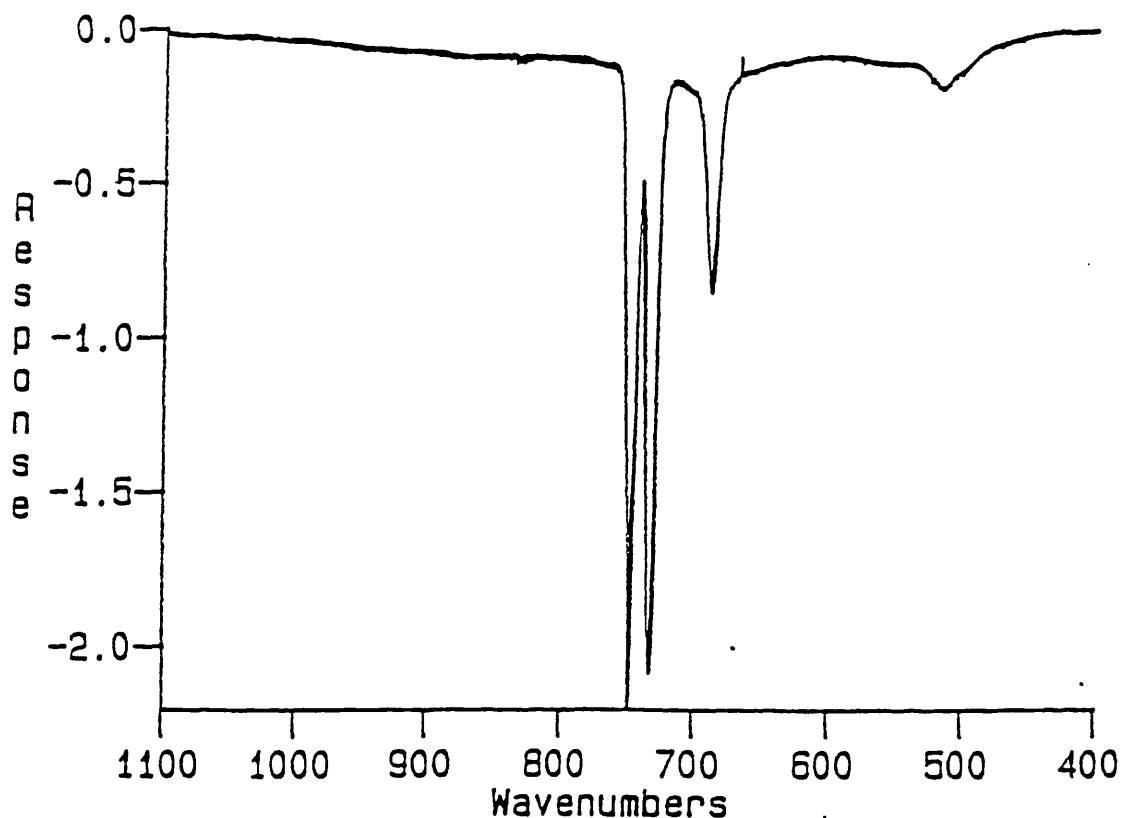


Figure 2.5:  $\text{NbF}_5$  Gas-Phase Infrared Spectrum at  $90^\circ\text{C}$ .

studies by gas-phase electric deflection mass spectrometry [14, 15], vapour density [12] and molecular weight determination [12] of gaseous  $\text{NbF}_5$  all show the presence of polymeric species at  $\approx 90^\circ\text{C}$ . In addition, the gas-phase Raman spectroscopy [11, 12] discounts the occurrence of large amounts of monomer at this temperature. An electron diffraction study [18] has shown that the predominant species is the trimer,  $\text{Nb}_3\text{F}_{15}$ , at this temperature. Thus the results from the other techniques show that the assignment by Blanchard [7] is incorrect. A more recent analysis [12] assigns the band at  $\approx 517\text{ cm}^{-1}$  as a fluorine-bridging mode, which is reasonable when compared with the corresponding band at  $514\text{ cm}^{-1}$  in the solid (see Table 2.3), the three bands at 748, 732 and  $688\text{ cm}^{-1}$  are assigned to a  $\text{C}_{2v}$ ,  $\text{MF}_4$  residue which is fluorine-bridged to form a polymer. However, this allows for the presence of different sized polymeric units at  $90^\circ\text{C}$ , when the trimer is believed to dominate. A further analysis [10], assigns the  $\text{NbF}_5$  spectrum on the basis of a  $\text{D}_{3h}$  trimeric molecule (see Figure 2.6). This is supported by the electron diffraction work [18], and has therefore been assumed to be correct for interpretive work in the present study and has been used in the analysis of the  $\text{NbF}_5:\text{TaF}_5$  [x:y] spectra. It should be noted here though that electron diffraction data can often be interpreted in a number of ways and so does not offer conclusive proof.

### 2.7.2 $\text{TaF}_5$

The gas-phase spectrum of  $\text{TaF}_5$  is shown in Figure 2.7 (and the frequencies are listed in Table 2.4) along with the spectrum recorded at room temperature, after the gas cell had cooled down. The spectrum has been reported previously [10,11], and appears different to that of  $\text{NbF}_5$  (Figure 2.5). However, gas-phase electric deflection mass spectrometry [14, 15] and electron diffraction [19] all suggest that  $\text{TaF}_5$ , like  $\text{NbF}_5$ , is trimeric at  $\approx 90^\circ\text{C}$ . The  $\text{NbF}_5$  spectrum consists of three bands between 748 and  $688\text{ cm}^{-1}$  and a fluorine-bridging mode at  $517\text{ cm}^{-1}$ , while the  $\text{TaF}_5$  spectrum shows six bands in the region  $\approx 750\text{--}650\text{ cm}^{-1}$  and a fluorine-bridging mode at  $520\text{ cm}^{-1}$ . However, when the  $\text{TaF}_5$  spectrum is recorded after cooling of the gas cell to room temperature the bands at 750, 739 and  $650\text{ cm}^{-1}$  remain (it

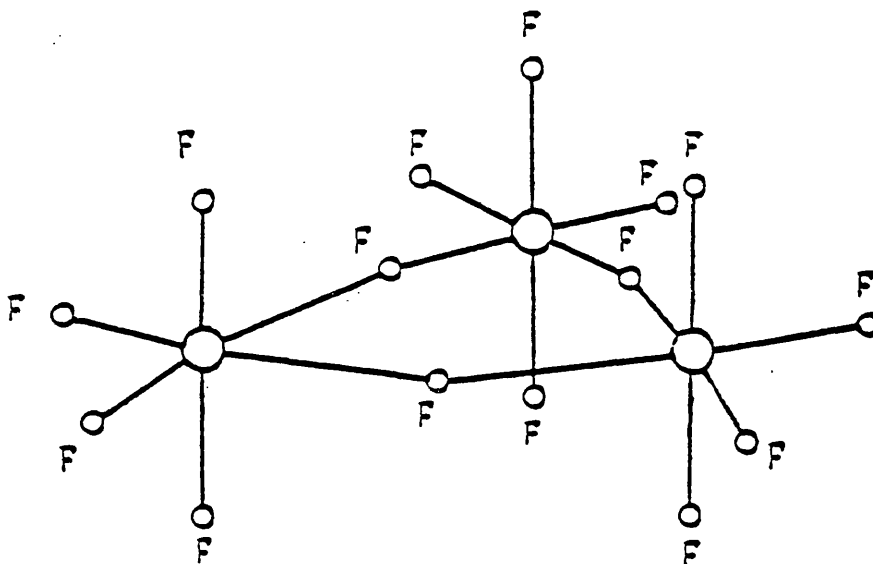


Figure 2.6: The Trimeric ( $D_{3h}$ )  $M_3F_{15}$  Molecule.

should be noted that this experiment requires extensive passivation of the gas cell to prevent decomposition). This implies that these bands arise from solid  $TaF_5$ , which has condensed on the AgCl windows of the gas cell and this is given greater credence by the fact that the shapes of the bands have similarities to those observed in the infrared of powdered  $TaF_5$  (see Table 2.3). If these bands are ignored, the gas-phase infrared spectrum is of a similar shape to that of  $NbF_5$ , with three bands at  $714\text{--}687\text{ cm}^{-1}$  and a fluorine-bridging mode at  $520\text{ cm}^{-1}$ . The assignment of the  $TaF_5$  gas-phase infrared spectrum is, therefore, assumed to be the similar to that for  $NbF_5$ .

### 2.7.3 $NbF_5:TaF_5$ [x:y]

Tentative assignments are suggested on the assumption that the main species at the temperature of the experiment are trimeric and that, within the solid state, the materials contain tetrameric rings containing Nb and Ta atoms in the ratios suggested

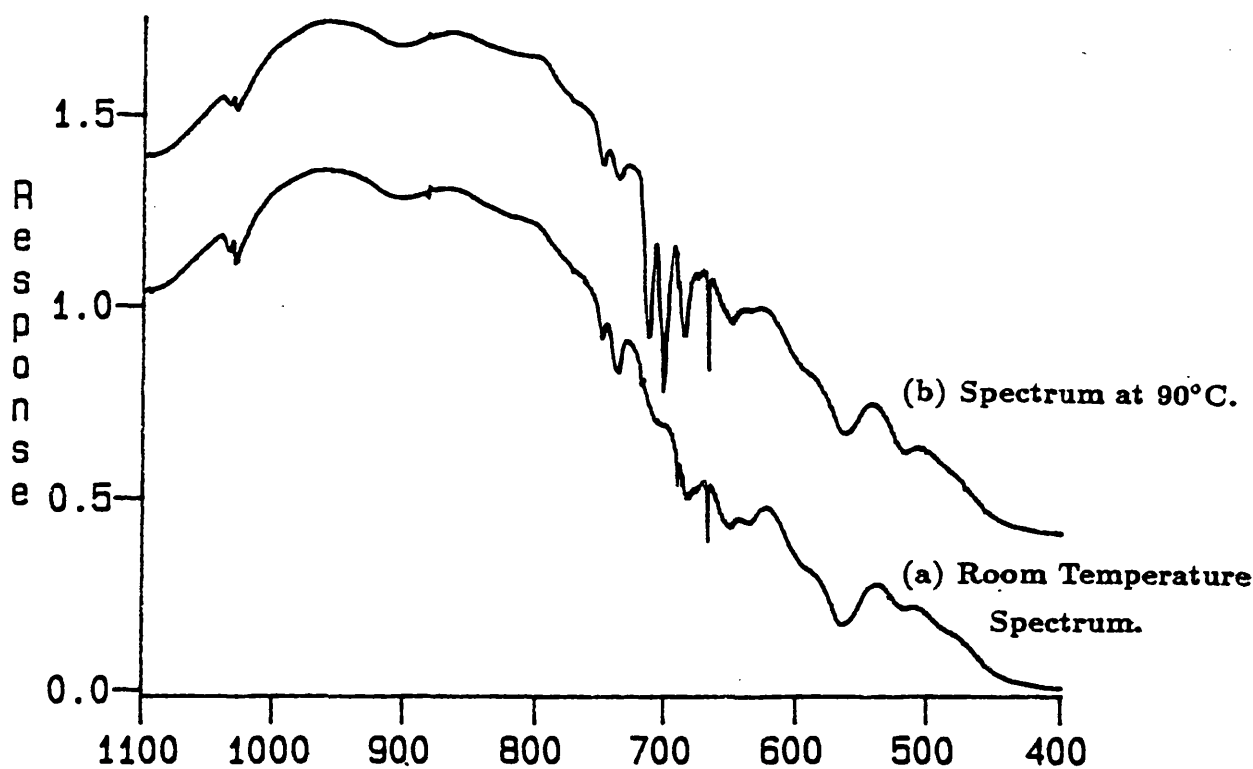


Figure 2.7: The  $\text{TaF}_5$  Gas-Phase Infrared Spectrum at  $90^\circ\text{C}$ , and at Room Temperature.

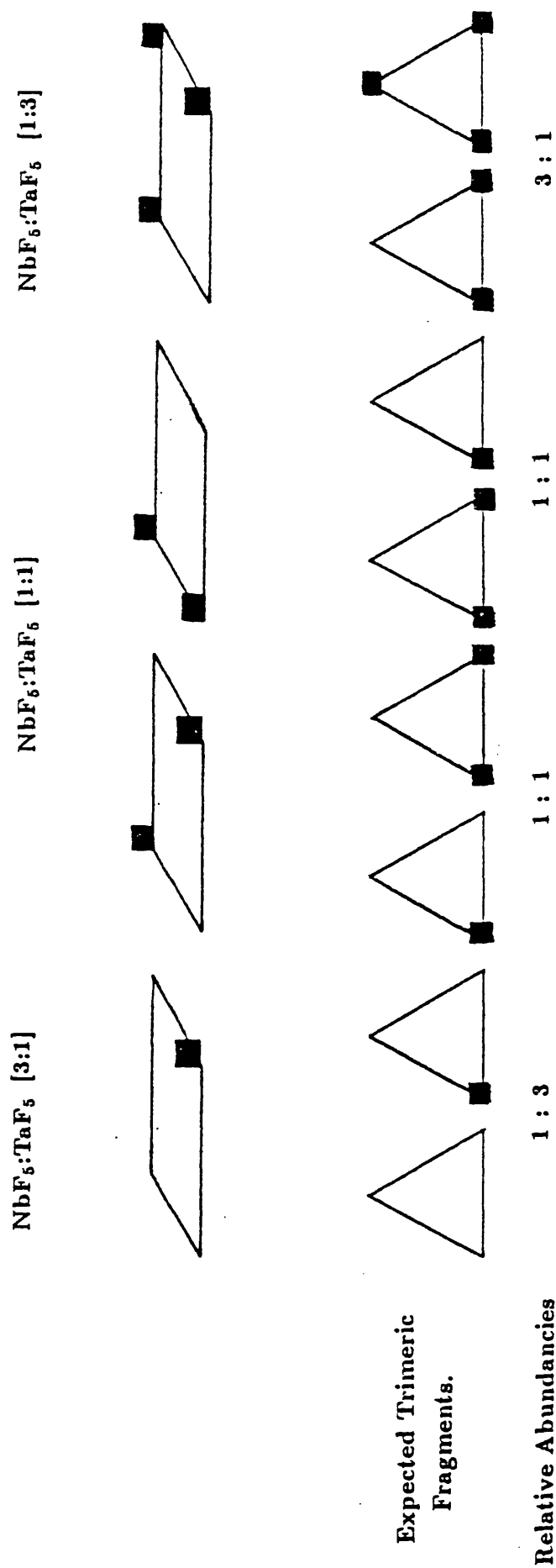
by the stoichiometries. The trimeric molecules which would be predicted to occur in the gas phase on the basis of these assumptions are shown in Figure 2.8.

#### $\text{NbF}_5:\text{TaF}_5$ [3:1]

The  $\text{NbF}_5:\text{TaF}_5$  [3:1] spectrum at  $89^\circ\text{C}$  is reported in Table 2.4 and shown in Figure 2.9. Both  $\text{Nb}_3\text{F}_{15}$  and  $\text{Nb}_2\text{TaF}_{15}$  should be present and, when the bands for the  $\text{NbF}_5$  trimer are subtracted, the three peaks remaining in the  $750\text{--}680\text{ cm}^{-1}$  region (at  $742$ ,  $705$  and  $691\text{ cm}^{-1}$ ) can be tentatively assigned to the  $\text{Nb}_2\text{TaF}_{15}$  trimer. The fluorine-bridging mode, for this molecule, is thought to be underneath the peak at  $517\text{ cm}^{-1}$ . This mode is expected to be very weak and broad in comparison to the stretching modes in these compounds, and it would also be expected to be in a very similar region to the equivalent band in  $\text{Nb}_3\text{F}_{15}$ .

Figure 2.8: The Expected Trimeric Molecules for  $\text{NbF}_5:\text{TaF}_5$  [3:1], [1:1] and [1:3]

(Based on Ordered Metal Sites).  $\blacksquare = \text{Ta}$



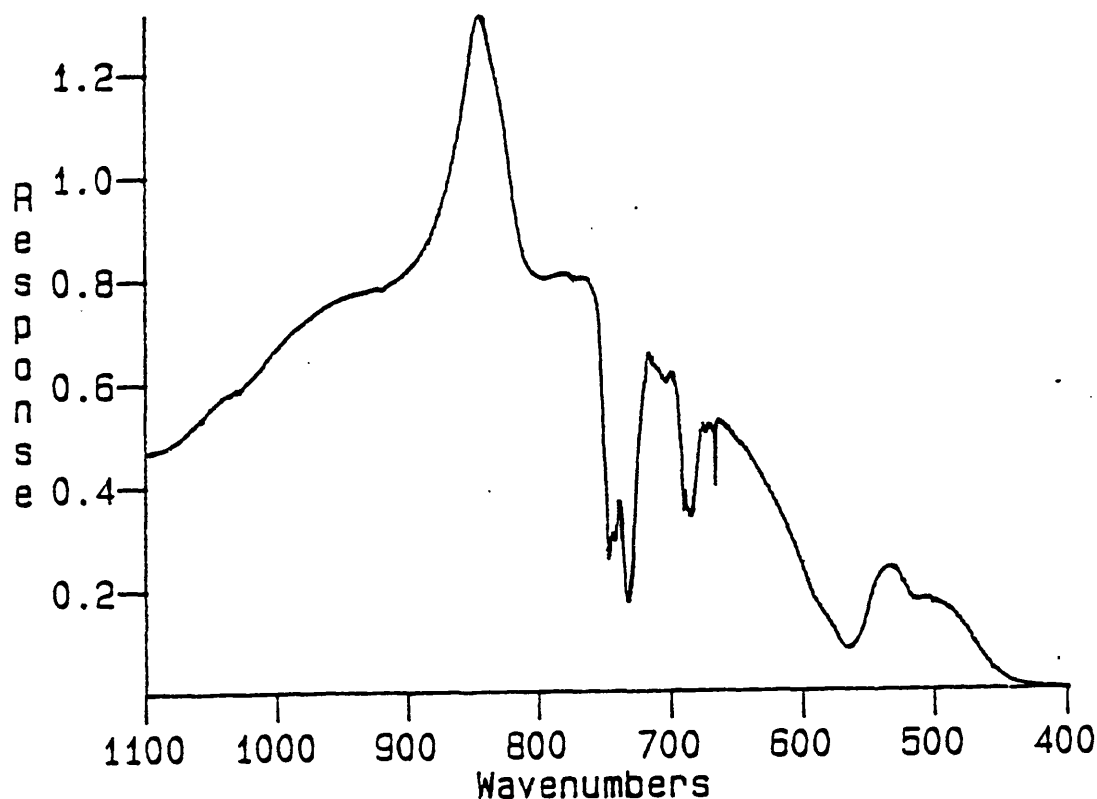


Figure 2.9: The  $\text{NbF}_5:\text{TaF}_5$  [3:1] Gas-Phase Spectrum at  $90^\circ\text{C}$ .

#### $\text{NbF}_5:\text{TaF}_5$ [1:1]

The  $\text{NbF}_5:\text{TaF}_5$  [1:1] spectrum, at  $90^\circ\text{C}$  (Table 2.4 and Figure 2.10), is more complicated than that of the analogous [3:1] and [1:3] spectra. The appearance of a shoulder at  $747\text{ cm}^{-1}$  suggests a trace amount of  $\text{Nb}_3\text{F}_{15}$ . The other bands for  $\text{Nb}_3\text{F}_{15}$  would be expected at  $732.5$  and  $688\text{ cm}^{-1}$ , but should be less intense than the  $747\text{ cm}^{-1}$  peak and so are probably beneath the large  $734$  and  $688\text{ cm}^{-1}$  peaks, respectively. The  $\text{Nb}_3\text{F}_{15}$  trimer can therefore be considered to be present only in a tiny amount, which may be due to a small amount of disorder in the solid or to some interaction between trimers as the compound is heated.

The  $\text{Nb}_2\text{TaF}_{15}$  species is predicted to occur in the gas phase of this material (see Figure 2.8) and may be observed with bands at  $742$ ,  $705$  and  $692\text{ cm}^{-1}$ , which correspond to similar bands tentatively assigned to the same species in the  $\text{NbF}_5:\text{TaF}_5$  [1:1] spectrum. In addition to the  $\text{Nb}_2\text{TaF}_{15}$  bands, there are peaks at  $734$ ,  $711.5$

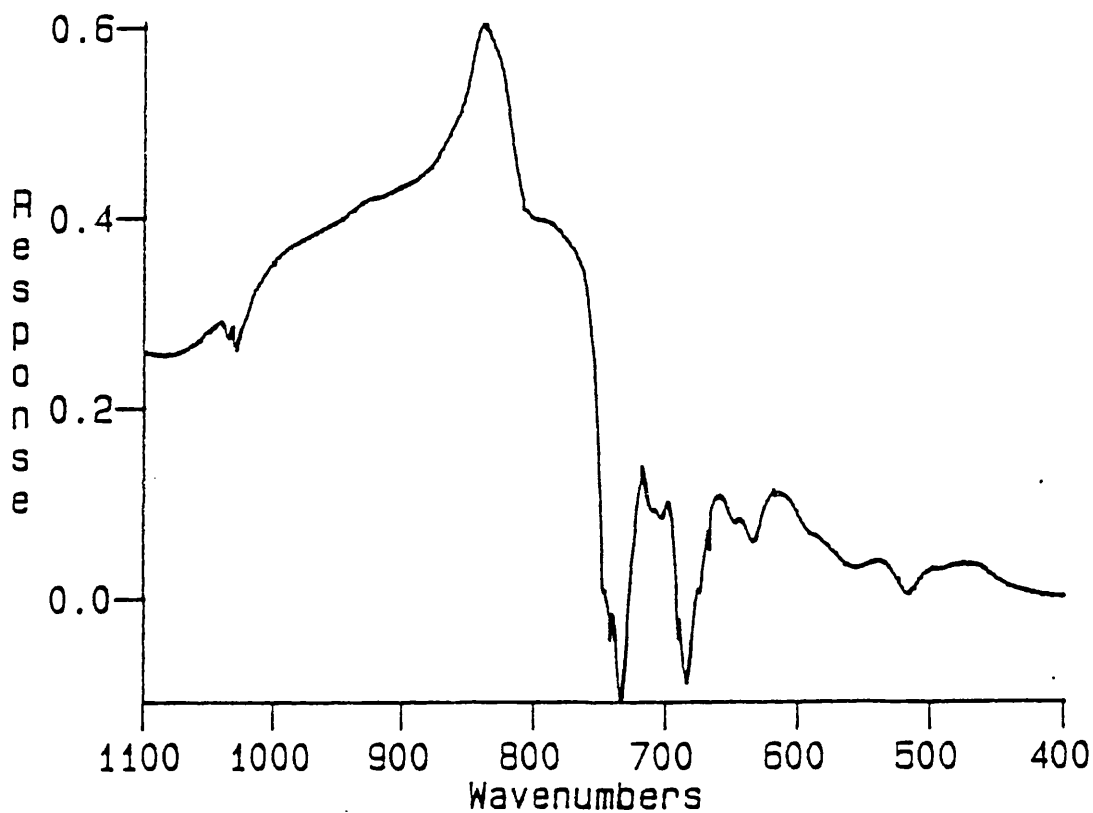


Figure 2.10: The  $\text{NbF}_5:\text{TaF}_5$  [1:1] Gas-Phase Infrared Spectrum at  $90^\circ\text{C}$ .

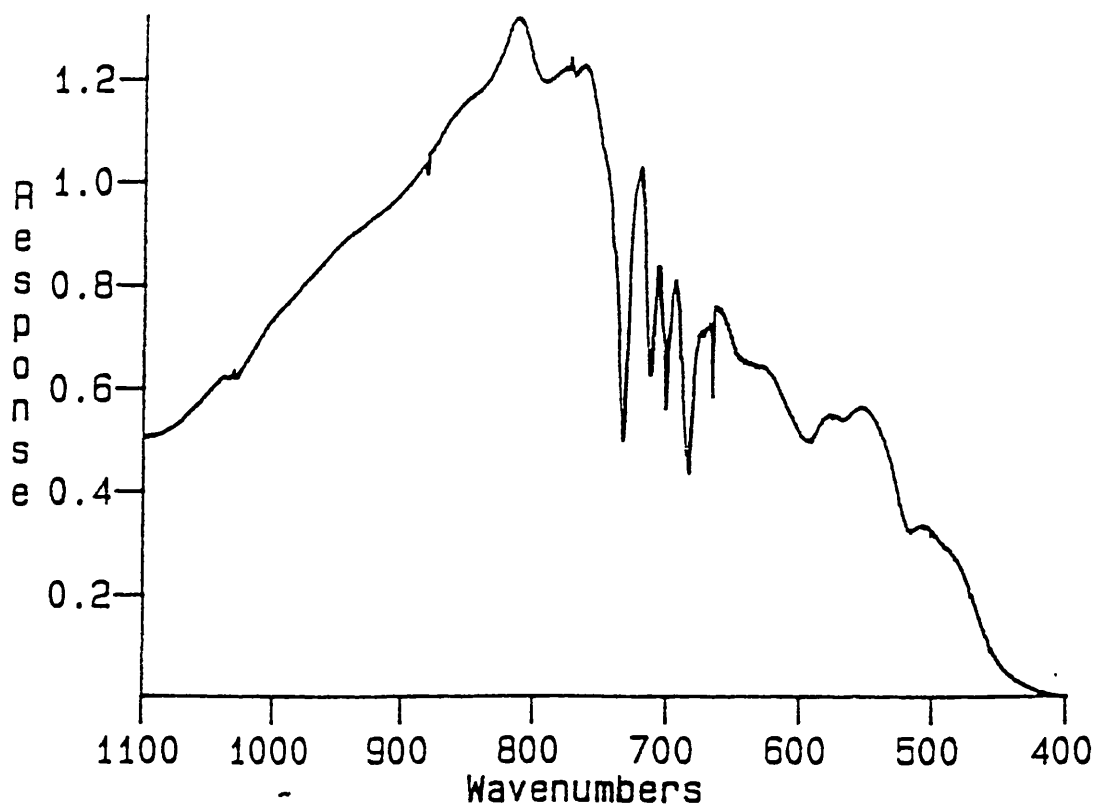


Figure 2.11: The  $\text{NbF}_5:\text{TaF}_5$  [1:3] Gas-Phase Infrared Spectrum at  $90^\circ\text{C}$ .

and  $685\text{ cm}^{-1}$  which are tentatively assigned to the  $\text{NbTa}_2\text{F}_{15}$  trimer also predicted to occur in the gas phase of this compound. assuming that the solid-state contains tetrameric rings of two Nb atoms and two Ta atoms, but regardless of the arrangement of these atoms within the rings. At  $517.5\text{ cm}^{-1}$ , there is a weak and broad band which is assumed to consist of the fluorine-bridging mode of each species present.

#### **$\text{NbF}_5:\text{TaF}_5$ [1:3]**

For  $\text{NbF}_5:\text{TaF}_5$  [1:3], the species expected are  $\text{NbTa}_2\text{F}_{15}$  and  $\text{Ta}_3\text{F}_{15}$  (Figure 2.8). The spectrum (Table 2.4 and Figure 2.11) confirms the presence of  $\text{Ta}_3\text{F}_{15}$  with bands at  $714$ ,  $702$  and  $685.5\text{ cm}^{-1}$ , and a fluorine-bridging mode at  $517.6\text{ cm}^{-1}$ , which can be compared with the analogous mode in the  $\text{TaF}_5$  spectrum in Figure 2.7. Also observed, is a strong peak at  $733.5\text{ cm}^{-1}$  which was present in the analogous [1:1] spectrum and was tentatively assigned to the  $\text{NbTa}_2\text{F}_{15}$  trimer. The other bands suggested to be associated with this species are a weak band at  $711.5\text{ cm}^{-1}$ , which may be hidden by the strong  $714\text{ cm}^{-1}$  band (from  $\text{Ta}_3\text{F}_{15}$ ), and a peak at  $685\text{ cm}^{-1}$  which would be almost coincident with the  $686\text{ cm}^{-1}$  peak of  $\text{Ta}_3\text{F}_{15}$ . It is assumed that any bridging mode for this species would be under the peak at  $517.6\text{ cm}^{-1}$ .

In this spectrum, there are also some very weak shoulders on some of the peaks which may be associated with the  $\text{Nb}_2\text{TaF}_{15}$  trimer (at  $741$  and  $691\text{ cm}^{-1}$ ), which is not predicted for this compound on the basis of ordered metal sites (see Figure 2.8). The other band suggested to be associated with this trimer is a weak stretch at  $705\text{ cm}^{-1}$  which may be under the peak at  $702\text{ cm}^{-1}$  from  $\text{Ta}_3\text{F}_{15}$ . This again may indicate some slight disorder in the compound or some interaction between molecules on heating.

## 2.8 X-ray Diffraction

### 2.8.1 X-ray Powder Diffraction Studies

Preliminary investigations into the structure of the  $\text{NbF}_5\text{:TaF}_5$  [x:y] compounds using X-ray powder diffraction show that all of these materials have diffraction patterns close to being identical to those of  $\text{NbF}_5$  and  $\text{TaF}_5$ . This suggests that the mixed niobium-tantalum pentafluorides are isostructural with  $\text{NbF}_5$  and  $\text{TaF}_5$  and that, as such, that they are fluorine-bridged tetramers.

### 2.8.2 X-ray Single Crystal Studies

X-ray structure determinations have been carried out on a single crystal of each stoichiometry (ie.  $\text{NbF}_5\text{:TaF}_5$  [3:1], [1:1] and [1:3]). This has confirmed the X-ray powder diffraction results in that all the crystals are monoclinic,  $C2/m$  and isomorphous with the crystals examined in the more recent  $\text{NbF}_5$  [4] and  $\text{TaF}_5$  structure determinations (Tables 2.5 and 2.6).

#### The $\text{TaF}_5$ Structure

The redetermined  $(\text{NbF}_5)_4$  and  $(\text{TaF}_5)_4$  structures (Tables 2.5 and 2.6) are three-dimensional investigations and have been solved using modern computer methods. They can therefore be considered to be more accurate than the original determinations which were two-dimensional, with the data collected photographically. One difference between the new and the old structures (see Table 2.7) is that the average  $\text{M-F}_t$  bond length in the new structures is 1.830(12) Å for  $\text{TaF}_5$  and 1.827(4) Å for  $\text{NbF}_5$  as compared with 1.77 Å in the original work [1]. The  $\text{M-F}_b\text{-M}$  bond angle is also different. In the new structures the values are 171.9(6)° for  $\text{TaF}_5$  and 173.0(1)° for  $\text{NbF}_5$  [4], which compare with 182.5(20)° in the first structure determinations. This departure from linearity of the  $\text{M-F}_b\text{-M}$  bond angle has repercussions in the discussions of the pentafluoride structures in that  $\pi$ -bonding can no longer be deemed to be important for the  $\text{TaF}_5$ -type structure (see Chapter 7).

Table 2.5: Data From Crystallographic Analyses of NbF<sub>5</sub>TaF<sub>5</sub> [3:1], [1:1], [1:3] and TaF<sub>5</sub>.

Compound	(TaF <sub>5</sub> ) <sub>4</sub>	3TaF <sub>5</sub> NbF <sub>5</sub>	2TaF <sub>5</sub> 2NbF <sub>5</sub>	TaF <sub>5</sub> 3NbF <sub>5</sub>
Formula*	F <sub>20</sub> Ta <sub>4</sub>	F <sub>20</sub> NbTa <sub>3</sub>	F <sub>20</sub> Nb <sub>2</sub> Ta <sub>2</sub>	F <sub>20</sub> Nb <sub>3</sub> Ta
M*	1103.8	1015.2	926.2	838.0
Crystal Symmetry	Monoclinic	Monoclinic	Monoclinic	Monoclinic
Space Group	C2/m	C2/m	C2/m	C2/m
a (Å)	9.631(27)	9.622(2)	9.634(19)	9.616(10)
b (Å)	14.466(41)	14.477(2)	14.471(28)	14.463 (10)
c (Å)	5.102(2)	5.093(1)	5.111(1)	5.112(1)
β (°)	96.34(2)	96.26(2)	96.06(1)	95.95(2)
V (Å <sup>3</sup> )	706.5 (3)	704(1)	709(3)	707(3)
Z †	4	4	4	4
Radiation Type	Mo-Kα	Mo-Kα	Mo-Kα	Mo-Kα
D <sub>c</sub> (gcm <sup>-3</sup> )	5.19	4.79	4.34	3.94
F (000)	944	880	816	752
Crystal Size (mm)	.12×.15×.35	.43×.27×.23	.14×.32×.48	-
μ(Mo-K) (cm <sup>-1</sup> )	297.6	239.6	162.4	96.0
Scan Width	1.4 + 0.7	Learnt Pro.	1.6 + 0.7	1.8 + 0.7
Scan Type	ω	ω - 2θ	ω	ω
Max. Bragg Angle (°)	60	45	54	52
Reflections Collected	978	1579	2914	1745
No. of Unique Reflections	769	470	681	636
No. of Variables	62	61	61	61
R = [Σ( F <sub>o</sub>  - F <sub>c</sub>  )/Σ F <sub>o</sub>  ]	0.070	0.0394	0.0447	0.0377
R <sub>w</sub> = [Σw( F <sub>o</sub>  - F <sub>c</sub>  ) <sup>2</sup> /Σw F <sub>o</sub>   <sup>2</sup> ] <sup>0.5</sup>	0.0705	0.0586	0.0466	0.0392
Weighting Factor (w)	0.019	0.0003	0.00077	0.0015
Max. Electron Density/e (Å <sup>-3</sup> )	3.7	1.82	2.6	1.8
Max. Final Shift/ e.s.d.	0.001	0.07	0.03	1.8

\* Refers to the molecular ratio of the adduct, with Z=2 equivalent.

† Refers to the averaged M<sub>2</sub>F<sub>10</sub> unit as C2/m.

### The NbF<sub>5</sub>:TaF<sub>5</sub> [3:1], [1:1] and [1:3] Structures

The X-ray single-crystal structure data (Table 2.6) from the mixed niobium-tantalum pentafluorides is consistent with the new data for NbF<sub>5</sub> and TaF<sub>5</sub>, and they can all be said to be isostructural, with similar bond lengths and angles within the experimental error. The near-linear fluorine-bridged tetrameric structure exhibited by these compounds, and by TaF<sub>5</sub>, is shown in Figure 2.12.

The possible arrangement of metal sites in a [3:1] mixed metal pentafluoride are shown in Figure 2.13. Ordered, disordered or random sites, as shown in this figure, are possible, but the ordered sites (Figure 2.13a) can be ruled out though on the basis of the X-ray single crystal data since, in the space group C2/m, two of the metal atoms in the tetramer occupy the m site (i), and two occupy the 2 site (g). Occupation of these sites does not allow a structure solution for either NbF<sub>5</sub>.TaF<sub>5</sub> [3:1] or [1:3] in which the single Nb or Ta atom occupy the same site in each tetramer throughout the lattice. This leads to an apparently random metal site occupancy in these mixed-metal structures.

The X-ray diffraction results on the NbF<sub>5</sub>.TaF<sub>5</sub> [x:y] compounds do not show whether there are (a) ordered metal sites within each tetramer (but that the tetramers are randomly arranged or arranged in a super-lattice as shown in Figure 2.13b), or (b) that there is a completely random arrangement of metal atoms (see Figure 2.13c).

## 2.9 Conclusions

Although the X-ray single crystal structure determinations of NbF<sub>5</sub>:TaF<sub>5</sub> [3:1], [1:1] and [1:3] do not distinguish between the metals in the tetramer, X-ray fluorescence analysis has confirmed the overall stoichiometry of the metals in these compounds. In addition, mass spectrometry has shown the presence of the mixed-metal frag-

Table 2.6: Selected Bond Lengths and Angles For NbF<sub>5</sub>, TaF<sub>5</sub> and NbF<sub>5</sub>:TaF<sub>5</sub> [3:1], [1:1] and [1:3].

Data	(TaF <sub>5</sub> ) <sub>4</sub>	NbF <sub>5</sub> .TaF <sub>5</sub> <sup>*</sup> [1:3]	NbF <sub>5</sub> .TaF <sub>5</sub> [1:1]	NbF <sub>5</sub> .TaF <sub>5</sub> [3:1]	(NbF <sub>5</sub> ) <sub>4</sub> [4]
M <sub>1</sub> -F <sub>eq</sub> (Å)	1.790(13)	1.85	1.819(6)	1.802(8)	1.812(3)
M <sub>1</sub> -F <sub>ax</sub> (Å)	1.873(10)	1.86	1.855(6)	1.840(9)	1.839(3)
M <sub>1</sub> -F <sub>b</sub> (Å)	2.070(12)	2.07	2.067(5)	2.090(6)	2.068(2)
M <sub>2</sub> -F <sub>eq</sub> (Å)	1.822(12)	1.78	1.803(6)	1.807(8)	1.807(3)
M <sub>2</sub> -F <sub>ax</sub> (Å)	1.862(25)	1.85	1.833(9)	1.858(13)	1.831(4)
	1.884(20)	1.87	1.863(9)	1.833(11)	1.846(4)
M <sub>2</sub> -F <sub>b</sub> (Å)	2.071(12)	2.06	2.070(5)	2.042(6)	2.063(2)
M <sub>1</sub> -F <sub>b</sub> -M <sub>2</sub> (°)	171.3(8)		172.8(3)	172.8(4)	173.0(1)

\* Data collected at Edinburgh University.

Table 2.7: Comparison of Selected Bond Lengths and Angles from the Original NbF<sub>5</sub> and TaF<sub>5</sub> Crystal Structures and the More Recent Redeterminations.

Data	NbF <sub>5</sub> and TaF <sub>5</sub> (Original Work <sup>1</sup> )	TaF <sub>5</sub> (Present Work)	NbF <sub>5</sub> (Recent Work <sup>4</sup> )
M <sub>1</sub> -F <sub>1</sub> (Å)	2.06(2)	2.070(12)	2.068(2)
M <sub>1</sub> -F <sub>2</sub> (Å)	1.78(5)	1.873(10)	1.839(3)
M <sub>1</sub> -F <sub>3</sub> (Å)	1.75(2)	1.790(13)	1.812(3)
M <sub>2</sub> -F <sub>1</sub> (Å)	2.07(2)	2.071(12)	2.063(2)
M <sub>2</sub> -F <sub>4</sub> (Å)	1.78(2)	1.862(25)	1.831(4)
M <sub>2</sub> -F <sub>5</sub> (Å)	1.75(5)	1.884(20)	1.846(4)
M <sub>2</sub> -F <sub>6</sub> (Å)	1.78(2)	1.822(12)	1.807(3)
M-F <sub>b</sub> -M (°)	182.5(25)	171.(8)	173.0(1)

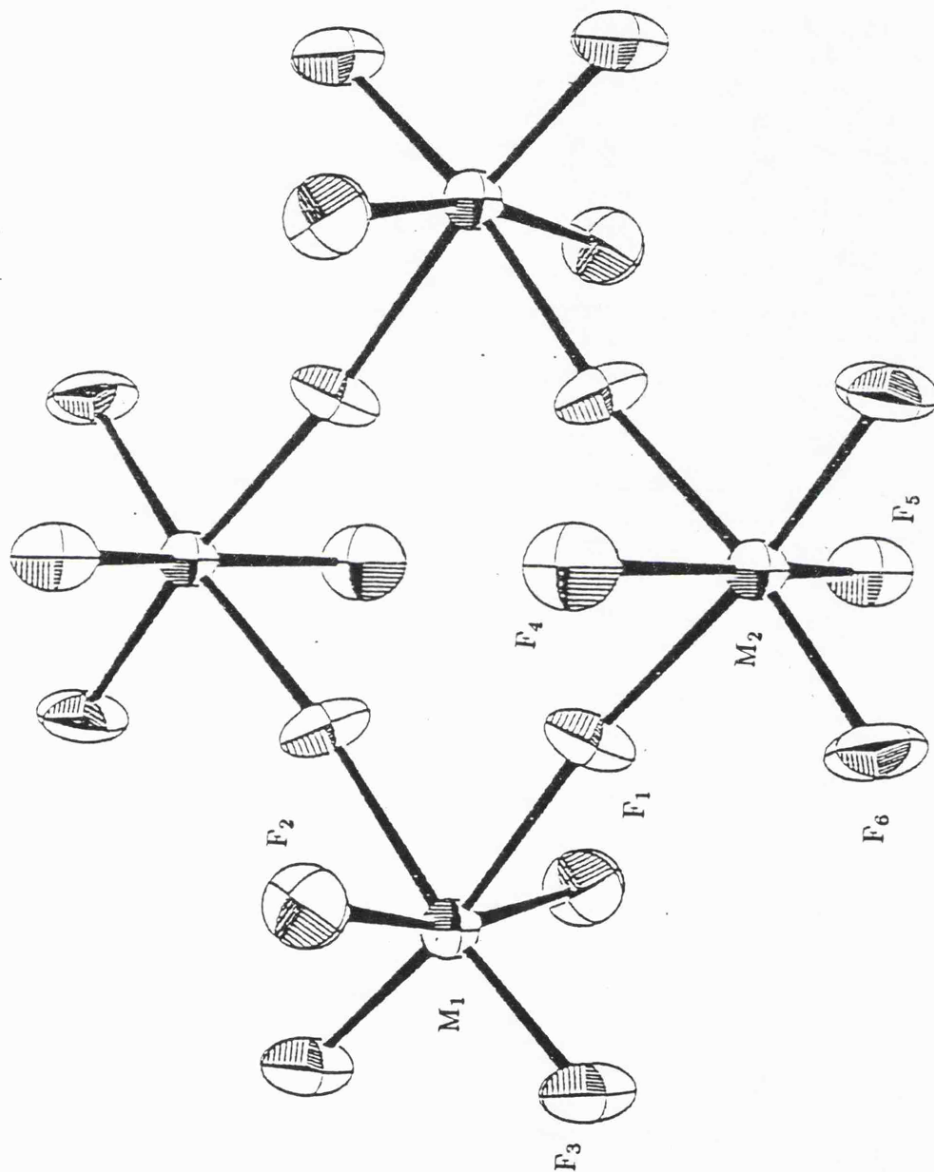
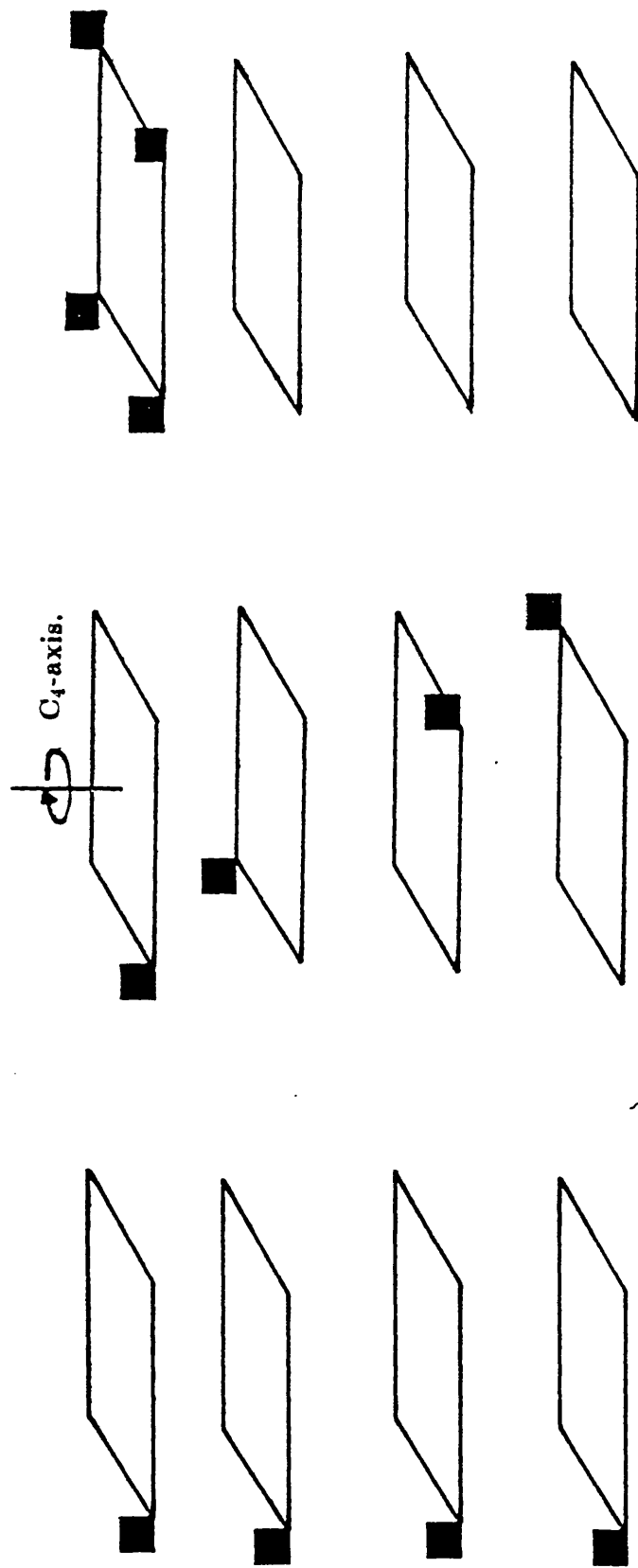


Figure 2.12: The Near-Linear Fluorine-Bridged Tetramer.

Figure 2.13: The Possible Arrangement of Metal

Sites in  $MF_5 \cdot M^{\circ}F_5 [3:1]$ .



(a) Ordered Metal Sites.

(b) Ordered Metal Sites in a Tetramer Superlattice.

(c) Disordered Metal Sites.

ments expected for each specific composition.

The mass spectrum of  $\text{NbF}_5 \cdot \text{TaF}_5$  [1:1], shows the presence of all the possible dimeric fragments. All of these could be present if the solid-state of this material contained tetrameric rings with two Nb and two Ta atoms in each tetramer regardless of the positioning of those atoms in the tetramer. However, the mass spectrum of  $\text{NbF}_5 \cdot \text{TaF}_5$  [3:1] has only a trace  $\text{Ta}_2\text{F}_9^+$  peak and that of  $\text{NbF}_5 \cdot \text{TaF}_5$  [1:3] has no peak for  $\text{Nb}_2\text{F}_9^+$ , which implies that the tetramers within the solid-state of these materials contain three Nb and one Ta atom and one Nb atom and three Ta atoms, respectively.

To investigate these compounds fully using mass spectroscopy it would be necessary to find out what larger fragments (ie. trimers and tetramers) are present in the samples.  $\text{BiF}_5 \cdot \text{SbF}_5$  [1:3], which also adopts the  $\text{TaF}_5$  structure, shows evidence for  $\text{BiF}_5 \cdot (\text{SbF}_5)_3$  tetramers in the gas phase [112]. Mass spectra in this thesis have only been recorded up to 520 a.m.u.. Although attempts have been made to record spectra up to higher masses (720 a.m.u.), this has not been successful due to the limitations of the mass spectrometer.

The solid-phase and gas-phase infrared spectra have been reported for characterisation purposes. The spectra have shown the presence of fluorine-bridging in the adducts and also that the solids are not made up of individual  $(\text{NbF}_5)_4$  and  $(\text{TaF}_5)_4$  tetramers. The gas-phase infrared spectra also appear to show that the structures are made up of mixed-metal tetramers with the expected number of Nb and Ta atoms within each tetramer in the lattice, according to the overall stoichiometries, and that the main species, in the gas phase of these compounds at  $\approx 90^\circ\text{C}$ , appears to be trimeric. However, infrared spectra can be interpreted in a number of ways and so these results are reported only tentatively. Raman spectroscopy also suggests the presence of mixed-metal tetramers.

In order to compare the relative Lewis acidities of  $\text{NbF}_5$  and  $\text{TaF}_5$ , it would

normally be possible to make a simple comparison of the bond lengths of the different metal sites of the  $\text{NbF}_5:\text{TaF}_5$  [x:y] single crystal structure determinations, the metal with the shorter M-F bond lengths being the stronger Lewis acid. Because individual Nb- and Ta-metal sites are not distinguishable, this has not been possible.

The fact that the M-F<sub>2</sub>-M bond angle in  $\text{NbF}_5$  and  $\text{TaF}_5$  is now known to be departed from linearity (at  $\approx 172^\circ$ ) reduces the importance of the fluorine  $\pi$ -bonding arguments in explaining these structures. Perhaps a more logical explanation of the close-packed structures, therefore, is based on the packing of the atoms in the solid state and this is considered in more detail in Chapter 7.

In order to determine if these mixed-metal pentafluorides have structures where the metal sites are completely randomly spread between Nb and Ta atoms according to the overall stoichiometry of the compound, the EXAFS (Extended X-ray Absorption Fine Structure) spectra have been recorded on selected compounds. The results are reported in Chapter 6. The analysis of the EXAFS has been used as a localised structural probe to distinguish the different metals present in each tetramer. This information, when allied with that of the crystal structure determination, presents a more complete structural characterisation of these materials.

## Chapter 3

# The Preparation and Characterisation of $\text{RuF}_5:\text{TaF}_5$ [3:1], [1:1] and [1:3].

### 3.1 Introduction

The Raman spectra of the products of the fusion of  $(\text{RuF}_5)_4$  and  $(\text{TaF}_5)_4$  have been previously investigated [113]. Holloway found that the spectra of the fusion products were not simply those of  $\text{RuF}_5$  and  $\text{TaF}_5$  superimposed one upon the other, but rather consisted of bands at intermediate values. No attempts were made at the time to assign these spectra. The main reason for this present study was to investigate the effect on the solid-state structure, when a near-linear bridged tetramer  $(\text{TaF}_5)_4$  was combined with a bent bridged tetramer  $(\text{RuF}_5)_4$ .

However the present study of  $\text{RuF}_5:\text{TaF}_5$  [3:1], [1:1] and [1:3] was undertaken not only to investigate the interaction of the two structural types, but also to (a) investigate the precise nature of the new compounds and to see if this would bring to light new information as to why the different metal pentafluoride structural types occur, (b) attempt to compare the relative Lewis acidities of  $\text{RuF}_5$  and  $\text{TaF}_5$  and (c) assess the physical properties of the new compounds with respect to the possibility

of using them as precursors for the CVD of metal alloys.

The first two reasons are similar to those for the  $\text{NbF}_5:\text{TaF}_5$  compounds (see Chapter 2). The possibility of using the  $\text{RuF}_5:\text{TaF}_5$  compounds as precursors for CVD of metal alloys is discussed in Chapter 8, and is based on the fact that the thermodynamics of reduction of  $\text{RuF}_5$  by hydrogen are favourable, while those for  $\text{TaF}_5$  are not. This leads to the possibility of forming RuTa alloys which would otherwise prove extremely difficult to prepare, due to the high melting point of Ta (3250 K [114]).

## 3.2 Preparation

$\text{RuF}_5:\text{TaF}_5$  [3:1], [1:1] and [1:3] have been prepared as described in Chapter 9. The materials have been stored in a dry box in stoppered, pre-seasoned 6mm FEP tubes and samples have been taken and analysed as required. The results of these analyses are reported below.

## 3.3 X-ray Fluorescence Analysis

The average values for the Ru:Ta ratios in  $\text{RuF}_5:\text{TaF}_5$  [x:y] are shown in Table 3.1, along with the values for the Ru/Ta mixed-powder samples, which have been analysed to check the accuracy of the technique. Bearing in mind that the metal atoms in the mixed-metal powder samples cannot be as intimately mixed as those in the hydrolysed  $\text{RuF}_5:\text{TaF}_5$  samples, the results seem to imply that the error on the analysis is of the order of  $\pm 4\%$ . The XRF analysis confirms the overall stoichiometry of the metals in the bulk samples. The crystal of  $\text{RuF}_5:\text{TaF}_5$  [1:3], for which a single crystal structure determination is reported, has also been analysed and these results also confirm the approximate Ru:Ta ratio of 1:3. Unfortunately, the single crystal of  $\text{RuF}_5:\text{TaF}_5$  [1:1], on which the X-ray structure determination has been carried out, has not been available as the X-ray data was collected at Edinburgh University.

Table 3.1: X-ray Fluorescence Data for  $\text{RuF}_5:\text{TaF}_5$  [3:1], [1:1], [1:3] and Ru/Ta Metal Powder Samples.

Sample	Ru Expected (%)	Ta Expected (%)	Ru Found (%)	Ta Found (%)
$\text{RuF}_5:\text{TaF}_5$ [1:1]	50	50	44.08	55.91
$\text{RuF}_5:\text{TaF}_5$ [1:3]	25	75	24.52	75.48
$\text{RuF}_5:\text{TaF}_5$ [1:3]*	25	75	21.61	78.39
Ru.Ta Metal Powders				
Ru:Ta Ratio [3:1]	75	25	69.72	30.28
Ru:Ta Ratio [1:1]	50	50	53.60	46.40
Ru:Ta Ratio [1:3]	25	75	26.71	73.29

\* This was the single crystal on which the X-ray structure determination has been carried out.

Although the data are quoted to 2 decimal places, the values are  $\approx \pm 4\%$ .

### 3.4 Infrared Spectroscopy of the Solids

The infrared spectra of  $\text{RuF}_5$ ,  $\text{RuF}_5:\text{TaF}_5$  [3:1], [1:1] and [1:3] and  $\text{TaF}_5$  have been recorded and the frequencies of the bands are reported in Table 3.2. As a consequence of the infrared spectra having been recorded on solid, powdered samples, the resolution of the peaks is poor and many of the bands are broad and intense. However, it is evident that the spectra are all of similar form in that there is a series of bands between  $\approx 750$  and  $650 \text{ cm}^{-1}$ , a band at  $\approx 580 \text{ cm}^{-1}$ , and another series of bands at  $\approx 500 \text{ cm}^{-1}$ . One difference is that those of  $\text{RuF}_5$ ,  $\text{RuF}_5:\text{TaF}_5$  [3:1] and [1:1] have a band at  $480 \text{ cm}^{-1}$ , which is not present in the others. In addition, the spectra of  $\text{TaF}_5$ ,  $\text{RuF}_5:\text{TaF}_5$  [1:1] and [1:3] all have a relatively sharp band at  $\approx 750 \text{ cm}^{-1}$ , whilst those of  $\text{RuF}_5$  and  $\text{RuF}_5:\text{TaF}_5$  [3:1] both have a much less well resolved peak at  $\approx 740 \text{ cm}^{-1}$ . These differences reflect the way in which the bands

Table 3.2: Infrared Frequencies of Solid, Powdered Samples of  $\text{RuF}_5$ ,  $\text{TaF}_5$ ,  $\text{RuF}_5:\text{TaF}_5$  [3:1], [1:1] and [1:3] ( $\text{cm}^{-1}$ ).

$\text{RuF}_5$	$\text{RuF}_5:\text{TaF}_5$ [3:1]	$\text{RuF}_5:\text{TaF}_5$ [1:1]	$\text{RuF}_5:\text{TaF}_5$ [1:3]	$\text{TaF}_5$
743 w	740 m	754m	753 s	753 m
		734 m,br	722 m	723 w
709 w,br				
	678 w	676 s	672 m	667 vw,br
654 s	664 m			
	645 m	655 vw	641 w	
588 w,shp	588 w,shp	588 w,shp		
	576 m	577 m	580 w	579 s
516 s,br	513 m,br	513 m,br	509 s,br	512 m,br
480 m	481 m	482 m		

of the  $\text{RuF}_5:\text{TaF}_5$  species fall at intermediate values between those of  $(\text{RuF}_5)_4$  and  $(\text{TaF}_5)_4$ . This, in turn, shows that although no detailed symmetry calculations have been carried out, the spectra appear to be the result of the vibrations of the whole molecule rather than individual metal sites, and that the  $\text{RuF}_5:\text{TaF}_5$  [x:y] solids seem to contain mixed-metal tetramers.

### 3.5 Raman Spectroscopy

The Raman spectra of solid samples of  $\text{RuF}_5$ ,  $\text{RuF}_5:\text{TaF}_5$  [3:1] and [1:1] and  $\text{TaF}_5$  are illustrated in Table 3.3. They are all of similar shape with one group of bands at  $\approx 760\text{--}660\text{ cm}^{-1}$ , which are believed to be M-F stretching modes, and another at  $\approx 300\text{--}200\text{ cm}^{-1}$ , which are assigned to M-F bending modes. It should be noted that the Raman spectra of  $\text{RuF}_5$ ,  $\text{RuF}_5:\text{TaF}_5$  [3:1] and [1:1] have all been recorded at low temperature,  $-196^\circ\text{C}$ ,  $-50^\circ\text{C}$  and  $-50^\circ\text{C}$  respectively. This is because the compounds

Table 3.3: Raman Spectra of  $\text{RuF}_5$ ,  $\text{TaF}_5$ ,  $\text{RuF}_5:\text{TaF}_5$  [3:1], [1:1] and [1:3] ( $\text{cm}^{-1}$ ).

$\text{RuF}_5^*$	$\text{RuF}_5:\text{TaF}_5$ [3:1]	$\text{RuF}_5:\text{TaF}_5$ [1:1]	$\text{RuF}_5:\text{TaF}_5$ [1:3] <sup>†</sup>	$\text{TaF}_5$
	762 m	763 m	-	
748 vs	739 s	738 s	-	757 s
722 m	724 vw	717 m	-	725 w
712 mw	712 m		-	
708 w		692 w	-	697 m
662 vs	658 s	660 s	-	646 w
		286 mw	-	
	275 m	271 m	-	272 m
	233 w	240 w	-	236 w
	212 w		-	222 vw

\* Spectrum recorded from 800–600  $\text{cm}^{-1}$  only.

† No spectrum has been recorded for this compound despite several attempts to do so.  
decompose in the laser at room temperature.

### 3.5.1 The Raman Spectra of $(\text{RuF}_5)_4$ and $(\text{TaF}_5)_4$ .

The Raman spectrum of  $\text{NbF}_5$  has been assigned [111] on the basis of the  $D_{4h}$  symmetry of the tetramer, found in the X-ray single crystal data [1, 4]. The similarity of the  $\text{TaF}_5$  structure and Raman spectrum to that of  $\text{NbF}_5$  has already been discussed (see Chapter 2). On the basis of this, it has been assumed that the  $\text{TaF}_5$  Raman spectrum is also associated with a tetrameric  $(\text{TaF}_5)_4$  molecule of  $D_{4h}$  symmetry.

The  $\text{RuF}_5$  Raman spectrum (Table 3.3) is, also, of similar overall form to that of  $(\text{TaF}_5)_4$ , but there are differences in the number and intensities of the bands and their precise frequencies. Symmetry group analysis of the  $\text{RuF}_5$  spectrum has not been attempted, but it seems reasonable to assume that the spectrum is based on the whole tetramer rather than on the individual metal sites.

Two important considerations when analysing a vibrational spectrum are the symmetry of the molecule and the force constants of the bonds which form the molecule. In  $\text{TaF}_5$  this symmetry is  $D_{4h}$ , whereas in  $\text{RuF}_5$  it is reduced to approximately  $D_{2d}$ . This reduction in the symmetry on going from  $\text{TaF}_5$  to  $\text{RuF}_5$  may explain the greater number of peaks in the  $\text{RuF}_5$  spectrum, whilst the influence of the force constants of the bonds would be to have an effect on the frequencies of the modes, because of differences in the strengths of the Ru-F bonds as compared to those of Ta-F. The bonding in these compounds must surely be an important factor in determining which type of structure they adopt.

### 3.5.2 The Raman Spectrum of $\text{RuF}_5:\text{TaF}_5$ [3:1]

The Raman spectrum of  $\text{RuF}_5:\text{TaF}_5$  [3:1] (see Table 3.3), though containing a series of M-F stretching ( $760\text{--}660\text{ cm}^{-1}$ ) and bending modes ( $270\text{--}200\text{ cm}^{-1}$ ) is quite different from those of  $(\text{RuF}_5)_4$  and  $(\text{TaF}_5)_4$ . This is despite the fact that  $\text{RuF}_5:\text{TaF}_5$  [3:1], on the basis of X-ray powder diffraction patterns and EXAFS (see Section 3.7 and Chapter 6 respectively), is believed to adopt a distorted version of the  $\text{TaF}_5$  structure.

A quantitative examination of the frequencies, reduced masses and symmetry of the modes in a Raman spectrum can give information on the force constants of a molecule. In turn, these give information about the bonding in the molecule. Although this spectrum has only been studied qualitatively, the fact that the detailed spectrum is unlike that of either  $\text{TaF}_5$  or  $\text{RuF}_5$  implies that the force constants and the bonding in this compound are different to either of these single-metal pentafluorides. In fact, it is believed that the bonding situation in the  $\text{RuF}_5:\text{TaF}_5$  [3:1] tetramer is intermediate between those for  $(\text{RuF}_5)_4$  and  $(\text{TaF}_5)_4$ . However, the overall structure of this compound is based on that of  $\text{TaF}_5$  because the larger  $\text{Ta}^{5+}$  ions dominate.

The complete change observed in the high resolution Raman spectrum of  $\text{RuF}_5:\text{TaF}_5$  [3:1] compared with those of  $\text{RuF}_5$  and  $\text{TaF}_5$  is different from the case for the  $\text{NbF}_5:\text{TaF}_5$  compounds (see Chapter 2). This is believed to be due to the fact that the  $\text{NbF}_5:\text{TaF}_5$  structures are based on those of  $(\text{NbF}_5)_4$  and  $(\text{TaF}_5)_4$ , and so the bonding energy levels in the mixed-metal tetramers would not be expected to alter greatly from those of the parent pentafluorides.

### 3.5.3 The Raman Spectrum of $\text{RuF}_5:\text{TaF}_5$ [1:1]

The Raman spectrum of  $\text{RuF}_5:\text{TaF}_5$  [1:1] is shown in Table 3.3. The spectrum is similar to that of  $\text{RuF}_5:\text{TaF}_5$  [3:1], but with slight differences in frequencies and intensities. Analysis of this spectrum is, therefore based on that of  $\text{RuF}_5:\text{TaF}_5$  [3:1], which itself adopts the  $\text{TaF}_5$  structure (see Section 3.7).

### 3.5.4 The Raman Spectrum of $\text{RuF}_5:\text{TaF}_5$ [1:3]

Several attempts have been made to record a Raman spectrum of this compound. The sample appears to burn in the laser at room temperature, and more slowly at  $-50^\circ\text{C}$ , with no decomposition at  $-196^\circ\text{C}$ . However, no bands are recorded under these conditions. The  $\text{Ar}^+$  green and blue lines have been used, as well as the  $\text{Kr}^+$  red line in order to see if the sample fluoresces. An attempt has also been made, at Southampton University, to record a spectrum using FT-Raman spectroscopy but without success. This is unfortunate and may be due to severe fluorescence of the sample, which was also found for  $\text{NbF}_5:\text{TaF}_5$  [1:3], although to a lesser extent.

## 3.6 Gas-Phase Infrared Spectroscopy

Because of the extreme moisture- and oxygen-sensitivity of  $\text{RuF}_5$ , peaks due to  $\text{RuO}_4$  [115] are also observed and, as such, the sensitivity of this technique to analyse  $\text{RuF}_5$ -containing species is reduced. This is despite extensive seasoning of the

Table 3.4: Gas-Phase Infrared Frequencies ( $\text{cm}^{-1}$ ) for  $\text{RuF}_5$ ,  $\text{TaF}_5$  and  $\text{RuF}_5:\text{TaF}_5$  [3:1], [1:1] and [1:3] at  $\approx 90^\circ\text{C}$

$\text{RuF}_5$	$\text{RuF}_5\text{TaF}_5$ [3:1]	$\text{RuF}_5\text{TaF}_5$ [1:1]	$\text{RuF}_5\text{TaF}_5$ [1:3]	$\text{TaF}_5$
749 m	744 sh	751 w	751 w	751 w*
721 s	739 m	739 w	739 w	739 w *
704 s	722 sh	723 sh	720 sh	714 m
659 w	705 vw,sh	705 sh	705 sh	
	691 vw	703 m	703 m	702.7 m
		692 vw,sh	691 sh	
		687 m	687 m	687 m
553 w,br	541 w,br			
	526 w,br	520 w,br	518 w,br	520 w,br

\* Assigned to non-gas phase species.

gas cell and is believed to be due to inefficient seals between the Cu cell body and the AgCl windows at elevated temperatures.

It should be noted that any assignments made of the gas-phase infrared spectra are only suggested tentatively as the data can be interpreted in a number of ways.

### 3.6.1 The Spectra of $\text{RuF}_5$ and $\text{TaF}_5$

The gas-phase infrared spectrum of  $\text{TaF}_5$  at  $90^\circ\text{C}$  has already been discussed in Chapter 2. The spectrum and frequencies are shown in Table 3.4 and Figure 2.7, along with the spectrum recorded at room temperature after the gas cell had cooled. The room-temperature spectrum shows that the peaks in the earlier spectrum, at 750 and  $739\text{ cm}^{-1}$ , are due to a non-gas-phase species. This is most probably solid  $\text{TaF}_5$  on the AgCl windows.

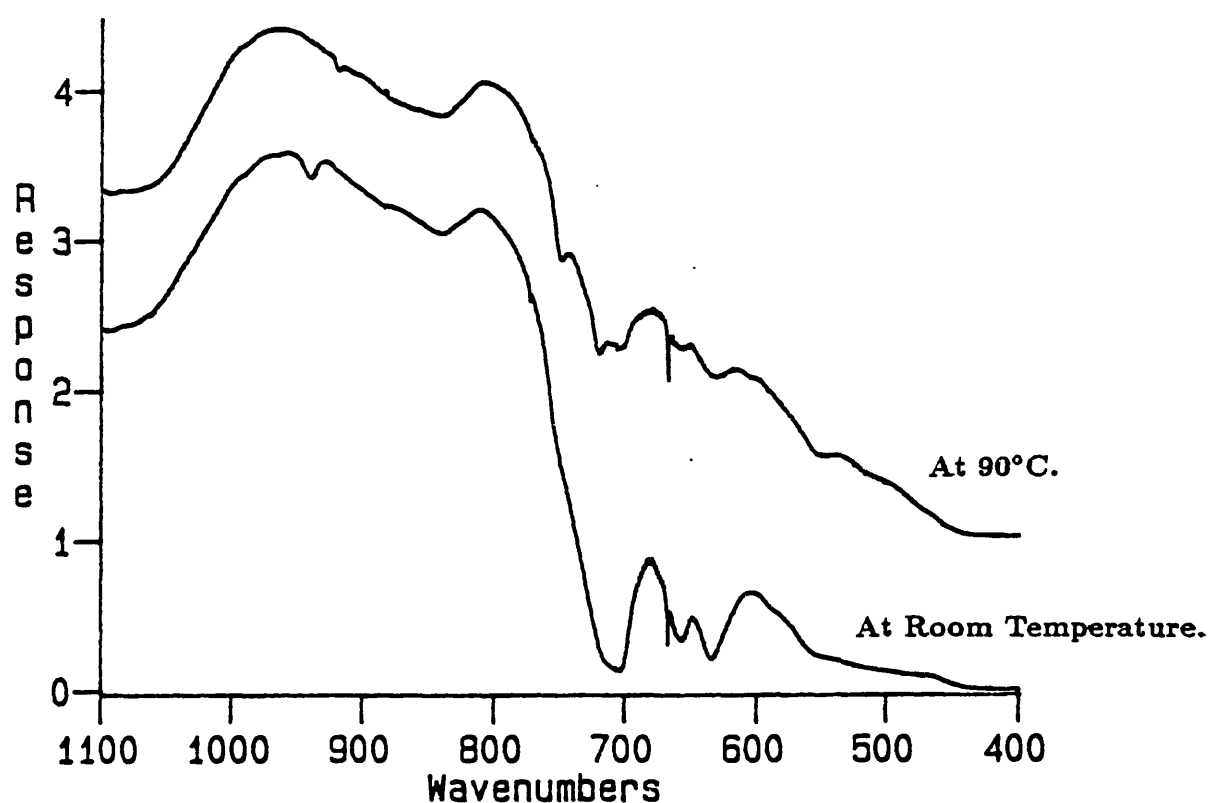


Figure 3.1: Gas-Phase Infrared Spectrum of  $\text{RuF}_5$  at  $90^\circ\text{C}$  and at Room Temperature.

The gas-phase infrared spectrum of  $\text{RuF}_5$  (Table 3.4 and Figure 3.1), at  $90^\circ\text{C}$ , is shown along with the spectrum recorded after the gas cell had cooled to room temperature. At room temperature, there are bands indicating that a solid species, most probably  $\text{RuF}_5$  tetramer, has condensed onto the  $\text{AgCl}$  windows.

The  $\text{RuF}_5$  spectrum is not as well resolved as those of  $\text{NbF}_5$  and  $\text{TaF}_5$ , which may be because there are bands associated with the solid on the  $\text{AgCl}$  windows which overlap with those from the gas phase species. However, it seems reasonable to assume that the band at  $720\text{ cm}^{-1}$  is due to a gas-phase  $\text{RuF}_5$  species, and those at  $750$  and  $705\text{ cm}^{-1}$  might be. It is interesting to note that the fluorine-bridging mode in this spectrum occurs at  $553\text{ cm}^{-1}$ , while the corresponding value for  $\text{TaF}_5$  spectrum is  $520\text{ cm}^{-1}$ .

The gas-phase infrared spectrum of  $\text{RuF}_5$  has been assigned on the basis of a trimeric molecule adopting  $D_{3h}$  symmetry [9, 10], similar to  $(\text{NbF}_5)_3$  and  $(\text{TaF}_5)_3$ .

A comparison of the frequencies from the niobium and tantalum studies and the present work is shown in Table 3.5. A schematic representation of the trimeric molecule is shown in Figure 2.6. Bearing in mind that some of the bands are broad, there is reasonable agreement between the present work and that of the literature.

### 3.6.2 RuF<sub>5</sub>:TaF<sub>5</sub> [3:1]

The spectrum at 75°C (Figure 3.2) is dominated by bands assigned to the TaF<sub>5</sub> trimer. This was not predicted as the TaF<sub>5</sub> trimer would be expected to be a minor component of the gas-phase. It is believed to dominate because of its relative chemical inertness with respect to the mixed-metal species. There are, however, other bands present, perhaps most notably two fluorine-bridging modes at 541 cm<sup>-1</sup> and 526 cm<sup>-1</sup>. These two values compare with those of 553 cm<sup>-1</sup> for RuF<sub>5</sub> and 520 cm<sup>-1</sup> for TaF<sub>5</sub>, which suggest that the mode at 543 cm<sup>-1</sup> is due to Ru-F-containing species.

There are also other bands, in the stretching region of the spectrum (750–650 cm<sup>-1</sup>), which are not due to (TaF<sub>5</sub>)<sub>3</sub>. These are all shoulders on intense TaF<sub>5</sub> bands. Two of them are at 744 and 722 cm<sup>-1</sup>, and there is also some evidence for a shoulder at 704 cm<sup>-1</sup>, but this is very weak. The bands at 722 and possibly 704 cm<sup>-1</sup> are assigned to the RuF<sub>5</sub> gas-phase trimer. The band at 750 cm<sup>-1</sup>, which would be expected for (RuF<sub>5</sub>)<sub>3(g)</sub> or for (TaF<sub>5</sub>)<sub>4(s)</sub>, is believed to be obscured by the shoulder at 744 cm<sup>-1</sup>. This shoulder is believed to be due to a novel gas-phase species as it is not present in either the TaF<sub>5</sub> or RuF<sub>5</sub> gas-phase spectra. It is perhaps most logical to assume that it is associated with a mixed RuF<sub>5</sub>:TaF<sub>5</sub> gas-phase species although no assignment is possible on the basis of a single band.

There is also a weak band at 812.8 cm<sup>-1</sup>. Due to the weakness of the band and the fact that it only occurred in one spectrum of the material it is assumed that it is due to a decomposition product.

Table 3.5: Comparison of Present and Published Gas Phase Infrared Frequencies ( $\text{cm}^{-1}$ ) for  $\text{RuF}_5$ .

Lit. Work [9]	Lit. Assignment [9]	Present Work
749 m	E'	749 m
726 m	A <sub>2</sub> '	721 m
698 s	E'	704 m
679 m	E'	659 w
523 w	E'	553 w,br

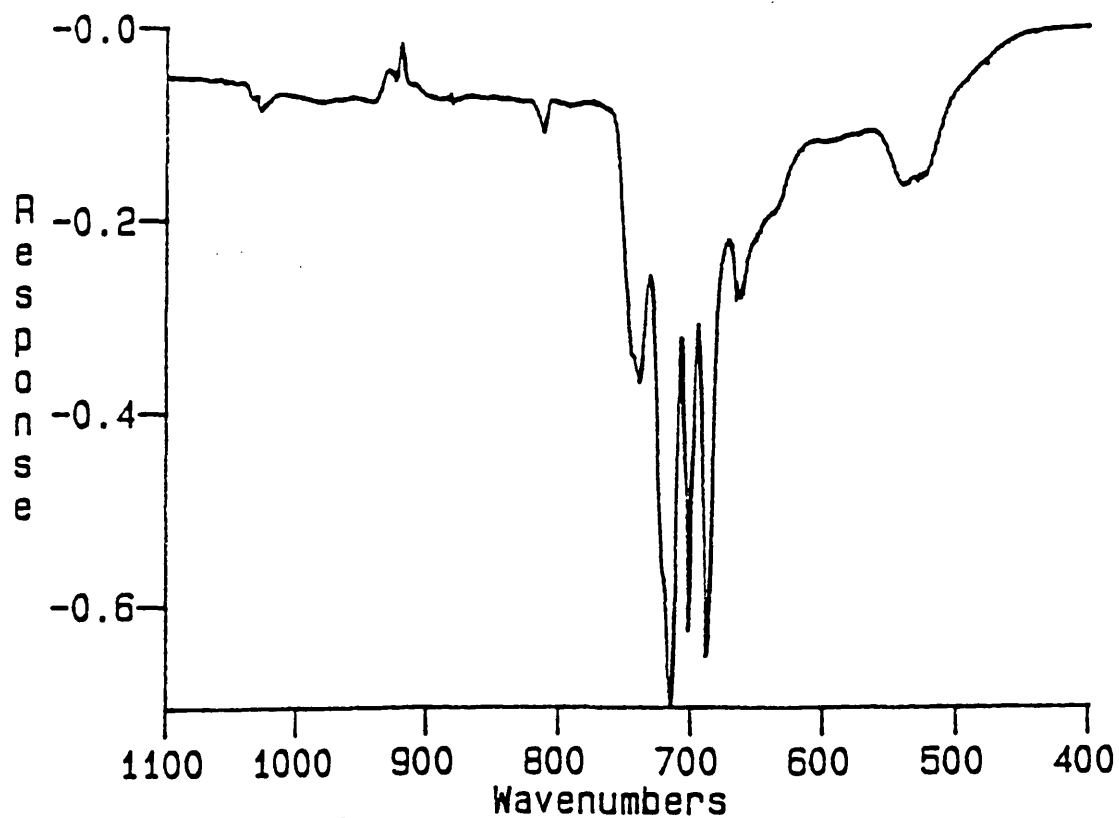


Figure 3.2: The  $\text{RuF}_5 \cdot \text{TaF}_5$  [3:1] Gas-Phase Spectrum at  $90^\circ\text{C}$ .

### 3.6.3 RuF<sub>5</sub>:TaF<sub>5</sub> [1:1]

The gas-phase spectrum of RuF<sub>5</sub>:TaF<sub>5</sub> [1:1] at 90°C is shown in Figures 3.3 with the frequencies listed in Table 3.4. The spectrum is again dominated by the bands associated with the TaF<sub>5</sub> trimer, but there is evidence for other species also. There are shoulders on the intense TaF<sub>5</sub> peaks at 722 and 705 cm<sup>-1</sup>, and there is also evidence for a weak shoulder at 691 cm<sup>-1</sup>. These peaks can be assigned to the RuF<sub>5</sub> trimer (see Figure 3.1). In addition, there is a band at 738 cm<sup>-1</sup> from solid TaF<sub>5</sub> on the AgCl windows. This band is broader than that in the TaF<sub>5</sub> gas-phase spectrum and there is an asymmetry to the peak shape. This broadening is sufficient to mask any peak at 750 cm<sup>-1</sup> (which might be expected for the RuF<sub>5</sub> trimer or solid TaF<sub>5</sub>), and may be indicative of a 744 cm<sup>-1</sup> peak similar to that in the RuF<sub>5</sub>:TaF<sub>5</sub> [3:1] spectrum. However, this is a very tentative suggestion. Finally, there is a tiny peak in this spectrum at 773 cm<sup>-1</sup>, which is present in other spectra and is thought to arise from fluorination of a contaminant in the gas cell.

### 3.6.4 RuF<sub>5</sub>:TaF<sub>5</sub> [1:3]

The gas-phase spectrum of RuF<sub>5</sub>:TaF<sub>5</sub> [1:3] (see Table 3.4 and Figure 3.4) shows mainly those bands associated with the gas-phase spectrum of TaF<sub>5</sub>, which includes the bands believed to be due to solid TaF<sub>5</sub> on the AgCl windows. Close inspection of the spectrum shows that there are weak shoulders on the intense (TaF<sub>5</sub>)<sub>3(g)</sub> bands at 721, 705 and 691 cm<sup>-1</sup>, which are assigned to a RuF<sub>5</sub> gas-phase trimer. No other bands are observed.

## 3.7 X-ray Powder Diffraction

The X-ray powder diffraction patterns of RuF<sub>5</sub>:TaF<sub>5</sub> [1:1] and [1:3] show that the samples are highly crystalline. On comparison with other patterns, it is evident that the structures of RuF<sub>5</sub>:TaF<sub>5</sub> [1:1] and [1:3] are similar to that of TaF<sub>5</sub>. In fact, the pattern of RuF<sub>5</sub>:TaF<sub>5</sub> [1:3] is essentially identical to that of TaF<sub>5</sub> indicating that

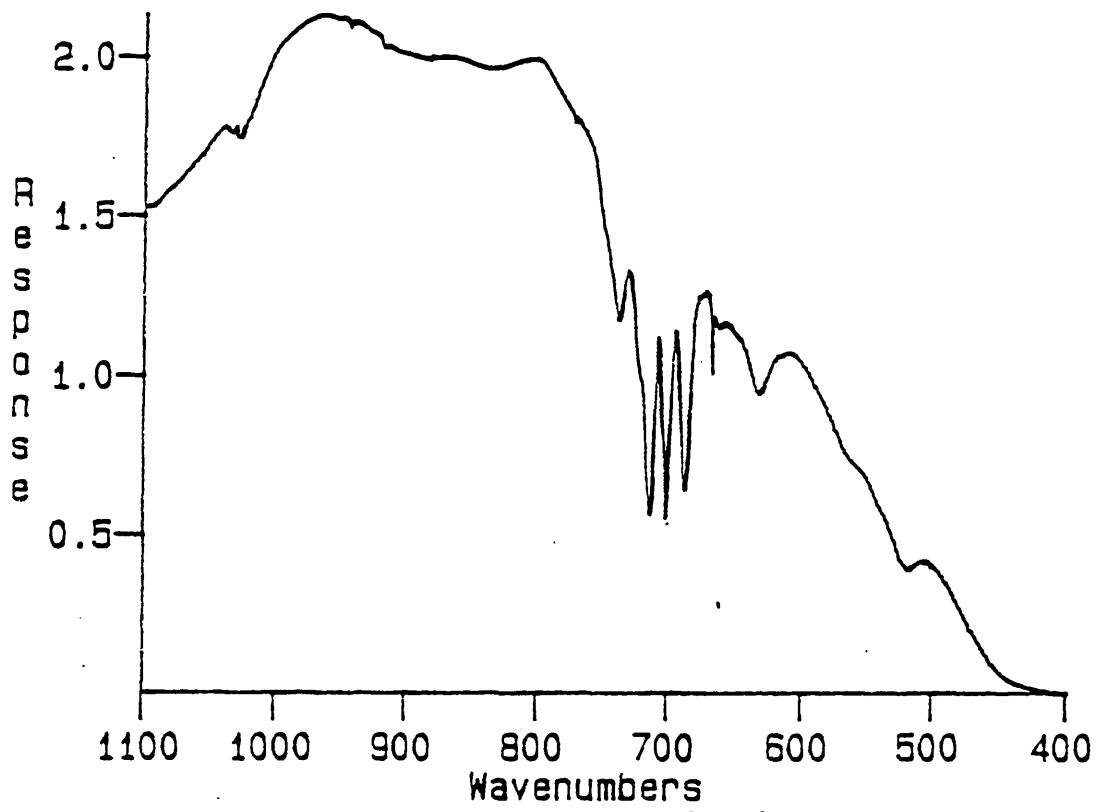


Figure 3.3: The  $\text{RuF}_5 \cdot \text{TaF}_5$  [1:1] Gas-Phase Infrared Spectrum at  $90^\circ\text{C}$ .

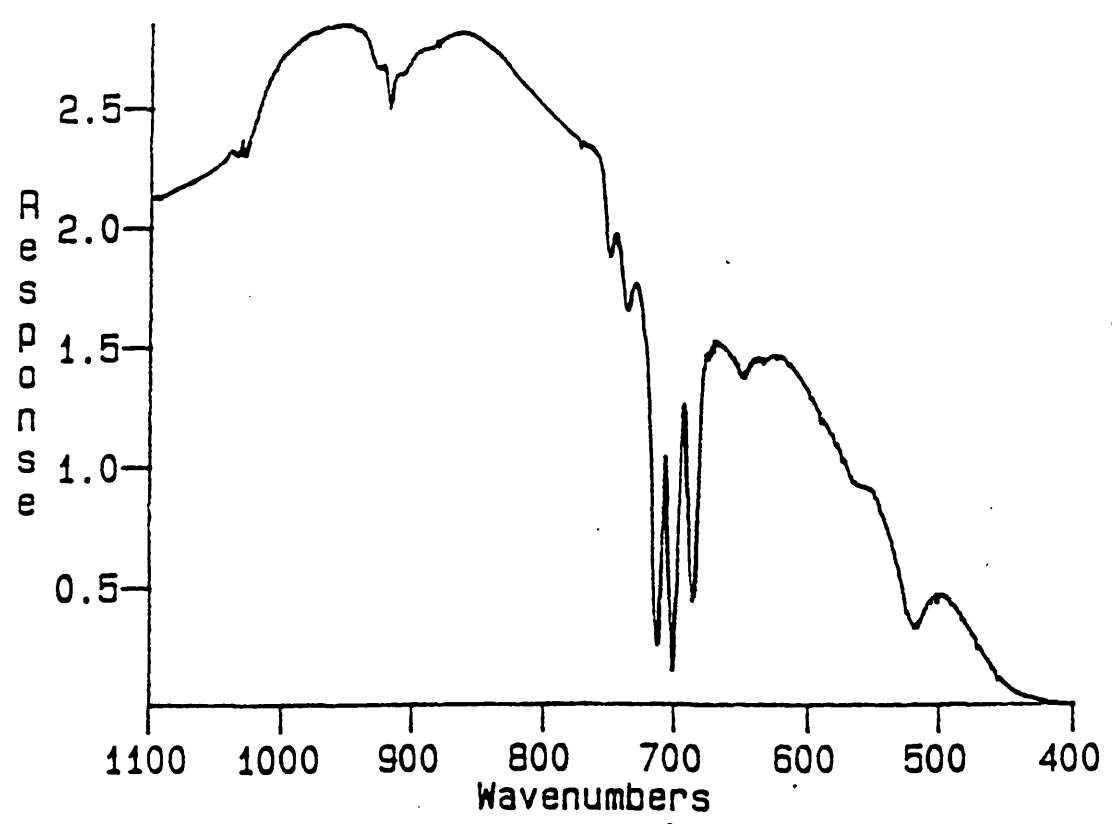


Figure 3.4: The  $\text{RuF}_5 \cdot \text{TaF}_5$  [1:3] Gas-Phase Infrared Spectrum at  $90^\circ\text{C}$ .

the two compounds are isomorphous, whilst that of  $\text{RuF}_5:\text{TaF}_5$  [1:1] shows slight differences in line spacings, indicating a similar but not identical structure.

The powder pattern of  $\text{RuF}_5:\text{TaF}_5$  [3:1] shows that this material is poorly crystalline even after sublimation. Careful comparison of this weak pattern with that of  $\text{TaF}_5$  shows that they are similar, but that all the lines on the  $\text{RuF}_5:\text{TaF}_5$  [3:1] pattern are more widely spaced. This implies a smaller unit cell for  $\text{RuF}_5:\text{TaF}_5$  [3:1] than  $\text{TaF}_5$ , which in turn implies a smaller tetramer. This is supported by the Ta  $L_{III}$ -edge EXAFS studies of this compound (see Chapter 6).

### 3.8 X-ray Single Crystal Diffraction Studies

X-ray crystal data have been collected and solved for single crystals, grown by sublimation, of  $\text{RuF}_5:\text{TaF}_5$  [1:1] and [1:3]. Both compounds are monoclinic, space group  $C2/m$  with tetrameric structures similar to that of  $\text{TaF}_5$ . A brief summary of the crystallographic data is shown in Table 3.6 for reference purposes.

#### 3.8.1 The $\text{RuF}_5:\text{TaF}_5$ [1:3] Structure

Some selected bond lengths and angles from this structure determination are shown in Table 3.7, along with those from related structures. The structure is tetrameric (see Figure 2.12), with an  $M-F_b-M$  bond angle of  $173.8(11)^\circ$ , which is comparable to that of  $171.3(8)^\circ$  for  $\text{TaF}_5$ . This is not surprising if it is assumed that there is only one Ru atom per tetramer, the other three atoms being Ta, which dominate the structure. The structure determination has been solved using an averaged situation for the metal site occupancy, between Ru and Ta, in the appropriate ratio. This apparent metal-site disorder is similar to that for  $\text{NbF}_5:\text{TaF}_5$  [3:1], [1:1] and [1:3] and is discussed in Chapter 2.

It should be noted that, because the structure is solved in space group  $C2/m$ ,

Figure 3.6: Data From Crystallographic Analysis of  $\text{RuF}_5\text{TaF}_5$  [1:1] and [1:3]

Compound	$\text{RuF}_5\text{TaF}_5$ [1:1]	$\text{RuF}_5\text{TaF}_5$ [1:3]
Formula*	$\text{F}_{20}\text{Ru}_2\text{Ta}_2$	$\text{F}_{20}\text{RuTa}_3$
$M^*$	944.0	1023.9
Crystal Symmetry	Monoclinic	Monoclinic
Space Group	C2/m	C2/m
$a$ (Å)	9.564*	9.640(25)
$b$ (Å)	14.354*	14.48(4)
$c$ (Å)	5.090*	5.104(3)
$\beta$ (°)	96.03	96.11(2)
$V$ (Å <sup>3</sup> )	695	708
$Z$ †	2	2
Radiation Type	Mo-K $\alpha$	Mo-K $\alpha$
$D_c$ (gcm <sup>-3</sup> )	4.51	4.80
$F(000)$	828	886
Crystal Size (mm)	*	.25 × .16 × .15
$\mu(\text{Mo-K})$ (cm <sup>-1</sup> )	171.7	232.7
Scan Width	4 circle learnt profile	$(1.6 + 0.7 \sin \mu / \tan \mu)^\circ$
Scan Type	$\omega$	$\omega$
Max. Bragg Angle (°)	*	54
Reflections Collected	732	816
No. of Unique Reflections	681	695
No. of Variables	34	60
$R = [\Sigma( F_o  -  F_c ) / \Sigma F_o ]$	0.091	0.061
$R_w = [\Sigma w( F_o  -  F_c )^2 / \Sigma w F_o ^2]^{0.5}$	0.058	
Weighting Parameter (g) ‡	0.018	0.0005
Max. Electron Density/e (Å <sup>-3</sup> )	-14-8.7	-8.0-3.6
Max. Final Shift/ e.s.d.	0.003	1.47

\* Refers to the molecular ratio of the adduct, with  $Z=2$  equivalent.

† Refers to the averaged  $\text{M}_2\text{F}_{10}$  unit as C2/m.

‡ Weighting  $w = 1/[\sigma^2(F) + g(F)^2]$ .

\* Data limited as collected at Edinburgh University.

Table 3.7: Selected Bond Lengths and Angles For  $\text{RuF}_5$ ,  $\text{TaF}_5$  and  $\text{RuF}_5:\text{TaF}_5$  [3:1], [1:1] and [1:3] from X-ray Single Crystal Studies.

Data	$(\text{RuF}_5)_4$ [5]	$\text{RuF}_5:\text{TaF}_5^*$ [1:1]	$\text{RuF}_5:\text{TaF}_5$ [1:3]	$(\text{TaF}_5)_4^\dagger$
$M_1\text{-F}_{eq}$ (Å)	1.796(1)	1.792(19)	1.867(25)	1.790(13)
$M_1\text{-F}_{ax}$ (Å)	1.819(1)	1.830(14)	1.878(25)	1.873(10)
$M_1\text{-F}_b$ (Å)	1.997(1)	2.050(14)	2.080(19)	2.070(12)
$M_2\text{-F}_{eq}$ (Å)	1.796(1)	1.809(18)	1.781(15)	1.822(12)
$M_2\text{-F}_{ax}$ (Å)	1.824(1) <sup>‡</sup>	1.85(3)	1.858(13)	1.862(25)
		1.842(18)	1.83	1.884(20)
$M_2\text{-F}_b$ (Å)	2.005(1)	2.075(13)	2.056(20)	2.071(12)
$M_1\text{-F}_b\text{-}M_2$ (°)	138.82(6) <sup>‡</sup>	167.4(10)	173.8(11)	171.3(8)

\* Data collected at Edinburgh University.

† Data redetermined as part of this thesis (see Chapter 2).

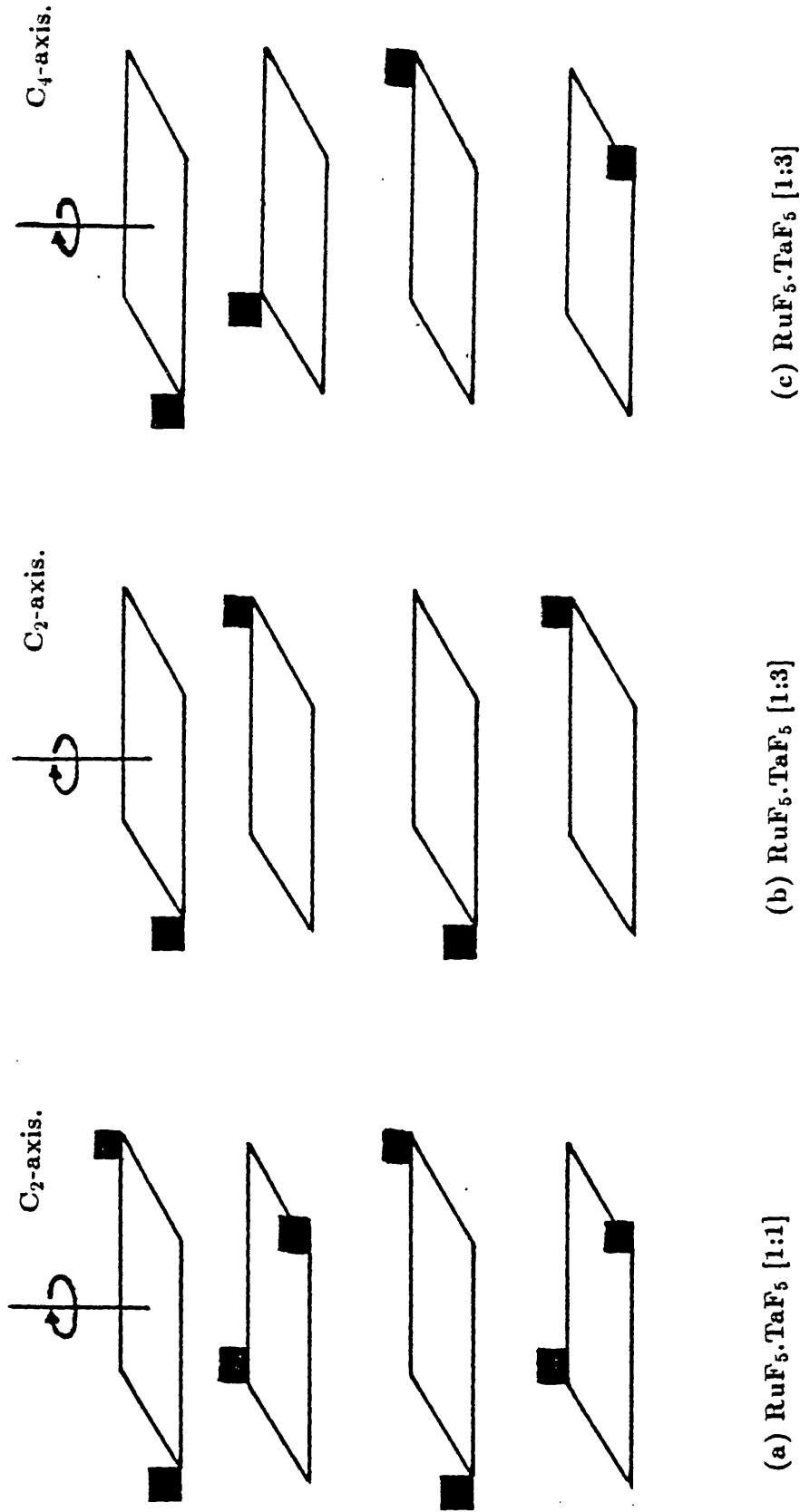
‡ Average value.

there are only two different metal sites in the structure solution, such that opposite corners of the tetramer are alike. The other metal site is then at the corner along one edge of the tetramer.

Close inspection of the bond lengths at the two metal sites ( $M_1$  and  $M_2$ ) shows that for the second metal site  $M_2$ , the  $M\text{-F}_{eq}$  bond length of 1.781(15) Å is shorter than the average  $M\text{-F}_{ax}$  distance of 1.84(3) Å. This is expected [5], as  $\text{Ru}^{5+}$  is  $d^3$  and  $\text{Ta}^{5+}$  is  $d^0$ . This is also the case for the first metal site  $M_1$ , but here the values are much more similar and are the same within experimental error.

A second difference between sites  $M_1$  and  $M_2$ , is that the  $M\text{-F}_t$  bond lengths for  $M_1$  are generally longer than those for  $M_2$  (average values are 1.873(25) and

Figure 3.5: Possible Superlattice Arrangements For  $\text{RuF}_5\cdot\text{TaF}_5$  [1:1] and [1:3] (Assuming Ordered Metal Sites).



1.820(30) Å respectively). There is also a difference in the M-F<sub>b</sub> distance for M<sub>1</sub> and M<sub>2</sub>. The M<sub>1</sub>-F<sub>b</sub> distance is 2.080(19) Å while the M<sub>2</sub>-F<sub>b</sub> distance is 2.056(20) Å. These values and those for the M-F<sub>t</sub> can also be considered to be the same within experimental error. However, on the assumption that these differences (though small) are real, the values can be compared to those for RuF<sub>5</sub> and TaF<sub>5</sub>. For TaF<sub>5</sub>, the average M-F<sub>t</sub> and M-F<sub>b</sub> distances are 1.853(20) and 2.070(9) Å and for RuF<sub>5</sub> they are 1.808(1) and 2.001(1) Å. It is, therefore, tentatively suggested that the metal site M<sub>1</sub> is more like those found in TaF<sub>5</sub>, while M<sub>2</sub> is more like those found in RuF<sub>5</sub>. This, in turn, may imply that although the metal site M<sub>1</sub> may not contain Ta atoms throughout the whole crystal, it may indeed be dominated by Ta atoms. This leads to a situation for the M<sub>2</sub> site which would be expected to have a metal site occupancy of 50% Ta atoms and 50% Ru atoms to make up the overall 1:3 ratio of Ru:Ta in the compound. However, as the M<sub>1</sub> site is not totally Ta atoms the M<sub>2</sub> site, in the crystal, might have a Ru:Ta ratio approaching 1:1, but with a slight excess of Ta atoms. This would lead to a situation where there would be three Ta atoms and one Ru atom in each tetramer in the lattice, but the Ru atom would not occupy the same metal atom throughout the lattice. Instead there would be a superlattice arrangement as shown in Figure 3.5b.

### 3.8.2 The RuF<sub>5</sub>:TaF<sub>5</sub> [1:1] Structure

Some selected bond lengths and angles from the RuF<sub>5</sub>:TaF<sub>5</sub> [1:1] crystal structure determination are shown in Table 3.7. The data shows that the compound is tetrameric and similar to that of TaF<sub>5</sub> (ie. monoclinic, space group C2/m). The two metal sites in the tetramer (M<sub>1</sub> and M<sub>2</sub>) can be considered to be the same when the error margins on the bond lengths and angles are taken into account. The average M-F<sub>b</sub>-M bond angle in this structure is 167.4(10)°, which reflects the fact that, assuming there are ordered metal sites, there are two Ru atoms and two Ta atoms in each tetramer. This represents a distortion of the TaF<sub>5</sub> structure and corresponds to an M-M° distance of 4.100 Å, compared with 4.129 Å for TaF<sub>5</sub>. These values can be compared to 138° and ≈ 3.7 Å for RuF<sub>5</sub>, respectively.

For both the  $M_1$  and  $M_2$  sites of the unit cell, the  $M-F_{eq}$  bond lengths (1.792(19) Å and 1.809(18) Å respectively) are shorter than the  $M-F_{ax}$  bond lengths, 1.830(14) Å and 1.828(20) Å respectively. These values can be considered the same within experimental error but, assuming the differences are real, then this is the situation which would be expected regardless of whether each site contained 100% Ta atoms or 100% Ru atoms [5].

If the metal sites are ordered, but the tetramers are not, then this would result in a superlattice arrangement of tetramers and an apparently random arrangement of metal atoms in the crystal structure determination. This is illustrated in Figure 3.5a. These structures are influenced by the packing of the atoms and so it would not be surprising if this compound formed a superlattice (Figure 3.5a), in order to accommodate the different ionic radii of  $Ru^{5+}$  (0.575 Å [67]) and  $Ta^{5+}$  (0.64 Å [67]) with a minimum distortion of the lattice.

### 3.9 Conclusions

It is unfortunate that it has not been possible to record the mass spectra of the  $RuF_5:TaF_5$  compounds. If the opportunity to record the mass spectra of these materials becomes available it would be very interesting to do so, especially bearing in mind the fact that the gas-phase infrared spectroscopy only shows limited evidence for mixed-metal species. Because of the lack of mass spectral and gas-phase infrared data, the only other evidence for the presence of mixed-metal tetramers is the Ta  $L_{III}$ -edge EXAFS of  $RuF_5:TaF_5$  [3:1] (Chapter 6), and the fact that the X-ray single crystal structure determinations of  $RuF_5:TaF_5$  [1:1] and [1:3] are not an average between those of  $RuF_5$  and  $TaF_5$ .

The characterisation of  $RuF_5:TaF_5$  [3:1], [1:1] and [1:3] in the solid state has proved more successful. The infrared spectra of solid, powdered samples show that all the  $RuF_5:TaF_5$  mixed-metal pentafluorides are fluorine-bridged, with peaks at

values intermediate between those of  $\text{RuF}_5$  and  $\text{TaF}_5$ , indicating their origin in the stretches and bends of the tetramer as a whole. This is reinforced by the Raman spectra of  $\text{RuF}_5:\text{TaF}_5$  [3:1] and [1:1] which, rather than being made up of the  $\text{RuF}_5$  and  $\text{TaF}_5$  Raman spectra superimposed on each other, are similar to each other but very different from those of either  $\text{RuF}_5$  or  $\text{TaF}_5$ . This implies a completely different bonding situation in the mixed-metal tetramers. This might be expected on mixing the  $\text{RuF}_5$  and  $\text{TaF}_5$ . For instance, the fluorine bridging in  $\text{TaF}_5$  is believed to be closer to being ionic than that of  $\text{RuF}_5$  [59, 80], and the terminal fluorine bonds are longer in the former than in the latter (1.853(20) Å versus 1.808(1)Å).

The X-ray powder diffraction patterns of  $\text{RuF}_5:\text{TaF}_5$  [3:1], [1:1] and [1:3] show that all these structures are based on that of  $\text{TaF}_5$ , and that there is an increasing distortion of the  $\text{TaF}_5$  structure in the series  $\text{RuF}_5:\text{TaF}_5$  [1:3] to [1:1] to [3:1]. This is to be expected bearing in mind the increased proportion of  $\text{RuF}_5$  units compared to  $\text{TaF}_5$ , across the series. The pattern of this distortion is most clearly shown by the M-F<sub>b</sub>-M bond angle. For  $\text{TaF}_5$ , this is 171.3(8)° and across the series  $\text{RuF}_5:\text{TaF}_5$  [3:1], [1:1] and [1:3], the corresponding values are 173.8(11)°, 167.4(10)° and 164°, respectively. The value for  $\text{RuF}_5:\text{TaF}_5$  [3:1] is based on the EXAFS spectrum, along with a number of assumptions and so cannot be considered to be as accurate as the crystal structure values.

The domination of the  $\text{RuF}_5:\text{TaF}_5$  structures by the  $\text{TaF}_5$  units present is extremely interesting from the point of view of why the different transition-metal pentafluoride structures are adopted. All the explanations of the structures based on  $\pi$ -bonding and/or fluorine bridging would predict that the  $\text{RuF}_5:\text{TaF}_5$  [3:1] structure would be based on that of  $\text{RuF}_5$ . This then leads to the suggestion that the packing of the atoms has a greater influence on these structures than was previously thought to be the case. This is discussed further in Chapter 7.

The crystal structure determination of  $\text{RuF}_5:\text{TaF}_5$  [1:3] seems to imply limited ordering of metal sites. The metal site  $M_1$  seems to be dominated by Ta atoms,

while  $M_2$  is occupied by approximately 50% Ru atoms and 50% Ta atoms. That these compounds have ordered metal sites is further supported by the Ta  $L_{III}$ -edge EXAFS of  $RuF_5:TaF_5$  [3:1], where the two metal atoms at the nearest metal sites to the Ta atom are confirmed as being Ru atoms. However, there is no apparent ordering of the metal sites from the  $RuF_5:TaF_5$  [1:1] crystal data, though this would still be the case if the two Ru and two Ta atoms in each tetramer were arranged as shown in Figure 3.5a. This fact can only be confirmed by the use of a localised structural probe, for instance, a complete analysis of each of the structures using EXAFS or solid-state NMR spectroscopy.

It has not been possible to assess the relative Lewis acidities of  $RuF_5$  and  $TaF_5$  as had been hoped originally, because of the random metal site occupancies in the crystal structures. However, a study of these compounds using a localised probe may give some indication of this, also.

## Chapter 4

# The Preparation and Characterisation of $\text{VF}_5:\text{TaF}_5$ [3:1], [1:1] and [1:3].

### 4.1 Introduction

Mixed-metal pentafluorides containing V and Ta have been prepared and characterised by XRF analysis, vibrational spectroscopy, EXAFS (see Chapter 6) and X-ray diffraction. The compounds are of particular interest as  $\text{TaF}_5$  forms a near-linear fluorine-bridged tetramer, and  $\text{VF}_5$  a fluorine-bridged endless chain, and it is hoped that mixed-metal compounds may yield further information about the arrangement of atoms in the parent pentafluorides, whilst the differing ionic sizes and atomic weights of Ta and V may present fewer difficulties in identifying the different metal sites within any single crystals formed and studied by X-ray diffraction. This has previously not been possible for the  $\text{RuF}_5:\text{TaF}_5$  and  $\text{NbF}_5:\text{TaF}_5$  single crystals. On the basis of the fact that the  $\text{RuF}_5:\text{TaF}_5$  solids are dominated by the Ta atoms (ie. they all formed tetramers), the  $\text{VF}_5:\text{TaF}_5$  materials have been prepared with V:Ta ratios of [3:1], [1:1] and [1:3].

The chemical reactivities of  $\text{VF}_5$  and  $\text{TaF}_5$  show similarities in that both com-

pounds form adducts with amines [107, 116, 117]. There are also some significant differences. For instance,  $\text{VF}_5$  appears to form  $\text{VF}_4^+ \text{X}^-$  salts far more readily than  $\text{TaF}_5$ , which suggests that although  $\text{VF}_5$  can act as a Lewis acid, it is a weaker one than  $\text{TaF}_5$  [118–120]. This may have some effect on the nature of the compounds formed between these materials.

The gas phase of  $\text{VF}_5$  is believed to be monomeric [17, 121, 122], whilst at  $\approx 90^\circ\text{C}$   $\text{TaF}_5$  is trimeric [10, 19]. The reasons for this difference are not yet fully understood, but studying the gas phase of any mixed species would therefore be of interest and the characterisation of any such species would have special relevance to the CVD work described in Chapter 8.

## 4.2 Preparation

$\text{VF}_5:\text{TaF}_5$  [3:1], [1:1] and [1:3] have been prepared as described in Chapter 9. The materials have been stored in stoppered, pre-seasoned 6mm FEP tubes in a dry box and samples transferred to the relevant pieces of apparatus for analysis.

## 4.3 X-ray Fluorescence Analysis

The results of the X-ray fluorescence analysis are shown in Table 4.1, along with the XRF analysis of intimately mixed V and Ta powders, for comparison. The data confirms the overall metal-atom ratio for  $\text{VF}_5:\text{TaF}_5$  [1:1]. Unfortunately, the single crystal for which X-ray diffraction data is reported in Section 4.8 has not been available for analysis, as the X-ray data was collected at Edinburgh University. Although the data are quoted to 2 decimal places, the values are  $\approx \pm 4\%$ .

Table 4.1: X-ray Fluorescence Data for  $\text{VF}_5:\text{TaF}_5$  [1:1] and V/Ta Metal Powder Samples.

Sample	V Expected (%)	Ta Expected (%)	V Found (%)	Ta Found (%)
$\text{VF}_5:\text{TaF}_5$ [1:1]	50	50	48.26	51.74
V.Ta Metal Powders				
V:Ta Ratio [3:1]	75	25	71.0	29.0
V:Ta Ratio [1:1]	50	50	42.8	57.2
V:Ta Ratio [1:3]	25	75	29.8	70.2

#### 4.4 Solid-Phase Infrared Spectroscopy

The solid-phase infrared spectroscopy has been recorded on selected  $\text{VF}_5:\text{TaF}_5$  compounds and the results are shown in Table 4.2. The data are shown for solid, powdered samples, for gaseous  $\text{VF}_5$  and also for  $\text{VF}_5$  held in a matrix at 12K [123]. The spectrum for solid  $\text{VF}_5$  is not shown as this would have required a far more sophisticated experiment and the  $\text{VF}_5$  data is shown only for comparison. There is evidence in some of the infrared spectra, and in some of the Raman spectra also, for a peak at  $1029\text{ cm}^{-1}$ , which is assigned to a metal oxide species, probably formed by contact with the air around the edge of the sample. However, the bulk of the sample appears not to be affected. This sensitivity to oxygen may indicate the need to handle these materials in fluorinated plastic containers rather than Pyrex glass.

##### 4.4.1 $\text{VF}_5:\text{TaF}_5$ [1:1]

The data for  $\text{TaF}_5$  and  $\text{VF}_5:\text{TaF}_5$  [1:1] show that both exhibit a fluorine-bridging mode at  $512$  and  $535\text{ cm}^{-1}$  respectively. This would be expected as the latter compound has been found to exhibit a  $\text{TaF}_5$ -like structure from X-ray diffraction work (see Section 4.8). It is surprising that there are no peaks at around  $800\text{ cm}^{-1}$ , which

Table 4.2: Infrared Frequencies of Solid, Powdered Samples of TaF<sub>5</sub>, VF<sub>5</sub>:TaF<sub>5</sub> [3:1], [1:1] and those of VF<sub>5(g)</sub> for Comparison (cm<sup>-1</sup>).

VF <sub>5</sub> [121]	VF <sub>5</sub> :TaF <sub>5</sub> [3:1]	VF <sub>5</sub> :TaF <sub>5</sub> [1:1]	TaF <sub>5</sub>
	1029 w	1029 w	
810 s	821 s		
784 s	799 s		
	792 s		
	753 s		753 s
		745 s	
	720 m		723 m
	674 m		667 m,br
	644 m		
		578 s	579 s
		535 m,br	512 m,br

might be expected for V-F stretching frequencies. However, it may be that these bands occur at very different frequencies when VF<sub>5</sub> is held in a lattice dominated by Ta atoms. This implies that even the V-F bonding is affected by the domination of the Ta atoms. This is perhaps not all that surprising as VF<sub>5</sub>, in the absence of TaF<sub>5</sub>, is monomeric at a similar temperature [121] and thus can be considered to have very different V-F bonding.

#### 4.4.2 VF<sub>5</sub>:TaF<sub>5</sub> [3:1]

The infrared spectrum of this compound shows a series of bands at  $\approx 800$  cm<sup>-1</sup>, which are assigned to a discreet VF-containing species. There may be some evidence for solid TaF<sub>5</sub> present in the sample with a sharp peak at 752 cm<sup>-1</sup> and a shoulder at 720 cm<sup>-1</sup>. However, the very strong 579 cm<sup>-1</sup> band for TaF<sub>5</sub> is not observed. If TaF<sub>5</sub> is present, then it may be as an impurity formed during preparation, as heating VF<sub>5</sub>.TaF<sub>5</sub> [1:3] causes it to decompose, and the spectrum was recorded on

the bulk material from the initial preparation.

The Ta  $L_{III}$ -edge EXAFS spectrum of this compound (see Chapter 6) suggests a discreet  $TaF_6^-$  unit, possibly with a  $V_3F_{14}^+$  counterion. Since the infrared spectrum seems to suggest that there is discreet, solid-phase  $VF_5$  species present, the occurrence of  $TaF_6^-$  might reasonably be expected. However, this would be expected to exhibit two bands in the infrared at 560 and 240  $cm^{-1}$  [124], the latter of which is obscured by the cut-off of the KBr plates at  $\approx 400\text{ cm}^{-1}$ . Unfortunately, there is also a series of very strong, broad peaks between 700 and 500  $cm^{-1}$ , which are believed to obscure the 560  $cm^{-1}$  peak. There is also no fluorine-bridging mode visible ( $\approx 500\text{ cm}^{-1}$ ), presumably for the same reason. These broad peaks may be due to further V-F stretching modes, or to  $TaF_5$  impurity from the initial preparation, but the lack of the strong 579  $cm^{-1}$  peak, seen in spectrum of pure  $TaF_5$  would not be predicted.

## 4.5 Raman Spectroscopy

The Raman spectroscopic data for  $VF_5:TaF_5$  [1:1] is shown in Table 4.3, along with that for  $TaF_5$  and  $VF_5$ . The Raman spectrum of  $VF_5:TaF_5$  [1:3] has not been recorded, whilst attempts to investigate the [3:1] compound by FT Raman have not been successful.

There are similarities between the [1:1] spectrum and its infrared spectrum in that there is not a series of peaks at around 800  $cm^{-1}$ , which might be expected for a discreet  $VF_5$  species. The spectrum appears closely related to that of  $TaF_5$  but there are additional bands, notably at 763, 364 and 343  $cm^{-1}$ . This is in keeping with the fact that this material is isostructural with  $TaF_5$ , but with different bonding within the tetramer, due to the V atoms. There may be further bands around 757  $cm^{-1}$ , as this band is very much broader than the corresponding one in  $TaF_5$ . Unfortunately, the spectrum is rather noisy and so some weaker peaks may not be visible. FT-Raman experiments confirm the frequencies from these spectra. At lower frequencies, the [1:1] spectrum seems to be a combination of those of  $VF_5$

Table 4.3: Raman Spectra of  $\text{VF}_5$ ,  $\text{TaF}_5$  and  $\text{VF}_5:\text{TaF}_5$  ( $\text{cm}^{-1}$ ).

$\text{VF}_5$ [121]	$\text{VF}_5\text{TaF}_5$ [1:1]	$\text{TaF}_5$
	1038 <sup>†</sup> w	
	1033 <sup>†</sup> w	
810	763 sh	
	757 s,br	757 s
719	727w	725 m
	700 m	697 m
		646 w
608		
	364 vw	
350	343 w	
282	272 m	272 m
	234 w	236 w
	222 vw	222 vw
$\approx 200$		

<sup>†</sup> Assigned to slight  $\text{VOF}_3$  impurity.

Table 4.4: Gas-Phase Infrared Frequencies ( $\text{cm}^{-1}$ ) for  $\text{VF}_5$ ,  $\text{VOF}_3$ ,  $\text{TaF}_5$ ,  $\text{VF}_5:\text{TaF}_5$  [1:1] and [1:3] at  $\approx 90^\circ\text{C}$  ( $\text{cm}^{-1}$ )

$\text{VF}_5$ [121]	$\text{VOF}_3$ [125]	$\text{VF}_5:\text{TaF}_5$ [1:1]	$\text{VF}_5:\text{TaF}_5$ [1:3]	$\text{TaF}_5$
	1057 m	1057 m	1057 m	
810 s		810 s	811 s	
	806 s	805 s	805 s	
784 s	792 m			
		753 w	753 w	751 w*
		739 w	739 w	739 w*
	721 m	721 m	721 m	
		714 m	714 m	714 m
		703 m	703 m	703 m
		687 m	687 m	687 m
		520 w	557 vw	520 w

\* Assigned to non-gas phase species.

and  $\text{TaF}_5$  with bands at  $\approx 350 \text{ cm}^{-1}$ ,  $270 \text{ cm}^{-1}$  and  $230 \text{ cm}^{-1}$ .

## 4.6 Gas-Phase Infrared Spectroscopy

The gas-phase infrared frequencies for  $\text{TaF}_5$ ,  $\text{VF}_5$ ,  $\text{VF}_5:\text{TaF}_5$  [1:1] and [1:3] are shown in Table 4.4 and the spectra in Figures 2.7, 4.1, 4.2 and 4.3, respectively. The spectrum of  $\text{TaF}_5$  has already been discussed (Chapter 2), whilst gaseous  $\text{VF}_5$  is believed to be monomeric [121, 122]. Despite extensive pre-seasoning of the gas cell with  $\text{F}_2$  and  $\text{ClF}_3$ ,  $\text{VOF}_3$  [125] is present in all of the spectra of the vanadium-containing species. This is illustrative of the extreme moisture and oxygen sensitivity of  $\text{VF}_5$  and the fact that elevated temperatures may cause leaks around the PTFE seals.

The gas phase above both  $\text{VF}_5:\text{TaF}_5$  [1:1] and [1:3] show evidence for a small

amount of  $\text{VF}_5(g)$ , even at room temperature. This may be due to slight decomposition of the samples at static vacuum, or to a slight excess of  $\text{VF}_5$ . On warming, the bands for  $\text{VF}_5$  increase in intensity, along with those for  $\text{VOF}_3$ . At  $\approx 60^\circ\text{C}$ , the  $\text{TaF}_5$  trimer is also present. There is no evidence in either spectra for mixed-metal species and the decomposition of the compounds, on heating, precludes their usage as precursors for CVD. However, thin layers containing Ta and V may still be formed by depositing  $\text{TaF}_5$  and  $\text{VF}_5$  together.

## 4.7 X-ray Powder Diffraction

The powder pattern of  $\text{VF}_5:\text{TaF}_5$  [1:3] shows it to be isomorphous with  $\text{TaF}_5$ , with little distortion of the latter structure. The corresponding [1:1] pattern shows that the arrangement of atoms in this compound is similar to that in  $\text{TaF}_5$ , but that there are some small differences in the spacings of the lines. This is confirmed by X-ray single crystal work.

## 4.8 X-ray Single Crystal Diffraction

The X-ray single crystal structural data of  $\text{TaF}_5$ ,  $\text{VF}_5$  and  $\text{VF}_5:\text{TaF}_5$  [1:1] are shown in Table 4.5 and the bond lengths and angles in Table 4.6.  $\text{VF}_5:\text{TaF}_5$  [1:1] is tetrameric and its structure is based on that of  $\text{TaF}_5$  structure. Unfortunately the data refines to a poor R-factor (13.2 %) which may be due to the fact that apparent M-F<sub>b</sub> bond lengths are an average of those of Ta-F<sub>b</sub> and V-F<sub>b</sub> in the crystal.

The compound contains  $\text{Ta}^{5+}$  and  $\text{V}^{5+}$  ions which have very different radii (0.64 Å and 0.54 Å [67], respectively). It might therefore be assumed that if the metal sites within the crystal are ordered, then this may be more apparent from the crystal data than for  $\text{NbF}_5:\text{TaF}_5$  or  $\text{RuF}_5:\text{TaF}_5$ , (for instance, from different M-F bond lengths) where the ionic radii of the metal ions are much more similar. The M-F<sub>t</sub> distances are all the same within the experimental error, but there is some evidence

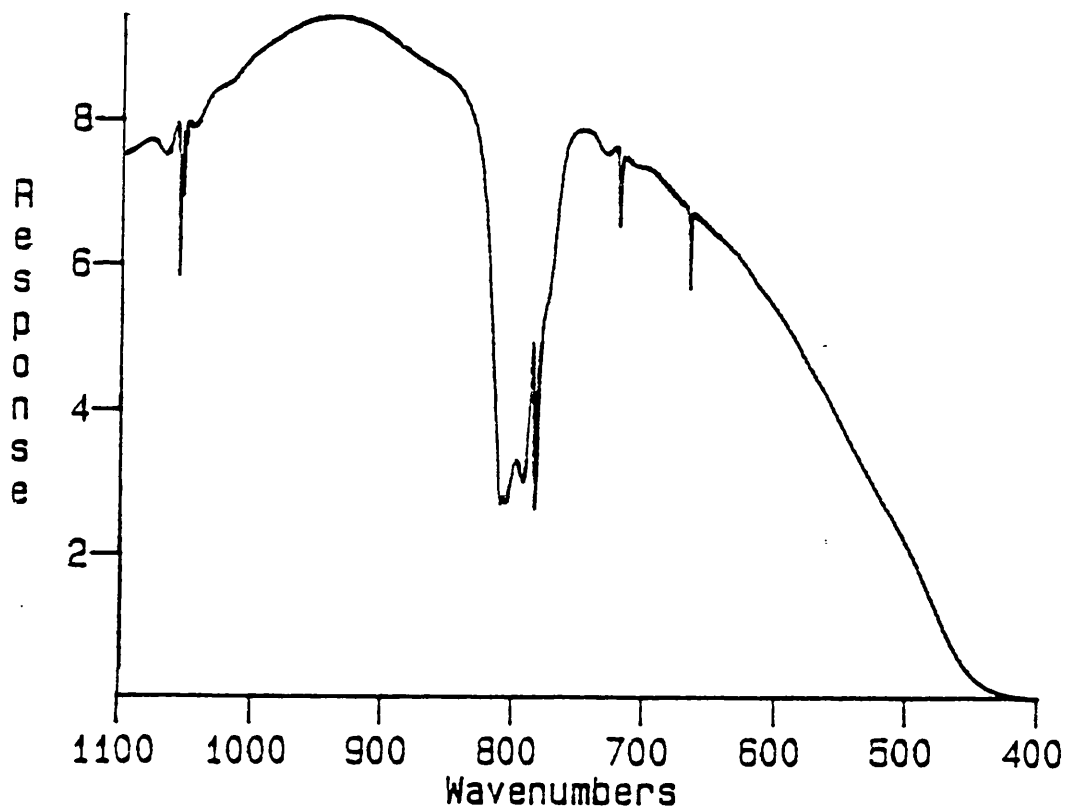


Figure 4.1:  $\text{VF}_5$  Gas-Phase Infrared Spectrum at  $17^\circ\text{C}$ .

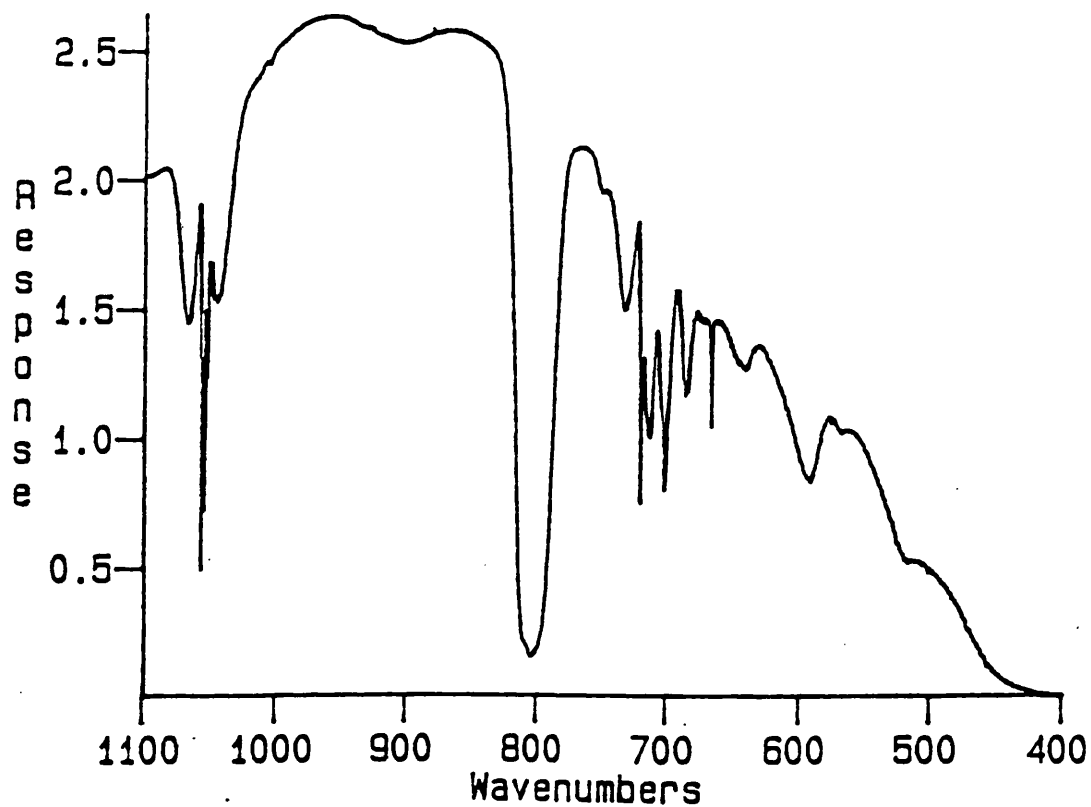


Figure 4.2: The  $\text{VF}_5\text{-TaF}_5$  [1:1] Gas-Phase Infrared Spectrum at  $90^\circ\text{C}$ .

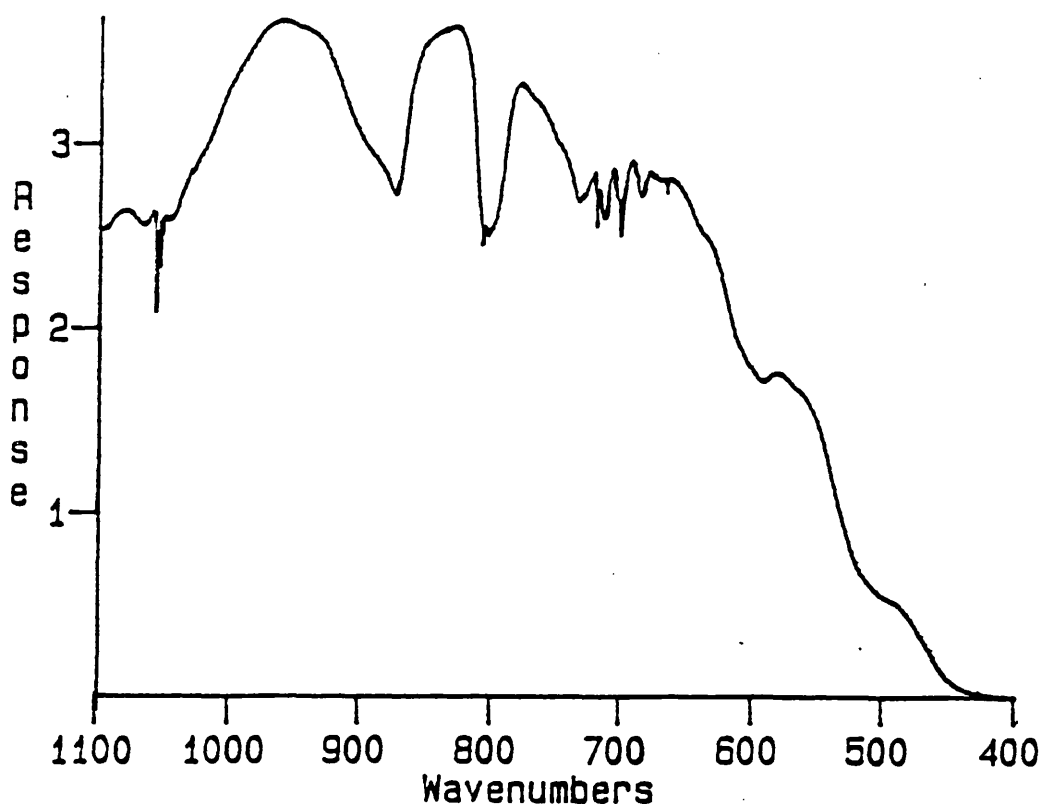


Figure 4.3: The  $\text{VF}_5 \cdot \text{TaF}_5$  [1:3] Gas-Phase Infrared Spectrum at  $90^\circ\text{C}$ .

for two different  $\text{M-F}_b$  bond lengths ( $2.10(3) \text{ \AA}$  and  $2.04(3) \text{ \AA}$ ). These values are the same within experimental error margins, but if this difference in the  $\text{M-F}_b$  bond lengths is real, this would be the first crystal structure evidence for asymmetric fluorine bridging in the mixed-metal pentafluorides.

It is not obvious whether the  $\text{TaF}_5$  or the  $\text{VF}_5$  units give rise to the longer  $\text{M-F}_b$  distance. It might reasonably be expected that, as  $\text{V}^{5+}$  is smaller than  $\text{Ta}^{5+}$ , the  $\text{V-F}_b$  distance would be the shorter. However, the Ta  $L_{III}$ -edge EXAFS of  $\text{VF}_5 \cdot \text{TaF}_5$  [3:1] (Chapter 6), suggests that this compound is of the form  $[\text{TaF}_6]^- [\text{V}_3\text{F}_{14}]^+$ , in which the Ta-F bond lengths are all much smaller than the V-F<sub>b</sub> distances of  $\approx 2.45 \text{ \AA}$ , which presumably tend towards being non-bonding distances. The smaller Ta-F distances are presumably due to the greater Lewis acidity of  $\text{TaF}_5$  over that of  $\text{VF}_5$ . When this thinking is applied to the  $\text{VF}_5 \cdot \text{TaF}_5$  [1:1] structure, it would seem reasonable that the shorter  $\text{M-F}_b$  bond lengths are for Ta-F<sub>b</sub>. This is supported by the Ta  $L_{III}$ -edge EXAFS (see Chapter 6) of this material which gives a Ta-F<sub>b</sub> bond

Table 4.5: Data From Crystallographic Analysis of  $\text{VF}_5\text{TaF}_5$  [1:1]

Compound	$\text{VF}_5\text{TaF}_5$ [1:1]
Formula*	$\text{F}_{20}\text{V}_2\text{Ta}_2$
$M^*$	843.7
Crystal Symmetry	Monoclinic
Space Group	$C2/m$
$a$ (Å)	9.631(5)
$b$ (Å)	14.449(7)
$c$ (Å)	5.093(3)
$\beta$ (°)	96.47(4)
$V$ (Å <sup>3</sup> )	704
$Z$ †	2
Radiation Type	Mo- $K\alpha$
$D_c$ (gcm <sup>-3</sup> )	3.98
$F(000)$	844
Crystal Size (mm)	.31 × .23 × .23
$\mu(\text{Mo-K})$ (cm <sup>-1</sup> )	228.1
Scan Width	4 circle learnt profile
Scan Type	$\omega$
Max. Bragg Angle (°)	*
Reflections Collected	488
No. of Unique Reflections	468
No. of Variables	36
$R = [\Sigma( F_o  -  F_c ) / \Sigma F_o ]$	0.1322
$R_w = [\Sigma w( F_o  -  F_c )^2 / \Sigma w F_o ^2]^{0.5}$	0.1324
Weighting Factor (g) ‡	0.0007
Max. Electron Density/e (Å <sup>-3</sup> )	-6.6–6.8
Max. Final Shift/ e.s.d.	0.476

\* Refers to the molecular ratio of the adduct, with  $Z=2$  equivalent.

† Refers to the averaged  $\text{M}_2\text{F}_{10}$  unit as  $C2/m$ .

‡ Weighting  $w = 1/[\sigma^2(F) + g(F)^2]$ .

\* Data limited as collected at Edinburgh University.

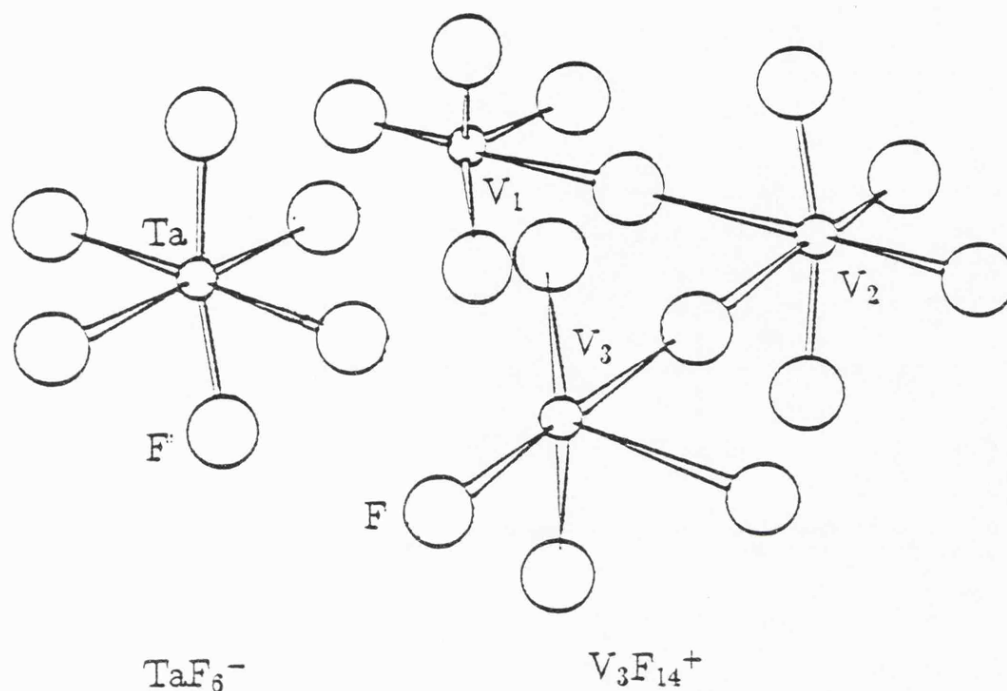


Figure 4.4: Suggested Structure for  $\text{VF}_5 \cdot \text{TaF}_5$  [3:1].

length of 1.973 Å. This is much shorter than either of the corresponding values from the crystal structure, but suggests that the Ta-F<sub>b</sub> distance is the shorter M-F<sub>b</sub>. However, this requires further information to be confirmed.

## 4.9 Conclusions

The vibrational spectroscopy of the solids shows that there is a complete change in the nature of the bonding on going from  $\text{VF}_5 \cdot \text{TaF}_5$  [1:1] to [3:1]. The [1:1] compound exhibits fluorine-bridging and is closely related to  $\text{TaF}_5$ , whereas the [3:1] compound shows bands attributed to a discrete  $\text{VF}_5$  derivative. It cannot be determined from this work whether there is fluorine-bridging or any  $\text{TaF}_6^-$  in this compound, as these modes would be hidden by other strong peaks in the spectrum. There may be some evidence, in an unpurified sample of  $\text{VF}_5 \cdot \text{TaF}_5$  [3:1], for  $\text{TaF}_5$ , but this could be removed by extensive pumping.

Table 4.6: Selected Bond Lengths and Angles For  $\text{VF}_5$ ,  $\text{TaF}_5$  and  $\text{VF}_5:\text{TaF}_5$  [1:1] from X-ray Single Crystal Work.

Data	$(\text{TaF}_5)_4$	$\text{TaF}_5 \cdot \text{VF}_5$ [1:1]	$\text{VF}_5$ [3]
$\text{M}_1\text{-F}_{(eq)}$ (Å)	1.790(13)	1.70(5)	1.68(1)
$\text{M}_1\text{-F}_{(ax)}$ (Å)	1.873(10)	1.75(4)	1.71(1)
$\text{M}_1\text{-F}_b$ (Å)	2.070(12)	2.04(3)	1.93(1)
$\text{M}_2\text{-F}_{(eq)}$ (Å)	1.822(12)	1.76(4)	1.65(1)
$\text{M}_2\text{-F}_{(ax)}$ (Å)	1.862(25)	1.72(5)	1.70(1)
$\text{M}_2\text{-F}_b$ (Å)	2.071(12)	2.10(3)	2.00(1)
$\text{M}_1\text{-F}_b\text{-M}_2$ (°)	171.3(8)	169.6(18)	149.6
Crystal Class	Mono	Mono	Orth
Space Group	C2/m	C2/m	Pmcn

Mono = Monoclinic.

Orth = Orthorhombic.

The gas-phase infrared spectra show that the [1:1] and [1:3] materials decompose on heating to form  $\text{VF}_5(g)$  and  $(\text{TaF}_5)_3(g)$ , which means that they would not be suitable as precursors for CVD. The decomposition of these materials also calls into question the suitability of using sublimation as a method of preparing single crystals for X-ray diffraction. This can certainly be ruled out for  $\text{VF}_5:\text{TaF}_5$  [3:1], as there does not appear to be any evidence of this subliming as ion pairs. For the [1:3] and [1:1] samples, the dominant species at the temperature of sublimation (40°C) is probably tetrameric. It may be that the tetramers are stable in the gas phase and it is their break-down to form trimers which initiates the decomposition to  $\text{VF}_5$  and  $\text{TaF}_5$ . If this is the case then the single crystal data for  $\text{VF}_5:\text{TaF}_5$  [1:1] can be considered to be correct. Unfortunately, the vapour pressure of the tetrameric species is too small to record a gas-phase infrared spectrum and so this cannot be investigated further by this technique, though mass spectrometry may offer a successful alternative. However, no  $\text{VF}_5$  forms on the upper surface of the tube when

the [1:1] and [1:3] compounds are sublimed which does occur for the [3:1] compound. Furthermore, XRF analysis confirms the correct stoichiometry for a sublimed [1:1] sample.

The very fact that these compounds decompose on heating may lend itself to a possible method of purifying Ta and V. For instance, if an ore contains both V and Ta, fluorination of the ground ore might yield a  $\text{VF}_5:\text{TaF}_5$  material, which on heating would decompose to  $\text{VF}_5$  and  $\text{TaF}_5$ . These could then be separated by fractional distillation.

The gas phase of the mixed-metal pentafluorides is interesting from the point of view that the thermal stability of the compounds seems to decrease across the series  $\text{NbF}_5:\text{TaF}_5 \rightarrow \text{RuF}_5:\text{TaF}_5 \rightarrow \text{VF}_5:\text{TaF}_5$ . This trend corresponds to an increase in the differences between the solid state structures of the two individual pentafluorides and is probably related to increasing differences in the bonding energy levels between the individual transition-metal pentafluorides.

Although the  $\text{VF}_5:\text{TaF}_5$  [x:y] compounds appear to be dominated by Ta atoms, this is not apparent in the [3:1] material where the  $\text{TaF}_5$  structure seems to be distorted to such a degree that  $\text{TaF}_6^- \text{V}_3\text{F}_{14}^+$  may be formed. A possible structure for this compound is illustrated in Figure 4.4, but is reported only tentatively and requires further evidence to be confirmed.

The main factors which seem to affect the nature of the solid state of  $\text{VF}_5:\text{TaF}_5$  [x:y] seem to be (a) the effect of the relative Lewis acidities of  $\text{VF}_5$  and  $\text{TaF}_5$  which result in changes in the bonding within the tetrameric unit, and (b) the packing of the atoms within the crystals. This is discussed further in Chapter 7.

## Chapter 5

# The Preparation and Characterisation of $\text{RuF}_5:\text{VF}_5$ [1:1], $\text{RuF}_5:\text{NbF}_5$ [3:1], [1:1] and [1:3].

### 5.1 Introduction

In addition to the compounds described elsewhere in this thesis, work is reported here for the materials mentioned above. This information is grouped together in this chapter because the data are not complete and so suggestions are made as to future experiments which might be valuable in this area.

#### 5.1.1 $\text{RuF}_5:\text{VF}_5$

The mixed-metal pentafluorides reported elsewhere in this thesis all contain a proportion of  $\text{TaF}_5$ , which dominates the majority of these structures.  $\text{RuF}_5:\text{VF}_5$  [1:1] is therefore interesting because no  $\text{TaF}_5$  is present. Thus, it seemed unlikely that this compound would adopt the  $\text{TaF}_5$  arrangement of atoms, but rather a combination of those of  $\text{RuF}_5$  and  $\text{VF}_5$ . This may be particularly important as it is believed that

the arrangement of atoms in  $\text{VF}_5$  more closely resembles that of  $\text{RuF}_5$  than  $\text{TaF}_5$  [3]. It was thought therefore that combining  $\text{RuF}_5$  and  $\text{VF}_5$  in the solid state might yield further insights into the precise nature of the parent pentafluorides themselves.

The chemical reactivities of  $\text{RuF}_5$  and  $\text{VF}_5$  show similarities in that they both exchange fluorine for chlorine on reaction with chlorofluorocarbons [126] and both form adducts with  $\text{XeF}_2$  [127] and [105] respectively. However, it seemed unlikely that they would have similar Lewis acid strengths and so putting the two into one material might indicate which is the stronger.

The possibility of using  $\text{RuF}_5:\text{VF}_5$  [1:1] as a precursor for CVD has been investigated by gas-phase infrared spectroscopy. The uses for RuV alloys may include, in the electronics industry for instance, metal contacts for semi-conductor devices. It is also known that both V and Ru are super-conducting at  $\approx 4\text{K}$  [128] and it may well be that an alloy of these metals would also exhibit this phenomenon. Much of the present research interest into super-conductors is involved in preparing novel materials which have a critical temperature,  $T_c$  (the temperature at which the electrical resistance of the superconductor drops to zero), nearer to room temperature. Although there has been interest in metals and alloys for this purpose, the bulk of the experimentation is now on compounds of the type  $\text{YBa}_2\text{Cu}_3\text{O}_{7-x}$ . Nonetheless, there may still be novel alloys of importance (which may include RuV alloys), which can be prepared with relative ease and control from the CVD of mixed-metal pentafluorides.

### 5.1.2 $\text{RuF}_5:\text{NbF}_5$

The  $\text{RuF}_5:\text{NbF}_5$  compounds should bear a close likeness to those of  $\text{RuF}_5:\text{TaF}_5$ . In order to collect high resolution EXAFS data, the Ru and Nb K-edge EXAFS have been recorded of  $\text{RuF}_5:\text{NbF}_5$  [1:1], to allow comparisons with  $\text{RuF}_5:\text{TaF}_5$  [1:1], whilst the [3:1] and [1:3] compounds have also been investigated to allow similar comparisons with the analogous  $\text{RuF}_5:\text{TaF}_5$  compounds. The main interest again is

centred on the bonding, structure, Lewis acidity comparisons and possible industrial importance of these materials.

## 5.2 The Preparation and Characterisation of $\text{RuF}_5:\text{VF}_5$ [1:1]

### 5.2.1 Preparation

$\text{RuF}_5:\text{VF}_5$  [3:1] and [1:1] have been prepared as detailed in Chapter 9 and stored in stoppered, pre-seasoned 6mm FEP tubes in a dry box. Samples have been analysed by XRF analysis, vibrational spectroscopy. X-ray diffraction and the results are detailed below.

### 5.2.2 X-ray Fluorescence Analysis

The XRF analysis of a sample of this compound gives Ru (55.3 %), as compared to 44.7 % for V, which confirms the expected metal ratio. The standardised samples of Ru and V powders have not been analysed as it is assumed, on the basis of the work detailed for the other mixed-metal pentafluorides, that the accuracy of this technique is  $\approx \pm 4$  %.

## 5.3 Solid-Phase Infrared Spectroscopy

The infrared data of  $\text{RuF}_5$ ,  $\text{VF}_5$  and  $\text{RuF}_5:\text{VF}_5$  [1:1] are detailed in Table 5.1. For  $\text{RuF}_5:\text{VF}_5$  [1:1], the frequencies can be grouped into three. Firstly, a group of two bands at 1385 and 1034  $\text{cm}^{-1}$ , which are believed to be due to a combination band and a metal oxide species respectively. The second group occur between 830 and 640  $\text{cm}^{-1}$  and are assigned to metal fluorine stretches, and the third set are a pair of fluorine-bridging modes at 542 and 525  $\text{cm}^{-1}$ . These last two bands constitute perhaps the most interesting part of the spectrum in that they imply that there are

Table 5.1: Infrared Frequencies of Solid, Powdered Samples of  $\text{RuF}_5$ ,  $\text{RuF}_5:\text{VF}_5$  [1:1] and  $\text{VF}_{5(g)}$  for Comparison ( $\text{cm}^{-1}$ ).

$\text{RuF}_5$	$\text{RuF}_5:\text{VF}_5$ [1:1]	$\text{VF}_{5(g)}$ [121]
	1384.8 w	
	1034 w	
	828 s	810 s
	792 s	784 s
743 w		
709 s,br	699 s	
654 s	645 w	
588 w,shp		
516 s,br	542 w	
	525 sh	
480 m	494 vw,sh	

two different metal sites within the compound. The bands at 828 and 792  $\text{cm}^{-1}$  are believed to be due to V-F stretching modes, whilst those for Ru-F are assigned to peaks at lower energies (for instance, the mode at 699  $\text{cm}^{-1}$ ). These values can be compared to those for  $\text{RuF}_{5(s)}$  and  $\text{VF}_{5(g)}$ , also in Table 5.1.

## 5.4 Gas-Phase Infrared Spectroscopy

There is some evidence for  $\text{VF}_5$  (spectrum shown in Figure 4.1) in the room temperature spectrum of  $\text{RuF}_5:\text{VF}_5$  [1:1], but bearing in mind the sensitivity of the spectrometer and the very small size of these peaks (compared to those at higher temperatures), these are assigned to either a small excess of  $\text{VF}_5$  or to some slight decomposition of the sample under static vacuum.

On warming the sample, the  $\text{VF}_5$  peaks increase in intensity and  $\text{VOF}_3$  [125] is

Table 5.2: Gas Phase Infrared Frequencies ( $\text{cm}^{-1}$ ) for  $\text{RuF}_5$ ,  $\text{RuF}_5:\text{VF}_5$  [1:1] at  $90^\circ\text{C}$  and  $\text{VF}_5(g)$  at  $17^\circ\text{C}$  for Comparison

$\text{RuF}_5$	$\text{RuF}_5:\text{VF}_5$ [1:1]	$\text{VF}_5(g)$ [121]
	1057 m	
	809 s	810 s
	793 s	
	783 s	784 s
749 m	731 sh	
721 m	721 m	
704 m	706 m	
659 w	658 w	
553 w,br	545 w,br	
	515 vw	

also observed (formed by partial hydrolysis). At  $90^\circ\text{C}$  (see Table 5.2 and Figure 5.1), there is evidence for the same species seen in the analogous  $\text{RuF}_5$  spectrum. Therefore, it is assumed that this material decomposes on heating to form monomeric  $\text{VF}_5$  and trimeric  $\text{RuF}_5$ . This may explain the colourless liquid which forms on the upper surface of the Pyrex tube (possibly this is  $\text{VF}_5$ ), when attempts are made to sublime this compound.

## 5.5 X-ray Powder Diffraction

The X-ray powder diffraction pattern of  $\text{RuF}_5:\text{VF}_5$  [1:1] resembles that of  $\text{RuF}_5$  at small  $\theta$ , but there are differences in the line spacings in that the lines are slightly closer together for this pattern compared to those of  $\text{RuF}_5$ . So  $\text{RuF}_5:\text{VF}_5$  [1:1] can be said to have an atomic arrangement based on that of  $\text{RuF}_5$ , but with some degree of distortion. The [1:1] pattern indicates that this sample has a unit cell larger

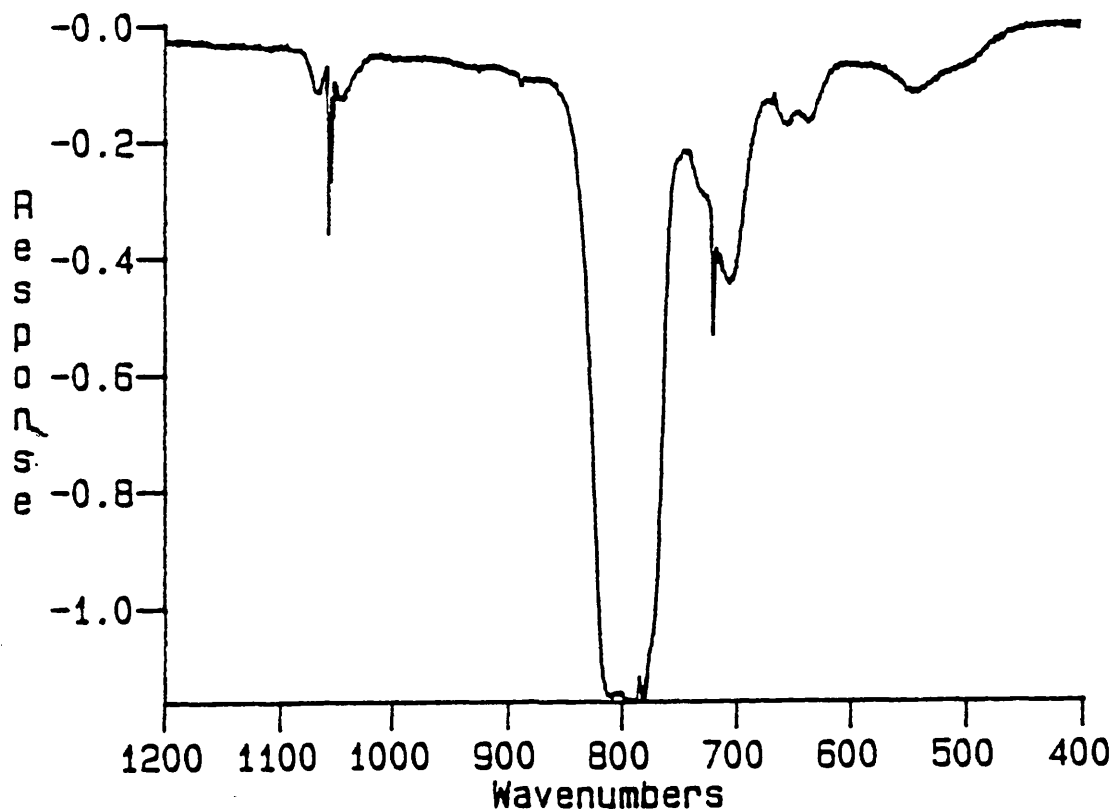


Figure 5.1:  $\text{RuF}_5\text{VF}_5$  [1:1] Gas-Phase Infrared Spectrum at  $90^\circ\text{C}$ .

than that of  $\text{RuF}_5$  and therefore, presumably, a larger tetramer. This ties in with the Ru K-edge EXAFS of this compound (see Chapter 6), where the Ru-V distance is  $3.873 \text{ \AA}$  as compared with  $\approx 3.7 \text{ \AA}$  for the analogous Ru-Ru $^\circ$  distance in  $\text{RuF}_5$  [5].

It is perhaps difficult, at first, to see why the replacement of two  $\text{Ru}^{5+}$  ions (radius  $0.575 \text{ \AA}$ ) by two  $\text{V}^{5+}$  ions (radius  $0.54 \text{ \AA}$ ) should result in an increase in the overall size of the tetramer. However, this is believed to be due to a departure of the M-F $_b$ -M bond angle from  $138^\circ$  in  $\text{RuF}_5$  to  $160^\circ$  (this value is calculated assuming the V-F $_b$  bond length to be  $1.96 \text{ \AA}$ , the average value in the  $\text{VF}_5$  structure [3]), and compares with  $149.7^\circ$  in  $\text{VF}_5$ . So it would appear that  $\text{VF}_5$  adopts a structure with a bond angle closer to that of  $\text{TaF}_5$  when in a lattice with  $\text{Ru}^{5+}$  ions, which are large enough to distort the octahedral holes of a theoretical, perfect lattice of fluorine ions ( $0.54 \text{ \AA}$ ). In  $\text{VF}_5$ , this is not the case. This is discussed further with respect to the  $\text{VF}_5$  structure in Chapter 7.

## 5.6 X-ray Single Crystal Studies

Ideally,  $\text{RuF}_5:\text{VF}_5$  [3:1], [1:1] and [1:3] should all be studied by single crystal X-ray work, but only the [3:1] has undergone preliminary investigation. However, the crystals were not of sufficiently high quality and so a full structure could not be calculated from them. No suitable single crystals of the [1:1] material have been obtained, as this decomposes on heating and attempts to grow crystals from HF solution have not been successful.

## 5.7 The Characterisation Of $\text{RuF}_5:\text{NbF}_5$ [3:1], [1:1] and [1:3]

### 5.7.1 Preparation

$\text{RuF}_5:\text{NbF}_5$  [3:1], [1:1] and [1:3] have been prepared as detailed in Chapter 9. Samples have been removed from stoppered, pre-seasoned 6mm FEP storage tubes and analysed. The results of this analysis are detailed below.

### 5.7.2 The Solid-Phase Infrared Spectroscopy

The infrared spectrum of powdered samples of  $\text{RuF}_5$ ,  $\text{NbF}_5$ ,  $\text{RuF}_5:\text{NbF}_5$  [3:1] and [1:3] are shown in Table 5.3. All the spectra exhibit a series of bands between 750 and 660  $\text{cm}^{-1}$ , assigned to M-F stretches, and a second group at 550–500  $\text{cm}^{-1}$  associated with fluorine-bridging modes. The spectra of  $\text{RuF}_5$  and  $\text{NbF}_5$  are fairly similar as are those of the mixed-metal pentafluorides formed by them. However, the spectrum of  $\text{RuF}_5:\text{NbF}_5$  [3:1] more closely resembles that of  $\text{RuF}_5$  than  $\text{NbF}_5$  and vice-versa for the [1:3] compound as expected. Because of the close similarities very little can be determined from the spectra except to say that they do not appear to be made up of frequencies associated with the individual metal-pentafluoride tetramers. There is also a weak band in both the [1:3] and [3:1] spectra at 1010  $\text{cm}^{-1}$  which is probably due to a metal oxide species formed by partial hydrolysis of the

Table 5.3: Infrared Frequencies of Solid, Powdered Samples of  $\text{RuF}_5$ ,  $\text{NbF}_5$ ,  $\text{RuF}_5:\text{NbF}_5$  [3:1] and [1:3] ( $\text{cm}^{-1}$ ).

$\text{RuF}_5$	$\text{RuF}_5:\text{NbF}_5$ [3:1]	$\text{RuF}_5:\text{NbF}_5$ [1:3]	$\text{NbF}_5$
	1010 w	1008 w	
743 w	735 w,br	748 m	748 m 723 w,sh
709 s,br	714 s 699 sh 682 sh	705 s 680 m	708 m 692 vw 667 s
654 s	652m	655 ms	661 s
588 w,shp			
516 s,br	544 w,br	504 m,br	498 s
480 m			

sample.

### 5.7.3 Gas-Phase Infrared Spectroscopy

The frequencies for  $\text{RuF}_5$ ,  $\text{NbF}_5$ ,  $\text{RuF}_5:\text{NbF}_5$  [3:1] and [1:3], at  $\approx 90^\circ\text{C}$  are shown in Table 5.4. For reference, the  $\text{RuF}_5$  and  $\text{NbF}_5$  gas-phase spectra are illustrated in Figures 3.1 and 2.5, respectively. The assignments made on the basis of these infrared spectra are reported tentatively as it may be possible to interpret the spectra in other ways.

The  $\text{RuF}_5:\text{NbF}_5$  [3:1] spectrum (see Figure 5.2) has bands at 749, 731 and 689  $\text{cm}^{-1}$ , which are assigned to the  $\text{NbF}_5$  trimer. There is also evidence for gaseous  $(\text{RuF}_5)_3$ , the 749  $\text{cm}^{-1}$  band is coincident with that of  $(\text{NbF}_5)_3$  and the bands at  $\approx 723$ , 706 and 658  $\text{cm}^{-1}$  are also present. There is evidence for a further gas-phase species with a peak at 765  $\text{cm}^{-1}$ . In addition there are three fluorine-bridging modes

Table 5.4: Gas-Phase Infrared Frequencies ( $\text{cm}^{-1}$ ) for  $\text{RuF}_5$ ,  $\text{NbF}_5$ ,  $\text{RuF}_5:\text{NbF}_5$  [3:1] and [1:3] at  $\approx 90^\circ\text{C}$  ( $\text{cm}^{-1}$ )

$\text{RuF}_5$	$\text{RuF}_5:\text{NbF}_5$ [3:1]	$\text{RuF}_5:\text{NbF}_5$ [1:3]	$\text{NbF}_5$
	765 sh		
749 m	749 s	747 s	747 s
	731 s	731 s	732 s
720 m	723 sh		
704 m	706 ms		
	689 s	687 s	688 m
659 w	658 m		
553 w,br	545 w	513 w	517 w
	523 sh		
	503 vw,sh	500 vw,sh	

at 545, 523 and 503  $\text{cm}^{-1}$ . The third species is tentatively assigned to a mixed-metal species, possibly  $\text{Ru}_2\text{NbF}_{15}$ .

The [1:3] data (Table 5.4 and Figure 5.3) closely resemble that of  $\text{NbF}_5$  with bands at 747, 731 and 687  $\text{cm}^{-1}$ . However, these bands are much broader than in the analogous  $\text{NbF}_5$  spectrum which, allied to the presence of two fluorine-bridging modes at 513 and 500  $\text{cm}^{-1}$ , tends to suggest a second gas-phase species with stretching mode frequencies very close to those of  $\text{NbF}_5$ . If this is assumed to be the case then the most likely species is  $\text{RuNb}_2\text{F}_{15}$ , but both these mixed-metal species are suggested very tentatively and further work is needed to confirm their existence.

#### 5.7.4 X-ray Powder Diffraction

One powder pattern of  $\text{RuF}_5:\text{NbF}_5$  [1:3] shows it to have a structure different from that of either  $\text{RuF}_5$  or  $\text{NbF}_5$ , and so results of the analysis of a single crystal struc-

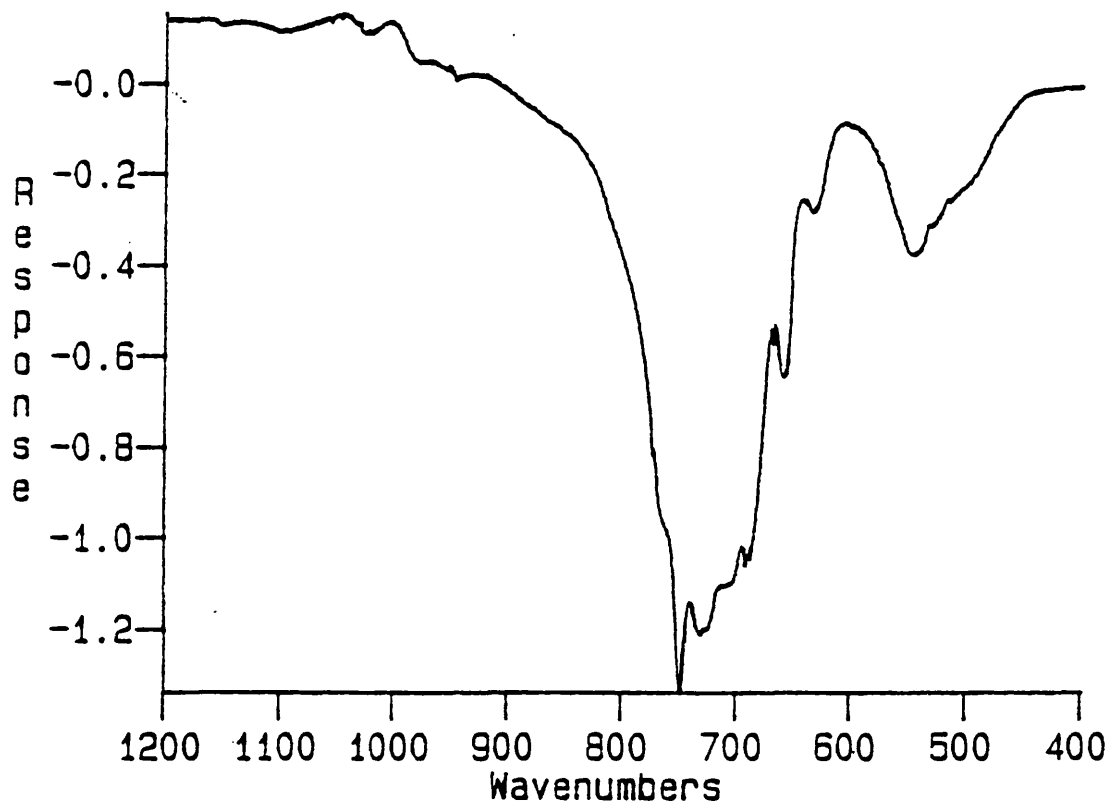


Figure 5.2: The  $\text{RuF}_5:\text{NbF}_5$  [3:1] Gas-Phase Infrared Spectrum at  $90^\circ\text{C}$ .

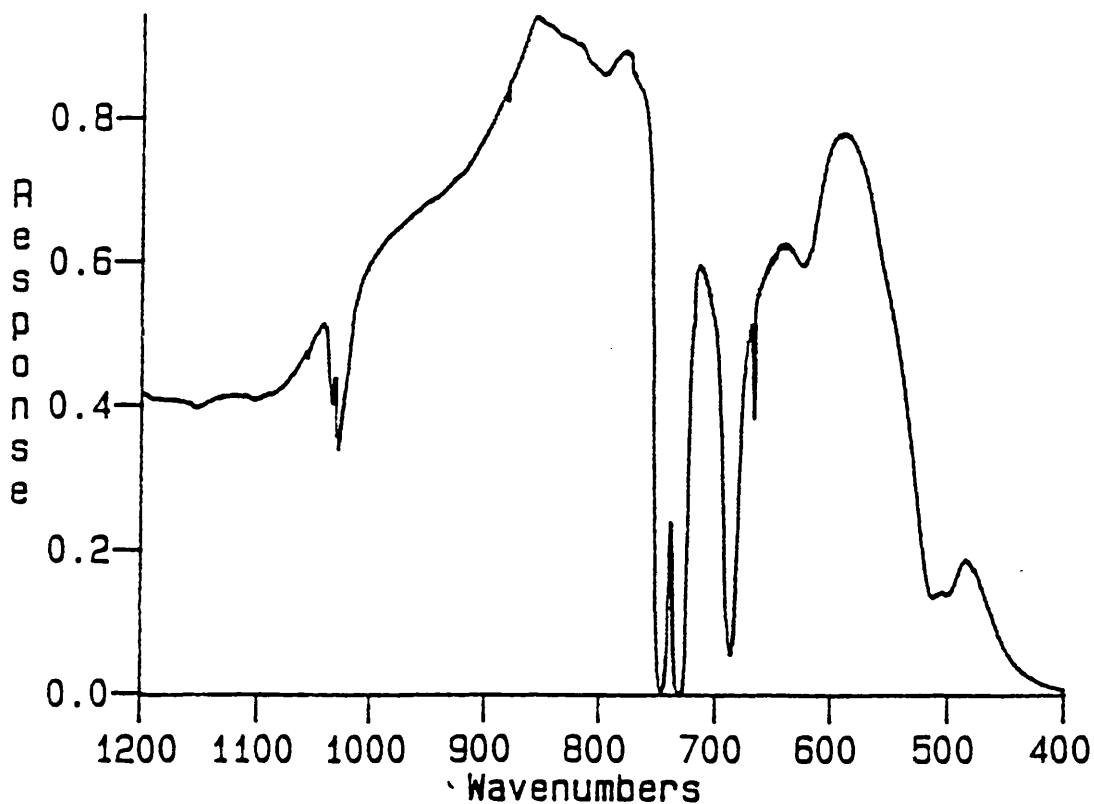


Figure 5.3: The  $\text{RuF}_5:\text{NbF}_5$  [1:3] Gas-Phase Infrared Spectrum at  $90^\circ\text{C}$ .

ture determination are reported in the next section. However, all other powder patterns of this material show that it has a structure based on that of  $\text{NbF}_5$  as expected. The sample which gives the pattern different to that of  $\text{NbF}_5$  is assumed to be a different structural form of this compound, which is assumed to adopt the  $\text{NbF}_5$ -type structure with time, at room temperature. This is similar behaviour to that of the red form of  $\text{RuF}_5$  which converts to the green form on gentle heating [65].

The [1:1] pattern is similar, but not identical to that of  $\text{NbF}_5$ . Likewise, the single crystal work on the analogous  $\text{RuF}_5:\text{TaF}_5$  [1:1] shows a reduction of the  $\text{M}-\text{M}^\circ$  distance and  $\text{M}-\text{F}_b-\text{M}$  bond angle from the values for  $\text{TaF}_5$  (4.129 Å to 4.100 Å and 171.8° to 167° respectively). The Nb and Ru K-edge EXAFS of  $\text{RuF}_5:\text{NbF}_5$  [1:1] (detailed in Chapter 6) shows that (a) there is a reduction in the  $\text{M}-\text{M}^\circ$  distance from 4.129 Å [4] in  $\text{NbF}_5$  to  $\approx 4.04\text{Å}$ , (b) there is a reduction of the  $\text{M}-\text{F}_b-\text{M}$  bond angle from 173.0° in  $\text{NbF}_5$  [4] to  $\approx 167^\circ$  (this value is calculated from the average  $\text{M}-\text{M}^\circ$  distance), and (c) that there is asymmetric fluorine-bridging. The  $\text{Nb}-\text{F}_b$  distance is 2.050 Å, whilst that for  $\text{Ru}-\text{F}_b$  is 2.007 Å. It is not clear as to whether these differences are based on Lewis acid considerations, or whether the  $\text{MF}_5$  units merely adopt the  $\text{M}-\text{F}_b$  bond lengths close to those in their respective single-metal pentafluorides. These distortions of the  $\text{NbF}_5$  structure are reflected in the powder patterns.

### 5.7.5 X-ray Single Crystal Diffraction Work

The X-ray structure determination data for a single crystal of  $\text{RuF}_5:\text{NbF}_5$  [1:3] are reported in Table 5.5, along with bond lengths and angles for this compound,  $\text{RuF}_5$  and  $\text{NbF}_5$  in Table 5.6. The compound is isostructural with  $\text{NbF}_5$ , which is expected since the analogous  $\text{RuF}_5:\text{TaF}_5$  [1:3] is isostructural with  $\text{TaF}_5$ . The  $\text{M}-\text{F}_{eq}$  bond lengths are slightly shorter than the  $\text{M}-\text{F}_{ax}$ , as would be expected for  $\text{Nb}^{5+}$  ( $d^0$ ) and  $\text{Ru}^{5+}$  ( $d^3$ ) [59]. There is no evidence for the asymmetric fluorine-bridging observed in the EXAFS of the [1:1] compound, and there appears to be random metal site occupation. This may be due either to a random arrangement, or to ordered metal sites arranged in a super-lattice, as detailed for the other mixed-metal pentafluorides

Table 5.5: Data From Crystallographic Analysis of  $\text{RuF}_5\text{NbF}_5$  [1:3]

Compound	$\text{RuF}_5\text{NbF}_5$ [1:3]
Formula*	$\text{F}_{20}\text{RuNb}_3$
$M^*$	759.8
Crystal Symmetry	Monoclinic
Space Group	$C2/m$
$a$ (Å)	9.631(27)
$b$ (Å)	14.466(41)
$c$ (Å)	5.103(2)
$\beta$ (°)	96.34(2)
$V$ (Å <sup>3</sup> )	706.5
$Z$ †	2
Radiation Type	Mo- $K\alpha$
$D_c$ (gcm <sup>-3</sup> )	3.57
$F(000)$	694
Crystal Size (mm)	.48 × .44 × .24
$\mu(\text{Mo-K})$ (cm <sup>-1</sup> )	32.7
Scan Width	$(1.6 + 0.7 \sin \mu / \tan \upsilon)^\circ$
Scan Type	$\omega$
Max. Bragg Angle (°)	54
Reflections Collected	788
No. of Unique Reflections	788
No. of Variables	61
$R = [\Sigma( F_o  -  F_c ) / \Sigma F_o ]$	0.0628
$R_w = [\Sigma w( F_o  -  F_c )^2 / \Sigma w F_o ^2]^{0.5}$	0.0684
Weighting Parameter (g) ‡	0.0137
Max. Electron Density/e (Å <sup>-3</sup> )	-2.6-2.9
Max. Final Shift/ e.s.d.	0.003

\* Refers to the molecular ratio of the adduct, with  $Z=2$  equivalent.

† Refers to the averaged  $\text{M}_2\text{F}_{10}$  unit as  $C2/m$ .

‡ Weighting  $w = 1/[\sigma^2(F) + g(F)^2]$ .

\* Data limited as collected at Edinburgh University.

Table 5.6: Selected Bond Lengths and Angles for  $\text{RuF}_5$ ,  $\text{NbF}_5$  and  $\text{RuF}_5:\text{NbF}_5$  [1:3] from X-ray Single Crystal Work.

Data	$\text{RuF}_5$ [5]	$\text{RuF}_5:\text{NbF}_5$ [1:3]	$\text{NbF}_5$ [4]
$M_1\text{-F}_{(eq)}$ (Å)	1.796(1)	1.827(7)	1.812(3)
$M_1\text{-F}_{(ax)}$ (Å)	1.819(1)	1.870(5)	1.839(3)
$M_1\text{-F}_b$ (Å)	1.997(1)	2.067(4)	2.068(2)
$M_2\text{-F}_{(eq)}$ (Å)	1.796(1)	1.820(6)	1.807(3)
$M_2\text{-F}_{(ax)}$ (Å)	1.824(1)	1.865(8)	1.837(4)
$M_2\text{-F}_b$ (Å)	2.005(1)	2.067(4)	2.063(2)
$M_1\text{-F}_b\text{-}M_2$ (°)	138.82(6) <sup>a</sup>	172.9(3)	173.0(1)
Crystal Class	Mono	Mono	Mono
Space Group	C2/m	C2/m	C2/m

<sup>a</sup> Average value.

Mono = Monoclinic.

(see Chapter 3). The EXAFS of the [1:1] compound supports the latter case.

## 5.8 Conclusions

### 5.8.1 $\text{RuF}_5:\text{VF}_5$

The majority of the data is reported for the [1:1] compound to coincide with the EXAFS detailed in Chapter 6. XRF analysis confirms the Ru:V ratio to be approximately 1:1 and the solid state can be said to be based on a distorted version of the  $\text{RuF}_5$  structure. These results show that, where single crystals are not available for more detailed X-ray work, solid materials of this type can be successfully studied using a series of more conventional analytical techniques in conjunction with EXAFS.

There is some evidence for asymmetric fluorine-bridging in this compound, as

there are two fluorine-bridging modes in the infrared of the solid. In fact, the M-F<sub>b</sub>-M bond angle has been calculated assuming that the V-F<sub>b</sub> bond length is 1.96 Å (the value in the VF<sub>5</sub> structure [3]) compared to that of 1.964 Å for RuF<sub>5</sub>, which implies symmetrical fluorine-bridging. The two fluorine-bridging modes could be the result of other factors, for instance if there were two different M-F<sub>b</sub>-M bond angles in the tetramer, and a complete structural characterisation would be necessary to confirm all the bond lengths and angles.

Both RuF<sub>5</sub>:VF<sub>5</sub> [3:1] and [1:1] would prove interesting candidates for further investigation, and it might be hoped that the [3:1] compound does not decompose on heating so that it can be used as a precursor for CVD. As for the arrangement of atoms in the mixed-metal pentafluorides, RuF<sub>5</sub>:VF<sub>5</sub> [1:3] also deserves attention, bearing in mind that the analogous VF<sub>5</sub>:TaF<sub>5</sub> [3:1] does not have a structure based on the TaF<sub>5</sub> tetramer.

### 5.8.2 RuF<sub>5</sub>:NbF<sub>5</sub>

RuF<sub>5</sub>:NbF<sub>5</sub> [3:1], [1:1] and [1:3] appear to be very similar to the analogous RuF<sub>5</sub>:TaF<sub>5</sub> compounds. The EXAFS of the [1:1] material shows asymmetric fluorine-bridging, which can only be possible if there are ordered metal sites in the tetramers, with like metal atoms at opposite corners. This could be the case for RuF<sub>5</sub>:TaF<sub>5</sub> [1:1] also, but further data is required to confirm this.

The infrared spectra of the solids are not well resolved and all the spectra are fairly similar, whilst the gas-phase infrared spectra of the [1:3] and [3:1] compounds are not conclusive in respect of which species are present at 90°C. There is evidence for decomposition to RuF<sub>5</sub> and NbF<sub>5</sub> trimers in the [3:1] spectrum as well as for mixed-metal trimers. This is again similar to the results observed for the RuF<sub>5</sub>:TaF<sub>5</sub> compounds, and requires further work to confirm the existence of mixed-metal species. This is especially important bearing in mind the favourable thermodynamics of reduction of RuF<sub>5</sub> by hydrogen compared to those of NbF<sub>5</sub> and TaF<sub>5</sub>,

and the very high melting points of Nb and Ta (2740 and 3250 K, respectively [114]).

Both the  $\text{RuF}_5:\text{NbF}_5$  [1:1] and [1:3] structures are dominated by the  $\text{Nb}^{5+}$  ion (radius 0.64 Å [67]), which is larger than  $\text{Ru}^{5+}$  (radius 0.575 Å [67]). This illustrates the importance of the packing of the atoms in these structures, whilst the asymmetric fluorine-bridging must surely be due to localised bonding.

## Chapter 6

# Structural Studies Using EXAFS.

### 6.1 Introduction

In order to study further the mixed-metal pentafluoride structures, EXAFS (Extended X-ray Absorption Fine Structure) data have been recorded and solved on selected compounds. The advantage of using EXAFS, in conjunction with X-ray diffraction is that EXAFS provides an element specific, localised structure probe, while X-ray diffraction data can provide information about the overall structure.

The EXAFS information is essential for a complete characterisation of the mixed-metal pentafluorides bearing in mind the fact that their X-ray single crystal structure determinations (Chapters 2, 3, 4 and 5) do not differentiate between the metal sites in the structures. The EXAFS technique, on the other hand, can confirm whether the mixed-metal pentafluorides are tetramers with random arrangements of metal atoms, or randomly arranged tetramers with the metal atoms in fixed positions.

It should be noted that to collect EXAFS does not require a crystalline sample, which is of particular use for compounds such as  $\text{RuF}_5:\text{VF}_5$  [1:1] and  $\text{RuF}_5:\text{TaF}_5$  [3:1], where it has not been possible to grow single crystals suitable for X-ray work (see Chapters 5 and 3, respectively).

As the analysis of EXAFS data is reliant on accurate phase shifts for each element, the EXAFS of the relevant hexafluoroanions ( $\text{KRuF}_6$ ,  $\text{KTaF}_6$ ,  $\text{KNbF}_6$  and  $\text{KVF}_6$ ) have been collected and modelled. The phase shifts from these compounds have then been used in the analysis of the EXAFS of the metal and the mixed-metal pentafluorides. Finally, to verify the accuracy of the distances from the EXAFS,  $\text{RuF}_5$ ,  $\text{TaF}_5$  and  $\text{NbF}_5$  have also been investigated and the data compared to those obtained from X-ray structure determinations.

Unfortunately, no V-edge EXAFS spectra have been recorded for the mixed-metal pentafluorides. This is because the V-edge EXAFS spectra must be recorded in fluorescence rather than in transmission mode because there was not sufficient transmission of the X-rays through the FEP sample holders to record a spectrum. The signal to noise ratio in fluorescence mode is poor for the number of scans which time allowed. This makes the analysis of shells at longer distances (greater than 3.5 Å), essential for the mixed-metal pentafluorides, unreliable.

## 6.2 EXAFS Theory

As EXAFS is a relatively novel technique, this section is an introduction to the theory surrounding the phenomenon and its analysis. For a more advanced treatment, the reader is directed to texts by Teo [129] and Corker [130] which adequately cover the area in more detail.

EXAFS is a final-state interference effect involving the scattering of an outgoing photoelectron from neighbouring atoms. The initial state of the electron can be described as the localised core level corresponding to the absorption edge, while the final state is the ejected photoelectron, represented as a spherical wave originating from the absorbing atom. If the absorbing atom has a neighbouring atom, then the outgoing photoelectron wave will be backscattered by it to produce an incoming wave. The incoming and outgoing waves can then interfere either constructively

or destructively to produce a sinusoidal variation of  $\mu$  vs  $E$  (where  $\mu$  is the X-ray absorption coefficient and  $E$  is the energy of the photoelectron), known as EXAFS. This is illustrated in Figure 6.1. If there is no neighbouring atom, then there would be no backscattering and no EXAFS. Instead, the decay of the post-edge would be smooth.

The amplitude and frequency of the EXAFS depends on the type and the bonding to the neighbouring atoms, as well as their distances from the absorbing atom. As such, EXAFS can provide a localised structure around the absorbing atom out to  $\approx 6 \text{ \AA}$ . This simple description of EXAFS is called the short-range single-electron single-scattering theory [129].

### 6.2.1 Short-Range Single-Electron Single-Scattering Theory.

For a monatomic gas with no neighbouring atoms, a photoelectron ejected by absorption of an X-ray photon travels as a spherical wave of wavelength,

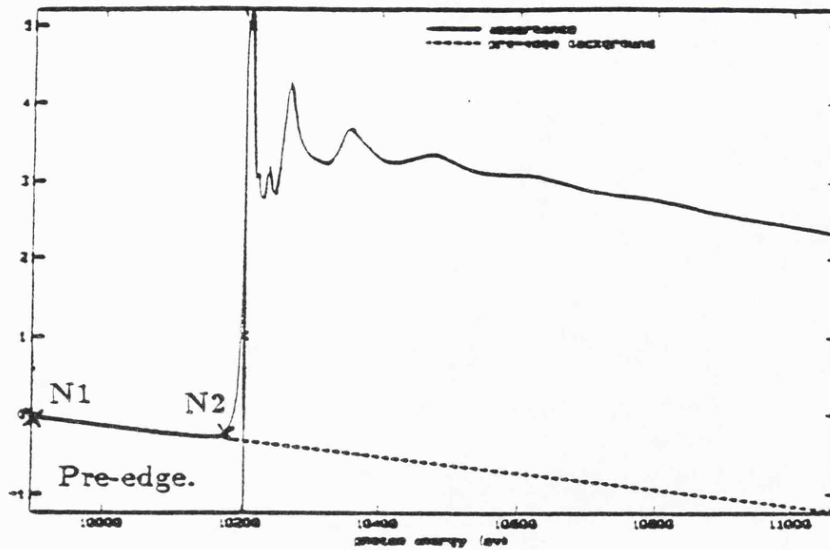
$$\lambda = \frac{2\pi}{k} \text{ where } k = \sqrt{\frac{2m}{\hbar^2} (E - E_0)}$$

The modulation of the absorption rate in EXAFS normalised to the background absorption ( $\mu^0$ ), assuming energy  $\geq 60 \text{ eV}$  and moderate thermal and static disorders, is given by,

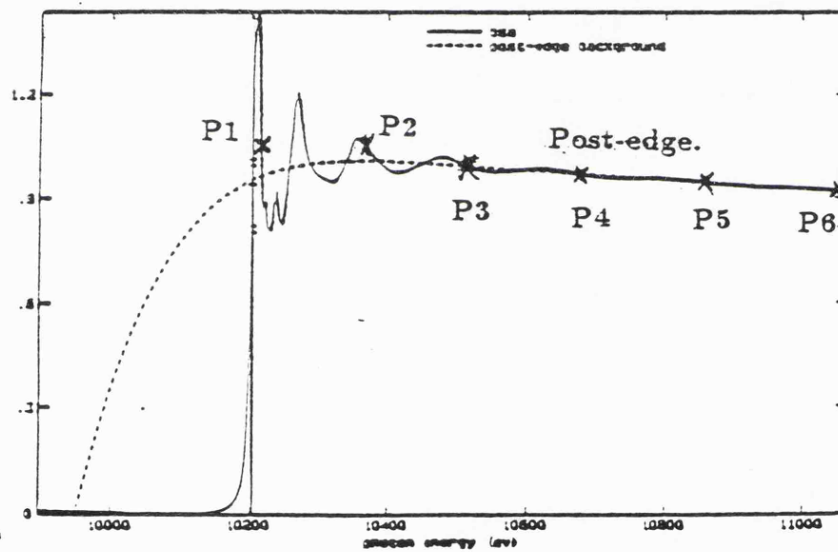
$$\chi(E) = \frac{\mu(E) - \mu_0(E)}{\mu_0(E)}$$

To relate  $\chi$  to structural parameters, it is necessary to convert energy to the photoelectron wavevector,  $k$ , using the equation above (in practice, it is the Fourier Transform with respect to photoelectron wavenumber which provides the structural information). So changing  $\chi(E)$  to  $\chi(k)$ , in  $k$  space, gives rise to,

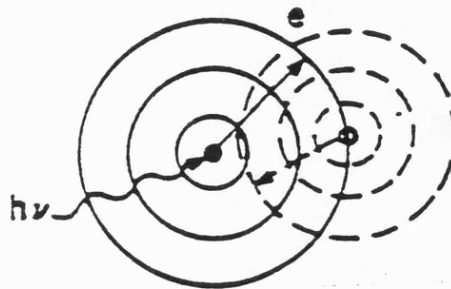
$$\chi(k) = \sum_j N_j S_i(k) F_j(k) e^{-2\sigma_j^2 k^2} e^{-2r_j \Lambda_j(k)} \frac{\sin(2kr_j + \phi_{ij}(k))}{kr_j^2}$$



(a) Pre-edge subtraction of EXAFS.



(b) Post-edge subtraction of EXAFS.



(c) EXAFS of a diatomic gas.

Figure 6.1: EXAFS Background Subtraction and a Schematic View of the EXAFS of a Monatomic Gas.

This equation is extremely complex and is only included to illustrate the factors important in the subsequent data analysis. For instance,  $F_j(k)$  is the backscattering amplitude from each of the  $N_j$  neighbouring atoms of the  $j$ th type, with a Debye-Waller factor of  $\sigma_j$ . The Debye-Waller factor accounts for thermal vibration (assuming harmonic vibration) and static disorder (assuming Gaussian pair distribution), at a distance  $r_j$  away. As a general rule in EXAFS analysis, the smaller  $\sigma_j$  is for each shell, the better the fit of the experimental and calculated data. The total phase shift experienced by the photoelectron,  $\Phi_{ij}(k)$ , and the term  $(e^{[-2\pi r_j/\lambda_j]})$  is due to the inelastic losses in the scattering process,  $\lambda_j$  being the mean free path. Finally,  $S_i(k)$  is the amplitude reduction factor due to many body effects, such as the shake up/off processes at the central atom, denoted by  $i$ .

### Multiple Scattering

The short-range single-electron single-scattering theory of EXAFS described here, makes use of the fact that in most cases multiple scattering (m.s.) of the photoelectron is not important. This assumption is normally valid as m.s. processes can be accounted for by adding all scattering paths that begin and end at the absorbing atom. Thus, the total scattering path length is much larger than that of the direct backscattering from nearest neighbour atoms, and so the m.s. gives rise to rapid oscillatory waves in  $k$  space, which tend to cancel out. However, m.s. becomes important when atoms are arranged in an approximately linear array, as for instance for Ta-F<sub>b</sub>-Ta in TaF<sub>5</sub>. In such cases, the outgoing photoelectron is forward scattered, resulting in a significant amplitude enhancement and modification of the phase. This effect drops off rapidly for bond angles less than 150° and so is not considered important for materials adopting the RuF<sub>5</sub>-type structure, where the M-F<sub>b</sub>-M bond angle is  $\approx 138^\circ$ .

The theory on which m.s. is based is extremely complicated and is dealt with elsewhere [129]. However, for a simple ABC system (such as Ta-F<sub>b</sub>-Ta in TaF<sub>5</sub>), the possible scattering pathways are shown in Figure 6.2. This illustrates the addi-

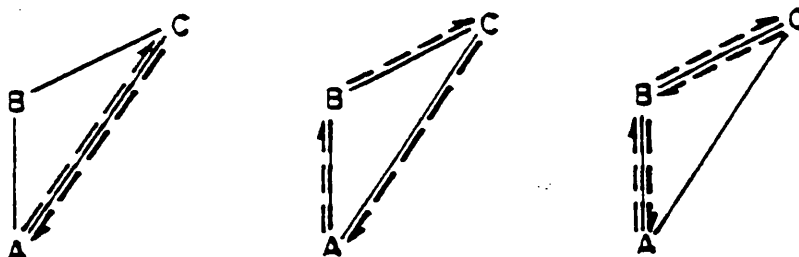


Figure 6.2: Possible Multiple Scattering Pathways in a Simple ABC System.

tional interactions which must be dealt with in the analysis in that there are three possible pathways which the backscattered photoelectron can take. One advantage of m.s. is that, without it, distances from the absorbing atom can be considered to be accurate ( $\pm 0.02 \text{ \AA}$ ) out to  $\approx 4 \text{ \AA}$ , but with m.s. this is possible out to  $\approx 8 \text{ \AA}$ .

### 6.2.2 Curved Wave Theory

The simple single-electron single scattering theory is described to give the reader an idea of the important parameters in the data analysis. In actual fact, a much better match over the whole energy range is achieved using curved wave theory [131], where the initial and final states of the photoelectron wavefunctions are described in terms of angular momentum. The final expression involves a matrix function describing all the effects of the scattering atom. This, however, is time consuming to solve and, in order to reduce the computational time, Gurman and co-workers [132, 133] have developed a simpler form, where random orientation of atoms is assumed and an angle averaged form of curved wave theory is used, resulting in only the diagonal matrix elements of the matrix being significant. This is the form which is currently used in curve fitting analysis. Detailed derivations of the curved wave expression are in references 131, 132 and 133.

### 6.2.3 EXAFS Data Analysis

EXAFS is the sum of the individual waves due to backscatter from different types of neighbouring atoms, or similar atoms at different distances. The EXAFS can be described thus,

$$\chi(k) = \sum_j A_j(k) \sin(2kr_j + \phi_{ij}(k))$$

where A is the amplitude thus,

$$A_j(k) = N_j S_i(k) F_j(k) e^{-2\sigma_j^2 k^2} e^{-2r_j/\lambda(k)} / (kr_j^2)$$

and the frequency is given by  $\sin(2kr_j + \Phi_{ij}(k))$ . The frequency of each individual EXAFS wave is determined by the distance between the absorbing and neighbouring atom. As the photoelectron travels from the former to the latter and back again, it experiences the phase shift (Coulombic interaction) of the absorbing atom twice and the neighbouring atom once (scattering). The phase shifts for the atoms in the metal and mixed-metal pentafluorides have been obtained from model compounds, the hexafluoroanions, and the distance from the absorbing to the neighbouring atoms have been calculated on the basis of these.

The amplitude of each individual EXAFS wave is dependent on the number and backscattering power of each neighbouring atom, and also on its bonding to and distance from the absorbing atom. The backscattering power is approximately related to the atomic weight of the atom, so that for fluorine, which is a light element (atomic number 9), the final R-factors for the solved EXAFS spectra,  $\approx 20\%$ , are acceptable. For heavier elements, lower R-factors would be expected.

#### Calibration, Averaging and Editing of Spectra

To solve EXAFS data, it is necessary to subtract the background absorption ( $\mu^0$ ), which has been done mainly using the EX computer programme [134]. The aver-

aging of several data sets has been found to improve the signal to noise ratio. The spectra are first calibrated with reference to the absorption edge of the relevant metal foil, before averaging. The editing facility, in the programme, allows for the removal of any spikes or glitches in the spectra, which is performed by the movement of individual points, in the y-axis direction. These glitches may be caused by sample inhomogeneity, beam movement or additional reflections in the monochromator, and those involving one or two points have been removed. However, every effort has been made to minimise the editing of the spectra for obvious reasons.

Once the spectra have been calibrated and averaged, the background absorption of the spectrometer and any other elements in the sample is removed so that the smooth part of the absorption, due to the defined central atom, is obtained. This leads to a normalised spectrum of  $\chi(k)$  versus  $k$  and is obtained, thus:

### **Pre-edge Background Subtraction**

The point at which  $k = 0 \text{ \AA}^{-1}$  is defined by assigning the energy zero,  $E^0$ , at the point on the absorption edge with the greatest derivative. The choice of  $E^0$  is important as it effects the phase of the oscillations being analysed. The pre-edge (see Figure 6.1a) is then removed by fitting a polynomial (order 1), between the points N1 and N2, chosen visually. A third point N3 is also used if this proves unsatisfactory. This process is important as a poor pre-edge subtraction will result in low frequency terms in the EXAFS spectrum and, therefore, lead to incorrect EXAFS amplitudes.

### **Post-edge Background Subtraction**

The post-edge subtraction is achieved by fitting a series (five or six) of linked polynomials (order 3), Figure 6.1b, such that the amplitude of the EXAFS oscillations is equally divided. The points ( $P_n$ ) where these polynomials start and finish are chosen equally along the post-edge. An indication of the success of the background subtractions can be judged by inspection of the Fourier transforms of the EXAFS.

## Excurve

Once the background subtraction is satisfactory, structural information is obtained from the EXAFS data using the Daresbury curve fitting programme EXCURVE [135]. This programme utilises the curved wave theory of Lee and Pendry [131], and the fast algorithms developed by Gurman et al [132, 133], to generate theoretical spectra. For each shell fitted after the first, a part of the EXCURVE computer programme is initiated [136] which makes a statistical check on that shell to ensure its validity. Unless otherwise stated every shell reported has a probability of less than 1 % of not being valid.

**Phase shifts** The phase shifts of the hexafluorometallates, used in the analysis of the other spectra, are calculated within EXCURVE using *ab initio* calculations. There are a number of assumptions involved, namely that (a) atomic wave function calculations assume that the charge density is that of a free atom calculated in a Hartree-Fock approximation [137], (b) that a constant potential (between the muffin-tin potentials [138]) exists outside the atom, (c) each atom possesses spherical symmetry with no overlap of potentials with other atoms, (d) that on ejection of a photoelectron, the resulting positive charge is shielded by the valence electrons, which are treated as being fully relaxed [139], and (e) as phase shifts are strongly dependent on inner electrons, they are independent of chemical environment [140, 141].

**Parameters** The individual sinusoidal waves corresponding to each set (shell) of neighbouring atoms are effectively solved separately, such that each shell has a set of parameters which are then altered to minimise the R-factor. The parameters are listed below:

$E^0$  : The magnitude of the photoelectron energy at zero wavevector. The value of  $E^0$  effects the value of  $k$ , and hence the phase shift function,  $\theta(k)$ . Thus, for the analysis of these spectra, where they are modelled using theoretically cal-

culated phaseshifts and an empirically calculated value of  $E^0$ , this parameter is refined in addition to the shell parameters.

**Ns** : The number of shells.

**Nn** : The number of atoms in shell n.

**Tn** : The type of atom in shell n, relative to the central atom 1.

**Rn** : The distance of shell n from the central atom.

**An** : The Debye-Waller factor corresponding to shell n. A is defined as  $2\sigma^2$ , where  $\sigma$  is the root mean square variation in the distance between absorber and scatterer. Values are typically 0.004–0.030 at room temperature. A Debye-Waller factor of  $\approx 0.010$  is considered acceptable for a given shell. Values greater than this are usually caused by either, a series of neighbouring atoms being grouped together in one shell which have different distances from the absorbing atom ( $\pm 0.2 \text{ \AA}$ ), or because the distance from the absorbing atom is large (greater than  $\approx 4 \text{ \AA}$ ).

**VPI** : The constant imaginary potential describing the lifetime of the photoelectron (ie. the factor which describes the effects of inelastic scattering in the curved wave theory). It is expressed in electron volts and typical values are between -1 and -6 eV.

**AFAC** : This describes the effects of multiple excitations which reduce the EXAFS amplitude. The value of AFAC is almost independent of the energy range and the chemical environment around the absorber, but is affected by the nature of

the absorbing atoms. Typical values are between 0.7 and 0.9.

**EMIN** : Minimum energy used to calculate the theoretical spectrum. It is defined in terms of the energy above the edge of the spectrum.

**EMAX** : Maximum energy used to calculate the theoretical spectrum.

**LMAX** : Maximum angular momentum used in phase shift calculation.

#### 6.2.4 Error Estimation

The errors on the EXAFS data are shown in brackets alongside the calculated structural information. However, these are based only on statistical errors for effects such as fluctuations in beam position, sample inhomogeneity, and electronic noise. Other errors, for instance incurred during background subtraction, are not accounted for and so the actual errors are larger than those reported. As a rough guide, the errors on the bond lengths are believed to be of the order of  $\pm 0.02 \text{ \AA}$ , but this increases with  $R_n$ . Some idea of these additional errors can be gauged by comparing the EXAFS data with the bond lengths from X-ray diffraction work, where available.

### 6.3 The Hexafluorometallates

The results of the analysis of the EXAFS of the relevant hexafluorometallates are shown in Table 6.1. All of the compounds have a single shell of six bonding fluorine atoms making up an  $\text{MF}_6^-$  unit at  $\approx 1.85 \text{ \AA}$ , along with some other fluorine atoms at non-bonding distances ( $\approx 3.5 \text{ \AA}$ ). In each case, the R-factor is acceptable bearing in mind that fluorine atoms are poor back-scatterers of X-rays (see theory section). The phaseshifts from these compounds have been calculated and used in the modelling of the metal and mixed-metal pentafluorides.

Table 6.1: Hexafluorometallate EXAFS Analyses

Hexafluorometallate	KNbF <sub>6</sub>	KTaF <sub>6</sub>	KRuF <sub>6</sub>	KVF <sub>6</sub>
R <sub>[min]</sub> (%)	14.86	18.89	17.32	16.92
F.I.	3.71	3.30	3.83	2.79
M-F(Å)*	1.893(2)	1.898(1)	1.850(2)	1.815(3)
σ <sup>2</sup> /Å <sup>2</sup> †	0.005	0.005	0.006	0.014
E <sub>0</sub>	23.80	8.25	30.10	20.10
VPI	-1.71	-1.36	-3.50	-4.93
AFAC	0.71	0.680	0.79	0.79
Range	3–14.5k	3–14k	3–14.5k	3.3–10k
Edge	Nb K	Ta L <sub>III</sub>	Ru K	V K

\* Bond distance for first shell of six fluorine atoms.

† Debye-Waller factor on shell 1.

The V K-edge EXAFS of KVF<sub>6</sub> is a small data set, because of the presence of a second edge at ≈ 12k which is believed to be due to contamination of the Be window from an earlier experiment.

## 6.4 The Metal Pentafluorides

### 6.4.1 Niobium Pentafluoride

The analysis of the NbF<sub>5</sub> EXAFS spectrum is shown in Table 6.2 and Figure 6.3. Table 6.2 shows the comparison of the bond lengths from the EXAFS with those from the original and the most recent X-ray structure determination [1,4]. The values for the bond lengths from the more recent structure should be more accurate and this fact is borne out by the much closer agreement between this data and the EXAFS bond lengths as compared with the original structural data.

Table 6.2: Niobium Pentafluoride EXAFS Analysis

Type of Data	Without M.S.	With M.S.	Crystal Data [2]	Crystal Data [4]
M-F <sub>t</sub> (Å)	1.831(1)	1.831(1)	1.77	1.822(4)
M-F <sub>b</sub> (Å)	2.059(2)	2.056(2)	2.06	2.066(2)
M-M°(Å)*	4.171(3)	4.085(3)	4.129 <sup>†</sup>	4.126 <sup>†</sup>
R <sub>[min]</sub> (%)	17.61	20.07	≈10.2	-
F.I.	1.31	1.60	-	-
E <sub>0</sub>	25.70	25.92	-	-
VPI	-2.79	-2.43	-	-
AFAC	0.79	0.75	-	-
Range	3-17k	3-17k	-	-

\* Non-bonding distance along one side of the tetramer.

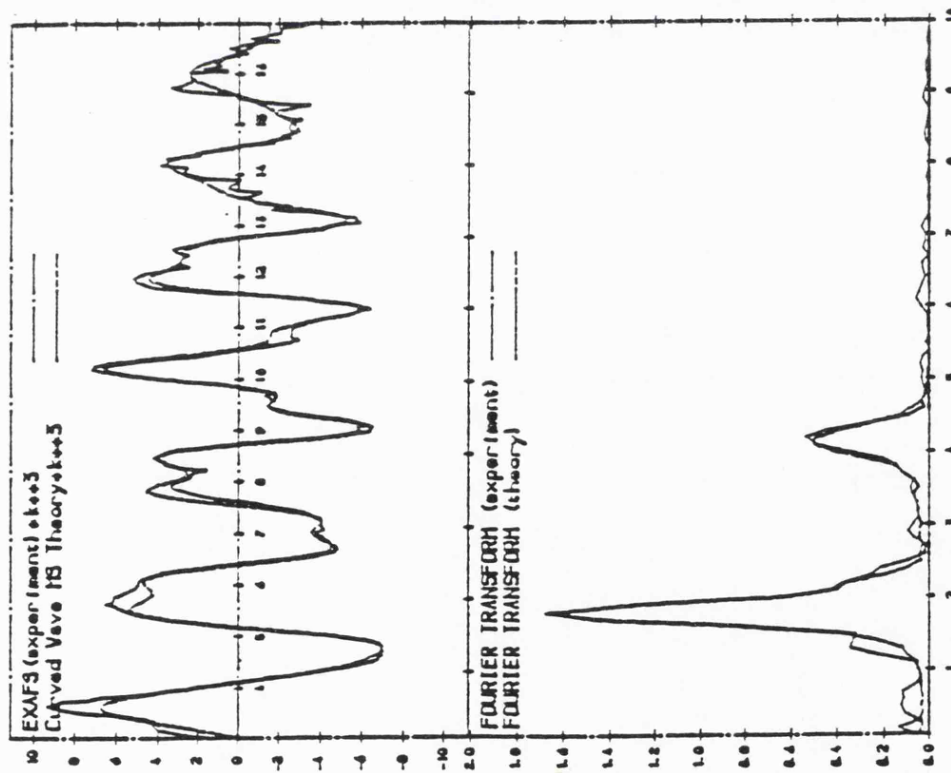
<sup>†</sup> Distance calculated from atom positions.

The EXAFS has been solved both with and without multiple scattering (see Section on EXAFS theory) and the results are shown for comparison in Table 6.2. Without multiple scattering, the Nb-Nb° distance (see Figure 6.8) is 4.171Å which is too long compared with the M-F<sub>b</sub> distance of 2.059Å. However, when multiple scattering is used the Nb-Nb° distance is 4.085Å, which corresponds to a M-F<sub>b</sub>-M bond angle of 166°. The Nb-Nb° length here is short compared to that calculated from the more recent crystal structure [4], but this illustrates the experimental error of the EXAFS technique. This data shows that EXAFS can be used to characterise these type of compounds, as long as the appropriate allowances are made for possible bond length errors.

Attempts to fit a shell corresponding to the M-M<sup>3</sup> distance have been unsuccessful as the extra shell does not pass the statistical significance test [136]. This is the case for all subsequent spectra as well. The atom type for shell 5 (the M-M<sup>2</sup>

Figure 6.3: Nb K-edge EXAFS Spectrum of NbF<sub>5</sub>

(with M.S.).



Shell	N	T	R	A
1	4	F	1.831	0.006
2	2	F	2.056	0.007
3	6	F	3.740	0.027
4	2	Nb	4.085	0.021
$R_{(min)}$			21.07	
F.I.			1.71	
$E_0$			25.92	
VPI			-1.71	
AFAC			0.75	
Range			3-17k	

distance along one side of the tetramer) has been verified as being Nb by running the analysis with either Ta, Ru or V atoms in place of Nb atoms. Of these three analyses the best fit gained is for Ru atoms ( $R_{min} = 20.6$ , F.I. = 1.69). As both of these parameters are lower in the Nb atom analysis ( $R_{min} = 20.07$ , F.I. = 1.61), this is assumed to be correct. This method of verifying the M-M<sup>2</sup> atom type has been used in all subsequent spectra. The verification of the M<sup>2</sup> atom type has been carried out with multiple scattering calculations included in the analysis in every compound where the M-F<sub>b</sub>-M bond angle is close to linear, as this is considered to give more accurate results.

#### 6.4.2 Tantalum Pentafluoride

Table 6.3 and Figure 6.4 show the bond lengths from the TaF<sub>5</sub> EXAFS analysis, along with those from the X-ray structure carried out as part of this thesis (see Chapter 2). The EXAFS has been solved with and without multiple scattering for comparison. The analysis which includes multiple scattering, has values which are in closer agreement with the crystal structure work than without multiple scattering. It is, therefore, suggested that using multiple scattering yields bond lengths with lower errors than when not using it, which must be considered when looking at the analyses of the mixed-metal pentafluorides which appear to be based on the TaF<sub>5</sub> structure.

Verification of the fact that the atom along one side of the tetramer from the absorbing atom is Ta has been confirmed by trying V, Nb or Ru atoms in the place of Ta atoms. Of these three the best fit is obtained for Nb ( $R_{min} = 19.29$ , F.I. = 1.54), but the M-M<sup>2</sup> distance is 4.221 Å. This is too long when compared to the M-F<sub>b</sub> distance of 2.076. In addition, the Debye-Waller value on this shell is 0.025, whilst the value for Ta atoms is lower at 0.017.

Table 6.3: Tantalum Pentafluoride EXAFS Analysis

Type of Data	Without M.S.	With M.S.	Crystal Data <sup>†</sup>
M-F <sub>t</sub> (Å)	1.847(2)	1.846(2)	1.836(12)
M-F <sub>b</sub> (Å)	2.080(4)	2.076(5)	2.071(12)
M-M <sup>o</sup> (Å)*	4.166(11)	4.128(11)	4.129
R <sub>[min]</sub> (%)	18.08	19.51	7.00
F.I.	1.35	1.59	-
E <sub>0</sub>	5.70	6.10	-
VPI	-1.36	-3.00	-
AFAC	0.71	0.77	-
Range	3.2–15k	3.2–15k	-

\* Non-bonding distance along one side of the tetramer.

† See Chapter 2.

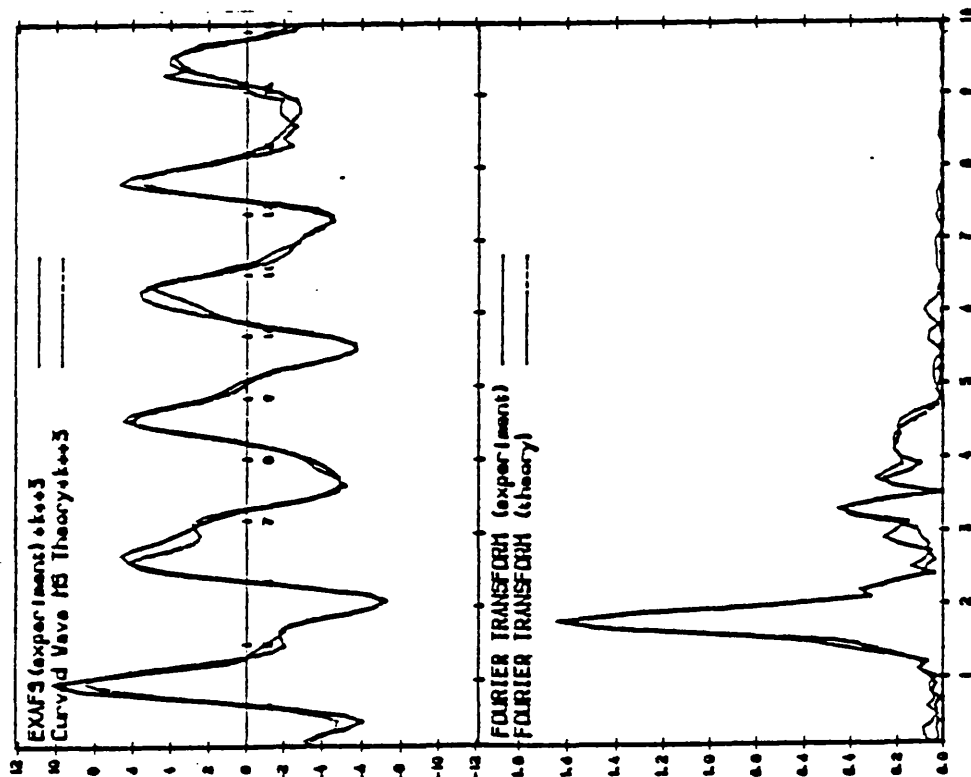
### 6.4.3 Ruthenium Pentafluoride

Ruthenium pentafluoride [2, 5] is known to have a different structure to NbF<sub>5</sub> [1, 4] and TaF<sub>5</sub> [1]. One difference between these structural types which needs to be considered with respect to the EXAFS, is that the M-F<sub>b</sub>-M bond angle in RuF<sub>5</sub> is  $\approx 138^\circ$  as compared to  $171.9(6)^\circ$  for TaF<sub>5</sub> (see Chapter 2) and  $173.0(1)^\circ$  for NbF<sub>5</sub> [4]. This means that no multiple scattering calculations have been used in the EXAFS analysis (see EXAFS theory section). This fact is supported by the good agreement between the EXAFS bond lengths (Table 6.4 and Figure 6.5) and those of the most recent and most accurate crystal structure [5]. The Ru-Ru<sup>o</sup> distance ( $3.700(6)\text{Å}$ ) gives a Ru-F<sub>b</sub>-Ru bond angle of  $\approx 136^\circ$  from the EXAFS, which corresponds to the equivalent bond angle in the crystal structure of  $138^\circ$ .

The atom type for shell 4 (the M-M<sup>2</sup> distance) has been checked by running the analysis with V, Nb or Ta atoms in place of Ru atoms. The best fit of these three

Figure 6.4: Ta *LIII*-edge Spectrum of TaF<sub>5</sub> (with

M.S.).



Shell	N	T	R	A
1	4	F	1.846	0.006
2	2	F	2.076	0.009
3	2	F	3.376	0.000
4	4	F	3.430	0.025
5	2	F	3.568	0.004
6	2	Ta	4.128	0.017

R<sub>[min]</sub> 19.50

F.I. 1.58

E<sub>0</sub> 6.10

VPI -3.00

AFAC 0.77

Range 3.3-15k

Table 6.4: Ruthenium Pentafluoride EXAFS Analysis

Type of Data	Without M.S.	Crystal Data <sup>3</sup>
M-F <sub>t</sub> (Å)	1.805(1)	1.808(1)
M-F <sub>b</sub> (Å)	1.993(3)	2.001(1)
M-M°(Å)*	3.700(5)	3.746 <sup>†</sup>
R <sub>[min]</sub> (%)	18.43	2.36
F.I.	1.44	-
E <sub>0</sub>	26.19	-
VPI	-2.43	-
AFAC	0.75	-
Range	3–16.3k	-

\* Non-bonding distance along one side of the tetramer.

<sup>†</sup> Calculated from atomic positions.

is for Nb atoms ( $R_{min} = 21.93$ , F.I. = 2.10). Both of these values are higher than those for the analysis using Ru atoms ( $R_{min} = 18.43$ , F.I. = 1.44) and so the Ru atom analysis is assumed to be correct.

## 6.5 The Mixed-Metal Pentafluorides

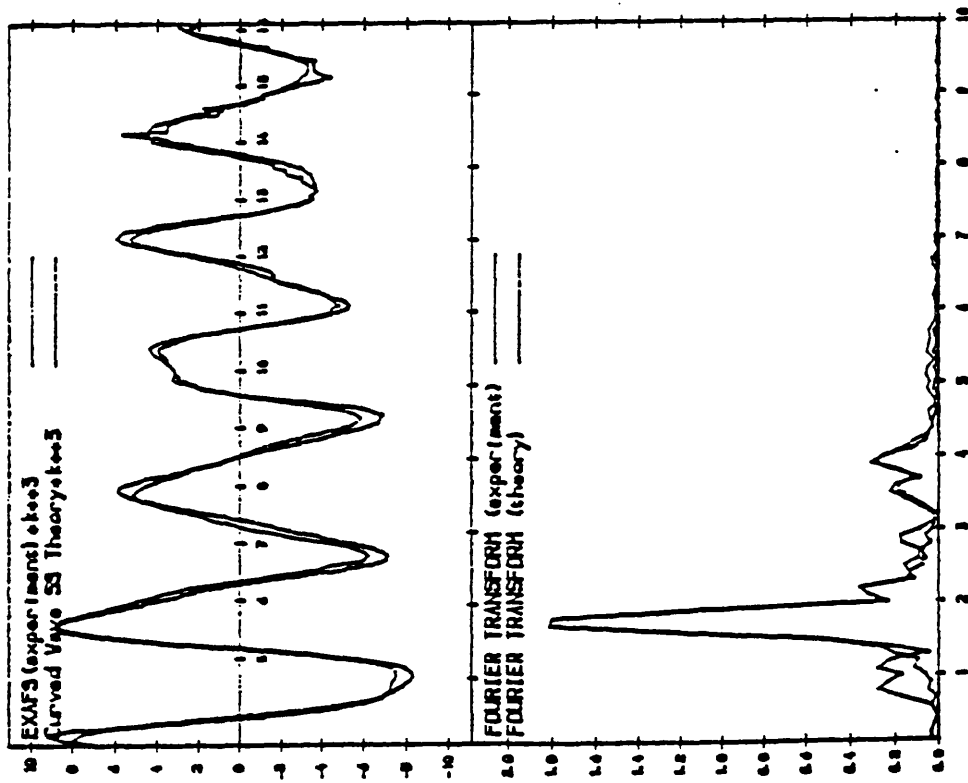
### 6.5.1 NbF<sub>5</sub>:TaF<sub>5</sub> [1:3]

In order to obtain a complete structural characterisation of this material in the solid state, both the Nb- and Ta-edge EXAFS spectra have been analysed and compared with the X-ray single crystal structure determination (see Chapter 2). The results are shown in Table 6.5 and Figures 6.6 and 6.7. Within experimental error ( $\pm 0.02\text{Å}$  on the EXAFS bond lengths), the EXAFS is in good agreement with the bond lengths from the crystal work.

From the Nb-edge EXAFS, it can be seen that there are two Ta atoms ( $M^2$  and

Figure 6.5: Ru K-edge EXAFS Spectrum of RuF<sub>5</sub>

(without M.S.).



Shell	N	T	R	A
1	4	F	1.805	0.005
2	2	F	1.993	0.007
3	2	F	3.625	0.031
4	4	F	3.700	0.018
$R_{[min]}$	18.42			
F.I.	1.43			
$E_0$	26.19			
VPI	-2.43			
AFAC	0.75			
Range	3-16.3k			

Table 6.5: NbF<sub>5</sub>:TaF<sub>5</sub>[1:3] EXAFS Analysis

Type of Data	No M.S.	M.S.	No M.S.	M.S.	Crystal Data <sup>‡</sup>
Edge	Nb K	Nb K	Ta L <sub>[III]</sub>	Ta L <sub>[III]</sub>	-
M-F <sub>i</sub> (Å)	1.824(1)	1.825(1)	1.849(2)	1.845(2)	1.844(14)
M-F <sub>b</sub> (Å)	2.051(3)	2.053(3)	2.061(3)	2.056(3)	2.065(9)
M-M° (Å)*	4.156(10)	4.054(12)	4.141(6)	4.099(10)	4.122 <sup>†</sup>
R <sub>[min]</sub> (%)	19.71	20.16	19.55	20.52	3.94
F.I.	2.08	2.00	0.94	1.23	-
E <sub>0</sub>	23.32	22.95	11.54	18.11	-
VPI	-1.00	-0.80	-3.14	-6.00	-
AFAC	0.71	0.71	0.79	0.91	-
Range	3-16k	3-16k	3.1-15k	3.1-15k	-

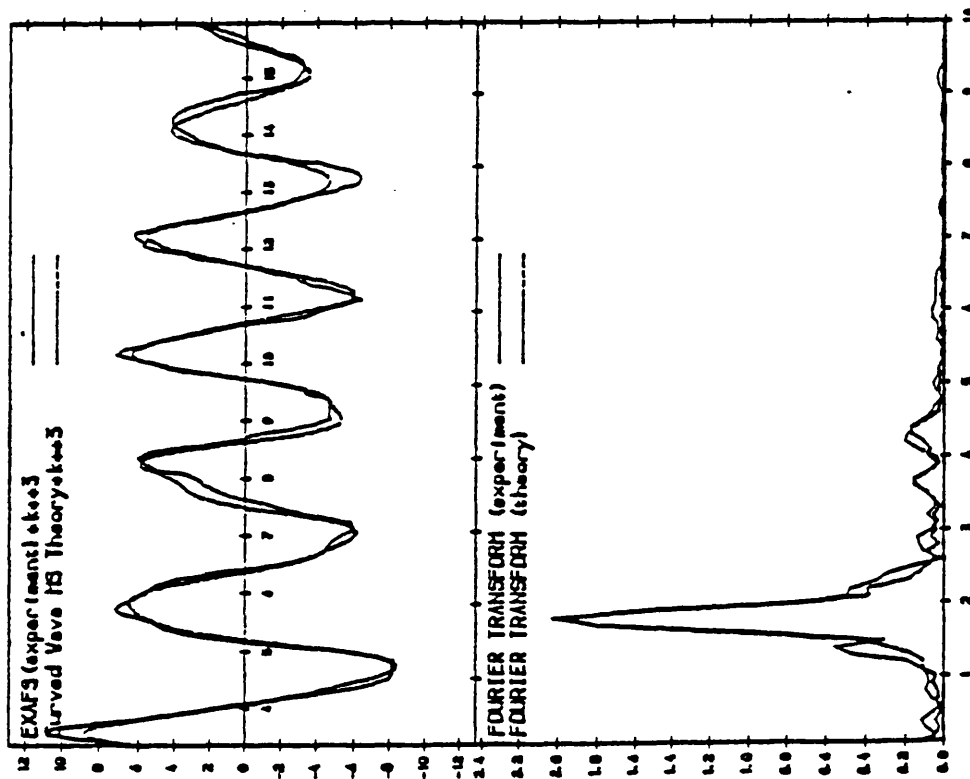
\* Non-bonding distance along one side of the tetramer.

† Distance calculated from atomic positions.

‡ Chapter 2.

Figure 6.6: Nb K-edge EXAFS Spectrum of

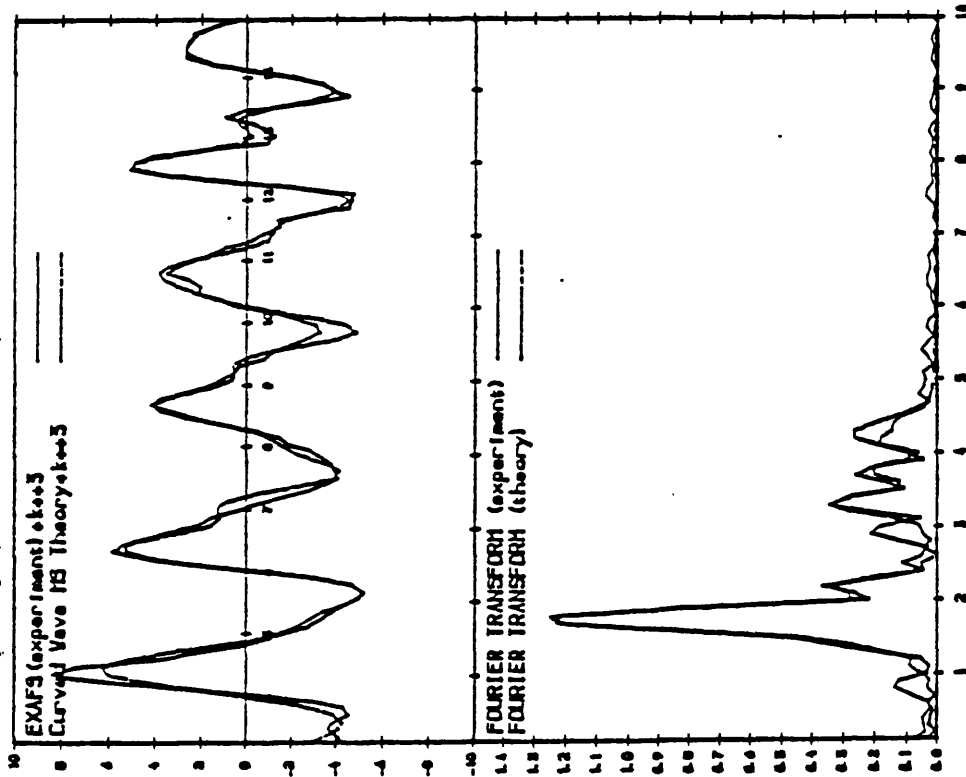
NbF<sub>5</sub>.TaF<sub>5</sub> [1:3] (with M.S.).



Shell	N	T	R	A
1	4	F	1.825	0.005
2	2	F	2.053	0.008
3	6	F	3.696	0.031
4	2	Ta	4.054	0.026
R <sub>(min)</sub>			20.16	
F.I.			2.00	
E <sub>0</sub>			22.95	
VPI			-0.80	
AFAC			0.71	
Range			3-16k	

Figure 6.7: Ta  $L_{III}$ -edge Spectrum of  $NbF_5 \cdot TaF_5$

[1:3] (with M.S.)



Shell	N	T	R	A
1	4	F	1.845	0.009
2	2	F	2.056	0.006
3	2	F	3.374	0.000
4	4	F	3.547	0.023
5	2	Ta	4.099	0.012
6	2	F	3.832	0.006
$R_{[min]}$	20.52			
F.I.	1.23			
$E_0$	18.11			
VPI	-6.00			
AFAC	0.91			
Range	3.1-15k			

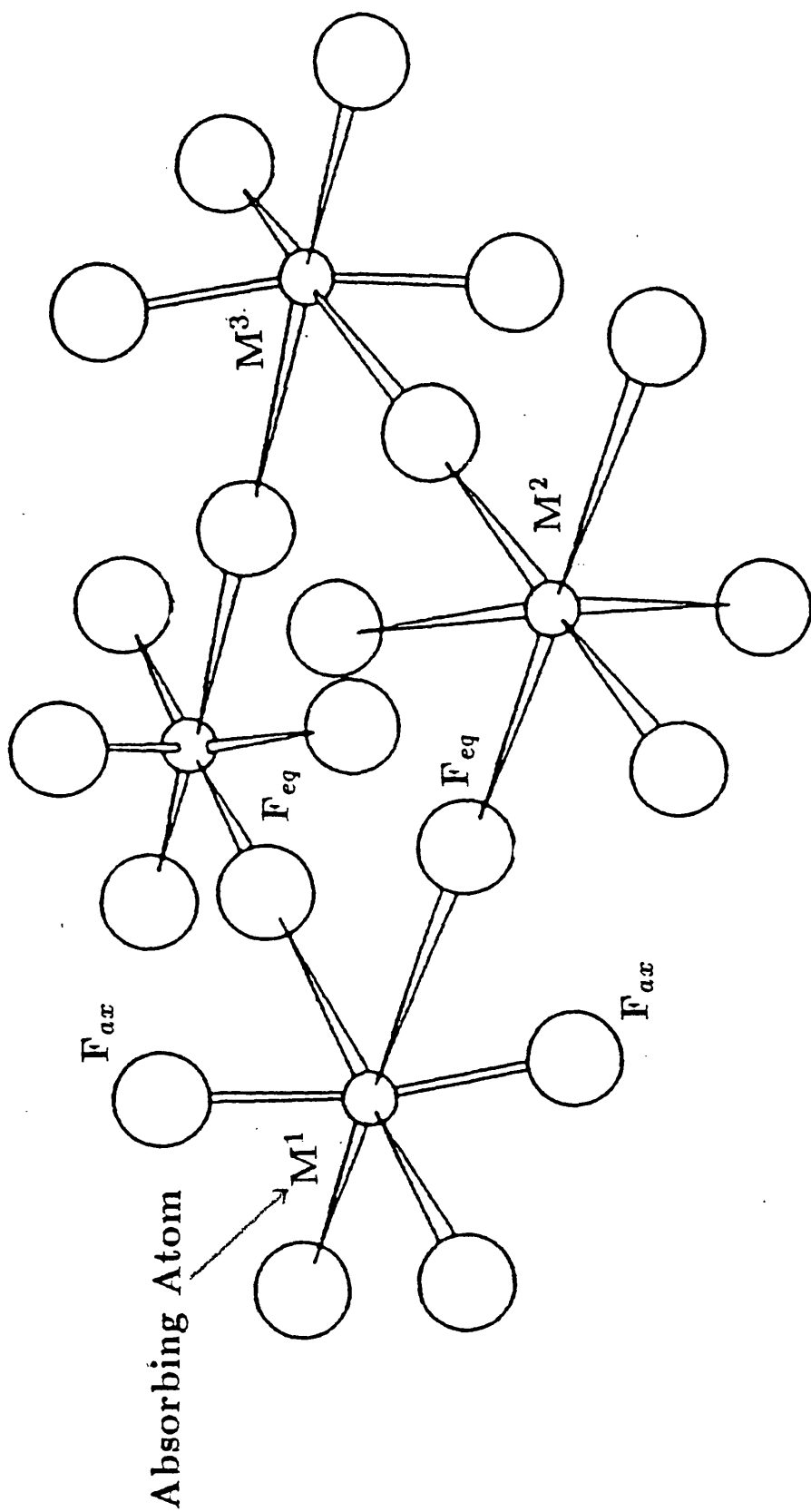


Figure 6.8: Schematic View of a TaF<sub>5</sub>-Type Tetramer.

$M^{2'}$  in Figure 6.8) on the nearest corners of the tetramer to the absorbing Nb atom. However, it cannot be confirmed whether  $M^3$  is a Ta atom because the Nb- $M^3$  distance ( $\approx 5.9\text{\AA}$ ) is at the limit of the reliability of the EXAFS technique. The atom along one side of the tetramer from the absorbing Nb atom has been confirmed as being Ta by comparing this analysis with those for Nb, Ru or V atoms. The best fit from these three is for Nb atoms ( $R_{min} = 20.3$ , F.I. = 2.11). Both these values are higher than those for the analysis using Ta atoms ( $R_{min} = 20.16$ , F.I. = 2.00), and so it is assumed that the  $M^2$  atoms are Ta. The fact that the nearest two metal atoms to the Nb are two Ta atoms supports the hypothesis that this compound has ordered metal sites, but that the tetramers are randomly arranged in the lattice.

The Ta-edge EXAFS (Figure 6.7) is more difficult to analyse. If the structure is assumed to have ordered metal sites as suggested by the Nb-edge EXAFS, then it will have two Ta environments, one (defined  $Ta_x$ ) has two Ta atoms in the nearest metal sites and the other (defined  $Ta_y$ ) has one Ta and one Nb atom. Problems are then incurred in the modelling of the EXAFS, as the phaseshifts of the atoms surrounding either  $Ta_x$  or  $Ta_y$  are different. By calculating the average situation between  $Ta_x$  and  $Ta_y$  based on the atomic weights of Nb and Ta, the atomic weight of the two nearest metal atoms to Ta is theoretically equivalent to two Eu atoms. When these are used in the modelling the R-factor is worsened ( $R_{min} = 22.39$ , F.I. = 1.25) compared to the analysis for two Ta atoms ( $R_{min} = 20.53$ , F.I. = 1.23), but the F.I. is slightly improved and the intensity on the  $M-M^\circ$  peak on the EXAFS FT appears to fit more closely. This may be because, although using the average atomic weight for a backscatter may be valid, the use of an average phase shift is not. For this reason, Eu has not been used to analyse this data but rather two Ta atoms. The use of the two Ta atoms has been further validated by comparing this analysis with those when Nb, Ru or V atoms are used instead. The best fit of these three is for Ru ( $R_{min} = 24.89$ , F.I. = 1.50). These values are both higher than when Ta atoms are used and so this is deemed to be correct.

As in the case of  $NbF_5$  and  $TaF_5$ , the analysis using multiple scattering appears

to afford the more accurate bond lengths when compared to the crystal data. This is expected bearing in mind the fact that the M-F<sub>b</sub>-M bond angle in these structures  $\approx 172^\circ$ , ie. close to linearity.

### 6.5.2 RuF<sub>5</sub>:NbF<sub>5</sub> [1:1]

The analysis of both the Nb and Ru-edge EXAFS of this compound are shown in Table 6.6, Figures 6.9 and 6.10. The similarity in the size and the phaseshifts of Ru and Nb mean that it is very difficult to differentiate between the metals in the tetramer, although the different metals do give different M-F<sub>b</sub> bond lengths. However, for the Ru-edge EXAFS the analysis where M<sup>2</sup> is taken to be Nb has been compared to those where M<sup>2</sup> is either Ru, Ta or V. Of these three the best fit is for V ( $R_{min} = 21.86$ , F.I. = 1.93). These values are comparable to those for Nb ( $R_{min} = 21.8$ , F.I. = 1.95). However, when M<sup>2</sup> is Ru the values are  $R_{min} = 21.93$  and F.I. = 1.97. Although these values are slightly higher than for Nb they indicate the difficulty in analysing the spectra because the differences are so small. When the Nb-edge EXAFS is considered the analysis where M<sup>2</sup> is Ru is compared with those where M<sup>2</sup> is either V, Nb, or Ta. The best fit of these three is for Ta ( $R_{min} = 19.79$ , F.I. = 2.33) but this can be discounted as the M-M<sup>2</sup> distance is too short at 3.968 Å and the material does not contain Ta. The analysis where M<sup>2</sup> is Nb ( $R_{min} = 20.01$ , F.I. = 2.42) is worse than that for Ru ( $R_{min} = 19.89$ , F.I. = 2.00) and so M<sup>2</sup> is assumed to be Ru although here again the differences are small.

The X-ray powder diffraction pattern shows that this structure is based on that of TaF<sub>5</sub> and, if it is assumed that both metals are present in the same tetramer, then this seems to imply that the Nb and Ru atoms are at opposite corners. This arrangement of metal atoms would retain the maximum symmetry of each tetramer. Mass spectrometry results on NbF<sub>5</sub>:TaF<sub>5</sub> [1:1], see Section 2.4.3, were not conclusive as to whether the metal atoms were on opposite corners or not and so the EXAFS results for RuF<sub>5</sub>:NbF<sub>5</sub> [1:1] may not be applicable in other systems. EXAFS data on the Nb and Ta edges of NbF<sub>5</sub>:TaF<sub>5</sub> [1:1] would resolve this.

Table 6.6: RuF<sub>5</sub>:NbF<sub>5</sub>[1:1] EXAFS Analysis

Type of Data	No M.S.	M.S.	No M.S.	M.S.
Edge	Nb K	Nb K	Ru K	Ru K
M-F <sub>i</sub> (Å)	1.823(1)	1.826(1)	1.828(1)	1.828(1)
M-F <sub>b</sub> (Å)	2.053(3)	2.051(3)	2.006(3)	2.006(3)
M-M° (Å)*	4.131(4)	4.055(4)	4.097(4)	4.012(4)
R <sub>[min]</sub> (%)	19.02	19.89	24.31	21.8
F.I.	2.41	2.00	2.50	1.957
E <sub>0</sub>	23.63	22.88	52.32	52.25
VPI	-2.43	-2.79	-1.36	-1.36
AFAC	0.87	0.87	0.75	0.75
Range	3-16k	3-16k	3-18.2k	3-18.2k

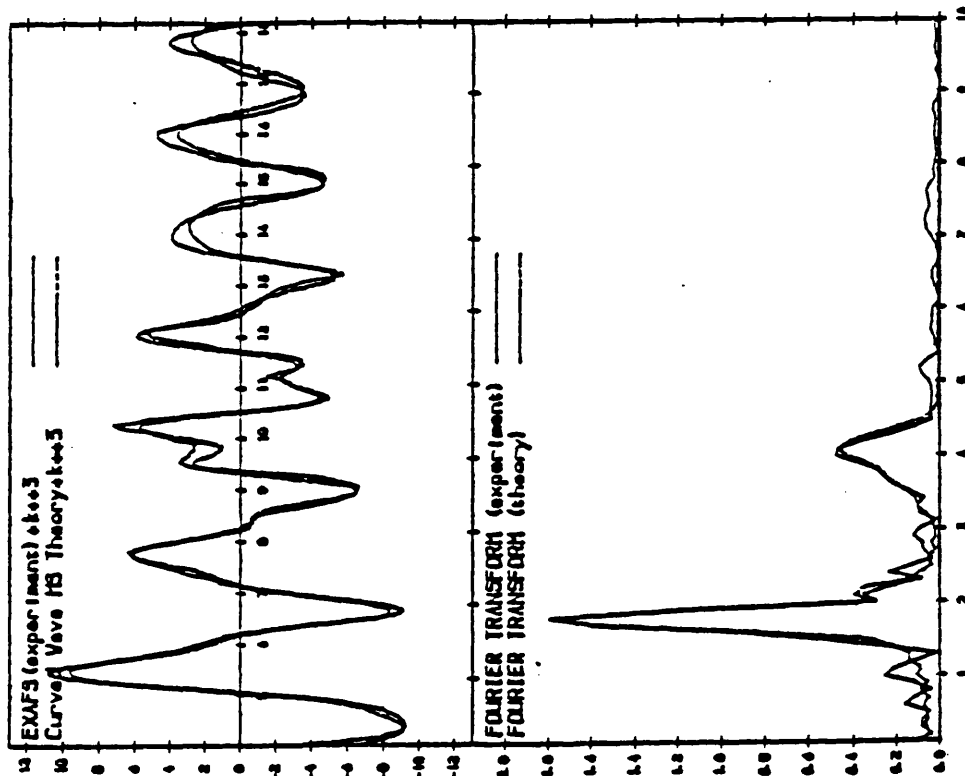
\* Non-bonding distance along one side of the tetramer.

The EXAFS shows a difference between this structure and that of TaF<sub>5</sub> in that there are two different metal sites. The Ru-F<sub>b</sub> bond length (2.006(2)Å) is shorter than that for Nb-F<sub>b</sub> (2.051(2)Å), which represents evidence for asymmetric fluorine bridging. It is not known whether this is due to the relative Lewis acidity of RuF<sub>5</sub> and NbF<sub>5</sub> or simply to differences in the bonding, but the latter is thought to have a greater influence.

A second difference between the structure of this compound and TaF<sub>5</sub> is that the average M-M° bond distance is 4.034(4)Å, whereas the analogous value in TaF<sub>5</sub> is 4.129Å. This corresponds to a less linear M-F<sub>b</sub>-M bond angle in RuF<sub>5</sub>:NbF<sub>5</sub> [1:1] of ≈ 167°. It is interesting to compare this value with the value from the crystal structure of the analogous compound RuF<sub>5</sub>:TaF<sub>5</sub> [1:1], which is 167°. However, there is no evidence in the RuF<sub>5</sub>:TaF<sub>5</sub> [1:1] crystal structure for two metal sites.

Figure 6.9: Ru K-edge EXAFS Spectrum of

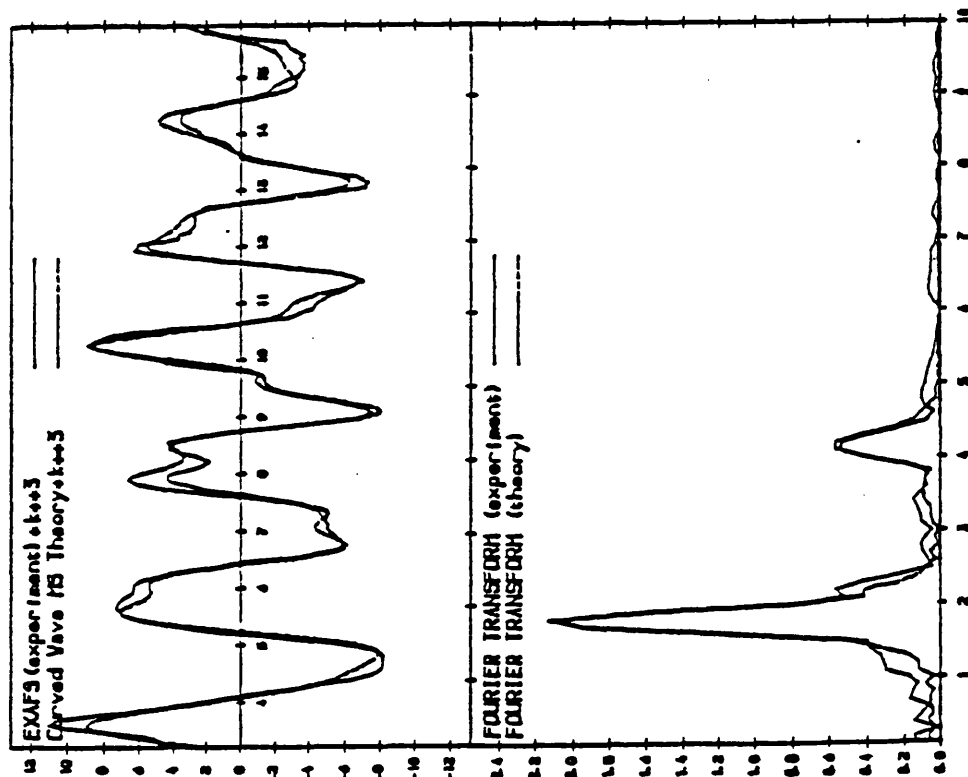
$\text{RuF}_5 \cdot \text{NbF}_5$  [1:1] (with M.S.).



Shell	N	T	R	A
1	4	F	1.828	0.004
2	2	F	2.006	0.005
3	6	F	3.667	0.016
4	2	Nb	4.012	0.019
$R_{[min]}$	21.80			
F.I.	1.957			
$E_0$	52.25			
VPI	-1.36			
AFAC	0.75			
Range	3-18k			

Figure 6.10: Nb K-edge EXAFS Spectrum of

$\text{RuF}_5\text{NbF}_5$  [1:1] (with M.S.).



Shell	N	T	R	A
1	4	F	1.826	0.005
2	2	F	2.053	0.008
3	6	F	3.749	0.028
4	2	Ru	4.055	0.021

$R_{\text{min}}$  19.89  
 F.I. 2.00  
 $E_0$  22.88  
 VPI -2.79  
 AFAC 0.87  
 Range 3-16k

The M-F<sub>b</sub>-M bond angle value of 167° is not surprising bearing in mind that there are two Ru atoms per tetramer and that RuF<sub>5</sub> is a bent fluorine-bridged tetramer [5] and NbF<sub>5</sub> a near-linear fluorine-bridged tetramer [4].

### 6.5.3 RuF<sub>5</sub>:VF<sub>5</sub> [1:1]

Table 6.7 and Figure 6.11 show the analysis of the Ru-edge EXAFS of RuF<sub>5</sub>:VF<sub>5</sub> [1:1]. The data shows that the nearest two metal atoms to Ru are two V atoms. This is confirmed when the analysis using V atoms as M<sup>2</sup> is compared to those where M<sup>2</sup> is either Ru, Nb or Ta. The best fit of these three is for Ta (R<sub>min</sub> = 18.79, F.I. = 1.51), which is comparable to that for V (R<sub>min</sub> = 18.80, F.I. = 1.49) but there is no Ta in the compound. The fit for Ru as M<sup>2</sup> (R<sub>min</sub> = 19.29, F.I. = 1.61) is worse than for V and so the M<sup>2</sup> atoms are assumed to be V. These V atoms are believed to be fluorine bridged to the Ru atoms. This is supported by the infrared spectrum which exhibits a fluorine-bridging mode (see Chapter 5). The X-ray powder diffraction pattern, in the same chapter, shows that this compound adopts a distorted version of the RuF<sub>5</sub>-type structure. The M-F<sub>b</sub>-M bond angle is calculated as 159.7°, which compares to that of 138° for RuF<sub>5</sub> [5], 150° for VF<sub>5</sub> [3] and 171.3(8)° for TaF<sub>5</sub> (Chapter 2.) The Ru-F<sub>b</sub>-V bond angle has been calculated assuming that the V-F<sub>b</sub> is the same as the Ru-F<sub>b</sub> bond distance of 1.966(5)Å, which is a reasonable assumption as the average V-F<sub>b</sub> distance from the VF<sub>5</sub> crystal structure is 1.97(1)Å [3]. It should be noted that, because the M-F<sub>b</sub>-M is so far from linearity in this compound, multiple scattering does not affect the bond distances (see EXAFS theory section).

### 6.5.4 TaF<sub>5</sub>:VF<sub>5</sub> [1:1]

An X-ray structure determination of a single crystal of this material (Chapter 4) shows that the arrangement of atoms is based on that of TaF<sub>5</sub>, and that there appear to be two slightly different metal sites at neighbouring corners of the tetramer. The Ta-edge EXAFS (Table 6.8 and Figure 6.12) seems to support this as the Ta-

Table 6.7: RuF<sub>5</sub>:VF<sub>5</sub>[1:1] EXAFS Analysis

Type of Data	Without M.S.	With M.S.
M-F <sub>t</sub> (Å)	1.800(1)	1.801(1)
M-F <sub>b</sub> (Å)	1.966(5)	1.970(5)
M-M <sup>o</sup> (Å)*	3.875(10)	3.870(10)
R <sub>[min]</sub> (%)	17.88	18.80
F.I.	1.39	1.49
E <sub>0</sub>	23.35	23.06
VPI	-2.43	-1.00
AFAC	0.75	0.68
Range	3-15.8k	3-15.8k

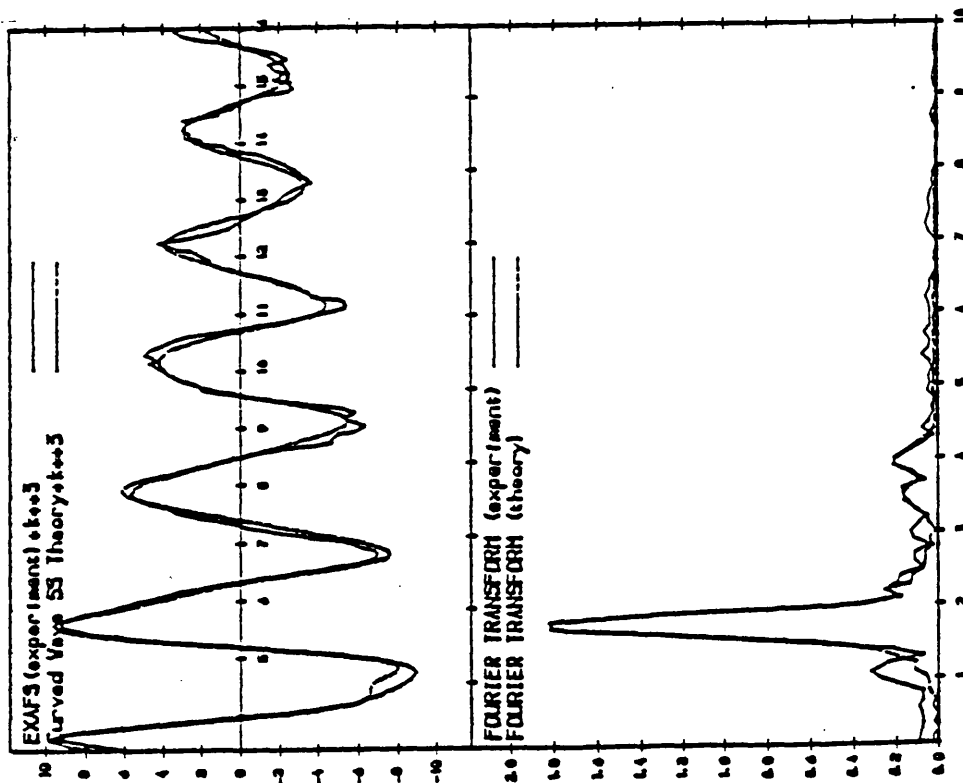
\* Non-bonding distance along one side of the tetramer.

F<sub>b</sub> bond length is 1.973 Å and the M-M<sup>2</sup> is 4.123 Å (see Chapter 4), which would lead to asymmetric fluorine bridging. Whether the nearest two metal atoms to Ta are two V atoms is not certain. The analysis where the M<sup>2</sup> atoms are V has been compared to those when M<sup>2</sup> is either Nb, Ru or Ta. The best fit of these three is for Ru (R<sub>min</sub> = 20.55, F.I. = 1.79) which compares to R<sub>min</sub> = 19.98, F.I. = 1.92 for V. So V can be said to be more favourable on the basis of the R-factor. This is also the case for when the M<sup>2</sup> atoms are Ta (R<sub>min</sub> = 20.61, F.I. = 1.87). However, in this case the M-M<sup>2</sup> distance is 4.117 Å, which is much closer to the crystal structure value of 4.123 Å than in the V analysis where the value is 4.019 Å. It is difficult to explain the Ta-F<sub>b</sub> bond distance though if the M<sub>2</sub> atoms are Ta and so it is tentatively suggested that they are V but that further work is needed to confirm this.

Assuming that the M<sup>2</sup> atoms are V, the M-M<sup>o</sup> distance when multiple scattering is not used, is 4.085(3) Å. This is in reasonable agreement with the the crystal structure value of 4.123 Å (see Chapter 4). However, if multiple scattering is used in the

Figure 6.11: Ru K-edge EXAFS Spectrum of

RuF<sub>5</sub>VF<sub>5</sub> [1:1] (with M.S.)



Shell	N	T	R	A
1	4	F	1.801	0.005
2	2	F	1.970	0.014
3	6	F	3.572	0.028
4	2	V	3.870	0.021
R <sub>[min]</sub> 18.80				
F.I. 1.49				
E <sub>0</sub> 23.06				
VPI -1.00				
AFAC 0.68				
Range 3-15.8k				

Table 6.8: TaF<sub>5</sub>:VF<sub>5</sub>[1:1] EXAFS Analysis

Type of Data	Without M.S.	With M.S.	Crystal Data <sup>‡</sup>
M-F <sub>t</sub> (Å)	1.828(3)	1.830(3)	1.74(5)
M-F <sub>b</sub> (Å)	1.971(9)	1.973(9)	2.04(3) or 2.10(3)
M-M <sup>o</sup> (Å)*	4.085(3)	4.019(28)	4.123 <sup>†</sup>
R <sub>{min}</sub> (%)	21.25	19.98	13.8
F.I.	2.17	1.92	-
E <sub>0</sub>	14.54	13.85	-
VPI	-1.50	-1.36	-
AFAC	0.80	0.78	-
Range	3-15.2k	3-15.2k	-

\* Non-bonding distance along one side of the tetramer.

<sup>†</sup> Distance calculated from atomic positions.

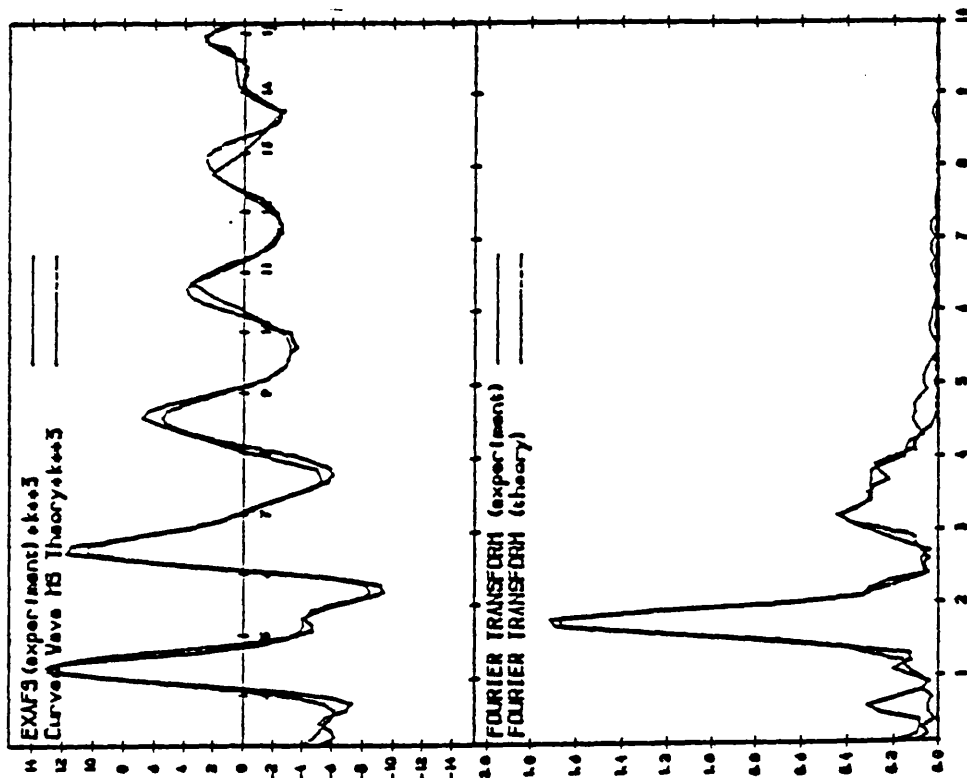
<sup>‡</sup> See Chapter 4.

analysis, the value from the EXAFS spectrum is 4.019(28)Å which does not correlate with the crystal structure even when the error margins are employed. Because of these differences and the fact that the V-F<sub>b</sub> distance is not known, the M-F<sub>b</sub>-M bond angle has not been calculated from the EXAFS. There are other differences between the bond lengths from the EXAFS and those from the X-ray structure determination. For instance, the Ta-F<sub>b</sub> bond length is 1.973(9)Å from the EXAFS, whilst the shorter M-F<sub>b</sub> from the crystal work is 2.04(3). These values are only close when the experimental errors are considered. This, in turn, would lead to the V-F<sub>b</sub> distance from the crystal structure being 2.10(3)Å, which can almost be considered as a non-bonding distance. It would also imply that TaF<sub>5</sub> is a stronger Lewis acid than VF<sub>5</sub>. This might be expected because Ta is a third row and V a first row transition metal.

It should be noted that the statistical test on shell 6 (the M-M<sup>o</sup> distance) for

Figure 6.12: Ta  $L_{III}$ -edge Spectrum of  $\text{VF}_5 \cdot \text{TaF}_5$

[1:1] (with M.S.).



Shell	N	T	R	A
1	4	F	1.830	0.008
2	2	F	1.973	0.011
3	2	F	3.285	0.001
4	4	F	3.428	0.007
5	2	F	3.897	0.007
6	2	V	4.019	0.034
$R_{\text{fit}}(\text{min})$	19.98			
F.I.	1.92			
$E_0$	13.85			
VPI	-1.36			
AFAC	0.78			
Range	3-15.2k			

both the analysis with and without multiple scattering states that the probability that this shell is not valid was only less than 5 %. This is believed to be due to the fact that V is a relatively light element and therefore a poorer backscatterer than heavier elements. It is also the case that fewer data points were collected for the Ta-edge spectra and so the signal to noise ratio of this spectrum may be worse than that for the Nb- and Ru-edge spectra. These facts may also explain the poor agreement of the Ta-V distance from the EXAFS and single crystal data. A further reason may be that the crystal structure data could not be solved below an R-factor of 13.8 %, even though the data appeared of reasonable quality. It is not known why this is the case, but this may lead to increased errors in the bond angles and distances from this work. To eliminate these problems would require the collection of a new single crystal diffraction data set, on a new crystal, and also to record the EXAFS spectrum again, with a greater number of scans. These are both possible ideas for future work.

#### 6.5.5 RuF<sub>5</sub>:TaF<sub>5</sub> [3:1]

The single crystal structure determinations of RuF<sub>5</sub>:TaF<sub>5</sub> [1:3] and RuF<sub>5</sub>:TaF<sub>5</sub> [1:1] have been carried out (see Chapter 3). It has not been possible to grow single crystals of RuF<sub>5</sub>:TaF<sub>5</sub> [3:1] of sufficiently high quality for X-ray diffraction work because this compound sublimates to give a poorly crystalline material. This means that the only structural data for this compound is based on EXAFS and X-ray powder diffraction work. The results of this Ta L<sub>III</sub>-edge EXAFS are shown in Table 6.9 and Figure 6.13.

The data has been analysed both with and without multiple scattering and in both cases the two nearest atoms to the Ta atom are Ru atoms. This has been verified by comparing the analysis using Ru atoms in shell 6 with those when Nb, V or Ta atoms are used. The best fit of these three is for Nb atoms ( $R_{min} = 19.65$ , F.I. = 3.84), which are values close to those for the Ru analysis ( $R_{min} = 19.77$ , F.I. = 3.75). However, this is believed to be the result of the fact that Ru and Nb have

Table 6.9: TaF<sub>5</sub>:RuF<sub>5</sub>[1:3] EXAFS Analysis

Type of Data	Without M.S.	With M.S.
M-F <sub>t</sub> (Å)	1.825(2)	1.825(2)
M-F <sub>b</sub> (Å)	2.053(4)	2.045(5)
M-M <sup>o</sup> (Å)*	4.097(19)	4.011(13)
R <sub>[min]</sub> (%)	17.92	19.77
F.I.	3.37	3.75
E <sub>0</sub>	14.57	14.12
VPI	-1.36	-1.36
AFAC	0.79	0.79
Range	3-15k	3-15k

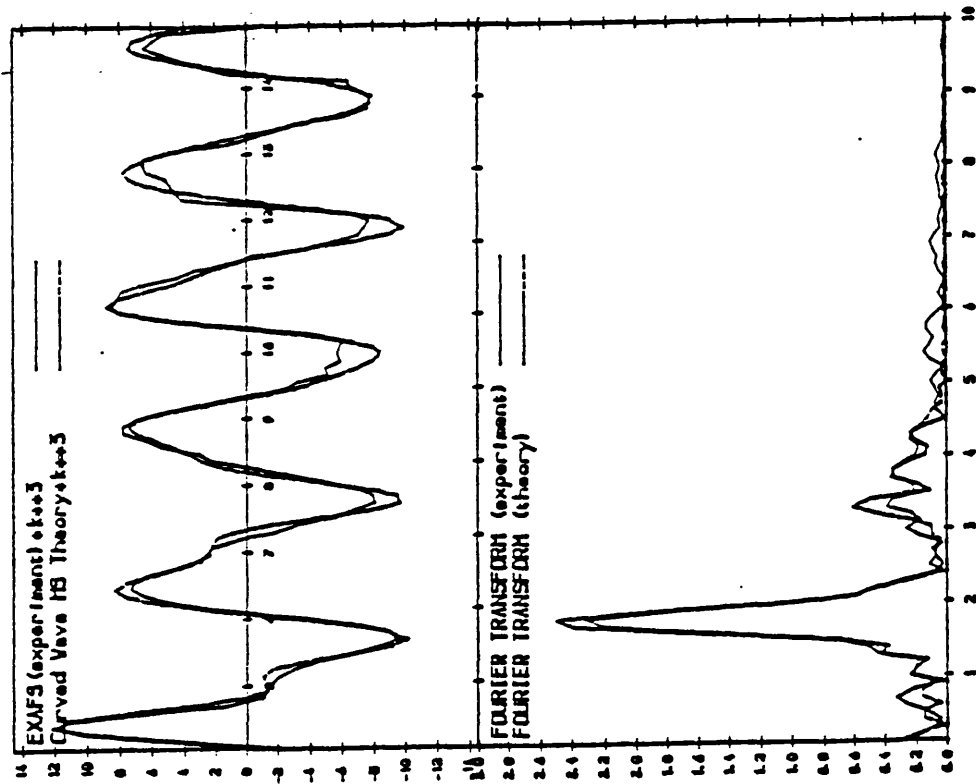
\* Non-bonding distance along one side of the tetramer.

similar atomic weights and phaseshifts. As no Nb is present in the compound this has been discounted and the analysis for Ta atoms checked instead. The values using Ta atoms ( $R_{min} = 20.26$ , F.I. = 3.92) are both higher than when Ru atoms are used, confirming that the M<sup>2</sup> atoms are Ru. This supports the hypothesis that this compound has ordered metal sites. The metal M<sup>3</sup> (cf. Figure 6.8) cannot be determined to be Ru because the Ta-M<sup>3</sup> distance of  $\approx 5.6\text{\AA}$  is at the limit of the reliability of the EXAFS technique.

However, the Ta-F<sub>t</sub> and Ta-F<sub>b</sub> bond lengths for RuF<sub>5</sub>:TaF<sub>5</sub> [3:1] are both reasonable values when compared, for instance, with TaF<sub>5</sub> (Table 6.3). The M-M<sup>o</sup> distance, as expected, is significantly altered by using multiple scattering. Without multiple scattering, this distance is 4.097(18)Å, but with multiple scattering the value departs to 4.011(13)Å. If it is assumed that the Ru-F<sub>b</sub> distance is  $\approx 2.00\text{\AA}$  (the value in RuF<sub>5</sub> [3] and RuF<sub>5</sub>:NbF<sub>5</sub> [1:1]) and that the M-M<sup>o</sup> distance is more accurately calculated using multiple scattering (which appears to be valid from the

Figure 6.13: Ta  $L_{III}$ -edge Spectrum of  $RuF_5 \cdot TaF_5$

[3:1] (with M.S.).



Shell	N	T	R	A
1	4	F	1.825	0.002
2	2	F	2.045	0.007
3	2	F	3.364	0.001
4	4	F	3.349	0.018
6	2	Ru	4.011	0.022
$R_{(min)}$	19.77			
F.I.	3.75			
$E_0$	14.12			
VPI	-1.36			
AFAC	0.79			
Range	3-15k			

metal pentafluoride EXAFS analyses), then the M-F<sub>b</sub>-M bond angle is  $\approx 163^\circ$ . This bond angle is reported only tentatively because it is calculated on the basis of a number of assumptions. However, the value of  $163^\circ$  does fit the trend exhibited by this series of compounds (see Table 6.10).

Table 6.10: M-F<sub>b</sub>-M Bond Angles For RuF<sub>5</sub>, TaF<sub>5</sub> and RuF<sub>5</sub>:TaF<sub>5</sub> [3:1], [1:1] and [1:3]

RuF <sub>5</sub>	RuF <sub>5</sub> :TaF <sub>5</sub> [3:1]	RuF <sub>5</sub> :TaF <sub>5</sub> [1:1]	RuF <sub>5</sub> :TaF <sub>5</sub> [1:3]	TaF <sub>5</sub>
138°	163°*	167°	173°	172°

\* This bond angle has been calculated from the Ru K-edge EXAFS spectrum of this compound. The other values in the table are calculated from X-ray single crystal data.

It should be noted that when multiple scattering is not used the probability that shell 6 is not valid is only less than 5 % but when multiple scattering is used the probability is less than 1 %. This tends to confirm that analysis of the TaF<sub>5</sub>-structural type is more accurate when multiple scattering is used.

### 6.5.6 TaF<sub>5</sub>:VF<sub>5</sub> [1:3]

The Ta-edge EXAFS spectrum (Table 6.11 and Figure 6.14) of this compound is particularly interesting because it seems to show a discreet TaF<sub>6</sub><sup>-</sup> ion. This means that the tetrameric structure based on TaF<sub>5</sub>, which is exhibited by TaF<sub>5</sub>:VF<sub>5</sub> [1:1], does not seem to exist in this compound. Instead, there is still octahedral coordination around the Ta atom, with the nearest two metal atoms to the Ta atom being two V atoms at a distance of 4.301(31)Å with multiple scattering and 4.434(34)Å without multiple scattering. The fact that the two M<sup>2</sup> atoms are V is confirmed by the comparison of this analysis with those when the M<sup>2</sup> atoms are either Nb, Ru or Ta. The best fit of these three is for Ta ( $R_{min} = 18.51$ , F.I. = 2.87) which compares to  $R_{min} = 18.64$  and F.I. = 3.13 for V. The values for Ta are better but

the  $M-M^2$  distance is only 4.065 Å. It is then difficult to reconcile the bond lengths around the absorbing Ta atom if the  $M^2$  atoms are also Ta atoms. They are therefore tentatively suggested to be V atoms, but further work is required to confirm this.

In the multiple scattering analysis, which is considered more accurate, the Ta- $F_b$  distance is calculated as 1.846 Å. This leads to a V- $F_b$  distance of at least 2.455 Å, which seems rather long to be a bonding distance. It should be noted that the differences in the Ta-F bond lengths are all the same until the multiple scattering shells are fitted. It may therefore be that they split into two groups as a result of the multiple scattering calculations rather than any real differences.

Whether there is another V atom or indeed any atom at position  $M^3$  (cf. Figure 6.8) cannot be determined from the EXAFS spectrum, although a  $TaF_6^- V_3F_{14}^+$  pseudo-tetramer (Figure 4.4) would perhaps be the most logical structure from this analysis. This is a very tentative suggestion as the probability that shell 6 is valid with and without multiple scattering is only less than 5 % and so this must be considered to make the errors associated with this shell greater than those for the others.

## 6.6 Conclusions

The analyses of the EXAFS spectra of the metal pentafluorides  $NbF_5$ ,  $TaF_5$  and  $RuF_5$  (section 6.4) show that this technique can be used as a non-destructive, localised probe of structure. By comparison with the relevant crystal structure determinations, it can be seen that the bond lengths from the EXAFS are, generally, in agreement within experimental error ( $\pm 0.02$  Å). It should be noted that the errors on the bond lengths from the EXAFS appear to increase as the distance from the absorbing atom increases. This is particularly important for distances greater than 3.5 Å.

The effect of using multiple scattering in the EXAFS analysis has also been considered. It appears that the closer to linearity the  $M-F_b-M$  bond angle becomes, the

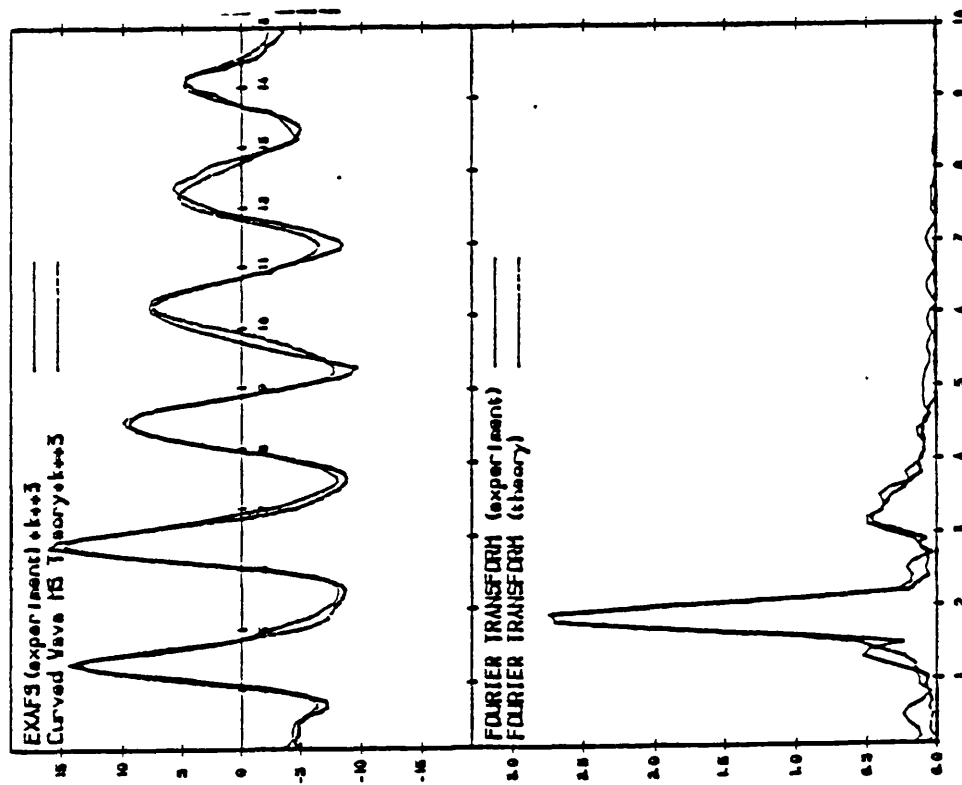
Table 6.11: TaF<sub>5</sub>:VF<sub>5</sub>[1:3] EXAFS Analysis

Type of Data	Without M.S.	With M.S.
M-F <sub>t</sub> (Å)	1.891(1)	1.902(10)
M-F <sub>b</sub> (Å)	-	1.846(21) <sup>†</sup>
M-M <sup>o</sup> (Å)*	4.434(31)	4.301(31)
R <sub>[min]</sub> (%)	18.60	18.64
F.I.	2.98	3.13
E <sub>0</sub>	9.16	10.48
VPI	-1.29	-1.50
AFAC	0.68	0.70
Range	3-15k	3-15k

\* Non-bonding distance along one side of the tetramer.

<sup>†</sup> The F atoms in this shell are defined as bridging for the purposes of the multiple scattering calculations and are not strictly speaking bridging F atoms. The difference between R1 and R2 shown in the table is only observed after the addition of multiple scattering calculations and so R1 and R2 are assumed to be the same within experimental error.

Figure 6.14: Ta  $L_{III}$ -edge Spectrum of  $VF_5 \cdot TaF_5$   
 [3:1] (with M.S.).



Shell	N	T	R	A
1	4	F	1.902	0.003
2	2	F	1.846	0.007
3	2	F	3.276	0.000
4	4	F	3.421	0.010
5	2	F	4.025	0.014
6	2	V	4.301	0.037

$R_{[min]}$  18.64

F.I. 3.13

$E_0$  10.48

VPI -1.50

AFAC 0.70

Range 3-15k

greater the influence of multiple scattering on the  $M-M^\circ$  distance. This fact is supported by the theory on which EXAFS analysis is based (see EXAFS theory section).

The reason for analysing the EXAFS spectra of the mixed-metal pentafluorides has been to establish whether the apparently random site occupancy of the mixed-metal pentafluoride tetramers determined by X-ray single crystal work is due to a random arrangement of metal atoms throughout the material (see Figure 2.13c), or to an ordered site occupancy within each tetramer, with a random arrangement of tetramers (see Figure 2.13b). The EXAFS supports the hypothesis that the mixed-metal pentafluorides have ordered metal sites in each tetramer, but that those tetramers are arranged in a superlattice. The arrangement of the tetramers can perhaps be explained by the fact that a superlattice arrangement would allow a minimum distortion of the fluorine atoms by the different ionic radii of the metal atoms.

The EXAFS spectra have also been collected and analysed on a number of mixed-metal pentafluorides where no X-ray single crystal determination has been carried out. The bond lengths and angles are subject to the normal errors associated with EXAFS analysis and a more complete understanding of these structures has only been possible using EXAFS in conjunction with other techniques (eg. infrared and X-ray powder diffraction). They do appear to have the structures which might be predicted for them, in that the structures are dominated by the larger  $M^{5+}$  ion. This, in turn, reinforces the importance of the packing of the atoms within these structures.

## Chapter 7

# Solid-State Structural Conclusions

### 7.1 Introduction

In this thesis, the main aim has been first to examine the relevant structural data already published for the transition-metal pentafluorides (held in Chapter 1), and then to investigate novel compounds involving them. From this work, further insights into the arrangement of the atoms in the pentafluorides have been gained and these are dealt with in this chapter.

Overall, it appears that the anion packing in the mixed-metal pentafluorides is dominated by the larger  $M^{5+}$  ion present. It also appears that the tetramers form superlattice arrangements, such that the metal sites occur randomly throughout the lattice. This is also believed to be due to packing considerations, as this allows for a minimum distortion of the anion lattice due to the different  $M^{5+}$  sizes.

A second area of interest lies in the localised bonding of the tetrameric molecules within the lattice, which seems to be influenced by the individual physical properties of the metal pentafluorides, rather than by packing. The fluorine bridging which joins the metal atoms is believed to be influenced both by packing and bonding. These ideas are thought to apply to both the mono-transition-metal and mixed-

transition-metal pentafluorides.

## 7.2 The TaF<sub>5</sub> Structure

A detailed explanation of the RuF<sub>5</sub> type-structure [5, 58, 59] is already in the literature. As a rough approximation, the first two reports deal with the packing of the atoms, and the other with the bonding within the structure. However, the mixed-metal pentafluorides studied by X-ray single crystal work all adopt the TaF<sub>5</sub> structure. This arrangement of atoms has already been described in terms of a c.c.p.-lattice of fluorine atoms [1], but a more detailed investigation of this structure is described here, on the basis of the redetermined structure which forms part of this work.

If the anions in TaF<sub>5</sub> form a perfect cubic-close packed lattice, then the M-F<sub>b</sub>-M bond angle would be 180° and the M-M° distance would be  $\approx 3.82 \text{ \AA}$  (based on a F<sup>-</sup> radius of 1.35  $\text{\AA}$  [67]). The actual values are 171.3° and 4.129  $\text{\AA}$ , which illustrates a distortion of the theoretical lattice. For perfect c.c.p., the radius of an octahedral hole within the lattice is 0.54  $\text{\AA}$ , while the actual Ta<sup>5+</sup> radius is 0.64  $\text{\AA}$  [67]. This discrepancy goes some way to explaining the observed distortion in TaF<sub>5</sub>, but the Ta<sup>5+</sup> radius is not sufficiently large to account for all of it. Instead, the additional distortion is probably due to the fluorine atoms themselves. For perfect c.c.p. to occur, all the fluorine atoms must be perfect spheres of equal size. However, the Ta-F<sub>b</sub> bond lengths are longer than the terminal ones and so, effectively, all the fluorine atoms are not of similar size. However, there seems to be a limit to the extent of this distortion of the TaF<sub>5</sub> tetramer. For instance, WOF<sub>4</sub> has a similar structure to TaF<sub>5</sub> with symmetrical fluorine bridges (2.11  $\text{\AA}$ ) and a bridging angle of 172.6°, which corresponds to a W-W° distance of 4.21  $\text{\AA}$ . MoOF<sub>4</sub> and ReOF<sub>4</sub> have asymmetric fluorine bridges of 2.00  $\text{\AA}$ , 2.32  $\text{\AA}$  and 1.94  $\text{\AA}$ , 2.29  $\text{\AA}$ , respectively. If these adopted the TaF<sub>5</sub> structure, then the M-M° distance would be  $\approx 4.3 \text{ \AA}$ , which would allow more space between the atoms and a greater distortion of the tetramer, which would presumably not hold together. They, therefore, adopt the

$\text{VF}_5$  endless-chain arrangement which is not close-packed and does not restrict the atomic arrangement in the same way. Indeed, this minimising the departure of the lattice from close packing may explain why the Ta-F<sub>b</sub>-Ta bond angle is not 180°. The departure from linearity may be in order to keep the M-M° distance to a minimum. The increase in the M-M° distance from 3.82 Å, for perfect packing, must give rise to space between the atoms, which in turn allows the fluorine-bridging bond angle to depart from 180°. Indeed it is stated earlier that the packing of the atoms dominates the overall structure while localised differences are due to the different physical properties of the pentafluorides. It is the departure from close packing that allows these localised differences to occur.

In  $\text{RhF}_5$ , the Rh-F<sub>b</sub> bonds are  $\approx 0.18$  Å longer than the terminal ones [59] and, as such, are believed to be due to one-electron and two-electron bonds respectively. In  $\text{TaF}_5$ , the difference is  $\approx 0.23$  Å and so it seems likely that this represents another type of fluorine bridging. A description of this in terms of the bridging-fluorine atom being some way along the ionisation path to  $\text{F}^-$ , held between two positive metal centres is already in the literature [59, 80].

### 7.3 Packing in the Transition-Metal Pentafluorides

Table 7.1 shows the transition-metal pentafluorides grouped into the three structural types, along with their appropriate ionic radii. For the second and third row transition-metal elements, there is a correlation between the two. For instance those which adopt the  $\text{TaF}_5$ -type structure have  $\text{M}^{5+}$  radii from 0.64–0.61 Å, whilst for those with the  $\text{RuF}_5$ -type structure, the range is 0.575–0.55 Å. In between these two, are  $\text{TcF}_5$  and  $\text{ReF}_5$  (0.60 Å and 0.58 Å respectively), which are believed to adopt a structure between those of  $\text{RuF}_5$  and  $\text{TaF}_5$ .

$\text{VF}_5$  and  $\text{CrF}_5$  have  $\text{M}^{5+}$  radii of 0.54 and 0.49 Å, respectively, and are grouped with  $\text{TcF}_5$  and  $\text{ReF}_5$ . However, both these metal ions are small enough to occupy an octahedral hole in either a c.c.p- or h.c.p.-fluorine lattice. Using  $\text{VF}_5$  in a c.c.p.

Table 7.1: Selected Physical Properties of the Transition-Metal Pentafluorides

Compound	d <sup>n</sup> -configuration	M <sup>5+</sup> Radius (Å) [67]	Formula Unit Volume (Å <sup>3</sup> ) [60]
VF <sub>5</sub>	0	0.54	84.9
CrF <sub>5</sub>	1	0.49	82.9
TcF <sub>5</sub>	2	0.60	94.9
ReF <sub>5</sub>	2	0.58	94.1
RuF <sub>5</sub>	3	0.565	83.3
OsF <sub>5</sub>	3	0.575	85.0
RhF <sub>5</sub>	4	0.55	84.4
IrF <sub>5</sub>	4	0.57	81.9
PtF <sub>5</sub>	5	0.57	82.2
AuF <sub>5</sub>	6	0.57	89 [48]
NbF <sub>5</sub>	0	0.64	88.3
TaF <sub>5</sub>	0	0.64	88.6
MoF <sub>5</sub>	1	0.61	87.8
WF <sub>5</sub>	1	0.62	89.3

lattice as an example, it can be seen that if there were four  $V^{5+}$  ions at the corners of a tetramer, there would be no distortion of the fluorine lattice. The V-V° distance would be  $\approx 3.82 \text{ \AA}$  and all the V-F bonds would be  $\approx 1.89 \text{ \AA}$ . It is very difficult to see how such a tetramer would be held together as all the V-F distances suggest a situation in which something approaching two-electron bonds are utilized and there would not be sufficient electrons for this to occur.

In the actual  $VF_5$  structure, the  $V^{5+}$  ions are arranged in a lattice where the anions are not close packed and as such there is no restriction on the bonding which can be adopted. The V-F<sub>b</sub> bonds (average  $1.965 \text{ \AA}$ ) are  $\approx 0.27 \text{ \AA}$  longer than the terminal bonds ( $1.697 \text{ \AA}$ ), which does not allow for the Pauling relationship described for the  $RuF_5$ -type structure [59]. The V-F<sub>b</sub>-V bond angle of  $149.6^\circ$  seems to discount the possibility of the fluorine bridging described for  $TaF_5$ . It is therefore assumed, on the basis of this bond angle, that the  $VF_5$  fluorine-bridge bonding lies between these two extremes,  $RuF_5$  and  $TaF_5$ . It would be extremely interesting to study the single crystal structure of either  $ReF_5$  or  $TcF_5$ , as the ionic radii of  $Re^{5+}$  and  $Tc^{5+}$  is so much closer to the other second and third row  $M^{5+}$  ions, and the bond lengths and angles would presumably be larger than those for  $VF_5$ . It would also be helpful to repeat the  $VF_5$  structure to get more accurate atomic positions. However, the overall  $VF_5$  structure previously reported [3] is believed to be correct.

## 7.4 Comparison Of H.C.P. and C.C.P. Fluorine Lattices

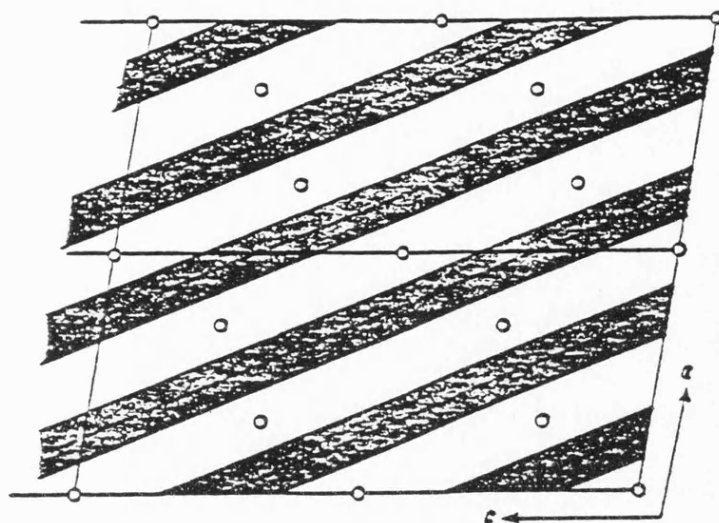
For either perfect close-packed arrangement, the volume occupied by the anions is 74% and the size of the octahedral holes is the same ( $0.54 \text{ \AA}$ ). For all the  $M^{5+}$  ions adopting these structures (see Table 7.1), their radii are too large to occupy this hole without distorting the lattice. On the other hand, the pentafluorides adopting the  $RuF_5$  arrangement have smaller  $M^{5+}$  ions (see Table 7.1), and, as such, distort the lattice less than those adopting the  $TaF_5$  structure. This is reflected in the smaller

formula unit volumes for the former case.

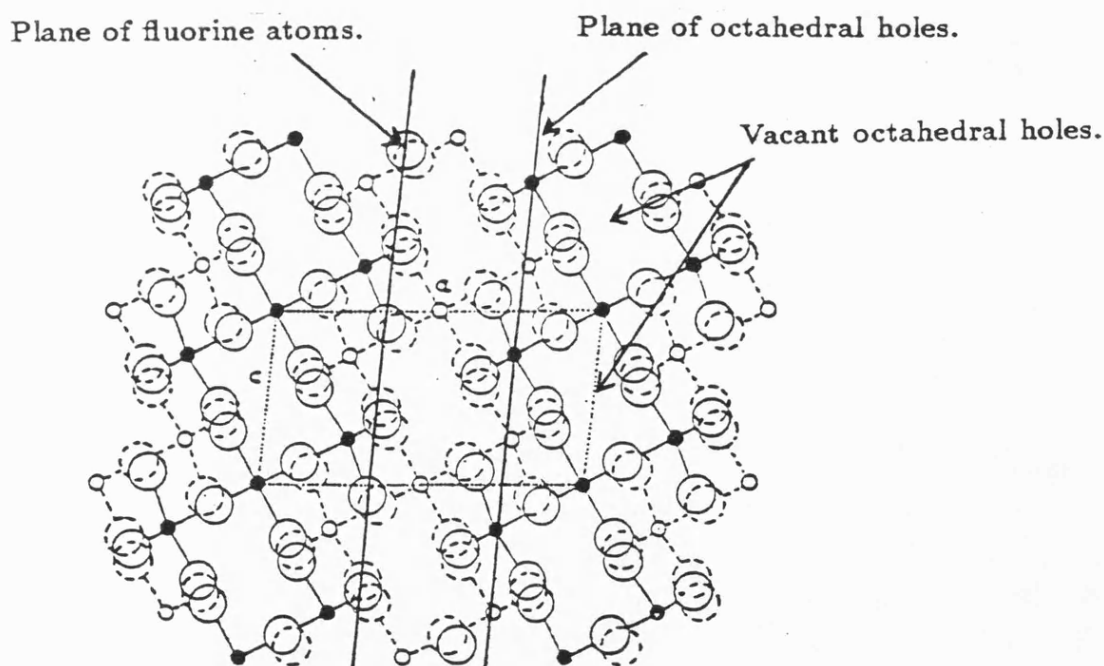
One difference between the h.c.p. and c.c.p. lattices is that the  $M-F_b-M$  bond angle for perfect packing is  $132^\circ$  and  $180^\circ$  respectively, and the metal atoms of the former are arranged in layers [58]. For  $TaF_5$  in a c.c.p. fluorine lattice, if there is a Ta atom on one octahedral site in a layer, there is a vacant octahedral site between this Ta atom and the next in the same layer. In  $RuF_5$ , where the metal ions are in the same layer, the  $M-M^\circ$  distance is shorter than for  $TaF_5$  ( $4.129 \text{ \AA}$ ), and there are three metal, non-bonding d-electrons. It may therefore be that there is some limited metal-metal interaction and that the non-linear fluorine bond angle does not prevent this occurring. This is illustrated in Figure 7.1

One of the original explanations for the different structures [23] is that there is  $\pi$ -bonding from the bridging fluorine atoms into the vacant d-orbitals of the metal atoms in the  $TaF_5$  structure. This is favourable where the  $d^n$  configuration is less than  $d^3$  and would require a bridging angle of  $180^\circ$ . The  $\pi$ -bonding argument is now clearly discredited on the grounds that (a) the  $M-F_b$  bond lengths are rather long, (b) the  $M-F_b-M$  bond angle for  $TaF_5$  is now known to depart from  $180^\circ$ , and (c) a similar tetrameric structure is adopted by  $Ba_3Al_2F_{12}$  [142], which has no low energy d-orbitals available for bonding.

Both the metal-metal bonding in  $RuF_5$  and  $\pi$ -bonding in  $TaF_5$  may occur to a limited extent, but in both cases the distances involved are too great to have a significant effect on the bonding of these molecules. It is surely more likely that it is the bridging-bond angle that gives rise to the adoption of one or other structure. This has been detailed before [59, 80], but must be allied to the anion packing and the metal ion size, which has not previously been thought to be important. Packing considerations have already been shown to explain the  $VF_5$  and  $CrF_5$  structures and it is also interesting to note that, in  $RhF_5$ , the fluorine-bridging bond angle ( $135^\circ$ ) is closest to that for perfect h.c.p. ( $132^\circ$ ), which corresponds to the  $Rh^{5+}$  radius ( $0.55 \text{ \AA}$ ) being the smallest ion in this group and only slightly larger than the octahedral



(a) Shaded areas represent layers of fluorine atoms.  
Open circles represent Ru atoms.



(b) Larger open circles represent fluorine atoms. Dark circles represent Nb atoms in a plane at  $b = 0$ . Small open circles represent Nb atoms at  $b = 0.5$ .

Figure 7.1: [001] Projection of (a) the  $\text{RuF}_5$ -Type Lattice and (b) [010] Projection of the  $\text{NbF}_5$ -Type Lattice.

hole (0.54 Å).

When the packing considerations are applied to the mixed-metal pentafluorides, it is not difficult to see why the structures are dominated by the larger  $M^{5+}$  ion. It is particularly interesting to look at structures such as  $VF_5:TaF_5$  [3:1] where the  $TaF_5$  arrangement of atoms does not occur, presumably because the smaller  $V^{5+}$  ions do not allow for a distortion of the anion lattice which occurs when a larger percentage of  $Ta^{5+}$  ions are present.

It is interesting to note that  $BiF_5$  and  $UF_5$  have the same  $M^{5+}$  radii (0.76 Å) and both crystallise as trans-fluorine bridged endless chains, though  $UF_5$  has a second form also.  $Sb^{5+}$  has a radius (0.60 Å) similar to  $TcF_5$  and  $ReF_5$  and has a structure based on alternating layers of h.c.p. and c.c.p atoms.  $ReF_5$  and  $TcF_5$  might also be expected to adopt this arrangement, but there must be another consideration (most probably based on the fluorine bridging) which prevents this.

## 7.5 Future Work

There are two main areas of future work, the first of which would be to confirm the EXAFS data that suggests that the metal sites in the mixed-metal pentafluorides are ordered, by X-ray crystallography. If  $RhF_5:TaF_5$  [3:1], [1:1] or [1:3] were prepared the  $Rh-F_{(ax)}$  bond lengths would be shorter than the equivalent equatorial bonds, whilst for the  $Ta-F_t$  bonds the opposite would occur, effectively labelling the metal sites. It might help to anneal the crystals, by slowly heating them to just below their m.p., so as to reduce any possible disorder. As the precise fluorine atom positions would be so important to this work, it might be necessary to collect neutron diffraction rather than X-ray data.

Another possibility would be to investigate  $ReF_5:VF_5$  [x:y], as both pentafluorides adopt the endless-chain structure. Disorder caused by rotation of tetrameric molecules within the lattice, to form a superlattice, would not be possible and an

ordered structure of this type is already known for  $\text{NbF}_5:\text{SbF}_5$  [1:1] [84]. The Re-F and V-F bond lengths in these compounds would presumably be very different, allowing the metal sites to be easily assigned.

The second area of future work would be to determine a full X-ray structure of either  $\text{TcF}_5$  or  $\text{ReF}_5$  as, although they are known to adopt the  $\text{VF}_5$  structure, the bond lengths and non-bonding distances must be very different. This is reflected by the very different ionic sizes and formula unit volumes of this group of pentafluorides (see Table 7.1).

It has been stated previously [143], that it would be interesting to study the high pressure forms of the transition-metal pentafluorides to investigate why tetramerisation occurs. This would not only be challenging intellectually, but also experimentally and might present a more complete explanation for the different structural types.

## Chapter 8

# Metal Inorganic Chemical Vapour Deposition Studies on Selected Metal Fluorides

### 8.1 Introduction

#### 8.1.1 Area of Study

Metal organic chemical vapour deposition (MOCVD) is a well established area for the preparation of materials for the electronics industry. However, this process uses organometallic compounds as precursors which can lead to problems of residual carbon content in the deposits. This contamination can affect the performance of the resulting electronic devices and much of the present research effort is centred on minimising this residual carbon content.

Metal inorganic chemical vapour deposition (MICVD) may offer advantages over MOCVD, from the point of view of reducing contamination in the deposit. The vast potential for the development of MICVD can perhaps be gauged by the large literature already published on  $\text{UF}_6$ ,  $\text{WF}_6$ ,  $\text{MoF}_6$  and  $\text{ReF}_6$  as precursors for deposition. Since the literature is large, only selected examples are mentioned in this introduction but, for a text covering all areas of thin film technology, reference can be made

to the Handbook of Thin Film Technology [144], and for a review of the platinum group metals in the electronics industry to the paper by Hagenmuller in *Inorganic Solid Fluorides* [145].

The normal limitations for a precursor, used for chemical vapour deposition (CVD), inevitably also apply to the metal fluorides. For instance, the precursor must be volatile at the temperature of the CVD apparatus (ideally this is room temperature), as it has to travel through the gas phase from source to substrate. Secondly, the precursor must be free from contamination at least to the parts per billion level or better, as the impurity may be transferred to the final deposit. The third requirement is that the precursor undergoes complete reaction, at a reasonable rate, to give a pure deposit, and that the by-products of that reaction are volatile and do not undergo secondary reactions with the substrate. The requirement for the precursor to react, at a reasonable rate, is rather vague and is dependent on what type of deposit is required [27]. If the process is used to form a large number of relatively low purity deposits (99.99 per cent pure), then a faster reaction rate will be advantageous. However, if a small number of very highly pure deposits are required (ie. contamination levels below parts per billion), then a slower reaction rate may not be a problem and may even be an advantage in gaining a more crystalline deposit. Since there is a tendency towards smaller electronic devices with more exacting specifications the latter case is now perhaps more usual.

### 8.1.2 Review of Previous Work

Although there has been work carried out on the reduction of the metal hexafluorides, there do not appear to be any reports in the literature of the use of transition-metal pentafluorides as precursors for CVD. However, the CVD of these compounds opens up the possibility of producing pure deposits containing V, Ta, and Nb, which do not form hexafluorides. Also, some of the transition-metal hexafluorides are difficult to prepare and indeed, in some cases, are most easily prepared from their respective pentafluorides (eg.  $\text{RhF}_6$  and  $\text{RuF}_6$  [146]). These compounds are very

reactive and moisture sensitive and, although  $\text{RuF}_5$  and  $\text{RhF}_5$  are also extremely moisture sensitive and less volatile, they offer more suitable candidates for CVD because they are easier to manipulate.

The published work on the hexafluorides has been concerned mainly with  $\text{WF}_6$ ,  $\text{MoF}_6$  and  $\text{ReF}_6$  (eg. [147–150]), and on the possible uses of deposits of W, Mo, Re and their respective alloys. In addition, there are a few reports of CVD using  $\text{IrF}_6$  and  $\text{PtF}_6$  [28, 151, 152], which are again associated with the electronics industry. There is also an extensive literature on the reduction of  $\text{UF}_6$ , which has been carried out mainly because of the importance of U in the nuclear industry. For a review of  $\text{UF}_6$  chemistry in the nuclear industry, the reader is referred to the review by Hagemuller [153]. The conversion of  $\text{UF}_6$  to  $\text{UO}_2$  is the process by which fuel rods are prepared for electricity generation, for some nuclear power stations. The depleted  $\text{UF}_6$ , which is the bi-product of the preparation of these fuel rods, is a potentially hazardous material, and it is thought that U metal would provide a safer storage option. The reduction of  $\text{UF}_6$  to U metal using  $\text{H}_2$  would also produce HF which could then be electrolysed to produce hydrogen and fluorine. This hydrogen would then be available to reduce more  $\text{UF}_6$ , whilst fluorine gas would be a valuable commodity for sale. If reduction using  $\text{H}_2$  is not possible, then the use of Si as a reductant would produce  $\text{SiF}_4$ . This has fewer potential uses than HF or  $\text{F}_2$ , but still offers U metal as a safer storage material.

Although a complete evaluation of the transition-metal pentafluorides as precursors for CVD would be the work of several PhD theses, a preliminary theoretical investigation and some experimental work is reported in this chapter, and compared with previously published work.

### **Uses for Deposits Formed by MICVD**

Some of the possible areas of industrial interest for MICVD are (a) for the electronics industry, (b) for the preparation of catalysts and (c) for the metallurgical

industry.

In the electronics industry  $WF_6$ , has been studied as a precursor for the preparation of metal contacts for semiconductors [27], for the development of electronic devices (eg. Schottky barrier [25]) and for use in solar cells [26]. Because some of these applications are dependent on the precise nature of the deposit (which can only be controlled during its formation), MICVD often provides the only method of preparation of the deposit required. Because of the nature of the reduction of  $WF_6$  by hydrogen, there is also potential to make very high quality W components without the need for high-temperature moulding or welding [30]. This is of particular importance where very demanding specifications are required (eg. space travel).

The need for very high purity platinum group metals (PGM's) as well as V, Cr, Nb and Ta have also been detailed in the literature [29]. For instance, their usage has been described in liquid crystals [155], layer resistors [156], electrode plating [157] and the formation of thin oxide layers [158]. Many of these applications require specific physical properties of the metals, which are only known to exist for the PGM's.

It is also known that some of the transition metals (including Nb  $\rightarrow$  Ru and Ta  $\rightarrow$  Ir) are superconducting at  $\approx 4K$  [128], that is, their electrical resistance reduces to zero at or below this temperature. It is also known that alloys involving these metals are superconducting (eg. WRe [159] and  $Nb_3Sn$  [160]). Potential uses for superconductors are believed to include magnetic energy storage, electrical transformers and even train locomotion [128], and it may be that new superconducting materials can be prepared from MICVD.

The use of Pt as a catalyst for organic reactions is well known. However, it may be that if Pt is doped with another metal the catalytic activity of the resultant material can be increased. This obviously leads to the possibility of co-deposition of  $PtF_6$  and another metal fluoride in the required ratio to form more highly active catalysts.

### 8.1.3 The CVD Technique

The MICVD technique involves allowing a volatile precursor (eg.  $\text{WF}_6$ ) to flow over a heated substrate (eg. Si). The precursor is reduced to the metal either by reaction with hydrogen to produce  $\text{HF}_{(g)}$ , or with the substrate itself (eg. the reaction with Si will produce  $\text{SiF}_{4(g)}$ ). The reaction with hydrogen, of course, has the advantage that it allows reduction on to any substrate. Other reductant gases can also be used, for instance,  $\text{CO}_{(g)}$  which forms  $\text{COF}_{2(g)}$  on reaction. A carrier gas, normally Ar to avoid side reactions, may also be fed through the reducing apparatus during the experiment.

It is important to keep the temperature of the substrate as low as possible, during reaction, to prevent decomposition of the substrate. The reduction of  $\text{WF}_6$  typically occurs between  $150^\circ\text{C}$  and  $750^\circ\text{C}$  [161]. At  $\approx 150^\circ\text{C}$ , the rate of deposition is slower compared to that at  $\approx 750^\circ\text{C}$ , but conversely in some cases there may be some decomposition of certain substrates at elevated temperatures, for example GaAs above  $\approx 600^\circ\text{C}$  [27].

## 8.2 Theoretical Thermodynamic Investigation of MICVD

### 8.2.1 The Transition-Metal Pentafluorides and Hexafluorides

Because of the wide range of transition-metal fluorides which have the potential to be used as precursors for CVD, the thermodynamics of the reactions of various metal fluorides, with both hydrogen and silicon, have been calculated. It is interesting to note that the thermodynamics for the reduction by Si, of a given fluoride, are more favourable than for the reduction by  $\text{H}_2$ .

In order for a reaction to take place spontaneously, the change in the Gibbs Free Energy of Reaction ( $\Delta G_r^\ominus$ ) must be negative. So in the case of the reduction of the

metal pentafluorides by hydrogen (Figure 8.1),  $\Delta G_f^\ominus$  [MF<sub>5</sub>] must be less negative than -1366.74 kJmol<sup>-1</sup>. Correspondingly, for the reduction of the metal pentafluorides by Si (Figure 8.2), the  $\Delta G_f^\ominus$  [MF<sub>5</sub>] must be less negative than -1966.8 kJmol<sup>-1</sup>. This shows that the formation of SiF<sub>4(g)</sub> provides a greater driving force for reaction than the formation of HF<sub>(g)</sub>. This compares with the reduction of the metal hexafluorides by hydrogen, where  $\Delta G_f^\ominus$  [MF<sub>6</sub>] (Figure 8.3) must be less negative than -1640.09 kJmol<sup>-1</sup> and for the reduction by Si, it must be less than -2360.18 kJmol<sup>-1</sup>. The calculated values for some transition-metal pentafluorides are shown in Table 8.1, and those for some hexafluorides in Table 8.2.

For any reaction it can be shown that:

$$\Delta H = \Delta G + T\Delta S$$

$\Delta H$  = change in enthalpy.

$\Delta G$  = change in the Gibbs Free Energy of Reaction.

T = temperature.

$\Delta S$  = change in the entropy of reaction.

The values reported are for the reduction of the metal fluorides to metal by a simple gas-phase reaction, and do not allow for any mechanism involving the substrate. It should be remembered that, although these values give an indication as to which reactions should be favourable, only experimental data can confirm or deny their validity.

The values should be compared with those of WF<sub>6</sub>, MoF<sub>6</sub> and IrF<sub>6</sub>, which are all known to be reduced to their respective metals, both in the reaction with H<sub>2</sub> and Si. For both MoF<sub>6</sub> and IrF<sub>6</sub>, the  $\Delta G_r^\ominus$  and  $\Delta H_r^\ominus$  are negative indicating that the reactions are favourable and exothermic. Unfortunately,  $\Delta G_f^\ominus$  [WF<sub>6</sub>] is not known, but the  $\Delta H_r^\ominus$  indicates an endothermic reaction. However, the widespread study of WF<sub>6</sub> shows that this does not prevent it being a useful precursor.

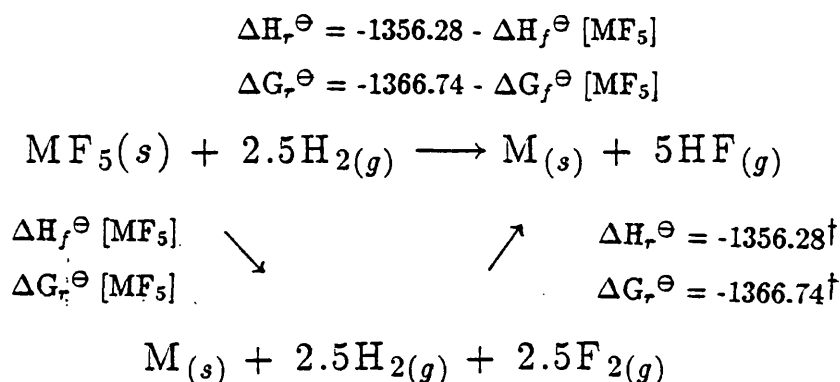


Figure 8.1: Thermodynamics of the Reduction of a Metal Pentafluoride by Hydrogen ( $\text{kJmol}^{-1}$ )

† Based on  $\Delta H_f^\ominus [\text{HF}] = -271.2 \text{ kJmol}^{-1}$  [162] and  $\Delta G_f^\ominus [\text{HF}] = -273.3 \text{ kJmol}^{-1}$  [162].

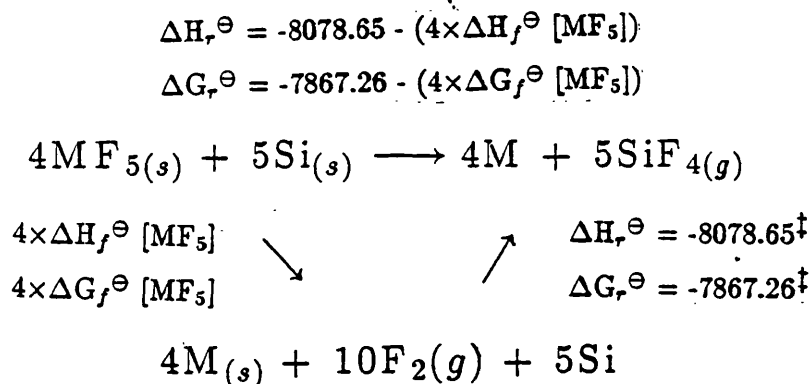


Figure 8.2: Thermodynamics of the Reduction of a Metal Pentafluoride by Silicon ( $\text{kJmol}^{-1}$ )

† Based on  $\Delta H_f^\ominus [\text{SiF}_4] = -1615.7 \text{ kJmol}^{-1}$  [162] and  $\Delta G_f^\ominus [\text{SiF}_4] = -1573.4 \text{ kJmol}^{-1}$  [162].

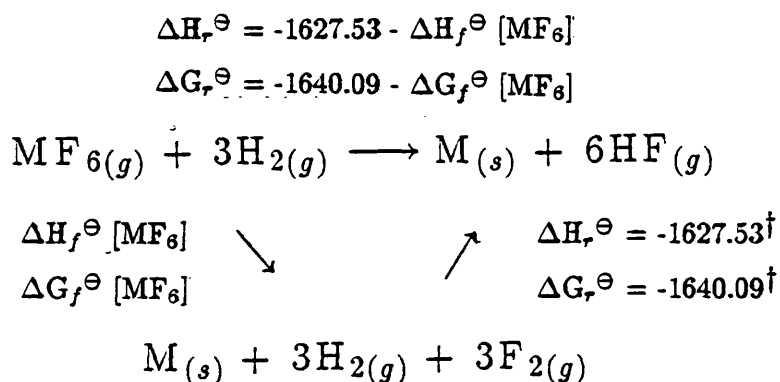


Figure 8.3: Thermodynamics of the Reduction of a Metal Hexafluoride by Hydrogen ( $\text{kJmol}^{-1}$ )

$^\ddagger$  Based on  $\Delta H_f^\ominus [\text{HF}] = -271.2 \text{ kJmol}^{-1}$  [162] and  $\Delta G_f^\ominus [\text{HF}] = -273.3 \text{ kJmol}^{-1}$  [162].

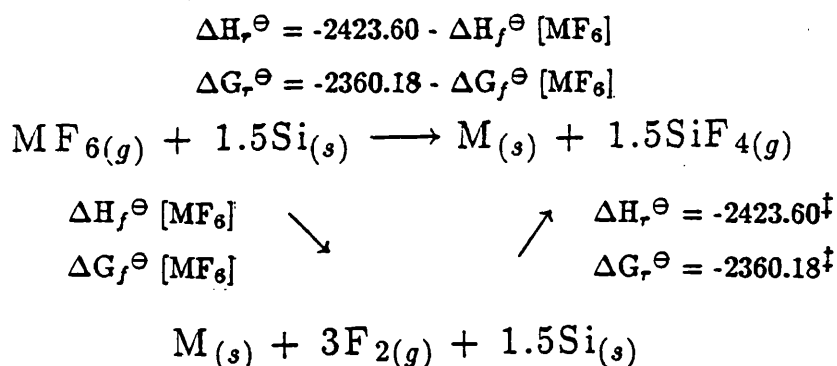


Figure 8.4: Thermodynamics of the Reduction of a Metal Hexafluoride by Silicon ( $\text{kJmol}^{-1}$ )

$^\ddagger$  Based on  $\Delta H_f^\ominus [\text{SiF}_4] = -1615.7 \text{ kJmol}^{-1}$  [162] and  $\Delta G_f^\ominus [\text{SiF}_4] = -1573.4 \text{ kJmol}^{-1}$  [162].

Of the transition-metal pentafluorides, only  $\text{RuF}_5$  appears to have a negative  $\Delta G_r^\ominus$  for the reaction with  $\text{H}_2$ . Although  $\Delta G_f^\ominus [\text{RuF}_5]$  is not known, the other pentafluorides shown exhibit a pattern whereby  $\Delta G_r^\ominus$  is more negative than the  $\Delta H_r^\ominus$ . Therefore, as the  $\Delta H_r^\ominus$  is negative for the reduction of  $\text{RuF}_5$  by  $\text{H}_2$ , the  $\Delta G_r^\ominus$  can also be assumed to be negative. However, all the metal fluorides listed have a negative value of  $\Delta G_r^\ominus$  for the reduction to metal by Si, and all of these reactions are exothermic. This is evidenced by the fact that stoichiometric amounts of Si are used to reduce the metal hexafluorides and pentafluorides to lower fluorides as a standard preparative route [94]. Therefore, all of the metal fluorides listed should make suitable precursors for deposition on to Si substrates.

The melting points and boiling points of some of the metal fluorides are also shown in Tables 8.1 and 8.2, to give some idea of their volatility. The more suitable precursors have high volatility at around room temperature. The boiling points of  $\text{WF}_6$  (17.5°C),  $\text{MoF}_6$  (37°C),  $\text{IrF}_6$  (53°C) and  $\text{VF}_5$  (48.1°C) [162] show that they all have suitable vapour pressures at around room temperature, whilst those of  $\text{RuF}_5$ ,  $\text{NbF}_5$  and  $\text{TaF}_5$  at room temperature are of the order of 0.1mm Hg [80]. Although this is sufficient for CVD in a dynamic vacuum system, it might also be necessary to heat them to increase the deposition rate.

One problem with the metal pentafluorides and hexafluorides, with respect to their use as precursors for CVD, is their extreme oxygen and moisture sensitivity. However, any materials for used for CVD in the electronics industry need to be handled under controlled conditions in order to ensure the very high purity required. By extending these techniques, it should be possible to use such materials without problems. Certainly, this has been possible for  $\text{WF}_6$ ,  $\text{ReF}_6$ ,  $\text{MoF}_6$  and  $\text{IrF}_6$ .

### 8.2.2 The Mixed-metal Pentafluorides

It has been assumed in these calculations, that the  $\Delta H_f^\ominus$  and  $\Delta G_f^\ominus$  values for a given mixed-metal pentafluoride are made up of the appropriate fraction of the values for each metal pentafluoride component. As the thermodynamics of the re-

Table 8.1: Thermodynamics of Reduction of Selected Transition-Metal Pentafluorides

Data	RuF <sub>5</sub>	VF <sub>5</sub>	TaF <sub>5</sub>	NbF <sub>5</sub>
$\Delta H_f^\ominus$ (kJmol <sup>-1</sup> )	-893.3 [162]	-1481.02 [162]	-1904.52 [162]	-1814.65 [162]
$\Delta G_f^\ominus$ (kJmol <sup>-1</sup> )	-	-1373.86 [162]	-1791.62 [162]	-1699.95 [162]
m.p. (°C)	86.5 [42]	19.5 [6]	95 [40]	80 [40]
b.p. (°C)	227 [42]	48.1 [6]	234.9 [40]	229 [40]
$\Delta H_r^\ominus$ [H <sub>2</sub> ] (kJmol <sup>-1</sup> )	-426.98	+124.74	+548.24	+458.37
$\Delta G_r^\ominus$ [H <sub>2</sub> ] (kJmol <sup>-1</sup> )	-	+7.12	+424.88	+333.21
$\Delta H_r^\ominus$ [Si] (kJmol <sup>-1</sup> )	-1073.5	-538.64	-115.14	-205.01
$\Delta G_r^\ominus$ [Si] (kJmol <sup>-1</sup> )	-	-592.96	-175.20	-266.87

duction of all the transition-metal pentafluorides by Si is known to be favourable, it is likely to be the case for the mixed-metal pentafluorides also. For the reduction by H<sub>2</sub>, only the reaction with RuF<sub>5</sub> is thermodynamically favourable and so only the compounds involving a proportion of RuF<sub>5</sub> are detailed below and the reactions of the others are assumed to be unfavourable.

From the calculations shown in Table 8.3, it is obvious that  $\Delta H_r^\ominus$  for the reduction by hydrogen for all the mixed-metal pentafluorides is negative except those for RuF<sub>5</sub>:TaF<sub>5</sub> [1:1], [1:3] and RuF<sub>5</sub>:NbF<sub>5</sub> [1:3]. Of these, the reduction of RuF<sub>5</sub>:TaF<sub>5</sub> [1:1] is believed to be favourable because  $\Delta G_r^\ominus$  is more negative than  $\Delta H_r^\ominus$  for analogous reactions. So, from the thermodynamics, it would appear that only the [1:3] compounds of RuF<sub>5</sub>:TaF<sub>5</sub> and RuF<sub>5</sub>:NbF<sub>5</sub> would not be suitable as precursors for CVD using H<sub>2</sub> as a reductant.

Also detailed in Table 8.3 are some of the results of the gas-phase infrared studies of these compounds. They show that RuF<sub>5</sub>:VF<sub>5</sub> [1:1] decomposes to RuF<sub>5</sub> and VF<sub>5</sub>

Table 8.2: Thermodynamics of Reduction of Selected Metal Hexafluorides

Data	WF <sub>6</sub>	MoF <sub>6</sub>	IrF <sub>6</sub>	UF <sub>6</sub>
$\Delta H_f^\ominus$ (kJmol <sup>-1</sup> )	-1722.98 [162]	-1586 [162]	-579.94 [162]	-2198.09 [162]
$\Delta G_f^\ominus$ (kJmol <sup>-1</sup> )	-	-1473 [162]	-461.89 [162]	-2069.58 [162]
m.p. (°C)	2.5 [162]	17.5 [162]	44.4 [162]	64.5 [154]
b.p. (°C)	17.5 [162]	37 [162]	53 [162]	56.2 [154]
$\Delta H_r^\ominus$ [H <sub>2</sub> ] (kJmol <sup>-1</sup> )	+95.45	-41.53	-1047.59	+570.56
$\Delta G_r^\ominus$ [H <sub>2</sub> ] (kJmol <sup>-1</sup> )	-	-166.27	-1060.15	+429.49
$\Delta H_r^\ominus$ [Si] (kJmol <sup>-1</sup> )	-700.62	-837.6	-1843.66	-225.51
$\Delta G_r^\ominus$ [Si] (kJmol <sup>-1</sup> )	-	-886.36	-1998.29	-290.60

on heating, and so the deposition of a RuV alloy could be more easily be achieved by co-depositing RuF<sub>5</sub> and VF<sub>5</sub>. Where the data is available, it appears that for all the other mixed-metal pentafluorides for which the thermodynamics seem favourable, there is some evidence for mixed-metal gas-phase species. Of these compounds, RuF<sub>5</sub>:MF<sub>5</sub> [3:1] (where M = Nb or Ta) deserve particular mention.

For the reduction by Si, since all the mixed-metal pentafluorides are believed to be reduced to alloys, the NbF<sub>5</sub>:TaF<sub>5</sub> [x:y] series might hold particular interest because it gives the most reliable evidence for mixed-metal species in the gas-phase (see Chapter 2).

Table 8.3: Thermodynamics of Reduction by Hydrogen of Selected Mixed-Metal Pentafluorides

Compound	$\Delta H_f^\ominus$ (kJmol <sup>-1</sup> )	$\Delta H_r^\ominus$ (kJmol <sup>-1</sup> )	Evidence for $M_xM_yF_{15}(g)$
RuF <sub>5</sub> :VF <sub>5</sub> [3:1]	-1040.02	-316.26	-
RuF <sub>5</sub> :VF <sub>5</sub> [1:1]	-1187.16	-169.12	None <sup>†</sup>
RuF <sub>5</sub> :VF <sub>5</sub> [1:3]	-1334.09	-22.19	-
RuF <sub>5</sub> :TaF <sub>5</sub> [3:1]	-1146.11	-210.17	Some <sup>†</sup>
RuF <sub>5</sub> :TaF <sub>5</sub> [1:1]	-1398.91	+42.63	Inconclusive <sup>‡</sup>
RuF <sub>5</sub> :TaF <sub>5</sub> [1:3]	-1651.72	+295.44	Inconclusive <sup>‡</sup>
RuF <sub>5</sub> :NbF <sub>5</sub> [3:1]	-1123.64	-232.97	Some <sup>†</sup>
RuF <sub>5</sub> :NbF <sub>5</sub> [1:1]	-1353.98	-2.3	-
RuF <sub>5</sub> :NbF <sub>5</sub> [1:3]	-1584.31	+228.03	Inconclusive <sup>‡</sup>

<sup>†</sup> See Chapter 5.

<sup>‡</sup> See Chapter 3.

### 8.3 The Reduction Apparatus

Three different pieces of equipment were used in the reduction experiments. These are designated Marks 1, 2 and 3 and are illustrated in Figures 8.5a, 8.5b and 8.6. A brief mention is made here as to the how the equipment has been developed on the basis of practical experience, whilst experimental details are in Chapter 9. The CVD experiments were initially based on a horizontal silica apparatus, Mark 1 (Figure 8.5a), in which the solid metal pentafluoride and the Al substrate were both held in the apparatus, which was heated externally. Hydrogen was used as the reductant and Ar was used as a carrier gas. There were problems with this in that reduction occurred on the surface of the silica, rather than the substrate. This led to inefficient deposition and caused problems in the analysis of the deposit by scanning electron microscopy (SEM) and X-ray fluorescence (XRF) analysis, which require predominantly flat surfaces. The advantage of this design was that the carrier gas and hydrogen passed through the apparatus with a highly laminar flow. This is

especially important in the area of the substrate where reaction is assumed to occur since an uneven gas flow can result in an uneven deposit.

A second apparatus, Mark 2, was developed in which the flow of gas was vertically downwards over the Al substrate (see Figure 8.5b). The metal pentafluoride was loaded into a side-arm on the apparatus, and the H<sub>2</sub> and Ar carrier gas were fed into the apparatus separately (the argon carrier gas passed over the metal pentafluoride source before reaching the substrate). This was to help prevent reduction before reaching the substrate. Again the apparatus was heated externally, and again deposition occurred on the inside of the apparatus walls rather than on the substrate. For both of these designs, there was a positive pressure of Ar and H<sub>2</sub> creating a flow system and the exhaust gases were chemically scrubbed.

Because of the problems of pre-reaction and deposition on the walls of the apparatus, a further piece of equipment has been designed after consultation with Dr Paul Huggett (Plessey Research Ltd). This is the apparatus which has been used in most of the experiments reported here. It is based on a vertical design with upward gas flow (see Figure 8.6), which prevents the problems of a non-laminar downward gas flow. This apparatus is hereafter described as reduction apparatus Mark 3. The substrate is heated from behind with a heating block, inside the apparatus, the main body of which is made of silica to reduce reaction with any HF produced. The silica is not heated externally and, as in the second apparatus, the Ar and H<sub>2</sub> are not mixed until close to the substrate. This equipment has been designed for maximum versatility so that changes in temperature, pressure and the Ar:H<sub>2</sub> ratio are all possible.

Unfortunately, it has not been possible to measure the exact flow rates of the gases through the equipment. Experiments have, therefore, been set up to investigate the effect of temperature on the reactions where all of the variables could be fixed with reasonable accuracy (substrate temperature, length of experiment, overall pressure etc.), but the flow rates of the gases have been calculated based on a

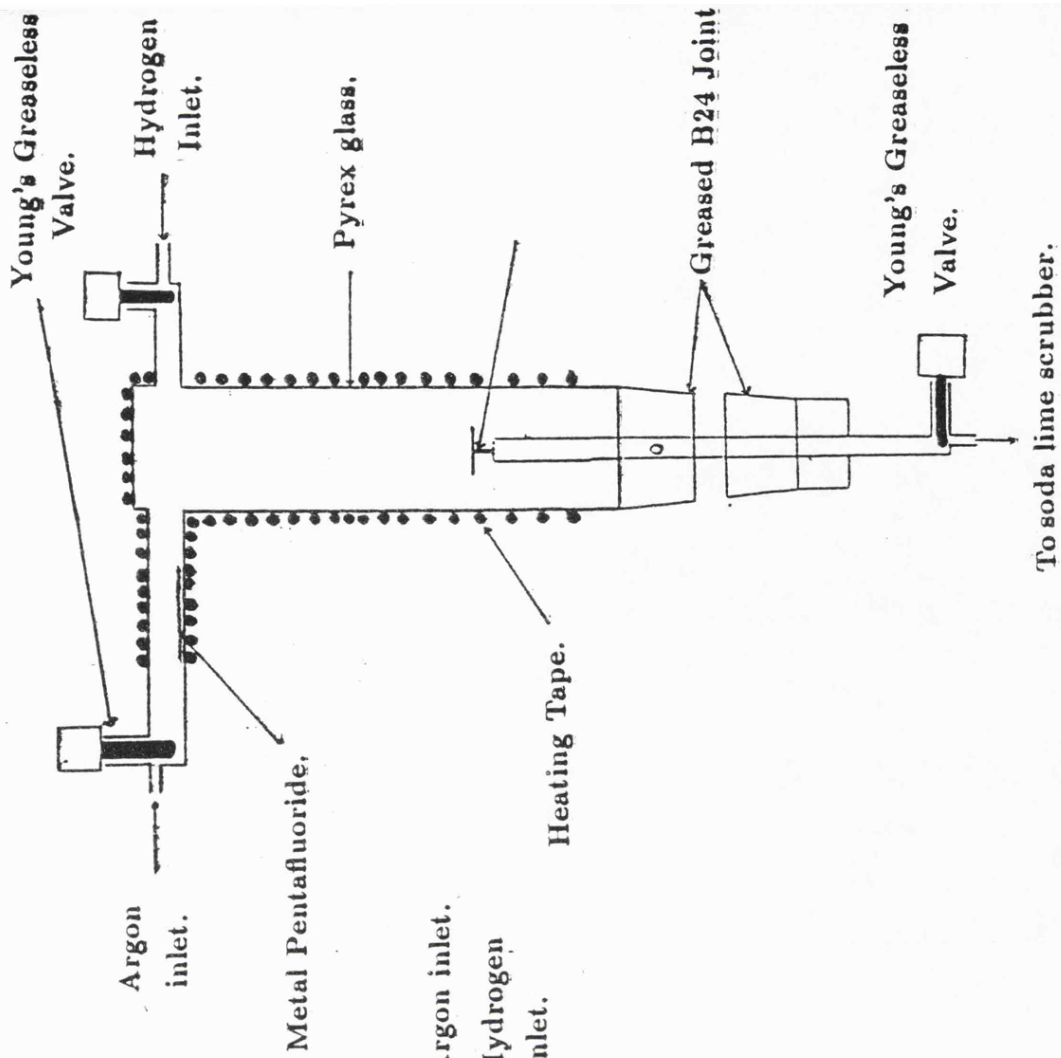


Figure 8.5a: Reduction Apparatus, Mark 1.

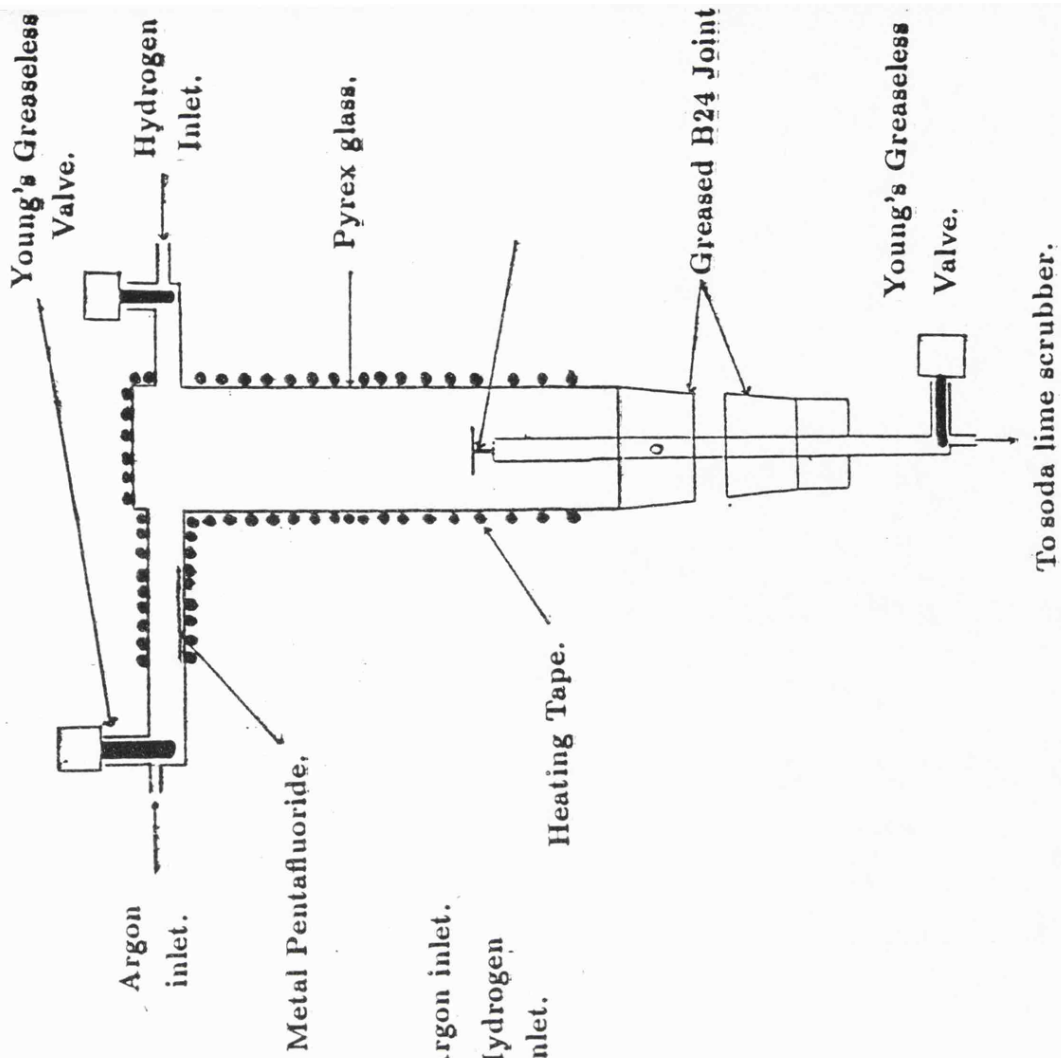


Figure 8.5b: Reduction Apparatus, Mark 2.

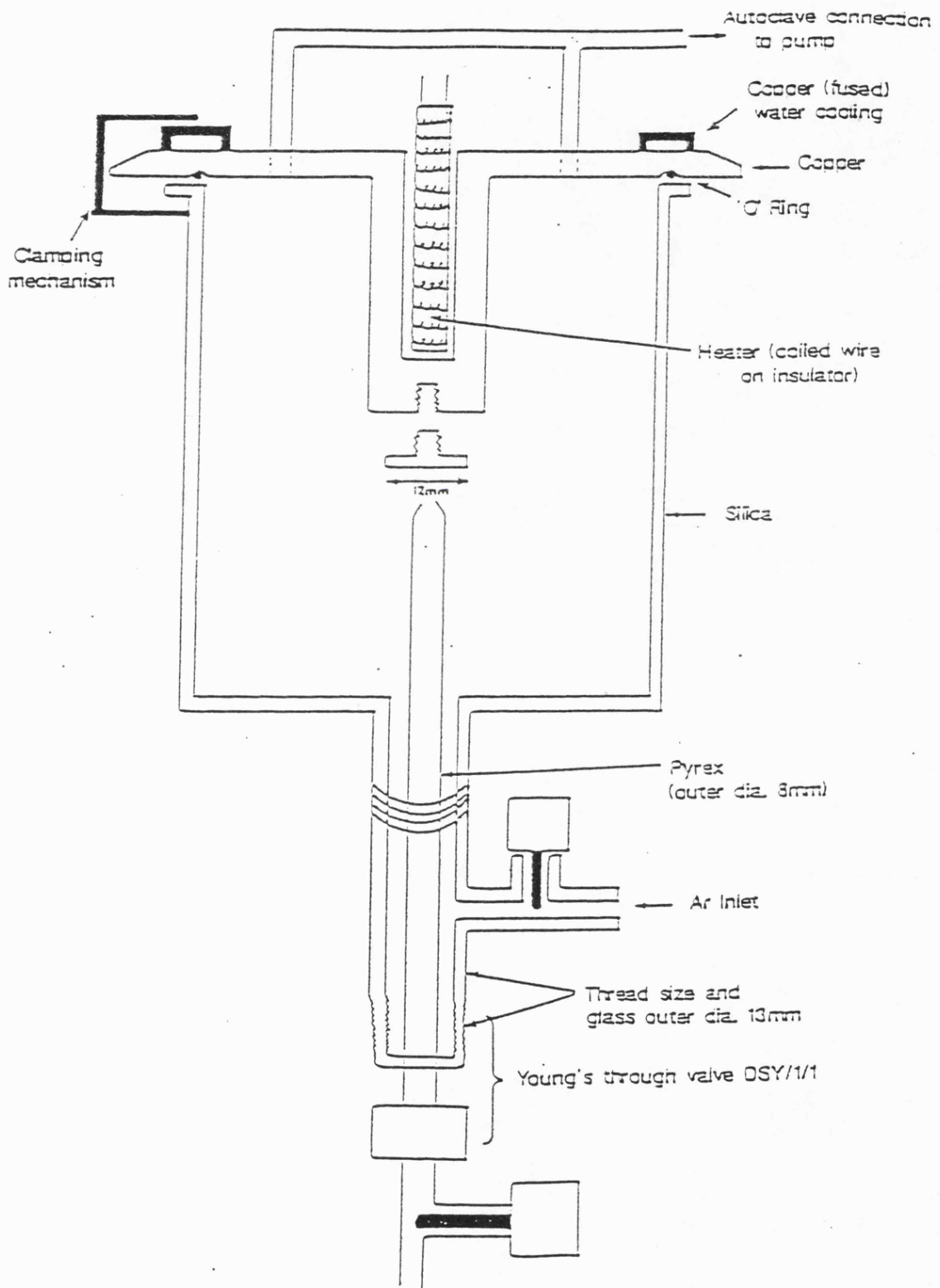


Figure 8.6: Reduction Apparatus. Mark 3.

measurement of the overall pressure of the system, under dynamic vacuum. This is rather unsatisfactory and, although every attempt was made to minimise errors between experiments, this fact should be borne in mind when considering the results.

## 8.4 Experimental Results

### **RuF<sub>5</sub>:TaF<sub>5</sub> [1:1] Reduction**

The results from the horizontal apparatus (Mark 1) have been very encouraging as, when RuF<sub>5</sub>:TaF<sub>5</sub> [1:1] is used as a precursor, an extensive, opaque, metallic-grey deposit forms on the surface of the silica. However, no data have been collected on this deposit.

### **NbF<sub>5</sub> Reduction**

The reduction of NbF<sub>5</sub> has been investigated on the second reduction apparatus (Mark 2). A pale blue, translucent thin film forms which is not firmly attached to the Pyrex-glass walls of the apparatus. Analysis of this deposit using SEM and XRF has shown that it contains Nb but low-element XRF-analysis for fluorine was not carried out. The pale blue colour implies a lower oxidation state than five (which would be d<sup>0</sup>) and also that the deposit is not Nb metal. The SEM showed a smooth surface with no blemishes and no apparent structure. The fact that NbF<sub>5</sub> is not apparently reduced to Nb metal by H<sub>2</sub> confirms the thermodynamics of the system (see Table 8.1). In the analogous NbCl<sub>5</sub> and NbBr<sub>5</sub> reduction experiments hydrogen was used as a reducing agent to form the respective tetrahalides [163]. However, NbF<sub>4</sub> is black and so the deposit is unlikely to be this.

Attempts have also been made, using this apparatus to study the reduction of NbF<sub>5</sub>:TaF<sub>5</sub> [1:1]. Although no significant deposits have been produced, that is nothing is visible to the naked eye or evidenced by SEM work, there is evidence for a very small deposit at a magnification of  $\approx 30000 \times$ , which contains Nb and

Table 8.4: Experimental Details of Some UF<sub>6</sub> Reduction Experiments with Hydrogen.

Expt. No.	Substrate	Substrate Temp. (°C)	≈ UF <sub>6</sub> :H <sub>2</sub>	U from XRF	Weight Uptake (mg)
1*	Cu	150	1 : 1	yes	-
2	Cu	150	1 : 1	yes	231
3	Cu	100	1 : 10	no	0
4	Cu	125	1 : 10	yes	0
5	Cu	150	1 : 10	yes	1
6	Cu	175	1 : 10	yes	2
7	Cu	200	1 : 10	yes	3
8	Cu	250	1 : 10	yes	-
9	Fe	150	1 : 10	yes	1

\* Experiment duration was 30 minutes. For all other experiments, this was 80 minutes.

Ta in approximately a 1:1 ratio. It is likely that this is due to hydrolysis of material which has sublimed on to the substrate rather than from any CVD process. No low element fluorine analysis has been carried out on the substrate after the reaction.

The reduction of WF<sub>6</sub>, UF<sub>6</sub>, TaF<sub>5</sub> and RuF<sub>5</sub> have been investigated on the third design of apparatus (Mark 3).

### UF<sub>6</sub> Reduction

The results of the experiments to reduce UF<sub>6</sub> using H<sub>2</sub> are shown in Table 8.4. This data shows that the amount of material deposited increases with temperature and that, at the temperatures at which these experiments are reported (100–250° C), there appears to be no self-limiting process in this reaction as has been observed for ReF<sub>6</sub> [161].

At a substrate temperature of 150°C, a grey deposit is formed. The SEM of

this material (Figure 8.7), shows an apparently amorphous deposit with no visible structure. The XRF analysis shows the presence of U, but no low-element XRF has been carried out. It is likely [164] that this material is not U metal, but probably a uranium oxide (the SEM was characteristic of  $\text{UO}_3$ ). This material may have been formed by the hydrolysis of  $\text{UF}_6$  by water, either on the surface of the substrate or from a leak of air into the apparatus. However, the deposits from subsequent experiments with other moisture-sensitive fluorides do not contain oxygen and so it may be that there is reaction with the silica glass in this case.

At a substrate temperature of  $175^\circ\text{C}$  (Figure 8.8), the deposit begins to show structure in the form of platelets. At  $200^\circ\text{C}$  (Figure 8.9), these platelets are more clearly defined and are characteristic of the formation of  $\text{UO}_2\text{F}_2$  [164]. Once  $\text{UO}_2\text{F}_2$  is formed, experience shows that deposits tend to retain this morphology during subsequent reactions. It is not certain, therefore, whether the material deposited is still  $\text{UO}_2\text{F}_2$ , uranium metal or a uranium fluoride. Subsequent low-element XRF analysis indicates a deposit of the order of  $10^{-6}$  m thickness containing U and F. Although oxygen is also present this is not confirmation of the presence of  $\text{UO}_2\text{F}_2$ , as the sample holder is made of Al which has an oxide layer. However, the presence of fluorine indicates that complete reduction to the metal has not occurred. Since the deposit is a thin film, a more quantitative analysis has not been carried out.

Experiments have also been carried out on the reduction of  $\text{UF}_6$  by  $\text{H}_2$  with a substrate temperature of  $250^\circ\text{C}$ . These experiments fit the pattern exhibited by those at lower substrate temperatures. The crystallites, believed to be due to the initial formation of  $\text{UO}_2\text{F}_2$  are present in the XRF of these deposits, but they cover a much smaller area (see Figure 8.10). This implies that less water is present in the system, presumably because of fluorination and pumping at a higher temperature. The remainder of the surface area of the deposit appears to be fairly amorphous with no apparent structure. Although no low-element XRF analysis has been possible on this deposit it may be that there has been reduction of  $\text{UF}_6$  to a lower fluoride (possibly  $\text{UF}_4$ ). This would be in line with the work already published in this area

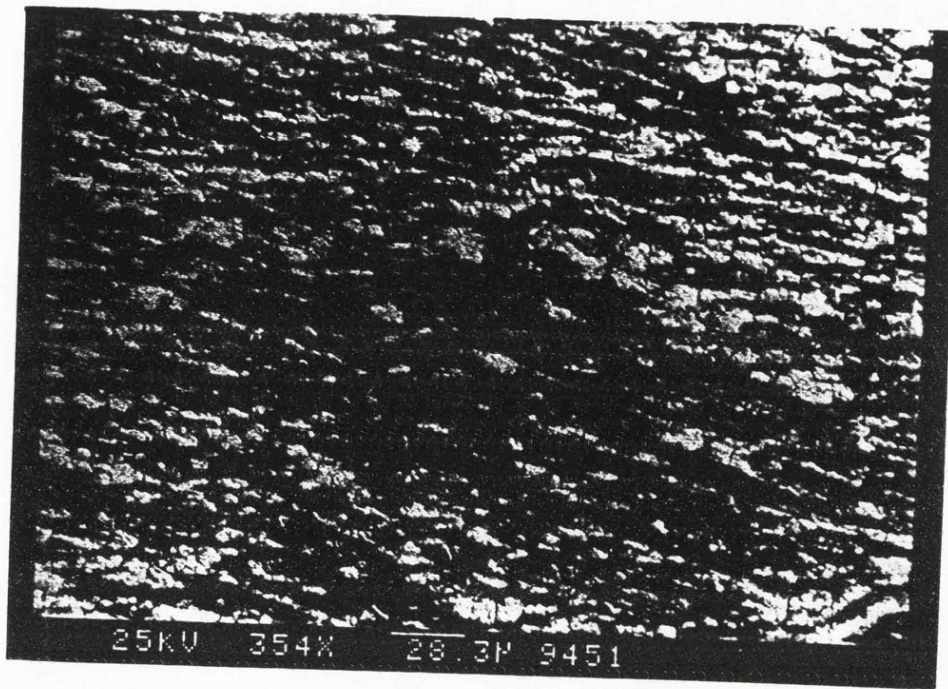


Figure 8.7: SEM of the Deposit Formed by the Reaction of  $\text{UF}_6$  and  $\text{H}_2$  at  $150^\circ\text{C}$



Figure 8.8: SEM of the Deposit Formed by the Reaction of  $\text{UF}_6$  and  $\text{H}_2$  at  $175^\circ\text{C}$

[eg. 165].

A second effect of the increasing substrate temperature, is that the rate of deposition increases. This is illustrated in Figure 8.11, where the number of counts for U from the XRF analysis is plotted against the substrate temperature. The experimental values used in Figure 8.11 are shown in Table 8.5. All other variables can be considered as constant. The graph shows the increase in the deposition rate with temperature and the exact shape of the graph is believed to be due to the fact that the number of U counts will be based on the thickness of the deposit rather than any property of the reaction itself.

### **WF<sub>6</sub> Reduction**

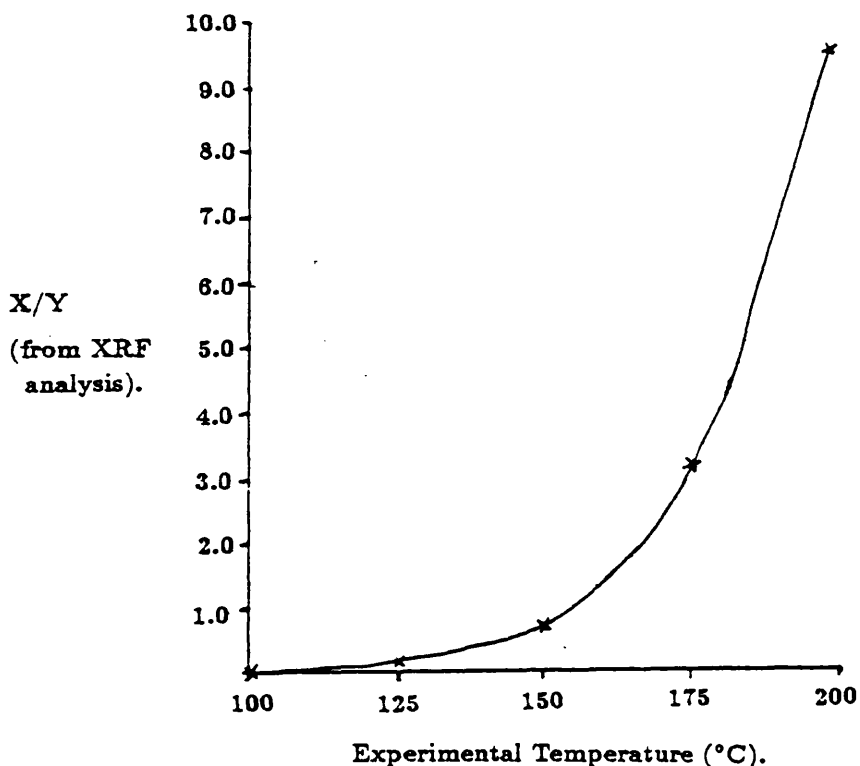
The reduction of WF<sub>6</sub> has been investigated in order to assess the present work with respect to that already published. It is already known that the reaction of WF<sub>6</sub> and H<sub>2</sub> between 150–250° C is slow [161], and that the deposits formed in this temperature range are very thin films. The results of this investigation confirm these findings in that, although W is found to be present from the XRF analysis from experiments with a substrate temperature of 150°C, only when this is raised to 200°C is any deposit evident from the SEM work. No low-element XRF-analysis has been carried out for fluorine because of the small amount of deposit but it is assumed, on the basis of the literature work, that the deposit is W metal. The deposit containing W from the experiment with a substrate temperature of 200° C is shown in Figure 8.12. The lighter areas correspond to W, which appears to be randomly distributed and without obvious structure. The surface of the substrate is far from smooth and later experiments have used polished substrates. There are problems with the reduction of WF<sub>6</sub> in that WF<sub>6</sub> has a vapour pressure around 1 atm at room temperature and so, even when the flow rate of WF<sub>6</sub> is controlled using needle valves, it is still found to be too fast. The WF<sub>6</sub> source has therefore been cooled to 0°C to reduce the WF<sub>6</sub> vapour pressure.



Figure 8.9: SEM of the Deposit Formed by the Reaction of  $\text{UF}_6$  and  $\text{H}_2$  at  $200^\circ\text{C}$



Figure 8.10: SEM of the Deposit Formed by the Reaction of  $\text{UF}_6$  and  $\text{H}_2$  at  $250^\circ\text{C}$



‡ At 100°C, there were no counts for U from the XRF analysis and so this ratio has been defined as zero.

Figure 8.11: Graph to Illustrate the Increasing Thickness of the U Containing Deposit with the Cu Substrate Temperature.

Table 8.5: Experimental Data of Number of Counts for U *L<sub>III</sub>*-Line from XRF Analysis Compared with the Cu Substrate Temperature.

Expt. No. *	Substrate Temp. (°C)	U Counts (from XRF) X	Cu Counts (from XRF) Y	X/Y
3	100	0	18692	-
4	125	6190	52690	0.117
5	150	27214	32155	0.846
6	175	44823	13010	3.445
7	200	67335	7414	9.07

\* See Table 8.4.

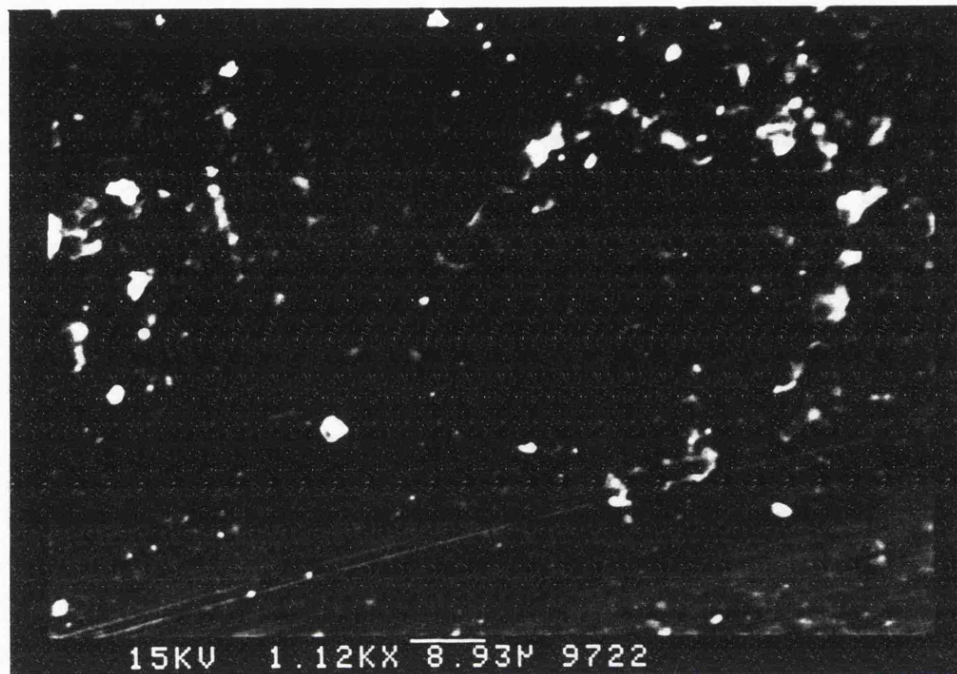


Figure 8.12: SEM of the Deposit Formed by the Reaction of  $WF_6$  and  $H_2$  at  $200^\circ C$

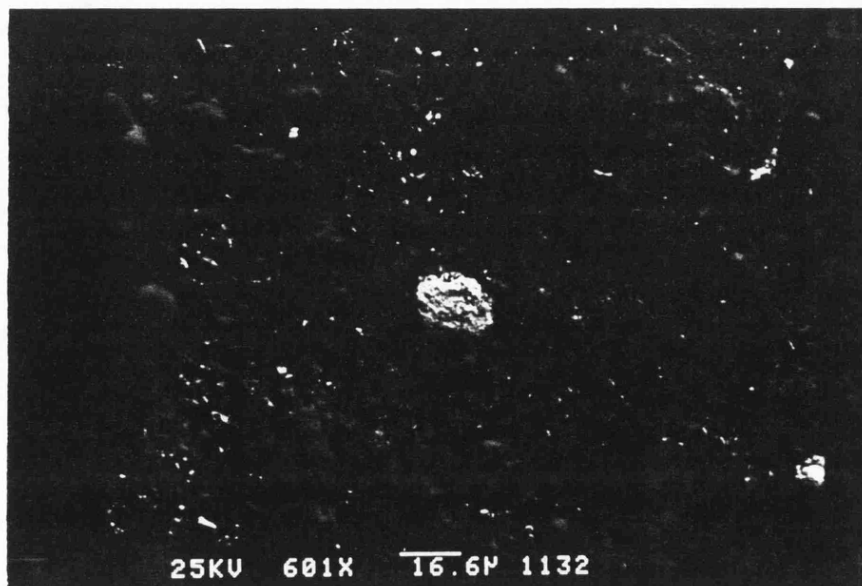


Figure 8.13: SEM of the Deposit Formed by the Reaction of  $TaF_5$  and  $H_2$  at  $250^\circ C$

### **TaF<sub>5</sub> Reduction**

Several attempts have been made to reduce TaF<sub>5</sub> using hydrogen at temperatures up to 250°C. On one substrate, from an experiment with a substrate temperature of 250°C, there was evidence from the XRF and SEM work for a tiny Ta-containing deposit (see Figure 8.13). It is not known if this is Ta metal or a lower fluoride as low element XRF is not reliable on such a small sample. Bearing in mind the thermodynamics and the lack of any deposit from other experiments, the latter seems more likely. This is unfortunate as the very high melting and boiling points for Ta (3250 K [114]) mean that sputtering techniques cannot be used for this metal. However, the thermodynamics indicate that the reduction of TaF<sub>5</sub> by Si is favourable, and so this could be used to obtain thin films of Ta metal.

### **RuF<sub>5</sub> Reduction**

By comparison with TaF<sub>5</sub>, the reduction of RuF<sub>5</sub> by hydrogen is expected to be favourable from the thermodynamic calculations and this is confirmed by experiment. In each experiment a grey, metallic deposit was formed on the substrate immediately on beginning the experiment. Subsequent SEM and XRF confirmed that a thin layer containing Ru had been deposited. Low element XRF analysis has determined that there is no fluorine in the deposit, and it is therefore assumed that the deposit is Ru metal. The only problem with these experiments is the extreme oxygen and moisture sensitivity of RuF<sub>5</sub>. However, RuF<sub>5</sub> is normally lime-green, but becomes black on hydrolysis and so any results from experiments where the RuF<sub>5</sub> hydrolyses have been disregarded.

The Ru deposit, from the reduction of RuF<sub>5</sub> by H<sub>2</sub> at 240°C, is spread over the entire surface of the substrate and is uniform over this area. There does appear to be structure to this deposit (see Figure 8.14), in the form of small crystallites, of similar shape and size. Because of the small size of these crystallites and their widespread occurrence, reduction at lower temperatures has been investigated to study the effect of this on the structure of the deposit. The result is that at 200 °C, a very thin film of Ru forms over the entire surface along with some straight-edged

crystallites randomly placed on this surface. An example of one of these crystallites is shown in Figure 8.15. However, not all of these crystallites are the same shape, and it is not known what factors effect their formation, except that it is assumed that the deposit is formed more slowly at a lower temperature.

## 8.5 Conclusions

The theoretical investigation of the thermodynamics of the reduction of selected metal fluorides shows that only  $\text{IrF}_6$ ,  $\text{MoF}_6$ ,  $\text{WF}_6$  and  $\text{RuF}_5$  should undergo favourable reaction with  $\text{H}_2$ , but that all of the transition-metal fluorides studied should undergo favourable reduction by Si. The studies of  $\text{UF}_6$  and  $\text{WF}_6$  by  $\text{H}_2$  seem to confirm the results already published, which validates the experimental techniques used in this work and the analysis of the deposits. The reduction of  $\text{RuF}_5$ ,  $\text{TaF}_5$  and  $\text{NbF}_5$  to their respective metals by hydrogen confirms the thermodynamic calculations for these materials in that the reduction of  $\text{RuF}_5$  occurs spontaneously at  $150^\circ\text{C}$ , whilst  $\text{NbF}_5$  and  $\text{TaF}_5$  do not appear to be reduced to metal. The thermodynamic calculations are further supported by the fact that there is evidence for reduction of  $\text{RuF}_5:\text{TaF}_5$  [1:1] by  $\text{H}_2$  at  $100^\circ\text{C}$ , to form a metallic grey deposit. This is extremely important from the point of view that this reduction of  $\text{RuF}_5:\text{TaF}_5$  [1:1] supports the suggestion that novel alloys might be prepared by the reduction of the mixed-metal pentafluorides. However, the deposit from the  $\text{RuF}_5:\text{TaF}_5$  [1:1] could not be fully analysed and so it may have contained only Ru.

## 8.6 Future Work

As the reduction of the metal pentafluorides is a novel area of research, there is a great deal of future work which could be based on these experiments. For the metal fluorides already studied, it would be interesting to develop more sophisticated experiments to investigate them further. Perhaps the most important improvement to the experimental design, bearing in mind the oxygen and moisture sensitivity of these high oxidation state metal fluorides, would be a method of accurately measur-

ing the vacuum in the apparatus so that leaks could be detected, for instance with a Penning gauge. There have also been problems measuring the exact flow rates. If mass/flow controllers could be used, this would allow measurement of the exact amount of gases flowing in and out of the apparatus and so give information on the efficiency of the system. It would also be interesting to trap the exhaust gases at low temperature so that they could be characterised by infrared spectroscopy.

The thermodynamic calculations show that while hydrogen reduces only some of the metal fluorides studied to their respective metals, using silicon as the reductant (and substrate) should reduce all of them. It would therefore be interesting to look into the reduction of the metal fluorides using a Si substrate. However, bearing in mind that the reactions are not only favourable on the basis of  $\Delta G_r^\ominus$  but are also exothermic, it would be necessary to exercise extreme caution as this system would be different from that using  $H_2$  in that using  $H_{2(g)}$  would give rise to  $HF_{(g)}$ , whilst  $Si_{(s)}$  would give rise to  $SiF_{4(g)}$ . This, therefore, could result in a large pressure increase on reaction and be potentially explosive. However, these experiments would hopefully produce thin films of Nb and Ta metals which have previously been difficult to prepare.

Following on from the successful reduction of  $RuF_5$ , it would seem likely that  $OsF_6$ ,  $OsF_5$ ,  $RhF_6$ ,  $RhF_5$ ,  $AuF_5$ ,  $CrF_5$  and  $TcF_6$  would also be reduced to their respective metals by hydrogen. Outside of the transition-metal fluorides, the importance of As-CVD work cannot be underestimated for the production of GaAs, and both  $AsF_3$  and  $AsF_5$  are volatile materials.

There is also industrial interest in the formation of metal oxide layers for catalysis, which might be an area where the reduction of metal oxide fluorides using CVD techniques could produce either novel oxide layers or novel preparative routes. Bearing in mind the close correlation between the thermodynamic calculations and the experimental data found for the transition-metal pentafluorides, this would perhaps also be an area for some theoretical investigation prior to experimentation.

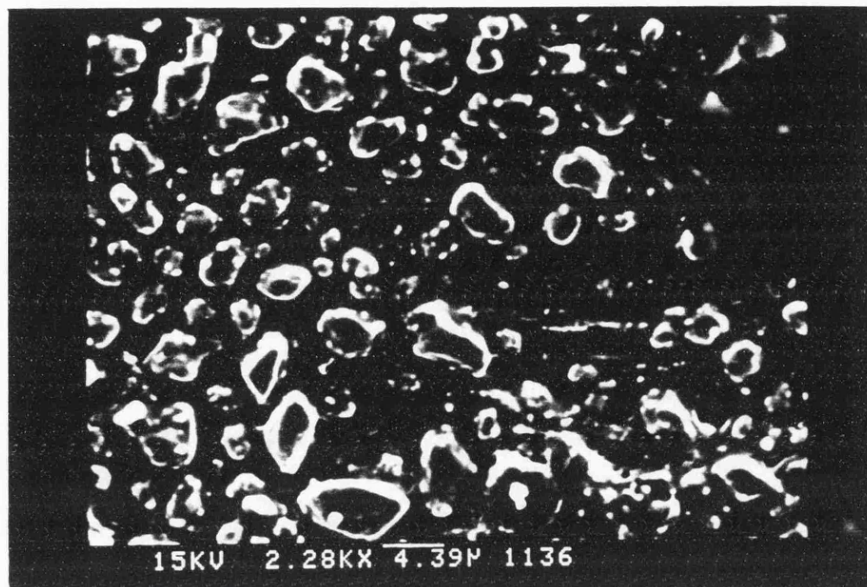


Figure 8.14: SEM of the Deposit Formed by the Reaction of  $\text{RuF}_5$  and  $\text{H}_2$  at  $240^\circ\text{C}$



Figure 8.15: SEM of the Deposit Formed by the Reaction of  $\text{RuF}_5$  and  $\text{H}_2$  at  $250^\circ\text{C}$

## Chapter 9

# Experimental

### 9.1 Handling of Materials

The transition-metal pentafluorides, mixed-metal pentafluorides and metal hexafluorides investigated in these studies are highly sensitive to oxygen and moisture. To prevent decomposition, they were handled either on a metal vacuum line (see Figure 9.1) to which glass or metal satellite lines were connected, or in a nitrogen dry box. For the reduction experiments, the materials were either handled in a sealed, silica-glass apparatus attached to a second vacuum line (see Figure 9.2), or in a dry box.

#### 9.1.1 Metal Vacuum Lines

The first of these consisted of 316 stainless steel or Monel Autoclave Engineers valves (AE-30 series) [Autoclave Engineers Inc., Erie, Pennsylvania, USA] connected via Autoclave Engineers connectors. Argon-arc welded nickel U traps were incorporated to permit separation and condensation of gases in the metal manifold. Inlets for argon [BOC special gases] and fluorine [Matheson Gas Products] (from a 1dm<sup>3</sup> nickel can) were positioned as shown in Figure 9.1. Rough pump outlets were connected to a soda-lime chemical scrubber unit of volume 1dm<sup>3</sup> which neutralised volatile fluorides, thereby protecting the rotary pump [Model PSR/2, NGN Ltd., Accrington, Lancashire] which provided a vacuum of 10<sup>-2</sup>mmHg. High vacuum was achieved

via outlets to a mercury diffusion pump coupled to a NGN rotary pump.

The pumping system, which provided a vacuum in the region of  $10^{-5}$ mmHg, was protected by two glass traps. The first was immersed in liquid nitrogen and was present to trap out volatile fluorides before they reached the mercury diffusion pump. The second was placed between the Hg diffusion pump and the rotary pump to trap out Hg before it reached the rotary pump.

Pressures of 0–1500mmHg were measured by Bourdon tube gauges [Type IF/66Z, Budenberg Gauge Co., Broadheath, Greater Manchester] and high vacuum was measured by a Penning Gauge [Model 2A, Edwards High Vacuum Ltd, Crawley, West Sussex] situated between the manifold outlet and the liquid nitrogen trap.

The second vacuum line was arranged as shown in Figure 9.2. It was also based on Autoclave Engineers valves and connectors and is similar to the main line.

### 9.1.2 Dry Box

Involatile materials were manipulated in an auto-recirculating positive-pressure dry box [Vacuum Atmospheres Co., VAC NE 42-2 Dri Lab] which provided a nitrogen atmosphere with a water and oxygen content less than 5ppm. The quality of the atmosphere was maintained via circulation through columns of manganese oxide and molecular sieves which removed oxygen and water respectively. The dry box was equipped with a Sartorius balance [Model 1601 MP8]. Static charge build-up was found to affect weighings, and so a Zerostat 3 anti-static gun was employed prior to weighing.

Figure 9.1: Metal Vacuum Line.

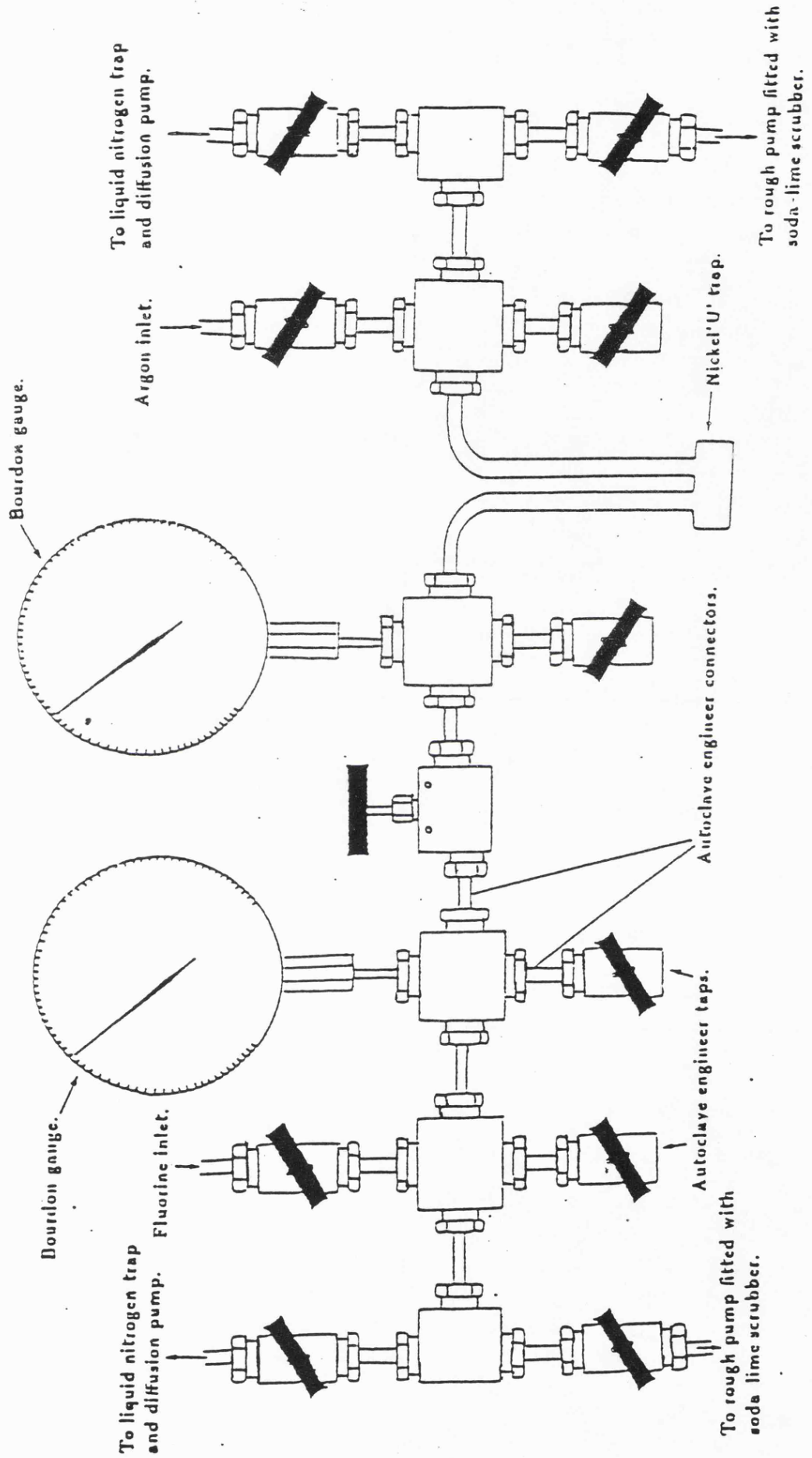
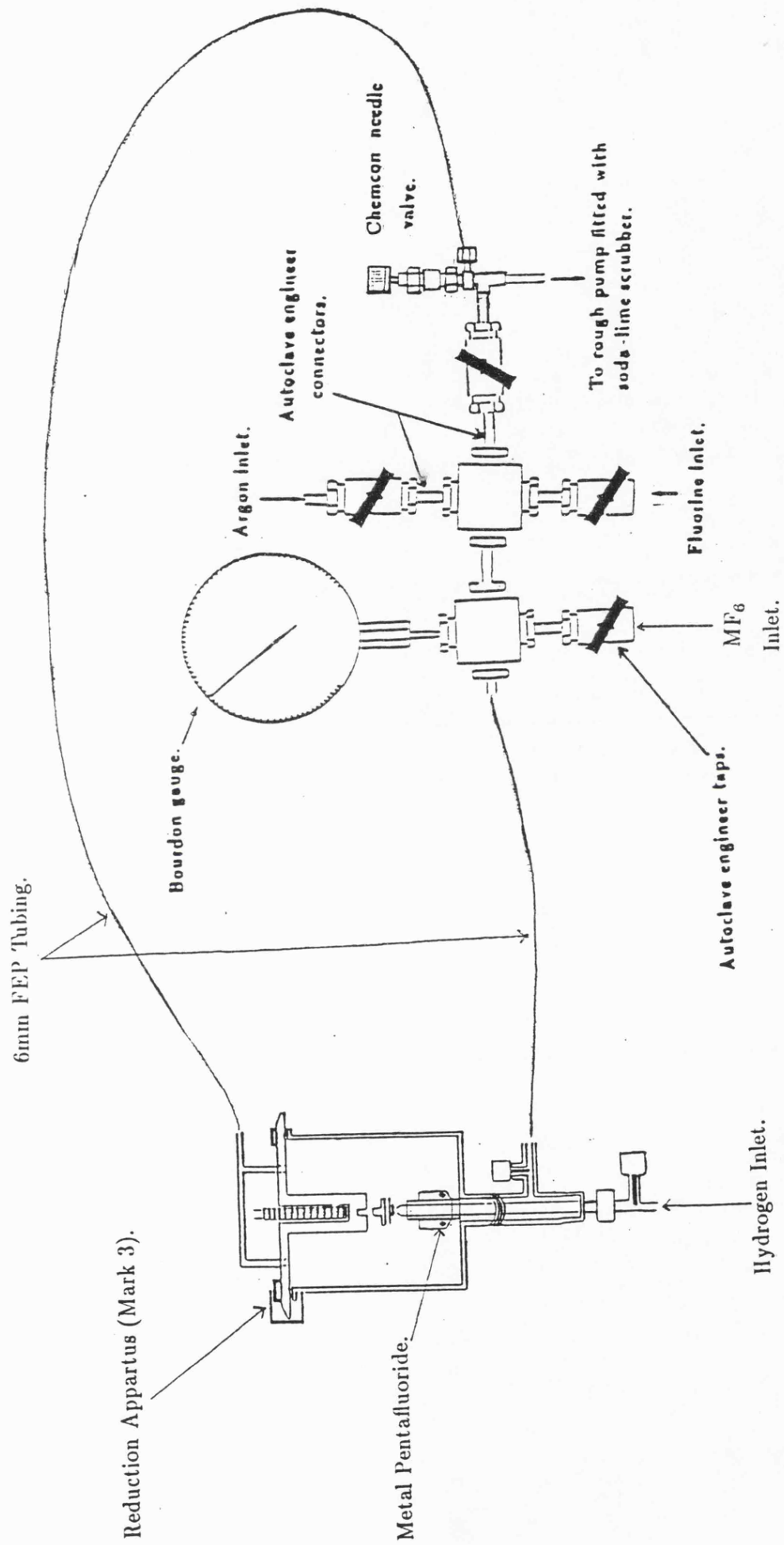


Figure 9.2: The Reduction Line.



### 9.1.3 Reaction Vessels

#### Metal Reactors

Metal reactors (eg. Figure 9.3), including the metal vacuum line, were pumped to high vacuum before use. They were then filled with two 500 mmHg quantities of fluorine gas (or, if elemental fluorine was used in the reaction, to the reaction pressure of fluorine). In the case of the metal vacuum line, two atmospheres of fluorine gas was left in the line to react overnight before pumping to high vacuum. The equipment was then filled with 100 mmHg of  $\text{ClF}_3(g)$  and left for an hour, before again pumping to high vacuum. For the metal reactors the fluorine gas was heated to the reaction temperature and left for the same periods of time as the experiment duration.

#### Glass Apparatus

Pyrex-glass apparatus was designed and prepared as required. A wide range of equipment was used, but the main types are shown in Figures 9.4 and 9.5. For the more moisture- and oxygen-sensitive compounds (for instance, those containing  $\text{RuF}_5$ ), break seals were used to transfer material between pieces of glassware.

The glass equipment was pumped to high vacuum and then gently flame dried with a gas torch. On cooling, 500 mmHg of fluorine gas was admitted to the system which was gently flamed again. The apparatus was then pumped to high vacuum and 100 mmHg of  $\text{ClF}_3$  was added to the system. This was left at room temperature for at least 20 minutes, and the glassware was pumped to high vacuum before use. It should be noted that  $\text{ClF}_3$  was used because it is a more powerful fluorinating agent than  $\text{F}_2$ . It is a very aggressive chemical and if, after addition of  $\text{ClF}_3$ , a yellow colour (chlorine gas) was observed in the apparatus, this was carefully pumped away and the process of passivation repeated.

For the reduction of the metal fluorides the equipment was designed incorpo-

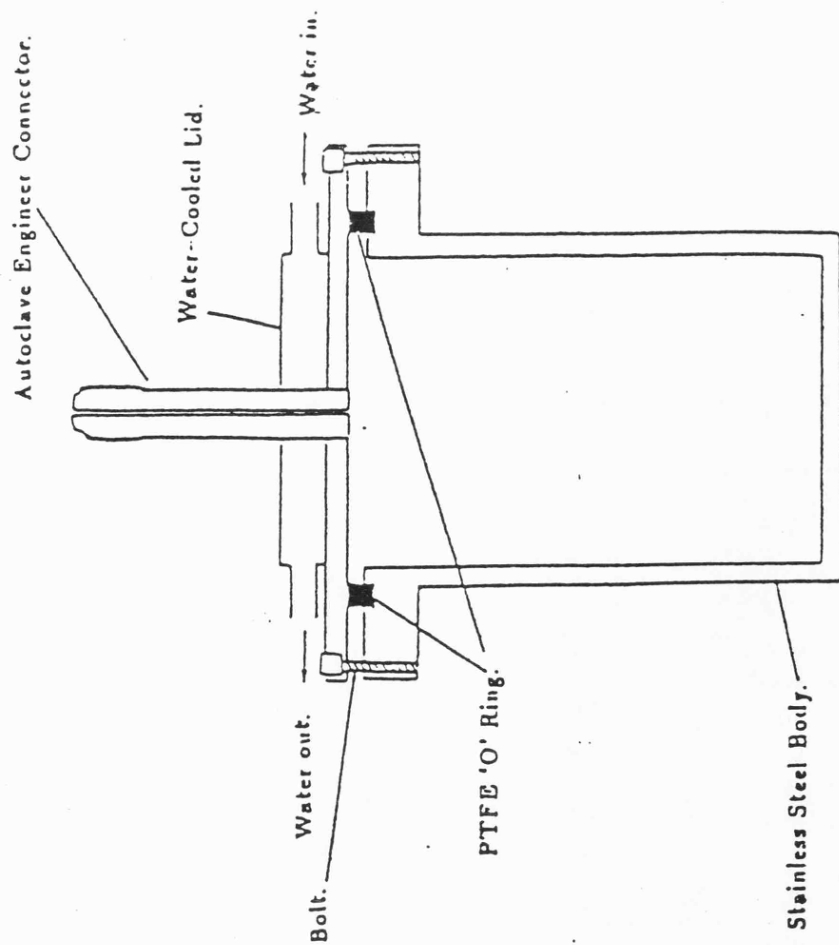
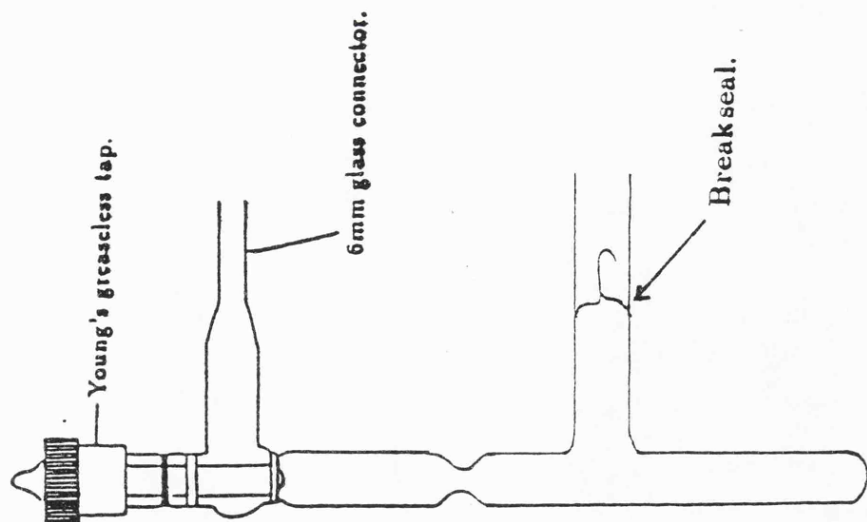


Figure 9.3: Autoclave for Metal-Pentafluoride

Figure 9.4: Pyrex Sublimation Apparatus.

Synthesis.

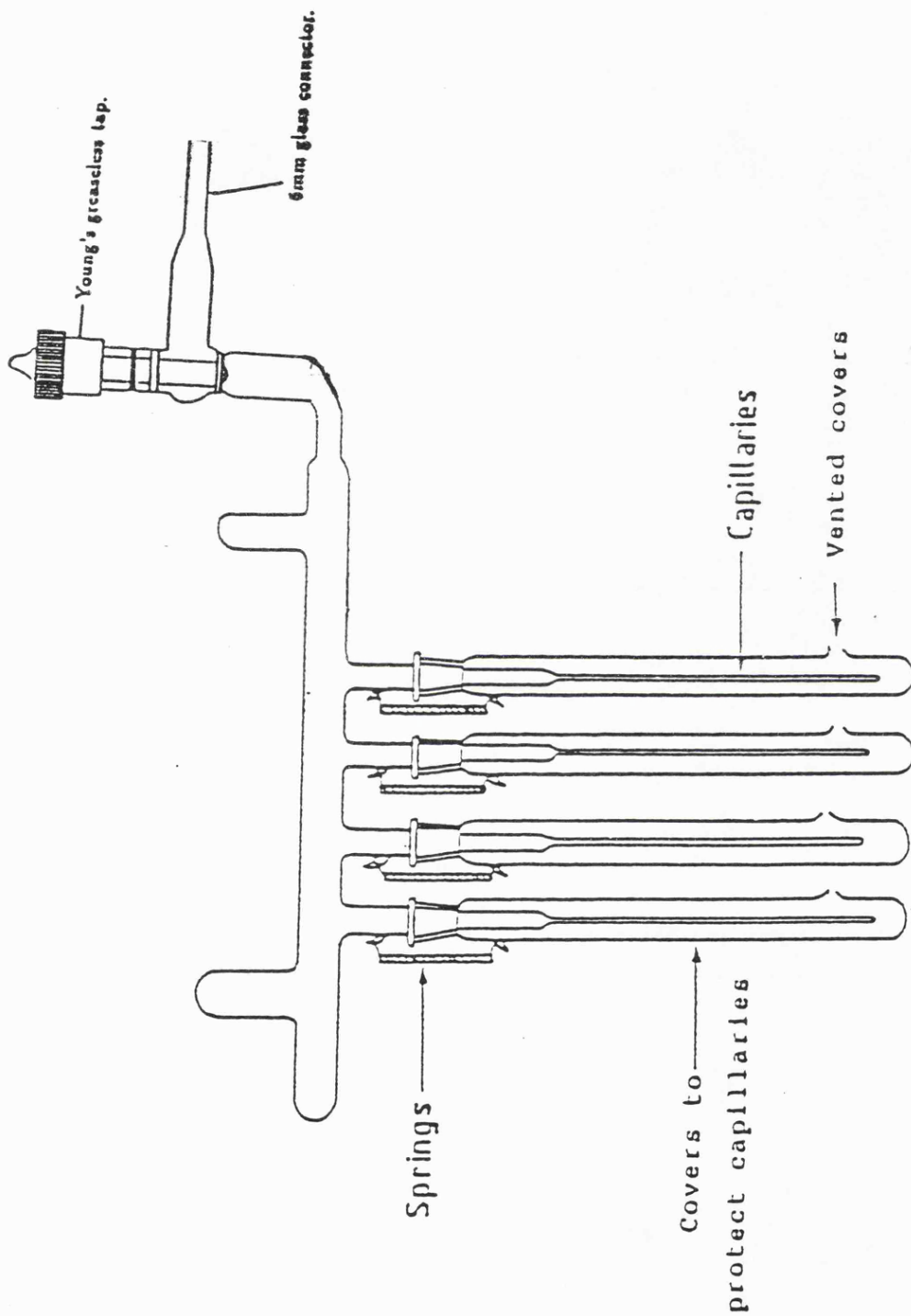


Figure 9.5: Pyrex Crystal Sorting Apparatus.

rating silica glass rather than Pyrex glass where possible, because of its greater resistance to HF. This apparatus was prepared by the departmental glassblower. As no equipment was available to accurately measure the vacuum in this equipment, leaks were tested for by pumping the apparatus for a period of at least 30 minutes, before leaving the system under static vacuum for 30 minutes. When there was no pressure increase over this time period, the apparatus was seasoned with 500 mmHg of fluorine gas for the duration and temperature of the experiment, before being pumped away and the system tested for leaks as before.

## 9.2 Analytical Techniques

### 9.2.1 Infrared Spectroscopy

Infrared spectra were recorded on a Digilab FTS-40 Fourier Transform spectrometer. Solid samples were run as powders prepared in the dry box and pressed between KBr discs. This was because solid materials appeared to react with Nujol.

Gas-phase spectra were recorded in a copper cell of 10cm path length fitted with AgCl windows. A seal was made between the AgCl windows and the cell body by two PTFE gaskets. Some of the gas-phase spectra were recorded above room temperature, which was achieved by wrapping a heating tape around the gas-cell body. The temperature of the gas cell was measured using a thermocouple. Spectra were recorded at 15°C intervals up to  $\approx 100^\circ\text{C}$ . At each new temperature, the gas cell was allowed to reach a steady state, before collection of the data, the temperature being manually controlled using a Variac potentiometer. One hundred scans were collected at each temperature. To ensure that the spectra above room temperature were due only to gas-phase species spectra were also recorded once the gas cell had cooled to room temperature.

## Raman Spectroscopy

Raman spectra were recorded on a Coderg T800 spectrometer, with either a 250 mW Ar<sup>+</sup> laser [Model 52, Coherent Radiation Laboratories] or a 500 mW Kr<sup>+</sup> laser [Model 164, Spectra Physics Inc.]. The Ar<sup>+</sup> laser provided exciting lines at 5145 Å (green) and 4880 Å (blue), whilst the Kr<sup>+</sup> laser provided an exciting line at 6471 Å (red).

Solid samples were either contained in pre-seasoned Pyrex glass capillaries sealed with dental wax [Glover Dental Services, Shrewbury], or in 6mm FEP tubes fitted with Chemcon PTFE valves [Production Techniques, Fleet, Hampshire]. Samples likely to decompose in the laser beam were cooled in an unsilvered glass Dewar filled with liquid nitrogen. The majority of spectra were recorded using the Ar<sup>+</sup> blue line (4880 Å) but, where this was not successful, the other laser lines were used. Before each spectrum was recorded, the Raman spectrometer was calibrated by recording the NbF<sub>5</sub> Raman spectrum and calibrating the instrument on the very strong 766 cm<sup>-1</sup> peak [111].

## Mass Spectrometry

Spectra were recorded on a VG Micromass 16B spectrometer. This equipment had a mass range up to 520 a.m.u. as standard and attempts were made to record spectra up to 720 a.m.u. but these were not successful. The solid samples were loaded into pre-seasoned Pyrex capillaries in a dry box. These were sealed temporarily using dental wax, and then permanently sealed on removal from the dry box, using a micro-torch [Model H164/1, Jencons, Hemel Hempstead, Hertfordshire]. The capillaries were introduced into the spectrometer on the end of a stainless steel probe fitted with a Teflon tip, by breaking them open and immediately inserting them into the spectrometer, to minimise exposure of the sample to air. To prevent hydrolysis inside the chamber, the system was flushed with a small quantity of fluorine gas before the sample was introduced.

Unfortunately, it was not possible to record the mass spectra of any materials containing ruthenium because of problems of this metal being deposited on the filament and on the inside of the chamber.

### **X-ray Fluorescence Analysis**

Samples of the mixed-metal pentafluorides were loaded onto Al stubs covered in an even, flat layer of plastic, carbon, conductive putty [Leit-C-Plast, Neubauer Chemikalien, W.Germany], in a dry box. The samples were allowed to hydrolyse in air before being transferred to a scanning electron microscope. The X-ray fluorescence analysis was recorded at a magnification of  $\approx 120\times$ , for the two metals present in the sample, on at least seven areas of each sample, and the average value reported.

Standard samples of the two metal powders were also placed onto Al stubs covered with the carbon putty and analysed in the same way. The error on the results was deemed to be of the order of  $\pm 4\%$  and was thought to be associated with the problems of sample preparation, as XRF requires a perfectly flat surface and a perfectly homogenous distribution of elements throughout the sample.

### **X-ray Powder Diffraction**

Samples were finely ground in a dry box and loaded into pre-seasoned capillaries, which were sealed using dental wax melted with a soldering iron. The capillaries were sealed permanently, immediately on removal from the dry box, using a microtorch [model as above]. X-ray powder diffraction photographs were recorded using a Phillips 116.4 mm diameter camera equipped with Koldirex KD59T film [Kodak Ltd]. Nickel filtered Cu-K $\alpha$  radiation was used with exposure times ranging from three to fifteen hours depending on the sample.

## X-ray Single Crystal Studies

For all of the compounds studied by single crystal X-ray diffraction the crystals were grown by sublimation at  $\approx 40^\circ\text{C}$ ,  $10^{-4}$  mmHg across a sealed Pyrex tube (inner diameter 8mm). The crystals were removed from the walls of the tube by cooling in liquid nitrogen followed by gentle tapping with a glass rod.

Single crystals were then loaded into a pre-seasoned crystal sorting apparatus (see Figure 9.5). Suitable crystals were chosen visually and manipulated into thin-walled capillaries on the apparatus. They were then wedged into the capillaries by gentle tapping, and the capillaries were sealed using a micro-torch. The most suitable single crystal was then chosen for X-ray studies. The collection of preliminary photographs, data sets and the solving of this data was carried out by the crystallography group at Leicester University, except for the data for single crystals of  $\text{TaF}_5$ ,  $\text{NbF}_5\text{TaF}_5$  [1:3] and  $\text{RuF}_5\text{TaF}_5$  [1:1], which were collected and partially solved at Edinburgh University.

## The Collection and Analysis of EXAFS Data

The moisture-sensitive pentafluoride samples were intimately mixed with pre-seasoned Teflon powder and loaded as thin layers into pre-seasoned, thin-walled, air-tight FEP holders (see Figure 9.6), in a dry box. Samples of  $\text{KNbF}_6$  and  $\text{KTaF}_6$  were intimately mixed with LiF and loaded into similar FEP sample holders.  $\text{KVF}_6$  was also intimately mixed with LiF and loaded as a thin layer in an FEP cavity. This cavity was sealed from the air with a Be window held in place with melted wax. This was carried out in a dry box.

All of the spectra were collected in transmission mode except for that of  $\text{KVF}_6$ , which was recorded in fluorescence mode. The data were recorded at the Daresbury Synchrotron Laboratory, Cheshire. The source ran at 2GeV and an average current of 190mA. The data were collected in  $k$  space with  $k^3$  weighting. For the hexafluorometallate samples three spectra were recorded, while for the other samples, where

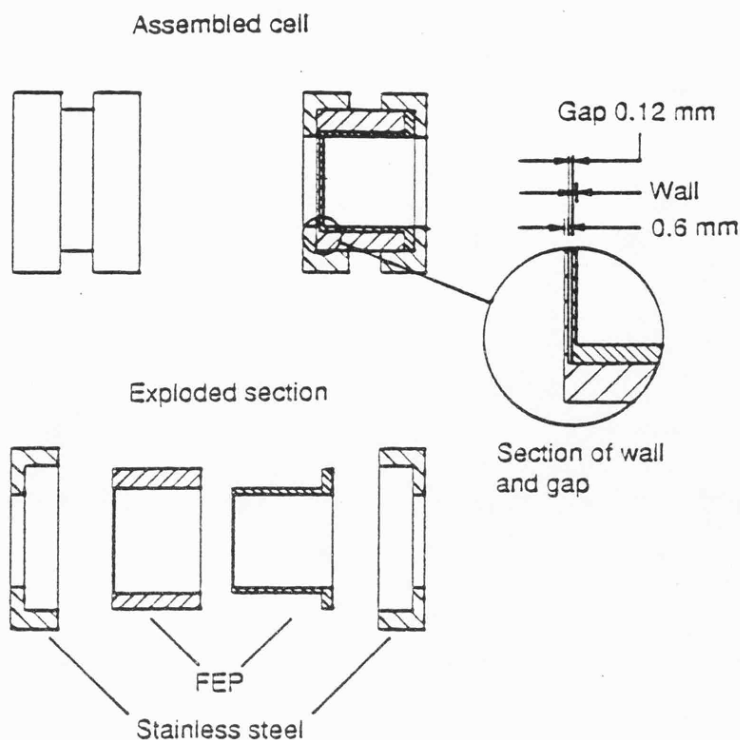


Figure 9.6: FEP EXAFS Sample Holder.

the K-edge was used, five spectra were recorded. For the  $L_{III}$  edges, ten spectra were recorded when time permitted.

Background subtraction of the EXAFS data was carried out using the EX computer programme [134]. Curve fitting was achieved using the EXCURV90 programme [135] and no Fourier Filtering was used in the spectral analysis.

### 9.3 The Preparation of the Transition Metal Pentafluorides and Mixed-Metal Pentafluorides

#### 9.3.1 $NbF_5$ , $TaF_5$ and $RuF_5$

These materials were prepared by the static fluorination of the appropriate activated metal powders (see Section 9.5). In a typical preparation, a metal autoclave (volume  $\approx 220\text{cm}^3$ ), Figure 9.3, was seasoned with neat fluorine gas, at the reaction

temperature and pressure, and pumped to high vacuum. Activated metal powder was then weighed and loaded into the autoclave. The mass of the metal powder was such that, at room temperature, with a pressure of fluorine gas of 5 atmospheres, there was a ten per cent excess of fluorine present in the reactor. The autoclave was then pumped to high vacuum again. Fluorine gas was carefully metered into the autoclave, which was held at  $-196^{\circ}$  by immersion in liquid nitrogen. It was then allowed to warm to room temperature and heated to  $\approx 120^{\circ}\text{C}$  in an oil bath, for at least three hours. After this time, the autoclave was allowed to cool to room temperature and the unreacted fluorine gas was pumped away via a soda-lime chemical scrubber. While the autoclave was cooled or heated, water was passed through the lid cavity to keep the PTFE seal as close to room temperature as possible to prevent leaks. The autoclave was then pumped to high vacuum for several minutes to remove any traces of  $\text{F}_2$  or  $\text{HF}$  and taken into a dry box. The  $\text{MF}_5$  formed as a crystalline solid on the lid and cooler parts of the autoclave, and was scraped out and loaded into a pre-seasoned 6mm FEP storage tube, fitted with a Pyrex stopper. This tube was then stored in a dry box.

Providing the autoclave was well passivated and the metal powder properly activated, yields were essentially quantitative. For the  $\text{RuF}_5$  preparation, occasionally when the autoclave was opened, the  $\text{RuF}_5$  had formed as a super-cooled liquid and so could not be easily scraped out. In these cases the autoclave was closed again and left overnight during which time the  $\text{RuF}_5$  solidified.

The product was purified by vacuum sublimation in a static vacuum ( $10^{-4}$  mmHg) across a sealed Pyrex tube (inner diameter 8mm) at  $40^{\circ}\text{C}$ . The purity of the products was checked by melting points, X-ray powder diffraction patterns and vibrational spectroscopy.

### 9.3.2 The VF<sub>5</sub> Preparation

This was essentially the same as those for NbF<sub>5</sub>, TaF<sub>5</sub> and RuF<sub>5</sub>. However, the reaction temperature was 250°C and the autoclave was held at this temperature for at least four hours. During this time, not only was water flowed through the lid cavity, but also through two copper blocks bolted on either side of the Autoclave Engineers valve on the top of the autoclave to prevent overheating of the valve. The autoclave was heated in a furnace filled with sand to ensure good thermal contact. After four hours, it was cooled to room temperature and unreacted fluorine gas was removed. VF<sub>5</sub> was distilled in small portions ( ≈ 0.5 g), into a pre-seasoned 6mm FEP storage tube fitted with a Chemcon valve ready for use. The bulk product was retained in the autoclave until required. Yields were again essentially quantitative providing there was adequate seasoning of the equipment and activation of the metal powder.

### 9.3.3 The Mixed-Metal Pentafluoride Preparation

The preparation of the mixed-metal pentafluorides was the same as for RuF<sub>5</sub>, NbF<sub>5</sub> and TaF<sub>5</sub>, except that two metal powders, in appropriate stoichiometries, were weighed out and loaded into the autoclave. The powders were intimately mixed before fluorine gas was condensed into the autoclave. All of the products were solid, except for some experiments involving the attempted preparation of TaF<sub>5</sub>.VF<sub>5</sub> [1:3], where VF<sub>5</sub> was formed.

## 9.4 The Reduction of the Metal Fluorides

### 9.4.1 The First and Second Types of Reduction Apparatus (Marks 1 and 2).

Experiments using the first and second types of reduction apparatus (Figures 8.5a and 8.5b) were run in a similar way. In a typical experiment, the apparatus was pre-seasoned with neat fluorine gas, at a static pressure of 500 mmHg and at 100°C

for at least 30 minutes. The residual fluorine was then pumped away through a soda-lime chemical scrubber and the equipment was taken into a dry box where a weighed amount of solid precursor was loaded into the equipment.

The experiment was then run at a positive pressure of Ar and H<sub>2</sub> in approximately a 5:1 ratio. There was no facility to measure the flow rates directly or the overall pressure of the system and so a silica oil bubbler was used. A trap, held at -78° C, was placed between the bubbler and the reduction apparatus to remove water from the inlet gas stream. The exhaust gases were passed through a soda-lime chemical scrubber to neutralise HF or volatile fluoride. Both the pieces of apparatus were heated using a heating tape, controlled by a Variac potentiometer and the temperature was measured using a thermocouple.

#### **9.4.2 The Third Type of Reduction Apparatus (Mark 3).**

##### **Reduction of the Metal Hexafluorides.**

After the apparatus (see Figure 8.6) was leak tested and seasoned with fluorine gas as detailed in Section 9.1.3, the substrate was heated to the required temperature and the metal hexafluoride, argon and hydrogen gas-inlet valves were opened. The experiment was then monitored for its duration (normally 80 minutes) to ensure the temperature and flow rates remained constant.

After the experiment had finished, the valves were shut and the system was pumped for at least 30 minutes to remove any HF. The apparatus was then opened to the atmosphere and the substrate removed to a sample tube. In later experiments, the substrate was removed from the equipment in an Ar-filled glove bag and placed in an Ar-filled sample tube. Where possible the substrate was weighed before and after the experiment.

### **The Reduction of the Metal Pentafluorides.**

The experiments were very much the same as those where a metal hexafluoride was used as a precursor, except that the solid precursor was weighed and loaded into a Pyrex glass boat, which was then placed in the reduction apparatus in a dry box. This necessitated re-checking for leaks as the previous seals were broken.

## **9.5 Sources of Chemicals and Methods of Purification**

**Fluorine Gas:**  $F_2$  Matheson Gas Products. This was used as supplied after being transferred to  $1\text{dm}^3$  welded nickel vessels for convenient use.

**Chlorine Trifluoride:**  $ClF_3$  Fluorochem Ltd, Derbyshire. This was used as supplied.

**Argon Gas:** Ar BOC Speciality Gases. Research grade; used as supplied.

**Tantalum:** Ta Aldrich Ltd. The metal was supplied as a fine powder which was activated by flowing hydrogen gas over the metal which was held in a porcelain crucible heated by a gas flame for an hour. Hydrogen gas was passed through the crucible, while the metal cooled. The aim of this activation was to remove any oxide coatings, and so the metal was then stored in a nitrogen-filled dry box.

**Niobium:** Nb Laboratory Reagents Ltd, Poole. This metal was supplied as a fine powder, and was activated in the same way as the Ta metal.

**Vanadium:** V Aldrich Ltd. This metal was supplied as a fine powder and was activated in the same way as for Ta metal. However, a lower temperature gas

flame was employed to prevent the formation of a blue coloured compound, believed to be a vanadium hydride species, which occurred during the initial attempt at activation.

**Ruthenium: Ru** Johnson Matthey Ltd. This metal was supplied as a fine powder which was activated in the same way as Ta.

**Tungsten Hexafluoride: WF<sub>6</sub>** Fluorochem Ltd, Derbyshire. This material was used as supplied after removal of the sufficient fractions to yield a gas phase-infrared spectrum indicating pure WF<sub>6</sub>.

**Uranium Hexafluoride: UF<sub>6</sub>** BNFL Ltd. This was used as supplied.

## References

1. A. J. Edwards, *J. Chem. Soc.*, 1964, 3714.
2. J. H. Holloway, R. D. Peacock, R. W. H. Small, *J. Chem. Soc.*, 1964, 644.
3. A. J. Edwards, G. Jones, *J. Chem. Soc. (A)*, 1969, 1651.
4. K. I. Khallow, PhD Thesis, University of Birmingham, 1983.
5. W. Casteel Jr., A. P. Wilkinson, H. Borrmann, R. E. Serfass, N. Bartlett, *Inorg. Chem.*, 1992, **31**, 3124.
6. H. J. Emeléus, H. C. Clark, *J. Chem. Soc.*, 1957, 2119.
7. S. Blanchard, *J. Chim. Phys.*, 1965, **62**, 919.
8. I. R. Beattie, R. Crocombe, A. German, P. Jones, C. Marsden, G. Van Schalkwyk, A. Bukovszky, *J. Chem. Soc., Dalton Trans.*, 1976, 1380.
9. G. Girichev, N. I. Giricheva, E. G. Rakov, A. S. Dudin, A. V. Dzhalavyan, B. Averbukh, *Koord. Khim.*, 1988, **14**, (6), 816.
10. G. Girichev, N. I. Giricheva, *Isv. Vyssh. Uchebn. Zaved. Khim. Technol.*, 1991, **34**, (7), 3.
11. L. E. Alexander, *Inorg. Nucl. Chem. Lett.*, 1970, **7**, 1053.
12. L. E. Alexander, I. R. Beattie, P. Jones, *J. Chem. Soc., Dalton Trans.*, 1972, 210.
13. L. E. Alexander, I. R. Beattie, *J. Chem. Phys.*, 1972, **56**, 5829.
14. W. E. Falconer, G. Jones, A. Muentner, M. J. Vasile, W. A. Sunder, T. R. Dyke, *J. Fluorine Chem.*, 1974, **4**, 213.
15. M. J. Vasile, G. R. Jones, W. E. Falconer, *J. Chem. Soc., Chem. Commun.*, 1971, 1355.
16. E. Lawless, *Inorg. Chem.*, 1971, **10**, (9), 2084.
17. G. Romanov, V. Spiridonov, *Zh. Str. Khimii*, 1966, **7**, (6), 882.
18. J. Brunvoll, A. Ischenko, I. Miakshin, G. Romanov, V. Sukhoverkhov, V. Spiridonov, T. Strand, *Acta Chem. Scand. A*, 1980, **34**, 733.
19. J. Brunvoll, A. Ischenko, I. Miakshin, G. Romanov, V. Sokolov, V. Spiridonov, T. Strand, *Acta Chem. Scand. A*, 1979, **33**, 775.

20. G. Girichev, V. N. Petrova, M. V. Petrov, K. Krasnov, V. Goncharuk, Zh. Strukt. Khim., 1983, **24**, (3), 54.
21. J. Brunvoll, A. Ischenko, A. Ivanov, G. Romanov, V. Sokolov, V. Spiridonov, T. Strand, Acta Chem. Scand., 1982, **36**, 705.
22. F. B. Clippard, L. Bartell, Inorg. Chem., 1970, **9**, (4), 805.
23. J. H. Canterford, R. Colton, T. A. O'Donnell, Rev. Pure and Appl. Chem., 1967, **17**, 123.
24. J. Fawcett, A. J. Hewitt, J. H. Holloway, M. A. Stephen, J. Chem. Soc., Dalton Trans., 1976, 2422.
25. K. Tsao, U. S. Pat. 4,587,710, 3 May, 1986, HOIL 21/26; BO5D 3/06.
26. J. Cuomo, J. Macpherson, J. Ziegler, U. S. Pat. 4,005,698, 1 Feb, 1977, F24J; 3/02.
27. P. Huggett, Plessey Research Ltd. (now at RSRE, Malvern), personal communication.
28. B. A. Macklin, J. C. Withers, Proc. Conf. CVD Refract. Metals, Alloys, Compounds; Gatlinburg, Tennessee, 1967, 161.
29. A. Rubezhov, Plat. Metals Review, 1992, **36**, (1), 26.
30. J. F. Clarke, U. S. Pat. 3,476,080, 4 Nov, 1969, Cl. 118-44; B21 cd BO5e.
31. F. Gortsema, R. Didchenko, Inorg. Chem. 1965, **4**, 182.
32. H. Schäfer, H. Schnering, K. J. Nieheuss, H. G. Nieder-Verenholz, J. Less Common Metals, 1965, **9**, 95.
33. A. F. Wright, B. E. F. Fender, N. Bartlett, K. Leary, Inorg. Chem., 1978, **17**, 748.
34. P. R. Rao, A. Tressaud, N. Bartlett, J. Inorg. Nucl. Chem. (Suppl.), 1976, 23.
35. N. Bartlett, A. Tressaud, Hebd. Sceances Acad. Sci., 1974, **C278**, 1501.
36. A. J. Jacobsen, L. McBride, B. E. F. Fender, J. Phys. Chem., 1974, **7**, 783.
37. L. Grosse, R. Hoppe, Z. Anorg. Allg. Chem., 1987, **552**, 123.
38. M. Pouchard, M. R. Torki, G. Demazeau, P. Hagenmüller, Hebd. Sceances Acad. Sci., 1971, **C273**, 1093.
39. A. J. Edwards, D. Hugill, R. D. Peacock, Nature, 1963, **200**, 672.
40. F. Fairbrother, W. C. Frith, J. Chem. Soc., 1951, 3051.

41. G. H. Cady, G. B. Hargreaves, *J. Chem. Soc.*, 1961, 1568.
42. J. H. Holloway, R. D. Peacock, *J. Chem. Soc.*, 1963, 527.
43. J. H. Holloway, P. R. Rao, N. Bartlett, *J. Chem. Soc., Chem. Commun.*, 1965, 306.
44. J. Schröder, F. J. Grewe, *Angew. Chem. (Int. Ed., Eng.)*, 1968, **80**, 118.
45. J. Schröder, F. J. Sieben, *Chem. Ber.*, 1970, **103**, 76.
46. N. Bartlett, D. J. Lohmann, *J. Chem. Soc.*, 1962, 5233.
47. A. J. Edwards, *Proc. Chem. Soc.*, 1963, 205.
48. Y. Kiselev, A. Popov, A. V. Goryunov, S. Spirin, V. B. Sokolov, L. N. Savinova, N. A. Chumaevskii, *Russ. J. Inorg. Chem.*, 1990, **35**, (3), 345.
49. J. H. Holloway, G. J. Schrobilgen, *J. Chem. Soc., Chem. Commun.*, 1975, 623.
50. A. J. Edwards, P. Taylor, *J. Chem. Soc., Chem. Commun.*, 1971, 1376.
51. W. H. Zachariasen, *Acta Cryst.*, 1949, **2**, 296.
52. P. Eller, A. Larson, *Inorg. Chim. Acta*, 1979, **37**, 129.
53. R. R. Ryan, R. A. Penneman, L. B. Asprey, R. T. Paine, *Acta Cryst.*, 1976, **B32**, 3311.
54. C. Hebecker, *Z. Anorg. Allg. Chem.*, 1971, **384**, 111.
55. A. J. Edwards, G. R. Jones, B. R. Steventon, *J. Chem. Soc., Chem. Commun.*, 1967, 462.
56. A. J. Edwards, R. D. Peacock, R. W. H. Small, *J. Chem. Soc.*, 1962, 4486.
57. A. J. Edwards, *J. Chem. Soc. (A)*, 1969, 909.
58. J. H. Holloway, S. J. Mitchell, *J. Chem. Soc. (A)*, 1971, 2789.
59. B. R. Morrell, A. Zalkin, A. Tressaud, N. Bartlett, *Inorg. Chem.*, 1973, **12**, (11), 2640.
60. A. J. Edwards, *Adv. Inorg. Chem. Radiochem.*, 1983, **27**, 83, (Acad. Press Inc.).
61. M. Akhtar, P. R. Rao, N. Bartlett, unpublished work.
62. B. G. Müller, M. Serafin, *Eur. J. Solid State Inorg. Chem.*, 1992, **29**, 625.
63. V. N. Ikorskii, K. A. Khaldoyanidi, *J. Struct. Chem. (Eng. Trans.)*, 1982, **23**, 302.
64. S. A. Brewer, J. Fawcett, J. H. Holloway, D. R. Russell, unpublished work.

65. J. H. Holloway, G. Stanger, E. G. Hope, D. A. Boyd, *J. Fluorine Chem.*, 1992, **56**, 77.
66. J. Fawcett, personal communication.
67. R. D. Shannon, *Acta Cryst.*, 1976, **A32**, 751.
68. N. Bartlett, P. R. Rao, *J. Chem. Soc., Chem. Commun.*, 1965, 252.
69. E. A. V. Ebsworth, D. W. H. Rankin, S. Craddock, *Structural Methods in Inorganic Chemistry* (1st Ed.), 1987, 322, (Blackwell Scientific Publ., Oxford), ISBN 0-632-01592-6.
70. A. K. Brisdon, personal communication.
71. V. B. Sokolov, Yu. V. Drobyshevskii, V. N. Prusakov, A. V. Rozhkov, S. S. Khorosov, *Dokl. Akad. Nauk. SSSR*, 1976, **229**, 641.
72. V. B. Sokolov, V. G. Tsinoev, A. V. Ryzhkov, *Teor. Eksp. Khim.*, 1980, **16**, 345.
73. F. W. Einstein, P. R. Rao, J. Trotter, N. Bartlett, *J. Chem. Soc. (A)*, 1967, 478.
74. A. J. Edwards, G. R. Jones, B. R. Steventon, *J. Chem. Soc., Chem. Commun.*, 1967, 462.
75. A. J. Edwards, G. R. Jones, *J. Chem. Soc. (A)*, 1968, 2074.
76. J. H. Canterford, R. Colton, *Halides of the Second and Third Row Transition Metals*, 1968, 2, (Wiley-Interscience).
77. O. Glemser, *J. Fluorine Chem.*, 1984, **24**, 319.
78. A. F. Wells, *Structural Inorganic Chemistry*, 1975, 4th Ed., 350, (Clarendon Press, Oxford).
79. V. D. Klimov, *Russ J. Inorg. Chem.*, 1990, **35**, (11), 1566.
80. R. D. Peacock, *Advances in Fluorine Chemistry*, 1973, **7**, 113, (Butterworth and Co. Ltd.).
81. L. Pauling, *The Nature of the Chemical Bond*, 1960, 3rd Ed., 225, (Cornell University Press, N.Y.).
82. *Tables of Interatomic Distances and Configurations in Molecules and Ions*, Chem. Soc. Publ., 1958, 11.
83. R. E. Rundle, *Rec. Chem. Progr.*, 1962, **23**, 195.

84. A. J. Edwards, *J. Chem. Soc., Dalton Trans.*, 1972, 2325.
85. U. Müller, *Acta Cryst.*, 1986, **B42**, 557.
86. J. H. Hollway, D. Laycock, *Adv. Inorg. Chem. Radiochem.*, 1984, **28**, 73, (Acad. Press Inc.).
87. P. J. Townson, 1991, PhD Thesis, Leicester University.
88. A. J. Edwards, W. E. Falconer, W. A. Sunder, *J. Chem. Soc., Dalton Trans.*, 1974, 541.
89. I. R. Beattie, D. J. Reynolds, *J. Chem. Soc., Chem. Commun.*, 1968, 1531.
90. L. B. Asprey, R. R. Ryan, E. Fukushima, *Inorg. Chem.*, 1972, **11**, 3122.
91. I. R. Beattie, K. M. S. Livingstone, D. J. Reynolds, G. A. S. Ozin, *J. Chem. Soc. (A)*, 1970, 1210.
92. A. J. Edwards, B. R. Steventon, *J. Chem. Soc. (A)*, 1968, 2503.
93. A. J. Edwards, G. R. Jones, *J. Chem. Soc. (A)*, 1968, 2511.
94. R. T. Paine, L. B. Asprey, *Inorg. Chem.*, 1975, **14**, (5), 1111.
95. A. J. Edwards, G. R. Jones, R. J. C. Sills, *J. Chem. Soc., Chem. Commun.*, 1968, 1177.
96. A. J. Edwards, G. R. Jones, R. J. C. Sills, *J. Chem. Soc. (A)*, 1970, 2521.
97. W. E. Falconer, R. D. Burbank, G. R. Jones, W. A. Sunder, M. J. Vasile, *J. Chem. Soc., Chem. Commun.*, 1972, 1080.
98. N. Bartlett, N. Nghi, *CR Acad. Sci. (Ser. C)*, 1969, **269**, 756.
99. W. E. Falconer, F. J. Disalvo, J. E. Griffiths, F. A. Stevie, W. A. Sunder, M. J. Vasile, *J. Fluorine Chem.*, 1975, **6**, 499.
100. M. A. Hepworth, P. L. Robinson, *J. Inorg. Nucl. Chem.*, 1957, **4**, 24.
101. H. G. Cady, G. B. Hargreaves, *J. Chem. Soc.*, 1961, 1568.
102. O. Ruff, E. Schiller, *Z. Anorg. Chem.*, 1911, **72**, 329.
103. H. Schafer, H. G. Schnering, K. J. Niehues, H. G. Nieder-Vahrenholz, *J. Less Common Metals*, 1965, **9**, 95.
104. J. H. Holloway, G. M. Staunton, K. Rediess, R. Bougon, D. Brown, *J. Chem. Soc., Dalton Trans.*, 1984, 2163.
105. A. Popov, V. Sukhoverkhov, N. Chumaevskii, *Russ. J. Inorg. Chem.*, 1990, **35**, (5), 626.

106. F. Fairbrother, K. H. Grundy, A. Thompson, *J. Chem. Soc.*, 1965, 765.
107. H. Clark, H. Emeléus, *J. Chem. Soc.*, 1958, 190.
108. J. C. Fuggle, R. W. H. Sharp, J. M. Winfield, *J. Fluorine Chem.*, 1971/2, 1, 427.
109. B. Frlec, J. H. Holloway, *J. Chem. Soc., Dalton Trans.*, 1975, 535.
110. J. H. Holloway, personal communication.
111. I. R. Beattie, K. M. S. Livingstone, G. A. Ozin, D. J. Reynolds, *J. Chem. Soc. (A)*, 1969, 958.
112. G. S. Chen, J. Passmore, P. Taylor, T. R. Whidden, P. S. White, *J. Chem. Soc., Dalton Trans.*, 1985, 9.
113. J. H. Holloway, unpublished work.
114. J. G. Stark, H. G. Wallace, *Chemistry Data Book (2nd Ed.)*, 1982, John Murray, London, ISBN 0-7195-3951-X.
115. R. S. McDowell, L. B. Asprey, L. C. Hoskins, *J. Chem. Phys.*, 1972, **56**, 5712.
116. R. Cavell, H. Clark, *J. Inorg. Nucl. Chem.*, 1961, **17**, 257.
117. P. J. Holliman, E. G. Hope, J. H. Holloway, unpublished work.
118. H. Selig, B. Frlec, *J. Inorg. Nucl. Chem.*, 1967, **29**, 1887.
119. A. F. Clifford, H. C. Beachall, W. M. Jack, *J. Am. Chem. Soc.*, 1953, **75**, 5221.
120. D. A. McCaulay, W. S. Higley, A. P. Lien, *J. Am. Chem. Soc.*, 1956, **78**, 3009.
121. H. Claassen, H. Selig, *J. Chem. Phys.*, 1965, **44**, 4039.
122. R. R. Holmes Snr., R. M. Deiters, J. A. Golen, *Inorg. Chem.*, 1969, **8**, (12), 2612.
123. E. G. Hope, *J. Chem. Soc., Dalton Trans.*, 1990, 723.
124. O. L. Keller, A. Cheetham-Strode, *Inorg. Chem.*, 1966, **5**, 367.
125. H. Selig, H. Claassen, *J. Chem. Phys.*, 1966, **44**, 1404.
126. W. W. Dukat, J. H. Holloway, E. G. Hope, M. Rieland, R. Powell, P. J. Townson, *Eur. Pat. Appl. No. 9105167.2*.
127. F. O. Sladky, P. A. Bulliner, N. Bartlett, *J. Chem. Soc. (A)*, 1969, 2179.

128. L. Smart, E. Moore, *Solid State Chemistry - An Introduction*, Chapman and Hall, 1992, 258.
129. B. K. Teo, *EXAFS: Basic Principles and Data Analysis*, 1986, Springer-Verlag, NY, ISBN 0-387-15833-2.
130. J. Corker, PhD Thesis, 1991, Southampton University.
131. P. A. Lee, J. B. Pendry, *Phys. Rev. B*, 1975, **11**, 2795.
132. S. J. Gurman, N. Binsted, I. Ross, *J. Phys. Chem.*, 1984, **17**, 143.
133. S. J. Gurman, N. Binsted, I. Ross, *J. Phys. Chem.*, 1986, **19**, 1845.
134. A. K. Brisdon, EX Programme, University of Leicester, 1991.
135. Daresbury Computer Programme, Version EXCURV90, Daresbury Laboratory, Cheshire.
136. R. W. Joyner, K. J. Martin, P. Meehan, *J. Phys. C: Solid State Physics*, 1987, **20**, 4005.
137. A. G. Turner, *Methods in Molecular Orbital Theory*, 1974, Prentice-Hall, New Jersey.
138. T. Loucks, *The Augmented Plane Wave Method*, 1967, Benjamin, New York.
139. P. A. Lee, G. Beni, *Phys. Rev. B*, 1977, **15**, 2862.
140. P. Eisenberger, B. Lengeler, *Phys. Rev. B*, 1980, **22**, 3551.
141. P. H. Citrin, P. Eisenberger, B. M. Kincaid, *Phys. Rev. Lett.*, 1976, **36**, 1346.
142. R. Domesle, R. Hoppe, *Angew. Chem. (Int. Ed., Eng.)*, 1980, **19**, (6), 489.
143. P. Hagenmüller (Ed.), *Inorganic Solid Fluorides*, 1985, 289, Acad. Press Inc., ISBN 0-12-313370-X.
144. L. I. Maissel, R. Glang, *Handbook of Thin Film Technology*, 1970, McGraw-Hill, New York.
145. P. Hagenmuller (Ed.), *Inorganic Solid Fluorides*, 1985, 594, Acad. Press Inc., ISBN 0-12-313370-X.
146. A. K. Brisdon, P. J. Jones, W. Levason, J. S. Ogden, J. H. Holloway, E. G. Hope, G. Stanger, *J. Chem. Soc., Dalton Trans.*, 1990, 715.
147. N. Lifshitz, *J. Electrochem. Soc.*, 1988, **135**, (7), 1832.
148. J. Kachnik, U. S. Pat. 4,654,266, 31st March 1987, E21B 43/26, a428-403.
149. R. Hozlzl, U. S. Pat. 3,565,676, 23rd Feb 1971, C23c 11/00, 13/02.

150. C. I. Fairchild, Proc. Conf. CVD Refract. Metals, Alloys, Compounds; Gatlinburg, Tennessee, 1967, 149.
151. T. Fukatsu, M. Takeuchi, K. Kazuyuki, Japanese Patent, JP 61127865, 1986.
152. E. Nishitani, S. Tsujiku, M. Nakatani, M. Maehara, M. Horiuchi, K. Mizukami, Japanese Patent, JP 63020481.
153. P. Hagenmüller (Ed.), Inorganic Solid Fluorides, 1985, 584, Acad. Press Inc., ISBN 0-12-313370-X.
154. D. R. Lide (Ed.), CRC Handbook of Chemistry and Physics (73rd Ed.), 1992-3, CRC Press Inc., Boca Raton, Florida, ISBN 0-8493-0473-3.
155. Hughes Aircraft Corp., British Patent 1,559,593, 1980.
156. Siemens, German Appl. 2,300,481, 1974.
157. J. Müller, D. Lohrberg, U. S. Pat. 3,788,968, 1974.
158. G. K. Acres, Plat. Metals Rev., 1980, 24, 25.
159. J. Federer, A. Schaffhauser, Thermodynamic Conv. Spring Conf. (9th), Miami Beach, 1970, 74.
160. R. Enstrom, N. Skillman, J. Appert, U. S. Pat. 3,484,208, 16th Dec 1969, C22c, 13/00, 31/00.
161. W. C. Robinson, F. H. Patterson, J. D. Fleming, C. W. Gorton, Proc. Conf. CVD Refract. Metals, Alloys, Compounds; Gatlinburg, Tennessee, 1967, 109.
162. R. C. Weast (Ed.), CRC Handbook of Chemistry and Physics (1st Student Ed.), 1987, CRC Press Inc., Boca Raton, Florida, ISBN 0-8493-0740-6.
163. F. A. Cotton, G. Wilkinson, Adv. Inorg. Chem., (5th Ed.), 1988, 791, Wiley-Interscience, New York.
164. M. Atherton, BNFL Fluorochemicals Ltd., Personal Communication.
165. F. S. Patten, J. M. Googin, W. L. Griffith, International Series of Monographs on Nuclear Energy, 1963, Pergamon, Oxford.

## Appendix:- Abbreviations

**PTFE:** Polytetrafluoroethane.

**F.E.P.:** Tetrafluoroethane-perfluoropropene copolymer.

**EXAFS** Extended X-ray Absorption Fine Structure.

**MICVD:** Metal Inorganic Vapour Deposition.

**s:** Strong.

**m:** Medium.

**w:** Weak.

**sh:** Shoulder.

**br:** Broad.

**shp:** Sharp.

**a.m.u.:** Atomic mass units.